

Aus dem Bereich Physiologie  
Theoretische Medizin und Biowissenschaften  
der Medizinischen Fakultät  
der Universität des Saarlandes, Homburg/Saar

# **Identification of novel pathogen-derived agonists for human and mouse formyl peptide receptors**

*Dissertation zur Erlangung des Grades eines Doktors*

*der Naturwissenschaften*

**der Medizinischen Fakultät**

der UNIVERSITÄT DES SAARLANDES

2015

vorgelegt von: Timo Schumann

geb. am: 07.03.1983 in Ottweiler

## **Dedication**

To my parents that always let my spirit soar and gave me a wonderful and happy life;

to my brother who keeps my inner child alive;

to my wife who supports my passionate curiosity;

to my daughter, the most wonderful thing I can imagine;

and to my yet unborn child: I desire to meet you healthy 😊.

I hope that this work will contribute to scientific progress in a way that good people can live a good life.

# Contents

## Table of Contents

---

<b>List of figures</b> .....	<b>VII</b>
<b>List of tables</b> .....	<b>IX</b>
<b>Abstract</b> .....	<b>X</b>
<b>Zusammenfassung</b> .....	<b>XII</b>
<b>Abbreviations</b> .....	<b>XIV</b>
<b>Chapter 1 - Introduction</b> .....	<b>1</b>
1.1. The Vomeronasal Organ .....	1
1.2. Expression of formyl peptide receptors .....	3
1.3. Physiological functions mediated by FPRs .....	4
1.4. Ligands of the FPR family .....	5
1.5. Structure and signaling of formyl peptide receptors .....	7
1.6. Hypothesis and aims of this work .....	9
<b>Chapter 2 – Materials &amp; Methods</b> .....	<b>10</b>
2.1. Molecular cloning of the formyl peptide receptors .....	10
2.1.1. Amplification of the FPR genes .....	10
2.1.2. DNA-purification via DNA Clean & Concentrator <sup>TM</sup> -5 -Kit .....	12
2.1.3. Gel electrophoresis .....	12
2.1.4. Expression vectors .....	12
2.1.5. DNA digestion .....	13
2.1.6. DNA ligation .....	14
2.1.7. Transformation .....	14
2.1.8. DNA isolation .....	14
2.1.9. Restriction analysis .....	15
2.1.10. Gel electrophoresis for restriction analysis .....	15
2.1.11. DNA purification and precipitation .....	15

2.1.12. DNA sequencing.....	16
2.2. HEK cell culture .....	16
2.2.1. Cell line and cultivation.....	16
2.2.2. Transient transfection .....	16
2.2.3. Handling of frozen cell stocks .....	17
2.3. Isolation and cultivation of primary cells .....	17
2.3.1. Human blood collection.....	17
2.3.1.1. Blood collection for isolation of human monocytes .....	18
2.3.1.2. Blood collection for isolation of human granulocytes.....	18
2.3.1.3. Collection of autologous serum.....	18
2.3.2. Isolation of human monocytes.....	18
2.3.3. Isolation of human granulocytes.....	19
2.3.3.1. Isolation of human granulocytes by Ficoll/dextran separation.....	19
2.3.3.2. Isolation of human granulocytes using CD16+ pluriBeads .....	20
2.3.4. Isolation of mouse leukocytes.....	20
2.3.4.1. Isolation of murine neutrophils from peripheral blood with Ly6G pluriBeads .....	20
2.3.4.2. Isolation of murine leukocytes from bone marrow .....	21
2.3.5. Dissociation of mouse vomeronasal sensory neurons .....	21
2.4. Mice .....	22
2.4.1. Mouse strains .....	22
2.4.1.1. Wild type mice.....	22
2.4.1.2. <i>Fpr1</i> -deficient mice.....	22
2.4.1.3. Mice heterozygous for <i>Fpr1</i> .....	22
2.4.1.4. Heterozygous <i>dOMP-GFP</i> mice.....	22
2.4.2. Mouse keeping and breeding .....	23
2.5. Immunocytochemistry .....	23
2.5.1. Antibodies.....	23
2.5.1.1. Primary antibodies .....	23
2.5.1.2. Secondary antibodies.....	24
2.5.2. Immunostaining .....	24
2.5.3. Analysis and evaluation of immunofluorescence .....	25
2.6. Calcium Imaging .....	25
2.6.1. G protein coupling of HEK293T cells .....	25
2.6.2. Ratiometric single cell calcium imaging .....	26

2.6.2.1. The BD Pathway 855 .....	26
2.6.2.2. Ratiometric dye Fura-2 AM .....	26
2.6.2.3. Loading procedure for conventional single cell imaging .....	27
2.6.2.4. Loading procedure for single cell imaging under perfusion conditions .....	27
2.6.2.5. Recording and evaluation .....	28
2.6.3. High-throughput calcium imaging of cell populations with the FLIPR .....	28
2.6.3.1. The FLIPR system (Fluorescence Imaging Plate Reader) .....	28
2.6.3.2. The calcium sensitive dye Fluo-4 AM .....	28
2.6.3.3. Loading procedure .....	28
2.6.3.4. Recording and evaluation .....	29
2.7. Detection of reactive oxygen species (ROS) .....	30
2.7.1. Radical detection with Amplex®UltraRed .....	30
2.7.1.1. The Amplex®UltraRed dye .....	30
2.7.1.2. Loading procedure of monocytes and granulocytes for ROS detection .....	30
2.7.1.3. Recording and evaluation of ROS detection experiments .....	30
2.8. Chemotaxis .....	31
2.8.1. Chemotaxis assay principle .....	31
2.8.2. Granulocyte stimulation for chemotaxis .....	31
2.8.3. Evaluation .....	31
2.9. Image processing software .....	32
2.9.1. Drawing of the ligand structures .....	32
2.9.2. Figures and images .....	32
2.10. Statistics and mathematics .....	32
2.10.1. Significance tests .....	32
2.10.2. Average and standard deviation .....	32
2.10.3. Concentration-response curves .....	33
2.11. Online tools and databases .....	33
2.11.1. Internet addresses .....	33
2.11.2. Prediction of transmembrane helices of cloned FPR constructs .....	33
2.12. Solutions, media and ligands .....	34
2.12.1. Ligands .....	34
2.12.2. Imaging buffers .....	36
2.12.3. Cell culture media .....	36
2.12.4. Bacterial growth media .....	37

2.12.5. Other solutions.....	37
<b>Chapter 3 – Results .....</b>	<b>38</b>
3.1. Pharmacological analysis of formyl peptide receptors of the immune and the vomeronasal system.....	38
3.1.1. Functional analysis of formyl peptide receptors in HEK293T cells.....	38
3.1.1.1. FPRs from the immune and vomeronasal system can be expressed in HEK293T cells .....	38
3.1.1.2. Heterologously expressed immune FPRs can be measured in calcium imaging .....	41
3.1.2. FPR agonist screening reveals divergent pharmacological profiles of immune FPRs and vomeronasal FPRs.....	48
3.1.2.1. Activation pattern of human FPRs.....	49
3.1.2.2. Activation pattern of mouse immune FPRs .....	50
3.1.2.3. Activation pattern of mouse vomeronasal FPRs.....	50
3.2. Structural requirements for activation of mFpr-rs1 by W-peptide .....	53
3.2.1. mFpr-rs1 shows stereo-selective tuning for related peptides containing D-amino acids .....	53
3.2.2. Activation of mFpr-rs1 requires the four C-terminal amino acids of W-peptide ...	56
3.2.3. Influence of C-terminal amidation of W-peptide on affinity to mFpr-rs1 .....	57
3.2.4. Activation of mFpr-rs1 by N-terminally formylated peptides.....	59
3.3. Vomeronasal sensory neurons of mice respond to the mFpr-rs1 ligand W-peptide.....	62
3.4. Formyl peptide receptor-dependent recognition of bacterial signal peptides by the mammalian innate immune system .....	65
3.4.1. Formyl peptide receptor-mediated recognition of bacterial signal peptides by human monocytes .....	67
3.4.1.1. Primary human monocytes can be measured by high-throughput calcium imaging... ..	67
3.4.1.2. Bacterial signal peptides activate human monocytes by utilizing FPRs.....	70
3.4.1.3. Primary human monocytes recognize bacterial signal peptides with high sensitivity .....	71
3.4.2. Human granulocytes detect bacterial signal peptides through formyl peptide receptors.....	75
3.4.2.1. Primary human granulocytes recognize signal peptides in high-throughput calcium imaging.....	75
3.4.2.2. Signal peptide recognition of human granulocytes is mediated by FPRs.....	78
3.4.2.3. Bacterial signal peptides activate primary human granulocytes with high affinity ....	80
3.5. Bacterial signal peptides trigger pathogen defense mechanisms in hum. phagocytes ..	82
3.5.1. Bacterial signal peptides induce chemotaxis in neutrophils .....	83

3.5.2. Monocytes and neutrophils produce reactive oxygen species when stimulated with bacterial signal peptides .....	84
3.6. Formyl peptide receptor-dependent activation of murine leukocytes by bacterial signal peptides .....	87
3.6.1. Signal peptides activate neutrophils isolated from mouse bone marrow.....	87
3.6.1.1. Immunocytochemical analysis of isolated bone marrow cells .....	87
3.6.1.2. Bone marrow leukocytes isolated from mice heterozygous for <i>Fpr1</i> can be activated by bacterial signal peptides.....	89
3.6.2. Signals induced by mFpr1-selective concentrations of Streptococcus-SP1 are abolished in <i>Fpr1</i> <i>-/-</i> mice .....	89
<b>Chapter 4 – Discussion.....</b>	<b>91</b>
4.1. DMSO is a newly identified FPR agonist with therapeutic potential.....	91
4.2. Recognition of pathogen-derived peptides by vomeronasal mFpr-rs1 .....	93
4.2.1. Activation of the vomeronasal receptor mFpr-rs1 by W-peptide and M-peptide...	93
4.2.2. Key structures for activation of mFpr-rs1 by small peptides.....	93
4.2.2.1. A core motif of four amino acids is necessary to activate mFpr-rs1 .....	94
4.2.2.2. mFpr-rs1 prefers peptides with C-terminal D-amino acids rather than L-amino acids .....	94
4.2.2.3. The double-bonded oxygen of terminal carbonyl groups is important for affinity of peptides to mFpr-rs1 .....	94
4.2.3. mFpr-rs1 detects pathogen-derived peptides: possible novel mechanisms to sense microbes .....	97
4.2.3.1. Detection of D-amino acid-containing peptides by mFpr-rs1 .....	97
4.2.3.2. Detection of N-terminally formylated peptides by mFpr-rs1 .....	98
4.2.3.3. Activation of vomeronasal sensory neurons by the mFpr-rs1 agonist W-peptide .....	99
4.3. Neo-functionalization of mouse Fpr-rs receptors expressed in the VNO .....	100
4.4. Recognition of bacterial signal peptides of innate immune cells is mediated by FPRs – evidence for a novel pattern recognition mechanism.....	102
4.4.1. Detection of signal peptides by innate immune cells occurs with extraordinary high affinity and receptor specificity .....	102
4.4.2. Biological significance of signal peptide detection by innate immune cells – evidence for a novel pattern recognition receptor .....	106
4.4.3. Occurrence of signal peptides and their N-terminal fragments in nature .....	108
4.4.3.1. Natural occurrence of bacterial peptides starting with N-terminally formylated methionine .....	108
4.4.3.2. Release of signal peptides and N-terminal signal peptide fragments in nature .....	109

4.5. Conclusion and Outlook ..... 111

**Literature ..... 113**

**Appendix ..... 122**

**Publications ..... 128**

**Acknowledgments and Contributions ..... 131**

**Curriculum vitae ..... 137**

## List of figures

---

### Chapter 1

**Figure 1-1** | Schematic overview of the olfactory subsystems in mice with a coronal section of the VNO \_\_\_\_\_ 2

**Figure 1-2** | Schematics of FPR-mediated signal transduction \_\_\_\_\_ 8

### Chapter 2

**Figure 2-1** | Schematics of expression vectors \_\_\_\_\_ 13

**Figure 2-2** | Schematics of blood separation by Ficoll density gradient centrifugation \_\_\_\_\_ 19

**Figure 2-3** | Schematics showing the construct used for targeted disruption of *Fpr1* in mice \_\_\_\_\_ 22

### Chapter 3

**Figure 3-1** | Expression of human and murine formyl peptide receptors in HEK293T cells \_\_\_\_\_ 40

**Figure 3-2** | Single cell calcium imaging of human and murine FPRs in HEK293T cells \_\_\_\_\_ 41

**Figure 3-3** | Mass population calcium imaging of human and murine FPRs in HEK293T cells \_\_\_\_\_ 42

**Figure 3-4** | Influence of G protein-chimeras on cal. imaging of human and murine FPRs in HEK293T cells \_\_\_\_\_ 44

**Figure 3-5** | Specific activation of hFPR2, mFpr1 and mFpr2 by DMSO \_\_\_\_\_ 45

**Figure 3-6** | Cell population-based calcium imaging of heterologously expressed FPRs \_\_\_\_\_ 47

**Figure 3-7** | W-peptide and M-peptide are activators of mFpr-rs1 \_\_\_\_\_ 48

**Figure 3-8** | Selective activation of mFpr-rs1 by disparate structures suggests a specific ligand recognition mechanism \_\_\_\_\_ 54

**Figure 3-9** | Single cell calcium imaging assay with buffer perfusion for repetitive stimulation \_\_\_\_\_ 55

**Figure 3-10** | Heterologously expressed mFpr-rs1 prefers C-terminal D-amino acids \_\_\_\_\_ 56

**Figure 3-11** | Amino acid residues of W-peptide critical for mFpr-rs1 activation \_\_\_\_\_ 57

**Figure 3-12** | Heterologously expressed mFpr-rs1 is selective towards C-terminally amidated W-peptide \_\_\_\_\_ 58

**Figure 3-13** | Stereo-chemical resemblance of D-methionine carrying a C-terminal formaldehyde function and L-methionine with N-terminal formylation \_\_\_\_\_ 59

**Figure 3-14** | Heterologously expressed mFpr-rs1 can be activated by formyl peptides \_\_\_\_\_ 60

**Figure 3-15** | Identification of acutely dissociated mouse vomeronasal sensory neurons \_\_\_\_\_ 62

**Figure 3-16** | Calcium imaging of vomeronasal sensory neurons \_\_\_\_\_ 64

**Figure 3-17** | Vomeronasal sensory neurons respond to W-peptide \_\_\_\_\_ 65

**Figure 3-18** | Heterologously expressed FPRs of human and mouse recognize bacterial signal peptides in single cell calcium imaging \_\_\_\_\_ 66

<b>Figure 3-19</b>   Calcium imaging of primary human monocytes upon stimulation with <i>Streptococcus</i> -SP1	67
<b>Figure 3-20</b>   Immunofluorescence of surface receptors on human monocytes	69
<b>Figure 3-21</b>   Cross-desensitization in human monocytes by the FPR1-preferential signal peptide SP1	70
<b>Figure 3-22</b>   Inhibition of signal peptide-induced calcium responses in monocytes by hFPR blockers	71
<b>Figure 3-23</b>   Human monocytes are activated by a range of bacterial signal peptides	72
<b>Figure 3-24</b>   Direct comparison between concentration-response curves of human monocytes and hFPR1-expressing HEK293T cells	73
<b>Figure 3-25</b>   Primary human granulocytes are activated by various bacterial signal peptides	76
<b>Figure 3-26</b>   Signal peptide-induced calcium signals are generated by primary human granulocytes	78
<b>Figure 3-27</b>   Block of signal peptide-induced calcium signals by hFPR1 and hFPR2 inhibitors in human granulocytes	80
<b>Figure 3-28</b>   Direct comparison between concentration-response curves of human granulocytes and hFPR1 or hFPR2 expressed in HEK293T cells	81
<b>Figure 3-29</b>   Human granulocytes show chemotactic activity towards signal peptides	84
<b>Figure 3-30</b>   Signal peptide-dependent formation of reactive oxygen species by human monocytes and granulocytes	86
<b>Figure 3-31</b>   Immunocytochemical analysis of mouse bone marrow leukocytes	88
<b>Figure 3-32</b>   Bone marrow leukocytes isolated from <i>Fpr1</i> <sup>+/-</sup> mice respond to signal peptides with intracellular calcium mobilization	89
<b>Figure 3-33</b>   Calcium signals in murine bone marrow leukocytes induced by 1 $\mu$ M <i>Streptococcus</i> -SP1 are abolished in <i>Fpr1</i> <sup>-/-</sup> mice	90

## Chapter 4

<b>Figure 4-1</b>   Retro-inversion of W-peptide reveals a common structural motif of N-terminally formylated and C-terminally amidated peptides	96
--	----

## Appendix

<b>Appendix 1</b>   The mFpr2 agonist CRAMP can elicit unspecific responses in HEK293T cells	122
<b>Appendix 2</b>   hFPR2 expression in human monocytes	122
<b>Appendix 3</b>   Determination of cross-reactivity of anti-hFPR antibodies with heterologously expressed FPRs	123
<b>Appendix 4</b>   Nucleotide sequence of the rhodopsin fusion element	125
<b>Appendix 5</b>   Full coding sequences of the cloned formyl peptide receptors	125

## List of tables

---

### Chapter 2

<b>Table 2-1</b>   Cloned genes, PCR primers and accession numbers of nucleotide sequences _____	<b>11</b>
<b>Table 2-2</b>   Primary antibodies used in this study _____	<b>23</b>
<b>Table 2-3</b>   Plasmids used for co-transfection encoding distinct G protein chimeras _____	<b>26</b>
<b>Table 2-4</b>   Ligands used in this study _____	<b>34</b>
<b>Table 2-5</b>   Buffers used for functional imaging _____	<b>36</b>
<b>Table 2-6</b>   Cell culture media _____	<b>36</b>
<b>Table 2-7</b>   Bacterial growth media _____	<b>37</b>

### Chapter 3

<b>Table 3-1</b>   Overview of cloned receptors, online accession, and detected amino acid exchanges _____	<b>39</b>
<b>Table 3-2</b>   Agonist profiling of FPRs in HEK293T cells _____	<b>52</b>
<b>Table 3-3</b>   mFpr-rs1 agonist motifs are frequently found in proteins of various pathogenic microorganisms __	<b>61</b>
<b>Table 3-4</b>   Human monocytes exhibit high affinity to bacterial signal peptides _____	<b>74</b>
<b>Table 3-5</b>   Human granulocytes exhibit high affinity to bacterial signal peptides _____	<b>82</b>

## Abstract

The mammalian innate immune system defines the first line of defense against pathogens. Immune cells expressing receptors that are specialized to recognize structures typical for pathogens play a central role in the detection of hostile organisms. One of these receptor-mediated mechanisms involves the formyl peptide receptors (FPRs). Their members, which are predominantly expressed on mammalian leukocytes of the innate immune system, are named after their affinity towards N-terminally formylated peptides, a pattern typical for bacterial metabolism. Besides formyl peptides, they recognize many exogenous and host endogenous substances that are involved in inflammatory processes. Interestingly, the vomeronasal organ of mouse, an accessory olfactory organ, expresses five structurally-related members of the formyl peptide receptor family. The current dissertation is based on the hypothesis that vomeronasal formyl peptide receptors of mice mediate the olfactory detection of pathogens. To test this hypothesis in the long run, profound pharmacological understanding of the vomeronasal formyl peptide receptors (mFpr-rs1, mFpr-rs3, mFpr-rs4, mFpr-rs6 and mFpr-rs7) is a prerequisite. Therefore, I cloned all five known vomeronasal formyl peptide receptors for high-throughput *in-vitro* pharmacological analysis in HEK293T cells. My initial observations with calcium imaging showed that the FPR family segregates into two functional groups: the promiscuous immune FPRs and the more stringent vomeronasal FPRs. In fact, only one of the vomeronasal receptors, mFpr-rs1, was able to induce calcium signals in response to certain peptides that exhibit chemical modifications characteristic for bacteria. Some of these peptides were also capable of activating vomeronasal sensory neurons, a cell type that naturally expresses mFpr-rs1. Interestingly, the corresponding peptide motifs are found in distinct pathogenic microorganisms, which is consistent with the idea that vomeronasal FPRs mediate the recognition of pathogens. Structure-function analysis of these peptides revealed a molecular signature important for activation of mFpr-rs1. Employing this knowledge, our group discovered that bacterially-derived signal peptides represent a large class of novel ligands for the FPR family, including mFpr-rs1 and human and mouse immune FPRs when expressed in HEK293T cells. With biochemical techniques as well as pharmacological and genetic manipulation, I show that these peptides specifically activate FPRs in primary innate human and mouse immune cells. Furthermore, my data provide clear evidence that signal peptides activate host anti-bacterial actions of human innate immune cells. With this, my work reveals conceptual insight into a possible novel detection mechanism by

which the mammalian immune system can sense the presence of bacteria at the molecular level.

## Zusammenfassung

Bei Säugetieren bildet das angeborene Immunsystem die erste Verteidigungslinie gegen Infektionen durch Pathogene. Bei der Detektion feindseliger Organismen spielen Immunzellen die spezialisierte Rezeptoren zur Erkennung pathogener Strukturen exprimieren eine zentrale Rolle. Einer dieser Rezeptor-vermittelten Mechanismen wird unter anderem von den Formylpeptid-Rezeptoren (FPRs) übernommen. Ihre Mitglieder, welche hauptsächlich auf Leukozyten von Säugetieren exprimiert werden, wurden nach Ihrer Affinität zu N-terminal formylierten Peptiden, ein Muster welches man dem bakteriellen Metabolismus zuschreibt, benannt. Neben den Formylpeptiden, erkennen sie auch viele exogene sowie wirtseigene Substanzen die bei entzündlichen Prozessen eine Rolle spielen. Interessanterweise exprimiert das Vomeronasalorgan der Maus, ein akzessorisches olfaktorisches Organ, fünf Struktur-verwandte Mitglieder der Formylpeptid-Rezeptor-Familie. Die vorliegende Arbeit basiert auf der Hypothese, dass die vomeronasalen Formylpeptid-Rezeptoren von Mäusen die olfaktorische Detektion von Pathogenen ermöglichen. Um diese Hypothese auf lange Sicht zu prüfen sind profunde pharmakologische Kenntnisse der vomeronasalen Formylpeptid-Rezeptoren (mFpr-rs1, mFpr-rs3, mFpr-rs4, mFpr-rs6 und mFpr-rs7) erforderlich. Daher habe ich alle fünf bekannten vomeronasalen Formylpeptid-Rezeptoren kloniert um sie mittels Hochdurchsatz-Kalzium-Imaging in HEK293T-Zellen pharmakologisch zu untersuchen. Meine ersten Beobachtungen zeigten, dass sich die FPR Familie in zwei funktionelle Gruppen aufteilt: die promiskuitiven Immun-FPRs und die stringenteren vomeronasalen FPRs. Genau genommen konnte nur ein vomeronasaler Rezeptor, mFpr-rs1, aktiviert werden. Dieser antwortete auf bestimmte Peptide, welche für Bakterien charakteristische chemische Modifikation trugen, mit Kalzium-Signalen. Einige dieser Peptide waren dazu in der Lage vomeronasale Neurone zu aktivieren. Die entsprechenden Peptid-Motive sind in bestimmten pathogenen Mikroorganismen zu finden, was mit der Idee, dass FPRs die Erkennung von Pathogenen vermitteln, einher geht. Struktur-Funktionsanalysen dieser Peptide offenbarten eine molekulare Signatur die wichtig zur Aktivierung des mFpr-rs1 ist. Durch Nutzung dieses Wissens entdeckte unsere Arbeitsgruppe, dass von Bakterien stammende Signal-Peptide eine riesige Gruppe neuer Liganden für heterolog exprimierte FPRs, inklusive der Immun- und der vomeronasalen FPRs, darstellen. Mit biochemischen Techniken sowie durch pharmakologische und genetische Manipulation, zeige ich, dass die FPRs in primären Zellen des angeborenen Immunsystems von Maus und Mensch, spezifisch durch diese Peptide

aktiviert werden. Darüber hinaus liefern meine Daten klare Beweise dafür, dass diese Signalpeptide wirtseigene anti-bakterielle Reaktionen in Zellen des angeborenen menschlichen Immunsystems auslösen. Damit liefert meine Arbeit konzeptionelle Einsichten in einen möglichen neuen Mechanismus, mit dem das Immunsystem von Säugetieren die Anwesenheit von Bakterien auf molekularer Ebene erkennen kann.

## Abbreviations

ABC	ATP binding cassette
ALX	lipoxinA4 receptor (a.k.a. hFPR2/ALX)
AM	acetoxymethyl (ester)
ATP	adenosine triphosphate
BGH	bovine growth hormone poly-adenylation site
Bioimager	BD pathway855 bioimaging system
BML	bone marrow leukocytes
cAMP	cyclic adenosine monophosphate
CCD	charge coupled device
CD	cluster of differentiation
CMV	cytomegalovirus
CO1	formylated N-terminal peptide fragment of cytochrome oxidase subunit I
CsH	cyclosporine H
DAG	diacylglycerol
DAMP	damage-associated molecular pattern
DMEM	dulbecco's modified eagle medium
DMSO	dimethyl sulfoxide
DPBS	dulbecco's phosphate buffered saline
EC <sub>50</sub>	half maximal effective concentration
EDTA	ethylenediaminetetraacetic acid
eGFP	enhanced green fluorescent protein
EPR	electron paramagnetic resonance
ER	endoplasmic reticulum
F <sub>0</sub>	baseline fluorescence
FCS	fetal calf serum (bovine)
FLIPR	fluorescence imaging plate reader

FPR	formyl peptide receptor (protein)
<i>FPR</i>	<i>formyl peptide receptor (gene)</i>
GDP	guanosine diphosphate
GFP	green fluorescent protein
G <sub>i,o,z,gust,α</sub>	G protein alpha subunits
GPCR	G protein-coupled receptor
GTP	guanosine triphosphate
HEK293T	human embryonic kidney cells (line 293, expressing the large T-antigen)
HeLA	cervical cancer cell line (Henrietta Lachs)
hFPR	human formyl peptide receptor (protein)
HL-60	human leukemia cell line
HRP	horse radish peroxidase
immune FPRs	hFPR1, hFPR2, hFPR3, mFpr1, mFpr2
IP <sub>3</sub>	inositol trisphosphate
IP <sub>3</sub> R	inositol trisphosphate receptor
IP-PLC <sub>β2</sub>	4,5–inositol-bisphosphate activating phospholipase C beta 2
jetPEI	jet polyethylenimine
K <sub>d</sub>	dissociation constant
LXA4	lipoxin A4
mAlx4r	murine Lipoxin A4 receptor, functional orthologue of hFPR2/ALX
MBU	molecular biology unit
mFpr	mouse formyl peptide receptor (protein)
mFpr-rs	mouse formyl peptide receptor - related sequence (protein)
MHC	major histocompatibility complex
MMP	matrix metalloproteinase
mock	negative control, same as sham
MUPs	major urinary proteins
NADH	nicotinamide adenine dinucleotide (reduced)
nh	hill coefficient

NMR	nuclear magnetic resonance
NOX	NADPH oxidase
NRP	non-ribosomal proteins
ORF	open reading frame
p. t.	post transfection
PAMP	pathogen-associated molecular pattern
PBMC	peripheral blood mononuclear cells
PBP10	phosphoinositide binding peptide (amino acids 1-10)
PBS	phosphate buffered saline
PCR	polymerase chain reaction
PIP <sub>2</sub>	4,5-phosphatidylinositol-bisphosphate
PKC	phosphokinase C
PLC	phospholipase C
PMN/PMNL	polymorph nuclear leukocytes
PRR	pattern recognition receptor
PTX	pertussis toxin
RCF	relative centrifugal force
RFU	relative fluorescence units
Rho	rhodopsin
ROIs	regions of interest
rpm	revolutions per minute
rsFpr	related sequence formyl peptide receptor
RT	room temperature
SD	standard deviation
SNP	single nucleotide polymorphism
SOD	superoxide dismutase
SP	signal peptide
SPF	specific pathogen-free (free of specific pathogens common for this organisms as defined by the FELASA)
T <sub>A</sub>	annealing temperature

TM	transmembrane (domain)
T <sub>m</sub>	melting temperature
TO	tetracycline operator
UTR	untranslated region
V1R	vomeronasal receptor type 1
V2R	vomeronasal receptor type 2
VNO	vomeronasal organ
vomeronasal FPRs	mFpr-rs1, mFpr-rs3, mFpr-rs4, mFpr-rs6, and mFpr-rs7
VSN	vomeronasal sensory neuron

# Chapter 1

---

## Introduction

---

### 1.1. The Vomeronasal Organ

---

Communication with the environment is of uttermost importance for every living organism. The detection of food and water, and the cognition of danger are mainly facilitated by systems of chemosensory perception. One of the most important chemosensory systems in mammals is the olfactory system, which is organized into distinct subsystems. The vomeronasal organ (VNO) of rodents has received special attention as it emerged to be important in pheromone-dependent conspecific communication and detection of predator associated kairomones (Chamero *et al.*, 2012). Recognition of these molecular cues is mediated by specific receptors that are expressed in the corresponding sensory system. The rodent VNO, encased in a bony capsule located at the ventral base of the nasal septum, (Døving and Trotier, 1998) comprises a large receptor repertoire, organized in a complex molecular architecture (Figure 1-1). Cell bodies of vomeronasal sensory neurons (VSNs) organize into distinct layers of the sensory epithelium (Ryba and Tirindelli, 1997). The apical layer comprises cell bodies predominantly expressing the G protein-coupled vomeronasal type 1 receptors (V1Rs) together with the G protein  $G_{\alpha_{i2}}$  (Berghard and Buck, 1996; Jia and Halpern, 1996). V1R expressing cells are involved in the detection of small organic molecules which provide information on the physiological status and hormone level of other animals (Leinders-Zufall *et al.*, 2000; Nodari *et al.*, 2008). Vomeronasal type 2 GPCRs (V2Rs) on the contrary, are predominantly expressed by neurons residing in the basal layer, co-localizing with the expression of  $G_{\alpha_o}$  (Berghard and Buck, 1996; Jia and Halpern, 1996). V2R-expressing neurons are activated by peptide cues, including exocrine gland-secreting peptides (Kimoto *et al.*, 2005), major urinary proteins (Chamero *et al.*, 2007), fragments of mitochondrial peptides (Chamero *et al.*, 2011), and MHC class I peptides (Leinders-Zufall *et al.*, 2004). More and more intriguing novel

findings are emerging, nourishing the hypothesis that the VNO represents an interface between the immune and the nervous system (Chamero *et al.*, 2012). Subsets of VSNs express molecules usually involved in immune surveillance. These include  $\beta$ 2-microglobulins (Ishii *et al.*, 2003; Loconto *et al.*, 2003) and members of the non-classical class 1b family of the major histocompatibility complex (MHC) (Ishii *et al.*, 2003; Loconto *et al.*, 2003). VSNs positive for non-classical MHC receptors recognize with high sensitivity formylated peptides that are presented by MHC molecules in the immune system (Leinders-Zufall *et al.*, 2014). Recent publications show that sensory neurons of the vomeronasal organ have extended their receptor repertoire by five members of the formyl peptide receptor family (Ibarra-Soria *et al.*, 2014; Liberles *et al.*, 2009; Rivière *et al.*, 2009).

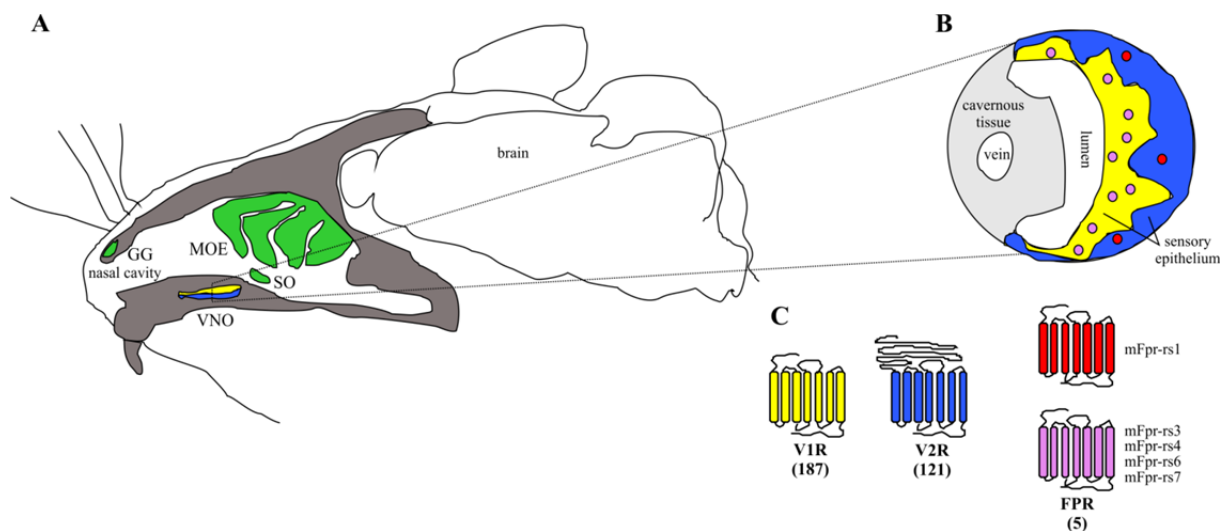


**Figure 1-1 | Schematic overview of the olfactory subsystems in mice with a coronal section of the VNO**

**[A]** Schematic overview of the anatomical organization of the distinct known olfactory subsystems in mice. Shown in green are the Main Olfactory Epithelium (MOE), the Septal Organ of Masera (SO) and the Grüneberg Ganglion (GG). The Vomeronasal Organ (VNO), embedded in the vomer bone, is shown in blue and yellow. **[B]** Coronal section of the VNO illustrating a simplified scheme its complex molecular architecture. The colors indicate the expression pattern of the receptors shown in C. **[C]** Three families of G protein-coupled receptors have been identified so far: vomeronasal receptors type 1 (V1R, yellow), vomeronasal receptors type 2 (V2R, blue) and formyl peptide receptors (FPR, red). The number of known receptor genes of a given family is indicated in parentheses.

Formyl peptide receptors (FPRs) which are constitutively expressed in cells of the innate immune system, contribute to host defence through recognition of pathogenic cues such as bacterial N-terminally formylated peptides or endogenous immunomodulatory molecules (Ye *et al.*, 2009). Four of its members (mFpr-rs3, mFpr-rs4, mFpr-rs6, and mFpr-rs7) are expressed in neurons of the VNO apical region while one receptor, mFpr-rs1, was found in VSNs residing in the basal layer (Figure 1-1). It has recently been confirmed that in mice the VNO mediates the avoidance of sick conspecifics (Boillat *et al.*, 2015). This avoidance is

presumably mediated through recognition of disease-related odours (Kavaliers *et al.*, 2005; Boillat *et al.*, 2015, Shirasu and Touhara, 2011). However, so far, there is no molecular mechanism known that mediates olfactory detection of pathogens. Intriguingly, it has been shown that bacterially-derived f-MLF, the prototypical FPR activator, can activate sensory neurons in the vomeronasal organ (Rivière *et al.*, 2009). Hence, formyl peptide receptors in the vomeronasal organ are excellent candidates for the olfactory detection of pathogen-derived molecules.

## 1.2. Expression of formyl peptide receptors

---

Formyl peptide receptors (FPRs) belong to the superfamily of seven transmembrane domain G protein-coupled receptors. First functional evidence for a formyl peptide receptor was described in 1975 when Schiffmann *et al.* (Schiffmann *et al.*, 1975) challenged human neutrophil granulocytes with N-terminally formylated peptides. These bacterially-derived peptides proved to be highly potent in attracting human granulocytes. Schiffmann's experiments suggested the presence of a surface receptor tuned for recognition of the eponymous formyl peptides. Fifteen years later this surface receptor turned out to be a germ line-encoded G protein-coupled receptor (Boulay *et al.*, 1990). Today the existence of three human formyl peptide receptors (hFPR1, hFPR2, and hFPR3) has been shown innumerable times. The prototypical hFPR1 and the homolog hFPR2<sup>1</sup> are both abundantly expressed in cells of the innate immune system, with neutrophil granulocytes being the most prominent ones found in peripheral blood (Durstin *et al.*, 1994). hFPR1 and hFPR2 have also been shown to be expressed in tissue-residing macrophages, microglia, dendritic cells, and their predecessors, monocytes (Lacy *et al.*, 1995; Durstin *et al.*, 1994; Migeotte *et al.*, 2005). Interestingly, hFPR3 was not found in human granulocytes and macrophages. Instead, it seems that its expression is restricted to monocytes and dendritic cells (Migeotte *et al.*, 2005). Besides cells of the myeloid lineage, FPR expression has been reported for many tissues and cell types (Migeotte *et al.*, 2006). Expression of FPRs is not restricted to humans. On the contrary: genes and active orthologs of FPRs are found not only in diverse mammalian species (Liberles *et al.*, 2009), but also in other phylogenetic classes like birds (Panaro *et al.*, 2007). In mice, like in other rodents, the FPR gene cluster has undergone species-specific expansion (Gao *et al.*, 1998; Wang and Ye, 2002). In addition to orthologs of hFPR1 and

---

<sup>1</sup> In this work hFPR2/ALX will simply be referred to as hFPR2. The name of the corresponding gene is *fprl1*. Many publications, especially the former ones, therefore use the name *FPRL1*.

hFPR2 (mFpr1 and mFpr2, respectively), mice express five related-sequence FPRs (mFpr-rs1, mFpr-rs3, mFpr-rs4, mFpr-rs6, and mFpr-rs7). In contrast to mFpr1 and mFpr2<sup>2</sup> (also called mFpr-rs2), which show tissue distribution resembling those of human FPRs, members of the FPR-rs subfamily (mFpr-rs1, mFpr-rs3, mFpr-rs4, mFpr-rs6 and mFpr-rs7) are predominantly found in sensory neurons of the vomeronasal organ. With exception of mFpr-rs1 all these receptor are localized in the apical zone of the vomeronasal sensory epithelium, where they are co-expressed with the G protein  $G_{\alpha i2}$  (Liberles *et al.*, 2009). mFpr-rs1, which has also been reported to be expressed in murine granulocytes (Takano *et al.*, 1997), is localized exclusively in the basal zone of the VNO, in cells expressing  $G_{\alpha o}$  (Liberles *et al.*, 2009).

### 1.3. Physiological functions mediated by FPRs

---

FPRs were originally identified as receptors for chemotactic peptides. The chemotactic capability of hFPR1 expressed in neutrophils was remarkable, as the calculated  $EC_{50}$  values were in the lower picomolar range (Schiffmann *et al.*, 1975). Nowadays, FPRs are thought to act as end-target chemotaxis receptors, meaning that in the signaling hierarchy they are above other chemotactic receptors, like for example chemokine receptors (Ye *et al.*, 2009). This means: when chemotaxis of human neutrophils is mediated via activation of FPRs, the cells do not migrate in the direction of chemokines. This underlines the biological significance of FPRs. It was later shown that FPR-induced activation of human neutrophils leads to a plethora of additional immunogenic responses like degranulation or superoxide production (Ye *et al.*, 2009). Activation of hFPR1 by the prototypical FPR agonist f-MLF quickly leads to secretion of several hydrolase-containing vesicles, a process called degranulation (Showell *et al.*, 1976). These vesicles are important for several reasons. First, they enable migration of the cells through extracellular matrices to approach their final target, the pathogen. Second, it is widely assumed that these hydrolases are involved in pathogen elimination (Kolaczowska and Kubes, 2013). Neutrophils and monocytes respond to FPR activation with the extracellular formation of reactive oxygen species, a process that is directly involved in pathogen killing (Klebanoff, 2005).

Mouse neutrophils exhibit immune responses very similar to their human counterparts when activated via FPR-dependent pathways. Experiments with *Fpr1* and *Fpr1/Fpr2* knockout mice have shown that in contrast to wildtype animals, the mice were highly susceptible to *Listeria*

---

<sup>2</sup> mFpr2 is also called mFpr-rs2. It is to note that mFpr1 and mFpr-rs1 are different receptors.

*monocytogenes* infection (Gao *et al.*, 1999; Liu *et al.*, 2012). FPRs have been put in context with many infectious and autoimmune diseases (Li and Ye, 2013). Uncontrolled activation of FPRs expressed in brain microglial cells may be a major determinant of neurogenic inflammation. However, in contrast to the immune FPRs, the function of the vomeronasal FPRs remains unknown. First clues indicating their potential function were obtained when Rivière *et al.* (2009) reported the activation of vomeronasal sensory neurons by classical formyl peptide receptor agonists.

#### 1.4. Ligands of the FPR family

---

The human FPR family has been described to be highly promiscuous with respect to ligand recognition. Their ligand repertoire encompasses bacterial (Schiffmann *et al.*, 1975) and viral peptides (Shen *et al.*, 2000; Moore *et al.*, 1995), host endogenous immune-modulatory peptides (Takenouchi and Munekata, 1995; Balbach *et al.*, 2000) and mitochondrial peptides (Rabiet *et al.*, 2005), neuro-protective and anti-microbial peptides (Ying *et al.*, 2004; Kurosaka *et al.*, 2005) and even anti-inflammatory fatty acid derivatives (Takano *et al.*, 1997). Human FPR1 is the most prominent receptor for bacterially-derived formyl peptides. It recognizes the eponymous N-terminally formylated peptides with high affinity (Schiffmann *et al.*, 1975). N-terminally formylated peptides are an evolutionary hallmark attributed to bacteria (Capecchi, 1966). Translation of bacterial proteins predominantly starts with a formylated methionine, underlining the immune defensive assignment of the FPRs. The prototypical formylated tripeptide f-MLF activates hFPR1 at concentrations in the upper picomolar range (Showell *et al.*, 1976). This was also shown for formylated mitochondrial peptides (Rabiet *et al.*, 2005; Carp, 1982). Release of mitochondrial peptides is usually a side effect of necrosis, which is why they define a damage-associated molecular pattern (DAMP) or danger signal (Pittman and Kubes, 2013). Although hFPR2 also recognizes formyl peptides, this generally occurs with significantly decreased affinity (Migeotte *et al.*, 2006). However, the complex pharmacological landscape of hFPR2 includes the recognition of many host-specific ligands. They include the human acute phase protein SAA (Su *et al.*, 1999a), the Alzheimer-related A $\beta$ <sub>1-42</sub> (Le, 2001), soluble uPAR (Resnati *et al.*, 2002), which is part of the plasminogen activating system and antimicrobial peptides like human LL37, a cleavage product of cathelicidin (De Yang *et al.*, 2000). In addition, hFPR2 binds several highly lipophilic organic compounds like Lipoxin A4 and some of its derivatives (Ye *et al.*, 2009) as

well as Resolvin D1 (Krishnamoorthy *et al.*, 2010) giving it the name of the lipoxin receptor or hFPR2/ALX (Ye *et al.*, 2009). hFPR3 (or FPRL2) the most-recently identified member of the human FPR family, is not well understood till now. Its small ligand repertoire includes the human neuro-protective humanin (Ying *et al.*, 2004) and parts of the heme-binding-protein F2L (Migeotte *et al.*, 2005). Although it can detect some formyl peptides, this happens at very high concentrations  $> 10 \mu\text{M}$  (Migeotte *et al.*, 2006).

Although the murine FPR family has not been as intensively studied as the human family, it is clear that they share common features with the human FPRs. mFpr1 and mFpr2, like their human orthologs, are able to recognize f-MLF and its formylated analogues. While mFpr1 seems to prefer formylated peptides as agonists, mFpr2 is also activated by many host-endogenous peptides, resembling the behavior of hFPR2. Two of the most potent naturally occurring agonists described so far are F2L and the antimicrobial peptide CRAMP, the murine ortholog of human LL37 (Kurosaka *et al.*, 2005). Interestingly, an allele of mFpr-rs1 (not mFpr2) was first described as the murine ortholog of the lipoxin receptor, named mLxa4r (Takano *et al.*, 1997). Unlike the murine immune FPRs, the recently discovered vomeronasal FPRs have not been investigated well. So far, only few agonists have been described for the vomeronasal FPRs. Rivière *et al.* (2009) reported the activation of heterologously expressed mFpr-rs3, mFpr-rs4, mFpr-rs6 and mFpr-rs7 by  $9 \mu\text{M}$  of the bacterial f-MLF in calcium imaging experiments. They also showed activation of these receptors, including mFpr-rs1, by  $5 \mu\text{M}$  antimicrobial CRAMP. Furthermore, they reported activation of mFpr-rs4 and mFpr-rs6 transfected cells with the immune-modulatory compounds Lipoxin A4 and uPAR, respectively (Rivière *et al.*, 2009). Intriguingly, application of these four classical FPR ligands was able to induce calcium signals in dendritic knobs of vomeronasal sensory neurons.

A number of inhibitors, selective for single members of the human FPR family, have been described during the last 40 years. Among the most prominent inhibitors for hFPR1 are N-*tert*-butoxy-MLF (tBoc1), N-*tert*-butoxy-FIFIF (tBoc2) and Cyclosporin H (CsH). In tBoc1 the formyl group of f-MLF is replaced by a urethane-linked *tert*-butyloxycarbonyl group. tBoc2 carries the same *tert*-butyloxycarbonyl moiety, probably competing for the same binding site on hFPR1 as f-MLF (Wenzel-Seifert, 1993). When used in higher micromolar concentrations, tBoc2 also partly antagonizes hFPR2 (Stenfeldt *et al.*, 2007; Wenzel-Seifert and Seifert 1993). The cyclic undecapeptide CsH (Wenzel-Seifert *et al.*, 1991) was determined to be highly selective for hFPR1 and is one of the most-potent hFPR1 antagonists so far (Ye *et al.* 2009; Wenzel-Seifert and Seifert, 1993). Besides tBoc2, which is a partial

inhibitor for hFPR2, there are two well-described blockers for this receptor. WRW4 is a hexapeptide that was identified as a selective antagonist of hFPR2 (Bae *et al.*, 2004). Another well-accepted inhibitor is the Gelsolin-derived peptide PBP10 (Forsman *et al.*, 2012). This cell-permeable RhodaminB-coupled decapeptide acts as an allosteric inhibitor on hFPR2 but not hFPR1. For hFPR3 no selective blockers are known at the moment.

In contrast to the human FPRs, inhibitors for mouse FPRs are only poorly investigated. tBoc2, mentioned above, is the only established antagonist for mFpr1 and mFpr2.

## 1.5. Structure and signaling of formyl peptide receptors

---

All above-mentioned FPRs are G protein-coupled receptors (GPCRs) that span the plasma membrane seven times. With their intracellular C-terminal tail immune FPRs interact with various heterotrimeric G proteins (Migeotte *et al.*, 2006). Although many alternative pathways are in discussion (Selvatici *et al.*, 2006), the most prominent one concludes direct interaction with G protein alpha subunit  $G_{\alpha i2}$  (Lad *et al.*, 1985, Wenzel-Seifert *et al.*, 1999). Upon agonist binding, the receptor activates the G protein alpha subunit, which catalyzes the exchange of GDP for GTP. This results in the dissociation of the alpha subunit and its corresponding beta and gamma subunits. The latter activate phospholipase  $C_{\beta 2}$  (Figure 1-2). The phospholipase catalyzes the cleavage of the membrane phospholipid phosphatidylinositol bisphosphate ( $PIP_2$ ) to inositol trisphosphate ( $IP_3$ ) and diacylglycerol (DAG). DAG then activates protein kinase C while  $IP_3$  activates the endoplasmic reticulum-membrane-bound  $IP_3$  receptor, leading to mobilization of endoplasmic calcium. Mouse immune FPRs have been described to employ similar pathways, including  $G_{\alpha i}$  and/or  $G_{\alpha q}$ -mediated signaling (Shi *et al.*, 2007). Because FPRs with related sequences (Fpr-rs) are expressed in sensory neurons that co-express either  $G_{\alpha i2}$  or the closely related  $G_{\alpha o}$ , it is possible that these receptors utilize the same signal transduction pathways.

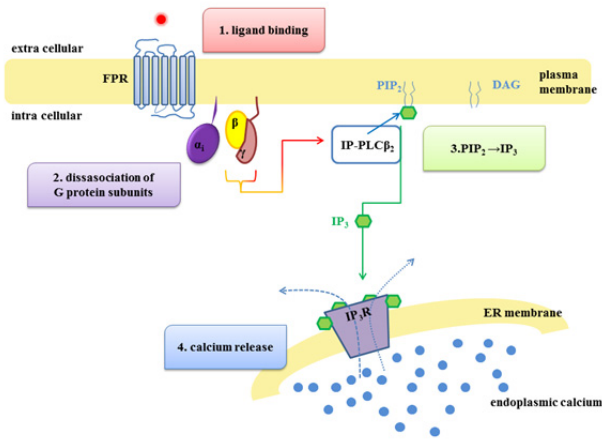


**Figure 1-2 | Schematics of FPR-mediated signal transduction**

Upon ligand binding, receptor conformational changes induce separation of heterotrimeric  $G_{i2}$  protein subunits ( $\alpha_2$ ,  $\beta$ ,  $\gamma$ ).  $\beta$  and  $\gamma$  subunits then activate phospholipase C $_{\beta 2}$  (PLC $_{\beta 2}$ ) which hydrolyzes phosphatidylinositol 4,5-bisphosphate ( $PIP_2$ ) to inositol 1,4,5-trisphosphate ( $IP_3$ ) and diacylglycerol (DAG).  $IP_3$  activates the  $IP_3$ -receptor ( $IP_3R$ ) which is a cooperative calcium channel situated in the membrane of the endoplasmic reticulum. Modified from Schumann, 2010.

## 1.6. Hypothesis and aims of this work

---

Formyl peptide receptors represent a key component in the attraction of phagocytes to sites of infection where they contribute to elimination of pathogens. During an evolutionary process, the FPR family of some rodents has extended into the olfactory system, thereby adding the FPR subfamily of FPR-rs to the receptor repertoire of the vomeronasal organ. In mice, five members of this subfamily are expressed in sensory neurons of the vomeronasal organ. However, although their function is not understood, it is assumed that they serve as detectors of pathogens or sick conspecifics. The current thesis is based on the idea that vomeronasal FPRs mediate the olfactory detection of pathogens.

To get first insights into the actual function of these receptors, profound knowledge of their pharmacology is a prerequisite. The aim is to understand, which classes of agonists can activate the vomeronasal FPRs and whether there are specific preferences of receptor for a given ligand. In order to see which agonists are able to activate vomeronasal FPRs, I tested an array of selected substances that are involved in inflammatory processes and screened them on heterologously expressed vomeronasal FPRs. To verify possible common ligands and common pharmacological properties, the resulting response profile was compared to that of FPRs expressed in the immune system. In order to investigate their pharmacology in a more physiological environment, newly identified ligands were tested on primary cells that naturally express the corresponding FPRs. For analyses of vomeronasal FPRs I employed single cell calcium imaging of isolated vomeronasal sensory neurons. For investigation of the immune FPRs I chose to observe innate immune cells of human and mouse. To get first insights into the biological significance of these newly identified ligands, I investigated their potential of inducing immune-defensive responses in human neutrophils and monocytes.

With this approach I am confident to contribute to a better understanding of the FPR family, including the immune FPRs and the vomeronasal FPRs, and their role in pathogen sensing.

## Chapter 2

---

### Materials & Methods

---

#### 2.1. Molecular cloning of the formyl peptide receptors

---

##### 2.1.1. Amplification of the FPR genes

The human receptor genes *hFPR1*, *hFPR2* and *hFPR3* were amplified from human genomic DNA, isolated from HEK293 cells. Mouse receptor genes *mFpr1*, *mFpr2* and *mFpr-rs3* were amplified from C57BL/6N genomic DNA during my diploma thesis (Schumann, 2010). *mFpr-rs1*, *mFpr-rs4*, *mFpr-rs6* and *mFpr-rs7* were amplified from cDNA of C57BL/6N mice. cDNA and genomic DNA were kindly provided by Dr. Bernd Bufe (Saarland University, Medical School Homburg, Department of Physiology). The necessary primers were chosen to amplify the complete open reading frame (consisting of one exon) between the exon's start codon (forward primer) and its stop codon (reverse primer). All forward primers contained an additional 5' sequence (5'-AAAGAATTCAAGCTTCCTGCAGGCGCCACC-3') upstream of the start codon (ATG), including a restriction site for *SbfI* (CCTGCAGG) and a consensus Kozak sequence (GCCACC) for enhanced ribosome binding. The reverse primers were fused with an additional sequence (5'-TTTCCTCAATTGGATATCGCGGCCGCAAGAGCTCA-3'), adding a stop codon (TCA) and a *NotI* restriction site (GCGGCCGC) for directed vector insertion to the 3' end of the amplified product. All primers were purchased from Sigma-Aldrich. PCRs were carried out using Phusion HF Master Mix (Thermo Scientific) according to manufacturer's protocol with the following agents:

- 10 µl 2x Phusion Master Mix
- 0.5 µl cDNA or 1 ng genomic DNA
- 0.5 µl forward primer (à 10 µM)
- 0.5 µl reverse primer (à 10 µM)
- ad 20 µl water (deionized)

All reagents were mixed on ice. PCR was run immediately on a My Cycler (Bio Rad) using the following program:

<b>Hot-Start</b>	at 98°C	
pre-denaturation:	98°C, 15 s	
denaturation:	98°C, 15 s	]—————   —————   —————   —————
annealing:	see Table 2.1, 15 s	
extension:	72°C, 35 s	
final extension:	72°, 1 min	
<b>hold</b>	at 4°C	34x

The amplified genes, their online reference numbers, and the used primer sequences are listed in Table 2-1.

**Table 2-1 | Cloned genes, PCR primers and accession numbers of nucleotide sequences\***

Receptor gene	Accession number	Specific sequences of primers <sup>#</sup> (forward) (reverse)	Annealing temperature [°C]
<i>mFpr1</i>	NM_013521.2	ATGGACACCAACATGTCTCTCCTCA TT TCCTCAATTG GATATC GCGGCCGC AA GAGC	59°C
<i>mFpr2</i>	NM_008039.2	ATGGAATCCAACACTCCATCCATCT TGGGGCCTTTAACTCAATGTCTG	64°C
<i>mFpr-rs1</i>	NM_008042.2	ATGGAATCCAACACTCCATCCATCT TATTGCCTTTATTCAATGTCTTCAGGAAG	64°C
<i>mFpr-rs3</i>	NM_008040.2	ATGGAAGCCAACCTCCTCCATC TAGTTCAGAGTCGGCAGGACATGA	64°C
<i>mFpr-rs4</i>	NM_008041.2	ATGGAAGTCAACATTTCAATGCCTCT GTCTTCCCTCAGGGCCCTCTC	64°C
<i>mFpr-rs6</i>	NM_177316.2	ATGGAAGCCAACCTTCTCCATACCTC GAGTCTTTGTGAAGACAAGTTTCTG	64°C
<i>mFpr-rs7</i>	AF437513.1	ATGGAAGCCAACCTTCTCCATACCTC GAGTCTTAAAGTTTGTGAAGACAAGTTTCTGATTT	64°C
<i>hFPR1</i>	NM_001193306.1	ATGGAGACAAATTCCTCTCTCCC CTTTGCCTGTAACCTCCACCTCTGC	65°C
<i>hFPR2</i>	NM_001462.3	ATGGAACCAACTTCTCCACTCCTCGCTTACCTCCT CATTGCCTGTAACCTCAGTCTCTGCA	65°C
<i>hFPR3</i>	NM_002030.3	ATGGAACCAACTTCTCCATTCTCCT CATTGCTTGTAACCTCCGTCCTCTC	65°C

\*Forward primers and reverse primers are listed in 5' to 3' direction. Shown are the specific primer sequences (= sequences complementary to target DNA). The reverse primers are given without the stop codon. <sup>#</sup>An extended nucleotide sequence was added to the 5'-end of all primers. All forward primers were fused to the sequence 5'-AAAGAATTCAAGCTTCCTGCAGGCGCCACC-3', which includes a restriction site for *Sbf*I (CCTGCAGG) and a Kozak-sequence (GCCACC). All reverse primers have been fused with the sequence 5'-TTTCCTCAATTGGATATCGCGGCCGCAAGAGCTCA-3' carrying diverse restriction sites, including that for *Not*I (GCGGCCGC) and the stop codon (TCA). Online accession numbers are valid for BLAST ([www.ncbi.nlm.nih.gov/blast/](http://www.ncbi.nlm.nih.gov/blast/)).

PCR products were purified subsequently.

### 2.1.2. DNA-purification via DNA Clean & Concentrator<sup>TM</sup> -5 -Kit

The PCR products were purified with the DNA Clean & Concentrator<sup>TM</sup> -5 kit (Zymo Research, D4003) according to manufacturer's protocol. In brief: PCR product was diluted 1:5 with the binding buffer. Mixture was transferred to a Zymo-Spin<sup>TM</sup> Column and then centrifuged at 14.000 rpm for 30 s. The columns were rinsed with the wash buffer and subsequently centrifuged. Elution of the DNA in deionized, sterilized, nuclease free water was done in a final centrifugation step. Following this, the purified PCR products were analyzed by separation with agarose gel electrophoresis.

### 2.1.3. Gel electrophoresis

To investigate the size and purity of the purified PCR products, they were separated on 1% [w/v] agarose gels (dissolved in TBE). The separation chamber was filled with 100 ml TBE that contained one drop of 1% [v/v] ethidium bromide (Roth, >98%). 10 µl of the DNA was mixed with 2 µl of 6x Fast Digest Loading Buffer (Fermentas) and then loaded on the agarose gel. Electrophoresis was performed in electrophoresis buffer containing 100 ml of 0.5% [v/v] TBE containing one drop of ethidium bromide. Electrophoresis was performed at 80 mV for 30 min, with a start current of 400 mA. Acquisition of the gels was performed with a Gel/ChemiDoc<sup>TM</sup> system (BioRad). Pure products of the correct size were used as inserts for cloning into target expression vectors.

### 2.1.4. Expression vectors

The amplified complete coding sequence of each gene was ligated into two distinct mammalian expression vectors (complete coding sequences are given in appendix 5). Both vectors are modified versions of commercially available plasmids, provided by Dr. Bernd Bufe (Saarland University, Medical School Homburg, department of Physiology). One plasmid is based on the pcDNA3.1(+) vector (Invitrogen) and was modified by inserting a *SbfI* restriction site between the *HindIII* and *NotI* restriction sites (Figure 2-1 A). It was used generally for functional studies<sup>3</sup>. All receptor genes cloned into pcDNA3.1 are referred to as unmodified or native receptors. The second plasmid is based on the pcDNA5/FRT/TO vector (Invitrogen) and was used for immunocytochemical detection (Figure 2-1 B).

<sup>3</sup> For functional analysis of mFpr-rs1 the pcDNA5/FRT/TO construct was used

pcDNA5/FRT/TO contains an additional *SbfI* restriction site between the restriction sites for *HindIII* and *NotI*. In addition, the plasmid contains a sequence that encodes a peptide comprising the first 39 amino acids of bovine rhodopsin, fusing this Rho-tag to the N-terminus of the receptor. This Rho-tag sequence serves as an N-terminal epitope for anti-Rho antibodies and therefore allows immunofluorescence analysis of receptor expression. The nucleotide sequence of the Rho encoding element is given in appendix 4. Both plasmids provide ampicillin resistance for selective growth in *E. coli*.

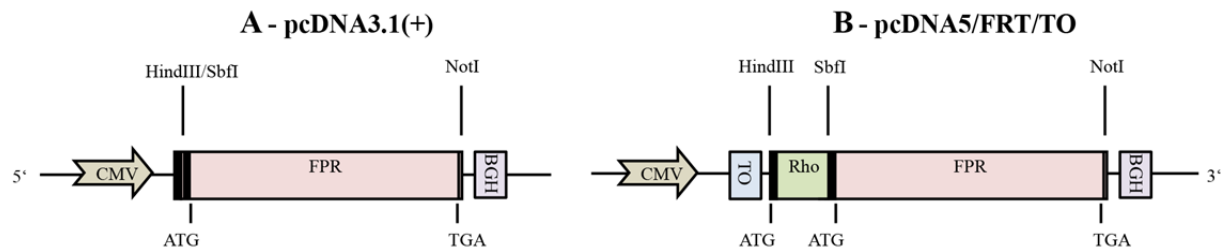


**Figure 2-1 | Schematics of expression vectors**

Shown is the insertion site for the PCR products. [A] Unmodified receptors cloned into pcDNA3.1(+) using *SbfI* and *NotI* restriction sites. [B] Receptors cloned into pcDNA5/FRT/TO carrying a 5' fusion sequence that codes the first 39 amino acids of bovine rhodopsin (Rho-tag). Start (ATG) and Stop (TGA) codons are indicated below gene cassettes. The first start codon of pcDNA5/FRT/TO belongs to the rhodopsin sequence. Restriction sites are indicated as black bars. Corresponding restriction enzymes are shown above the gene cassettes. Abbreviations: BGH = Bovine Growth Hormone poly-adenylation site, CMV = cytomegalovirus promoter sequence, Rho = rhodopsin-derived fusion sequence, TO = tetracycline operator (image and text adapted from Schumann, 2010).

All PCR products were cloned into the vectors by using *SbfI* and *NotI* as restriction enzymes.

### 2.1.5. DNA digestion

For a directed ligation into the plasmid, purified PCR products as well as target vectors were digested with two different octamer-cutting restriction endonucleases (*SbfI* and *NotI*). Digestion was performed according to the Fast Digest digestion enzyme protocol (Fermentas):

- 1  $\mu$ l 10x Fast Digest Buffer (Fermentas)
- 0.5  $\mu$ l *NotI* (= 10 Units)
- 0.5  $\mu$ l *SbfI* (= 10 Units)
- PCR product (150-200 ng) or vector plasmid (1  $\mu$ g), respectively
- The reaction was adjusted to a final volume of 10  $\mu$ l with deionized H<sub>2</sub>O
- To prevent re-circularization all plasmids were dephosphorylated adding 0.5  $\mu$ l (1 MBU) of thermosensitive alkaline phosphatase (Promega) to the reaction

After incubation at 37°C for 45 minutes, the reaction was ready for ligation.

### 2.1.6. DNA ligation

The sticky ends of the digested DNA (plasmid and PCR products, respectively) were ligated according to the fast-link-ligation protocol (Fermentas). The reaction contained the following components:

- 0.5 µl 10x ligation buffer (Fermentas)
- 0.5 µl ATP (Fermentas)
- 0.5 µl T4-DNA-ligase (Fermentas)
- Insert (= PCR products), 10-20 ng
- Target-plasmid, 5-10 ng
- Adjust volume to 5 µl with H<sub>2</sub>O (de-ionized)

The whole reaction was mixed on ice and then incubated at RT for 60 min. After this, the resulting receptor constructs were ready for transformation.

### 2.1.7. Transformation

Heat shock transformation was performed with chemically highly competent *E. coli* cells (NEB 10-β, >10<sup>9</sup>, New England Biolabs). Bacterial stocks were stored at -80°C and thawed on ice. 15 µl of the thawed stocks were incubated with 1 µl of the ligation reaction on ice for 10 min. Water bath heat shock was performed for 30 s at 42°C and the reaction was subsequently cooled on ice for 60 s. For regeneration, bacteria were suspended in 150 µl SOC-medium (RT) and then incubated for 1 h at 37°C, shaking. Bacteria were grown over night at 37°C on agar plates containing 50 µg/ml ampicillin.

### 2.1.8. DNA isolation

For each genetic construct, at least three ampicillin-resistant clones were picked for restriction analysis. In addition, all picked clones were plated on a replica plate for back-up. The clones that were picked for restriction analysis were suspended in 5 ml of 2YT-medium in 15 ml reaction tubes and kept shaking overnight at 37°C. Grown bacteria were harvested by centrifugation (3200 x g, RT, 10 min) and plasmids were purified using the Promega PureYield™ Plasmid Miniprep kit according to the manufacturer's protocol.

### 2.1.9. Restriction analysis

To identify bacterial clones carrying the desired insert, restriction analyses were conducted with the purified plasmids. Digestion was usually performed with *EcoRI* and *SacI* following the Fast Digest protocol (see 2.1.5.). Prediction of the restriction sites was performed with the Vector NTI® software (life technologies). Specific restriction patterns were analyzed via separation by agarose gel electrophoresis.

### 2.1.10. Gel electrophoresis for restriction analysis

Digested DNA was separated on 1% [w/v] agarose gels as described in 2.1.3. Clones exhibiting the correct restriction pattern were chosen for large-scale DNA purification in order to precipitate high amounts of the desired plasmid.

### 2.1.11. DNA purification and precipitation

Clones carrying the desired constructs were picked from the replica plate and suspended in 250 ml of 2YT-medium, supplemented with ampicillin (1 µg/ml) and incubated overnight at 37°C. Bacteria were then harvested and the plasmids were isolated according to the PureYield™ Plasmid Midiprep system (Promega). The purified DNA was precipitated (see below) and dispensed in deionized water to a concentration of 1 µg/µl.

Precipitation protocol:

- 10% (v/v) of 3 M sodium-acetate pH 5.2 were added to the purified plasmid DNA
- absolute ethanol (> 99,8% [v/v]) was added at 250% [v/v], with a final concentration of 70% enabling overnight precipitation at -20°C
- precipitated reaction was then centrifuged at 12,000 rpm at 4°C for 15 min and then washed with 1 ml 80% [v/v] ethanol
- after centrifugation (5 min, 12,000 rpm, 4°C) the precipitate was dried at RT and resuspended in deionized water.

### 2.1.12. DNA sequencing

The insert sequences of the resuspended plasmids were sequenced by MWG-Biotech AG using Sanger technology. The sequencing Probes were dispatched as premixes containing the forward or reverse primers, respectively, and the DNA templates. The primers were synthesized by Sigma-Aldrich. Forward primer: 5'-cgcaaattgggtaggcgtg-3', anneals to the CMV promoter sequence ( $T_m = 76.8^\circ\text{C}$ ). Reverse primer: 5'-tagaaggcacagtcgagg-3', anneals to the BGH poly adenylation site ( $T_m = 59^\circ\text{C}$ ). Plasmids carrying the desired genes were stored at  $-20^\circ\text{C}$  and used for transfection in HEK cells.

## 2.2. HEK cell culture

---

### 2.2.1. Cell line and cultivation

Authenticated, mycoplasma-free HEK293T PEAKrapid cells were obtained from ATCC® (CRL2828™). This immortalized cell line is retrieved from fetal human embryonic kidney cells that were transformed with adenovirus 5 DNA. The cells were grown in 75 cm<sup>2</sup> cell culture flasks in 20 ml cell culture medium (DMEM with [4.5 g/l] glucose (Invitrogen) + 5% [v/v] heat-inactivated bovine calf serum (Biochrom), 10,000 U/ml penicillin G (Sigma), 10 mg/ml streptomycin and 2 mM L-glutamine (Sigma) and kept until 80 - 90% confluence. Culture propagation was performed by rinsing cells in Dulbecco's Phosphate Buffer (Sigma-Aldrich) until the cells were detached from the flask bottom. For regeneration, cell culture medium was added to the phosphate buffer (9/1). After centrifugation (900 rpm, 3 min) cells were resuspended in 10 ml fresh culture medium. One ml of the suspension was used to inoculate a new flask. For experimental analysis, cells were seeded at 20 - 30% confluence on poly-*D*-lysine (Sigma) coated optic 96-well  $\mu$ -clear plates (greiner bio-one). The coating procedure was performed with 50  $\mu$ l of 10  $\mu$ g/ml poly-*D*-lysine (dissolved in PBS) per well and incubated for 30 min at RT. The cell line was generally propagated until 35 passages were reached. Then a new aliquot was thawed.

### 2.2.2. Transient transfection

Cells were seeded in 96-well plates as described above (chapter 2.2.1) and transfected after 48 h at a confluence of 50-70%. Transient transfection was accomplished with the poly-

cationic DNA transfection-reagent jetPEI<sup>TM</sup> (PeqLab), according to manufacturer's instruction: For one well, 0.25 µg of plasmid-DNA was diluted in 150 mM NaCl to a final volume of 10 µl, gently mixed and spun down. At the same time, 0.5 µl of jetPEI<sup>TM</sup> were diluted in 150 mM NaCl to a final volume of 10 µl, and mixed thoroughly. The 10 µl jetPEI<sup>TM</sup> solution and the 10 µl DNA solution were combined, mixed and spun down. The mixed solution was then incubated for 30 minutes at RT. Before transfection, the cell culture medium in each well (100 µl) was replaced once to remove dead cells and debris. For the actual transfection, 20 µl of the jetPEI<sup>TM</sup>/DNA mix were added to each well. The plates were carefully swirled and then incubated for 48 h (37°C, 5% [v/v] CO<sub>2</sub>). For calcium imaging experiments, cells were generally co-transfected with the G protein alpha subunit Gα<sub>16</sub> (if not stated otherwise, see chapter 2.6.1). Both plasmids were mixed in equal amounts while the total amount of transfected DNA was kept constant. Cells were imaged 48 h after transfection, with a cell density of approximately 50,000 cells / well.

### **2.2.3. Handling of frozen cell stocks**

HEK293T cell aliquots were kept in cell culture medium (chapter 2.2.1.) supplemented with 10% [v/v] DMSO and an additional 10% [v/v] FCS according to the instructions of the ATCC and then frozen to -80°C at a rate of 1°C/min using a Nalgene cryo container. Cells were then transferred to liquid nitrogen at -196°C and stored until use. For inoculation of new cell passages, stock cells were thawed at 37°C and then transferred to cell culture medium in a 10 cm diameter culture dish. The medium was replaced after 4 h to wash out remaining DMSO and cell debris.

## **2.3. Isolation and cultivation of primary cells**

---

### **2.3.1. Human blood collection**

All donors were apparently healthy adults of both genders that volunteered for the blood donation. Use of human blood for the investigation of monocytes and granulocytes has been approved by the local ethics committee.

### ***2.3.1.1. Blood collection for isolation of human monocytes***

Blood for monocyte purifications was kindly provided by the Institute of Clinical Haemostaseology and Transfusion Medicine, University of Saarland School of Medicine, under direction of Prof. Dr. Hermann Eichler. All donors donated whole blood for thrombocyte collection. Therefore, thrombocytes were filtered out of the blood. The thrombocyte-depleted blood was kept in leukocyte-reducing-system chambers at RT for 2 h before it was used for the monocyte isolation. All donations were anonymous to me.

### ***2.3.1.2. Blood collection for isolation of human granulocytes***

Whole blood was taken from adult volunteers in accordance with Ethics commission application HA249/11 (11-21-2011, Ärztekammer des Saarlandes). Blood was collected into blood collection tubes containing 16 international units (I.U.) heparin (S-Monovette Li-Heparin<sup>®</sup>, SARSTEDT) and was subsequently used for granulocyte isolation. All donors were familiar to me.

### ***2.3.1.3. Collection of autologous serum***

Autologous (= donor self) serum was collected by draining the donor's blood into serum collection tubes with silicate as clot activator (S-Monovette Serum-Gel<sup>®</sup>, SARSTEDT). For clotting, the tube was inverted several times and the blood was incubated for 30 min at RT. After centrifugation, (2500 x g, 10 min at 20°C) supernatant autologous serum was ready for use. For each experiment, only freshly prepared serum was used.

## **2.3.2. Isolation of human monocytes**

Peripheral blood leukocytes (PBLs) were purified from thrombocyte-filtered blood by Ficoll density gradient centrifugation using Leucosep<sup>™</sup> filter columns (greiner bio-one) according to the manufacturer's instructions: Blood was transferred to Leucosep<sup>™</sup> columns filled with Ficoll (LSM1077, PAA) and centrifugalized (1000 x g, 10 min, RT). Centrifugation of human blood in a separation medium like Ficoll results in four phases or bands (Figure 2-2). The uppermost phase contains serum or plasma, respectively. The second band is the cell-enriched interphase (or buffy coat) comprising peripheral blood mononuclear cells (PBMCs, = lymphocytes, macrophages and monocytes). The third phase contains the separation medium and the last phase encompasses granulocytes and erythrocytes. The cell-enriched fraction, which contained PBMCs was harvested and washed three times with HBSS (Sigma-Aldrich)

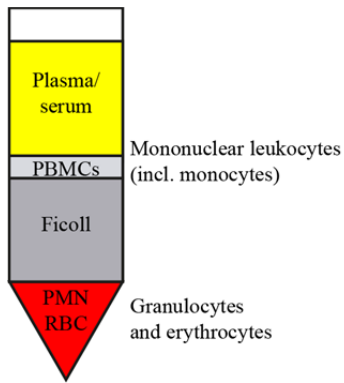


**Figure 2-2 | Schematics of blood separation by Ficoll density gradient centrifugation**

Shown is the dispersion of the blood into different phases after centrifugation. PBMC = Peripheral blood mononucleated cells. PMN = Polymorph nucleated cells. RBC = Red blood cells.

by centrifugation (250 x g, 10 min, RT). The resulting pellet was resuspended in 5 ml HBSS. Remaining erythrocytes and thrombocytes were abolished by lysis for 2 min (lysis buffer in mM: 155 NH<sub>4</sub>Cl, 10 KHCO<sub>3</sub> and 0.13 EDTA in H<sub>2</sub>O, pH 7.3). Lysis was stopped by washing with HBSS and leukocytes were resuspended in PBS supplemented with 0.5% BSA [w/v]. PBMCs were enriched in a cell incubator through adhesion in standard culture flasks containing monocyte cell culture medium (RPMI1640 + 10% FCS [v/v] + 1% [v/v] penicillin/streptomycin). During this procedure, monocytes will adhere to the flask bottom, while lymphocytes will remain in suspension and can hence be washed out. After two hours, the medium was exchanged and the supernatant (including non-adherent lymphocytes) discarded. After overnight incubation at 37°C and 5% [v/v] CO<sub>2</sub>, the cells were washed with PBS plus

0.5% [w/v] BSA, scratched from the flask surface and resuspended in fresh medium. For regeneration, cells were then seeded in 24-well Ultra-Low attachment plates (Corning, 3473) at a density of 1 - 4 x 10<sup>6</sup> cells/ml, and incubated overnight at 37°C and 5% [v/v] CO<sub>2</sub>. Cells were then ready for experiments.

### 2.3.3. Isolation of human granulocytes

#### 2.3.3.1. Isolation of human granulocytes by Ficoll/dextran separation

10 ml of heparinized whole blood were supplemented with 17 ml of cool Ca<sup>2+</sup>/Mg<sup>2+</sup> - free Dulbecco's Phosphate Buffered Saline (DPBS). Then, 13 ml of the separation medium (FicoLite-H, Linaris) was layered above the cell suspension and subsequently centrifuged (560 x g, 25 min, RT and with brakes turned off). The PBMC interphase and the Ficoll supernatant were withdrawn and discarded. The remaining phase, containing granulocytes and red blood cells was then transferred to a new 50 ml reaction tube and DPBS was added to a maximal volume of 25 ml. 3% Dextran solution (T500, Pharmacosmos A/S) was added 1/1 and mixed well. Cells were incubated for 15-30 min at RT. Dextran promotes erythrocyte rouleaux formation, resulting in differential sedimentation of the erythrocytes and leukocytes, the latter of which will remain in the supernatant. The supernatant, including the cells was

then transferred to a new tube and filled with DPBS to a volume of 50 ml and then centrifuged (339 x g, 6 min and 4°C). For hypotonic lysis of remaining erythrocytes, the resulting supernatant was removed and the cell pellet was gently suspended in 5 ml of sterile water (Aqua ad iniectabilia, Braun). To stop the lysis, 45 ml of DPBS were added after 30 seconds. The complete lysis was repeated once. The resulting granulocyte pellet was gently resuspended in autologous medium (RPMI 1640 + L-Glutamine + 1% [v/v] Na-Pyruvate + 1% [v/v] Pen-Strep and + 1% [v/v] autologous Serum) and kept on ice until use. Granulocytes were now ready for use in chemotaxis assays, ROS detection, calcium imaging, and immunocytochemistry.

#### ***2.3.3.2. Isolation of human granulocytes using CD16<sup>+</sup> pluriBeads***

Isolation of human granulocytes by the pluriBead kit (CD16 S-pluriBeads® anti-hu, 19-01600-10, pluriSelect) enables direct purification of granulocytes from whole blood without the use of separation media. This method relies on specific antibodies targeted against the surface marker CD16, which is expressed in high amounts on human granulocytes. The antibodies are chemically conjugated to polystyrene beads, which are 30 µm in diameter and cannot be phagocytized. Cells bound by these antibodies are retained by a 27 µm cell strainer (size exclusion) while non-bound cells will run through. Granulocytes were prepared from heparinized whole blood according to the manufacturer's protocol. After harvesting, the cells were suspended in the corresponding calcium imaging loading solution.

#### **2.3.4. Isolation of mouse leukocytes**

##### ***2.3.4.1. Isolation of murine neutrophils from peripheral blood with Ly6G pluriBeads***

Mice were euthanized by introduction of CO<sub>2</sub> and subsequently decapitated. Blood (~ 500 µl / mouse) was squeezed out of the body and collected into a polystyrene tube. The blood was directly supplemented with 4 mM EDTA to suppress coagulation. Isolation of murine granulocytes using the pluriBead kit (S-pluriBeads® anti-mouse-Ly6G, 21-Ly6G0-11, pluriSelect) was carried out according to the manufacturer's instructions. This method works equivalent to the CD16<sup>+</sup> pluriBeads kit described above, but relies on specific antibodies targeted against Ly6G, which is located in the plasma membrane of murine neutrophils. After harvesting, the cells were suspended in the corresponding calcium imaging loading solution (chapter 2.12.2.).

#### **2.3.4.2. Isolation of murine leukocytes from bone marrow**

Bones represent an excellent source for large numbers of white blood cells, as they are developed and stored within the bone marrow. Isolation of fresh mouse bone marrow leukocytes was performed according to Boxio (Boxio *et al.*, 2003). Adult mice (male and female) were euthanized by CO<sub>2</sub> introduction and subsequently decapitated. Abdomen and legs were rinsed with 70% [v/v] ethanol prior to organ collection. Tibia from both hind legs was freed of soft tissue and stored in cooled Ca<sup>2+</sup>/Mg<sup>2+</sup> - free HBSS buffer for 10 minutes. Epiphysis was cut off both sides and 3 ml buffer was forced through the diaphysis (bone shaft) with a syringe (needle: 20G) to flush out the bone marrow. The resulting solution was strained with a 100 µm cell strainer (BD) and then centrifuged (300 x g, brake on lowest level) for 8 min at 4°C. Supernatant was discarded, cells were counted with a MOXI™ Z cell counter and softly resuspended in HBSS (Ca/Mg) + 1/1000 Fluo-4 AM. 150,000 cells were seeded per well (100 µl) in uncoated µ-clear plates (greiner) and incubated for 45 min at RT. Wells were rinsed two times with HBSS prior to experiment. Calcium responses of bone marrow neutrophils to several ligands were compared to responses of neutrophils isolated via Ly6G beads from peripheral blood. I could not detect a significant functional difference and decided to use the direct isolation from bone marrow as it yielded ~ 10 times more healthy cells.

#### **2.3.5. Dissociation of mouse vomeronasal sensory neurons**

Adult OMP/GFP mice (Potter *et al.*, 2001) were anesthetized and killed by introduction of CO<sub>2</sub> and subsequent decapitation. The VNO sensory epithelium was isolated as described before (Chamero *et al.*, 2011). In brief: the vomeronasal sensory epithelia of adult mice (usually three per experiment) were detached from the cartilage of the vomer bone and transferred to PBS at 4°C. With a scalpel, the epithelia were minced in freshly prepared dissociation solution, which contained 2.2 units/ml Papain (Worthington), 1.1 mM EDTA (Fermentas), 5.5 mM cysteine-HCl (Sigma), and 50 units DNaseI (Fermentas) in PBS. The minced tissue was slightly triturated with a 1 ml pipette tip prior to incubation in the incubator (37°C, 24% [v/v] O<sub>2</sub>, 5% [v/v] CO<sub>2</sub>) for 18 minutes. Afterwards cells were triturated using a 200 µl pipette tip and incubated for 2 min at RT. The reaction was stopped by adding stopping solution containing high-glucose DMEM (Invitrogen), 10% [v/v] FBS (Biochrom), and 1% [v/v] P/S (Sigma). Cells were then collected by centrifugation (0.2 rcf, 5 min, pre-cooled to 8°C). After suspension in loading solution the cells were ready for calcium imaging.

## 2.4. Mice

### 2.4.1. Mouse strains

#### 2.4.1.1. Wild type mice

Adult C57Bl/6NCrI were purchased from Charles River and classified as specific pathogen-free (SPF). These animals served as wild type controls for the knockout experiments and are denoted as +/+ mice.

#### 2.4.1.2. *Fpr1*-deficient mice

Mice with a global deficiency in *Fpr1* (C57BL/6NTac-*Fpr1*<sup>tm1Gao</sup>N6, denoted as -/- mice) were obtained from Taconic and reported as SPF. The *Fpr1* ablation was created by targeted disruption of the *Fpr1* open reading frame by a neomycin resistance cassette (Gao *et al.*, 1999) (Figure 2-3).

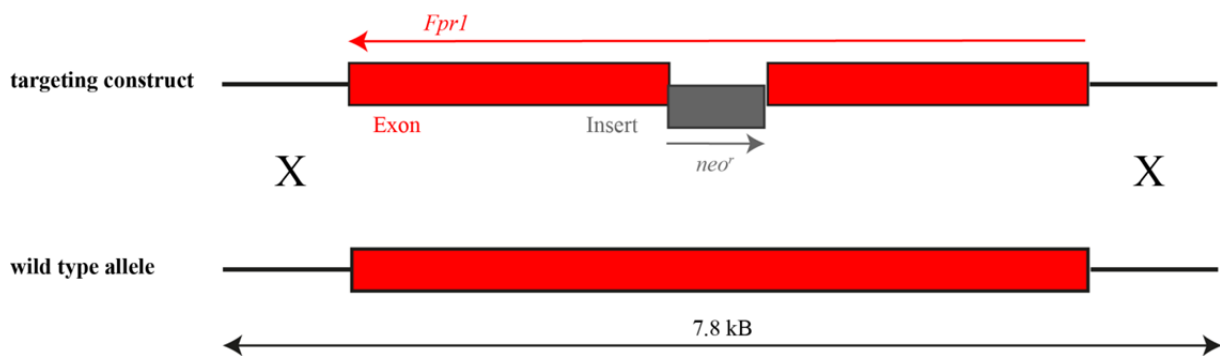


**Figure 2-3 | Schematics showing the construct used for targeted disruption of *Fpr1* in mice** Shown are schematics of the targeting construct and the wild type locus of *Fpr1*. In the targeting construct a neomycin resistance gene (*neo'*), shown in gray, is replaced 150 bp of the FPR open reading frame (red). The single headed arrows indicate open reading frames. The construct was targeted to a 7.8 kilo bases-encompassing allele in the wild type mouse. *Modified from Gao et al., 1999.*

#### 2.4.1.3. Mice heterozygous for *Fpr1*

Heterozygous control animals (+/-) were bred by pairing C57BL/6NTac-*Fpr1*<sup>tm1Gao</sup>N6 with C57Bl/6NCrI mice.

#### 2.4.1.4. Heterozygous *dOMP-GFP* mice

In *dOMP-GFP* mice, B6;129P2-OMP<sup>tm3Mom</sup>-MomJ, the coding region of the *OMP* (= olfactory marker protein) gene and part of the 3' untranslated region was replaced by *GFP* (Potter *et al.*, 2001). This process results in GFP expression in olfactory sensory neurons (Potter *et al.*, 2001). Mice are available from the Jackson Laboratory (Stock number: 006667). To create heterozygous mice, *dOMP-GFP* mice were paired with C57Bl/6NCrI mice.

## 2.4.2. Mouse keeping and breeding

Breeding pairs were kept in SPF areas. Offspring was kept in SPF areas until weaning (~ 3-4 weeks). A 12-hour light-dark cycle was set, starting at 7.15 MET. Sterile water and food (Teklad 18% Protein Rodent Diet, Harlan) were fed *ad libitum* by the personnel of the animal facility. Mice used for experiments were between 5 and 12 weeks old. The German Animal Protection Act has been complied during husbandry and experiments.

## 2.5. Immunocytochemistry

### 2.5.1. Antibodies

#### 2.5.1.1. Primary antibodies

All primary antibodies used in this study are summarized in Table 2-2.

**Table 2-2 | Primary antibodies used in this study\***

Antibody	Target	Clonality	Isotype	Provider	Order number	Used concentration
hFPR1	human FPR1	monoclonal	mouse IgG <sub>2A</sub>	R&D Systems	MAB3744	1 µg/ml
hFPR2	human FPR2	monoclonal	mouse IgG <sub>1,κ</sub>	SANTA CRUZ BIOTECHNOLOGY, INC.	sc-57141	0.2 µg/ml
hFPR3	human FPR3	monoclonal	mouse IgG <sub>2B</sub>	R&D Systems	MAB3896	1 µg/ml
Rho	4D2 of bovine rhodopsin	polyclonal	not determined	Centre for Macular Research, University of British Columbia, Canada	Dr. R. Molday,	1/500
CD14	human CD14	monoclonal	mouse IgG <sub>1,κ</sub>	Biolegend	325601	0.5 µg/ml
CD66	human CD66abce	monoclonal	mouse IgG <sub>2B</sub>	Miltenyi Biotech	130-093-155 (APC)	33 ng/ml
Ly-6G	mouse Ly6G	monoclonal	Rat IgG <sub>2a, κ</sub>	Biolegend	127601	5 µg/ml
KLH	Keyhole Limpet Hemocyanin	monoclonal	mouse IgG <sub>2A</sub>	R&D Systems	MAB0031	1 µg/ml
MOPC-21	unknown	monoclonal	mouse IgG <sub>1,κ</sub>	Biolegend	400101	0.2 µg/ml (hFPR2) 0.5 µg/ml (CD14)

\*The table lists all primary antibodies used in this study. Shown are their specific targets, clonality, isotype of their constant region, provider, order number and the final concentrations at which they were used. The hFPR2 antibody of Santa Cruz is the same as GM-0601 of aldevron, which has been used in many studies.

All shown antibodies are directed against extracellular epitopes. Besides the CD66 antibody, which was conjugated with allophycocyanin, all other antibodies were unconjugated for

staining with a secondary antibody. Antibodies were stored and handled according to the provider's instructions.

#### **2.5.1.2. Secondary antibodies**

The secondary antibodies used in this study were polyclonal goat anti-mouse antibodies, conjugated with either Alexa Fluor 488 or Alexa Fluor 555 (Invitrogen). They were used in final concentrations of 2 µg/ml. Alexa 488 was used in conjunction with the Rho-antibody while the Alexa 555 antibody was used for stainings with the remaining primary antibodies. Antibodies were stored and handled according to the provider's instructions.

#### **2.5.2. Immunostaining**

HEK293T cells were fixated for 4 min at RT in 4% [v/v] methanol-free paraformaldehyde (Polyscience Inc.). Human monocytes and granulocytes as well as mouse leukocytes were fixated with 3% [v/v] methanol-free paraformaldehyde. All wells were washed three times by complete exchange of solutions by PBS. This procedure was used to fixate the cells without permeabilization of the plasma membrane, enabling analysis of cell surface expression. To permeabilize the cells (for visualization of total cellular expression), 0.3% [v/v] Triton-X was added for 30 min at RT after the fixation step. After blocking with 5% [v/v] FCS in PBS for 30 min, the cells were incubated overnight at 4°C with the corresponding antibody in blocking solution. After washing three times, cells were incubated with the secondary antibody (dissolved in blocking solution) for 45 min at RT. The total number of nucleated cells was obtained by a counterstaining of the cell nuclei with 1 µg/ml Hoechst 33342 (Hoechst) diluted with the secondary antibody. All wells were washed three times and subsequently analyzed. In general, only non-stimulated cells were used for immunocytochemical analysis.

White blood cells naturally express receptors for binding of the constant regions of antibodies (Fc receptors), which can result in strong background signals during immunostainings. Therefore, so-called isotype controls are commonly used as background controls for immunofluorescence. These controls are of the same isotype as the desired antibody but targeted against antigens that are not present in the target cells. Isotype controls used were KLH for hFPR1 and MOPC-21 for hFPR2 and CD14.

### 2.5.3. Analysis and evaluation of immunofluorescence

Pictures were taken with the imaging system BD Pathway Bioimager 855 (BD Bioscience) and quantified with the delivered software BD-image Explorer. Layer thickness (z-axis) of confocal images was 2.7  $\mu\text{m}$ .

## 2.6. Calcium Imaging

---

### 2.6.1. G protein coupling of HEK293T cells

Formyl peptide receptors are described as  $G_{\alpha i2}$ -coupled GPCRs that employ signal transduction pathways utilizing phospholipase beta 2 ( $\text{PLC}_{\beta 2}$ ) to increase intracellular calcium levels (see chapter 1.5). However, the used cell line does not express all components of the signal transduction cascade required for intracellular calcium mobilization. To enable FPR-dependent mobilization of internally stored calcium, a plasmid encoding the G alpha subunit  $G_{\alpha 16}$  was co-transfected for calcium imaging experiments.  $G_{16}$  is a human G protein of the  $G_q$  type, naturally expressed in cells of the myeloid lineage (Tenailleau *et al.*, 1997), which is known to couple a variety of GPCRs to the  $\text{PLC}_{\beta 1}/\text{IP}_3$  signaling pathway (Offermanns and Simon, 1995). Once activated, the catalytic domain of  $G_{\alpha 16}$  activates the  $\text{PLC}_{\beta 1}/\text{IP}_3$  signaling cascade, resulting in an increase of intracellular calcium. It was tested, whether FPRs interact with distinct G proteins. To couple the GPCR interacting C-terminus of distinct G protein alpha subunits to the  $G_{\alpha 16}$ -induced  $\text{PLC}_{\beta 1}/\text{IP}_3$  signaling pathway, G protein chimeras were used. These chimeras were created by substituting the last 44 to 47 C-terminal amino acids of human  $G_{\alpha 16}$  or mouse  $G_{\alpha 15}$  by amino acids of other G protein alpha subunits (Table 2-3).

**Table 2-3 | Plasmids used for co-transfection encoding distinct G protein chimeras\***

Name of co-transfected plasmid as listed in the lab	Encoded protein or chimera	C-terminal sequence derived from G protein type
<b>PHB102</b>	G <sub>16</sub> -G <sub>i2</sub> -44	human G <sub>i2</sub> , G <sub>i</sub> type
<b>PHB21</b>	G <sub>16</sub> -G <sub>z</sub> -44	human G <sub>z</sub> , G <sub>z</sub> type
<b>PHB185</b>	G <sub>16</sub> -G <sub>o1A</sub> -44	human G <sub>o1A</sub> , G <sub>o</sub> type
<b>PHB9</b>	G <sub>16</sub> -G <sub>gust</sub> -44	human gustducin, G <sub>i</sub> type
<b>PHB4</b>	G <sub>16</sub> (unmodified)	human G <sub>16</sub> , G <sub>q</sub> type
<b>PHB3</b>	G <sub>15</sub> (unmodified)	murine G <sub>15</sub> , G <sub>q</sub> type
<b>PHB226</b>	G <sub>15</sub> -G <sub>olf</sub> -47	human G <sub>olf</sub> , G <sub>s</sub> type

\*All vectors coding for chimeras and G proteins were provided by Dr. Bernd Bufe Bufe (Saarland University, Medical School Homburg, Department of Physiology). For creating the chimeras, the alpha subunit of human G<sub>16</sub> was modified by replacing the last 44 amino acids with that of the indicated G proteins. The G<sub>15</sub>-G<sub>olf</sub>-47 chimera was created by replacing the last 47 amino acids of G<sub>15</sub> with that of G<sub>olf</sub> (table and text adapted from Schumann, 2010).

## 2.6.2. Ratiometric single cell calcium imaging

### 2.6.2.1. The BD Pathway 855

Automated high-throughput Ca<sup>2+</sup> imaging with single-cell resolution was performed with the BD Pathway 855 (BD Bioscience) bioimaging system. This fully automated confocal microscope allows high content kinetic live-cell imaging with an optional confocal setup. An automated liquid handling unit enables programmed application of liquids (e.g. ligands) in 96-well plates with simultaneous live-cell imaging of individual cells. Coordinates of the imaged cells are saved and can be monitored after the experiment, enabling *post-hoc* analysis (e.g. with immunocytochemistry). Light is generated by 103 W mercury short arc lamps, which provide a broad excitation spectrum of 330 to 900 nm. A variety of excitation/emission spectra are made possible by a set of dichroic mirrors, excitation- and emission filters. Signals are detected by a Hamamatsu ORCA ER CCD camera.

### 2.6.2.2. Ratiometric dye Fura-2 AM

For ratiometric calcium imaging cells were loaded with the calcium sensitive dye Fura-2 AM (Molecular Probes). The acetoxymethyl ester of Fura-2 (Fura-2 AM) can pass the plasma membranes of cells. The ester moiety is then cleaved by intracellular esterases, yielding free Fura-2. This has its excitation maximum at 365 nm in calcium-free state. However, when bound to calcium, the excitation maximum of Fura-2 shifts to 340 nm and the emitted fluorescence increases with rising calcium concentrations. At the same time, the fluorescence

decreases when excited at 380 nm (Grynkiewicz *et al.*, 1985). Calculation of the 340/380 nm ratio enables measuring of intracellular calcium concentrations independent from the intracellular dye concentration. Fura-2 was excited at 340 nm and 380 nm, respectively. Emission was measured at 435 nm due to preset filter sets. Hence, the calcium-induced Fura-2 fluorescence intensity is given as the ratio of 340/380 nm.

#### ***2.6.2.3. Loading procedure for conventional single cell imaging***

Fura-2 AM was dissolved 2 mM in DMSO. Cells in 96-well plates were loaded by exchange of culture medium with the corresponding loading solution (see chapter 2.13.) plus 2  $\mu$ M Fura-2 AM. HEK cells, monocytes and granulocytes were then incubated at RT for three and one hour respectively. The HEK cells were loaded 48 h after transfection; granulocytes 30 minutes and monocytes 48 h post isolation. Dissociated vomeronasal sensory neurons were suspended in loading solution (chapter 2.3.5 and 2.12.2), plated on Concanavalin A Type V – coated (1 mg/ml, Sigma) 384-well plates (greiner, 655090) and incubated for 45 minutes on ice. All plates were then rinsed three times using the ELx50 ELISA cell-washer (BioTek).

Loading solutions (buffer formulation is given in Table 2-5)

- HEK293T cells: C1 + 2  $\mu$ M Fura-2 AM
- Human monocytes: Ringer + 2  $\mu$ M Fura-2 AM
- Human granulocytes: Ringer + 2  $\mu$ M Fura-2 AM
- Mouse leukocytes: HBSS (Ca/Mg) + 2  $\mu$ M Fura-2 AM
- Mouse vomeronasal sensory neurons: C1 + 3  $\mu$ M Fura-2 AM + 1/20 BD Signal enhancer (BD Biosciences, 644243)

#### ***2.6.2.4. Loading procedure for single cell imaging under perfusion conditions***

48 h post-transfection, cells were resuspended in imaging solution (chapter 2.12.2) + 2.2  $\mu$ M Fura-2 AM (Invitrogen) by vigorous pipetting. Cells were then seeded into Poly-D-Lysine-coated (10  $\mu$ g/ml in PBS, Sigma)  $\mu$ -slides (ibiTreat 6-channel  $\mu$ -slides VI0.4, ibidi) to a confluency of 80-90% according to manufacturer's protocol and incubated for 2 h at ambient temperature to load and adhere to the slide. Prior to imaging, each channel was rinsed with three volumes of C1 buffer solution to remove dye precipitates and other debris. Stimulation was done by application of 1.5 volumes of the diluted ligands and incubation for 30 seconds. Cells were rinsed for three minutes with a total of 256 volumes of bath solution after each stimulation. Calcium-dependent fluorescence signals of eGFP-positive cells were recorded at

0.5 Hz. Images were taken with the Bioimager 855 system and quantified using Attovision software (BD Bioscience).

#### **2.6.2.5. Recording and evaluation**

Fluorescence images were recorded at 0.5 Hz and analyzed with the attovision software. Ratiometric fluorescence maxima recorded from HEK293T cells were quantified by using the BD-image Explorer software (BD Bioscience) and plotted with Excel2007.

### **2.6.3. High-throughput calcium imaging of cell populations with the FLIPR**

#### **2.6.3.1. The FLIPR system (Fluorescence Imaging Plate Reader)**

The FLIPR system (Molecular Probes) is predominantly used in industry for pharmacological screenings. The system can detect fluorescence signals in all 96 wells of a given micro plate simultaneously. It is equipped with an automated pipetting robot that applies fluids to all 96 wells at the same time. Excitation light is provided by an argon laser, exciting probes with 488 nm. The fluorescence detection technology of the FLIPR is based on a cooled charge-coupled device set-up (CCD camera). The detection optics is optimized to detect signals of a cell monolayer at the bottom of each well.

#### **2.6.3.2. The calcium sensitive dye Fluo-4 AM**

Similar to the Fura-2 AM described in chapter 2.6.2.2, Fluo-4 AM is an acetoxymethyl-esterified product of Fluo-4 (Molecular Probes) which passes the plasma membrane and is then hydrolyzed intracellularly. Increase of intracellular  $\text{Ca}^{2+}$  levels leads to enhanced formation of calcium complexes with the dye, resulting in an increased fluorescence signal. Fluo-4, in contrast to Fura-2, is not ratiometric. Thus, the observed signals are not only dependent on calcium, but also on the intracellular dye concentration. It is to note that in several cell types anionic forms of the dye are actively extruded into the extracellular medium by ABC transporters (Di Virgilio *et al.*, 1990). For experiments with HEK293T cells, the anionic-exchange-protein inhibitor probenecid (Sigma-Aldrich) was used to block the anion transport systems.

#### **2.6.3.3. Loading procedure**

Fluo-4 AM was dissolved 2 mM in DMSO. Cells in 96-well plates were loaded by exchange of culture medium with 50  $\mu\text{l}$  of the corresponding loading solution (Table 2-5). Cells were

then incubated at RT in the dark for 4 h (HEK293T cells), 2 h (human monocytes), 1 h (human granulocytes) or 45 min (mouse leukocytes) respectively. HEK293T cells were loaded 48 h after transfection and monocytes 48 h post isolation. Granulocytes and mouse leukocytes were loaded directly after isolation. The 96-well plates were then rinsed 3 times using the ELx50 ELISA cell-washer (BioTek) and measured subsequently. For hFPR2 blocking experiments in granulocytes, 5  $\mu$ M PBP10 was added to the loading solution.

Loading solutions (buffer formulation is given in Table 2-5)

- HEK293T cells: C1 + 2  $\mu$ M Fluo-4 AM, + 50  $\mu$ M probenecid
- Human monocytes: Ringer + 2  $\mu$ M Fluo-4 AM
- Human granulocytes: Ringer + 2  $\mu$ M Fluo-4 AM
- Mouse leukocytes: HBSS (Ca/Mg) + 2  $\mu$ M Fluo-4 AM

For calcium imaging with human granulocytes, two loading procedures were compared. One loading solution was in the above listed Ringer. The other one was in culture medium. Both worked similarly well.

#### ***2.6.3.4. Recording and evaluation***

Fluorescence was measured in relative fluorescence units (RFU) and signal analysis was performed with the FLIPR software. The fluorescence baseline was recorded before ligand application (ten images, in intervals of two seconds). The recorded baseline signal inherits information about the loading condition of the cells since it is measured in absence of physical and chemical stimuli. This baseline signal ( $F_0$ ) was used for normalization of the recorded fluorescence amplitudes after stimulation ( $dF$ ). Signal amplitudes ( $dF$ ) were determined as the maximal signal minus the minimal signal after application of the ligand. Normalization of calcium responses was calculated by dividing the maximal change in fluorescence after stimulation by baseline fluorescence ( $dF/F_0$ ). Evaluation was performed with Excel2010 (Microsoft). Dose-response curves were calculated using GraphPad Prism 5.0 (see below). Experiments were routinely performed in duplicates. Experiments on HEK293T cells, human monocytes and granulocytes were generally performed as duplicates. Experiments on mouse leukocytes were generally done in triplicates.

## 2.7. Detection of reactive oxygen species (ROS)

---

### 2.7.1. Radical detection with Amplex®UltraRed

#### 2.7.1.1. *The Amplex®UltraRed dye*

Monocyte/granulocyte-dependent radical production was measured using the hydrogen peroxide (H<sub>2</sub>O<sub>2</sub>) reactive Amplex®UltraRed (Molecular Probes). Amplex®UltraRed is not cell permeable and thus, enables exclusive measurement of extracellular reactive oxygen species (ROS). This assay does not discriminate between the distinct ROS as the substrate does only react with H<sub>2</sub>O<sub>2</sub>. Upon stimulation, phagocytes respond primarily by producing superoxide radicals, which in turn can also react to form H<sub>2</sub>O<sub>2</sub>. Therefore, this assay was used for detection of ROS in general. Amplex®UltraRed is a fluorogenic substrate for horseradish peroxidase (HRP) which catalyzes the H<sub>2</sub>O<sub>2</sub>-dependent reduction of the reagent to the fluorescent dye Resorufin (global excitation/emission maxima: 568 nm / 581 nm). To accelerate the formation of hydrogen peroxide, superoxide dismutase (SOD) that catalyzes the dismutation of superoxide into oxygen and hydrogen peroxide was added.

#### 2.7.1.2. *Loading procedure of monocytes and granulocytes for ROS detection*

Amplex®UltraRed was dissolved in DMSO to a concentration of 5 mM. After isolation, the cells were transferred into Ringer solution containing 50 µM Amplex®UltraRed, 0.1 Units/ml HRP (Sigma-Aldrich) and 10 Units/ml SOD (Sigma). The cells were then carefully seeded in black 96-well µ-clear plates (greiner bio-one) to the following densities: monocytes ~ 30,000; granulocytes ~ 100,000 per well in 180 µl). The subsequent application of stimuli was done manually directly before measurement.

#### 2.7.1.3. *Recording and evaluation of ROS detection experiments*

The plates were placed in a pre-heated (37°C) fluorescence plate reader (Tecan GENios Pro) and rocked for 30 s. The fluorescence dye was excited at 535 nm excitation and emission was recorded at 590 nm with bottom reading settings. H<sub>2</sub>O<sub>2</sub> concentrations were calculated from relative fluorescence units (RFU) 10 min after application by employing H<sub>2</sub>O<sub>2</sub> calibration curves. Experiments were routinely performed as duplicates.

## 2.8. Chemotaxis

---

### 2.8.1. Chemotaxis assay principle

For chemotaxis experiments HTS Transwell® chambers (pore size: 3 µm; Corning) were used. This assay uses an upper Transwell® insert that is placed on a clear 96-well cell-culture plate (lower compartment). The cells are seeded into chambers of the Transwells while the stimuli are present in the lower compartment. The bottom of the Transwells® is made up by a polycarbonate membrane with pores of 3 µm in diameter (pore density:  $2 \times 10^6$  pores per cm<sup>2</sup>). Human neutrophils, which are between 12 to 15 µm in diameter, can only pass the membrane by morphological changes during active processes like diapedesis. Therefore, only adequately activated cells will migrate through the membrane. Since the stimuli are dissolved in the lower compartments and not in the Transwell® inserts, a concentration gradient is established by diffusive exchange of the media components through the pores. After 2 hours, the cells that adhered to the bottom of the lower compartment were counted in the BD pathway 855. To facilitate automatic focusing, the cells were stained with the live cell plasma membrane stain CellMask™ Deep Red.

### 2.8.2. Granulocyte stimulation for chemotaxis

Migration assays were performed according to the manufacturer's protocol. Briefly: chambers of the lower compartment were filled with 235 µl of medium supplemented with the desired stimulus or control, respectively. The Transwell insert was then placed on the plate. For each chamber, 100,000 granulocytes were suspended in 75 µl medium (supplemented with 1/10,000 CellMask™ Deep Red) and then seeded into a chamber of the Transwell insert. The cells were incubated for 2 h in a cell culture incubator (37°C, 5% [v/v] CO<sub>2</sub>) and then counted with the BD pathway855 at RT. For the counting, the Transwell insert was discarded.

### 2.8.3. Evaluation

The number of transmigrated cells was determined by automated counting with the BD Pathway 855 system. Measurements were always done in duplicates.

## 2.9. Image processing software

---

### 2.9.1. Drawing of the ligand structures

Natta projections of chemical structures of amino acids and modifications were drawn with Accelrys Draw, 4.1 (accelrys).

### 2.9.2. Figures and images

Fluorescence images were processed with Adobe Photoshop Elements 10 (Adobe systems Incorporated). All figures were composed and processed in Adobe Illustrator CS6 (32-bit) on a computer using Microsoft Windows 7. The schematic organization of the olfactory system was composed and processed with Corel DRAW<sup>®</sup>X5 version 15.0.0.486 (Corel Corporation).

## 2.10. Statistics and mathematics

---

### 2.10.1. Significance tests

Statistical significance was generally calculated with Excel2010 (Microsoft), using the formula for unpaired, two-tailed t-tests with unequal variance (heteroscedastic t-test). Each t-test was performed by including all population sample values (i.e. each single data point).

### 2.10.2. Average and standard deviation

Experiments were generally performed in duplicates or triplicates. Calculation of the experiment's sample average was done with the basic calculation for arithmetic mean for each experiment (= experimental mean). Subsequently, all experimental mean values (obtained from independent experiments, e.g. transfection, donors) were averaged with the basic calculation for the arithmetic mean. Empirical/population standard deviation was calculated using the formula  $\sqrt{\frac{\Sigma(x-\bar{x})^2}{n}}$ , with  $\bar{x}$  being the sample's arithmetic mean and n being the sample size. Error bars show the empirical standard deviation of the average, if not stated otherwise.

### 2.10.3. Concentration-response curves

Maximal amplitudes of normalized curves were set to 100% and curves were calculated with Graph Pad Prism 5.0 (GraphPad Software) using the equation for sigmoidal dose response with variable slope (“log(agonist) vs. normalized response -- Variable slope”). Normalization was used for comparison of ligand affinities. Usually, the difference of EC<sub>50</sub> values obtained with normalized and non-normalized curves was not higher than a factor of 2. Curves with non-normalized peaks were calculated using the following equation: “log (agonist) vs. response -- Variable slope”. For statistical analysis, only curves with calculated R<sup>2</sup>-values > 0.95 were used in general. The absolute sum of squares for normalized curves was generally < 900. Usually, 10 μM was the highest ligand concentration used to create concentration-response curves. Empirical standard deviation and average were calculated from independently obtained EC<sub>50</sub> values.

## 2.11. Online tools and databases

---

### 2.11.1. Internet addresses

Signal peptide database (update 2010-06-11) <http://www.signalpeptide.de/>

Virulence Factor database (update 2014-22-01) <http://www.mgc.ac.cn/VFs/main.htm>

Sequence blast (latest access 2014/08) <http://blast.st-va.ncbi.nlm.nih.gov/Blast.cgi>

TMHMM Server v. 2.0 (latest access 2015/01) <http://www.cbs.dtu.dk/services/TMHMM/>

### 2.11.2. Prediction of transmembrane helices of cloned FPR constructs

Prediction of transmembrane helices of cloned FPR constructs was performed with the online tool for “Prediction of transmembrane helices in proteins” (TMHMM) of the Center for Biological sequence Analysis, Technical University of Denmark.

## 2.12. Solutions, media and ligands

### 2.12.1. Ligands

Substances were routinely dissolved in watery solutions (C1, Ringer) to concentrations between 0.1 and 1 mM. Strongly hydrophobic substances were generally dissolved as 10 mM stocks in DMSO (99.7%, Sigma). All stocks were stored in small aliquots at -20°C until use. All ligands are listed in Table 2-4.

**Table 2-4 | Ligands used in this study\***

Ligand	Primary structure	Provider and purity	Solvent
<b>Organic compounds</b>			
LXA4 (LipoxinA4)	C <sub>20</sub> H <sub>32</sub> O <sub>5</sub>	Biozol, Cayman Chemical, ≥95%	Ethanol
ATL (15-R-Epi-Lipoxin)	C <sub>20</sub> H <sub>32</sub> O <sub>5</sub>	Biozol, Cayman Chemical, ≥95%	Ethanol
DMSO	C <sub>2</sub> H <sub>6</sub> OS	Sigma, 99,73%	/
n-pentyl acetate	CH <sub>3</sub> CO <sub>2</sub> (CH <sub>2</sub> ) <sub>4</sub> CH <sub>3</sub>	abcr, ≥ 99%	/
2-heptanone	CH <sub>3</sub> (CH <sub>2</sub> ) <sub>4</sub> COCH <sub>3</sub>	Sigma, ≥ 99%	/
LPS	Lipopolysaccharide extract of <i>Salmonella typhimurium</i>	Sigma (L2262)	Water
<b>Naturally-derived peptides</b>			
CRAMP33	GLLRKGGKEKIGEKLLKIGQKIKNFFQKLVPOPEQ	Innovagen, >95%	C1
CRAMP39	ISRLAGLLRKGGEKIGEKLLKIGQKIKNFFQKLVPOPEQ	Innovagen, >95%	C1
rCRAMP33	GLLRKGGKEKFGKELRKGKIKDFQKLAPEIEQ	Innovagen, >95%	C1
Temporin A, amide	FLPLIGRVLSGIL-NH <sub>2</sub>	Anaspec/MoBiTec ≥95%	C1
CO1	f-MFINRWLFS	GenScript Corporation, >96,9%	DMSO
ND1-6I	f-MFFINILTL	Gen Script Corporation, >95,3%	DMSO
ND1-6T	f-MFFINTLTL	Gen Script Corporation, >98,2%	DMSO
f-MLF	f-MLF	Sigma, ≥97%	C1
T20 (DP178, Enfuvirtide)	Ac-YTSLIHSLEESQNQQEKNEQELLELDKWASLWNWF-NH <sub>2</sub>	Anaspec/MoBiTec ≥95%	C1
V3 [ADP715]	RKRIHIGPGRAFYTTKN	Anaspec/MoBiTec, ≥95%	C1
V3 gp120 HIV (JR-FL)	SIHIGPGRAFYTT	Anaspec/MoBiTec, ≥95%	C1
V3 gp120 HIV (BK-130)	RIHIGPGRALYTT	Anaspec/MoBiTec, ≥95%	C1
μPAR (84 – 95)	Ac-AVTYSRSRYLECNH <sub>2</sub>	Anaspec/MoBiTec, ≥95%	C1
Beta – Amyloid (16 – 22)	KLVFFAE	Anaspec/MoBiTec, ≥95%	C1
Beta – Amyloid (35 – 42)	MVGGVVIA	Anaspec/MoBiTec, ≥95%	C1
Ac2-26	Ac-AMVSEFLKQAWFIENEEQEYVQTVK	Toocris, 95%	C1
Substance P	RPKPKQFFGLM-NH <sub>2</sub>	Biotrend, 98,1%	C1
RANTES (11 – 22)	CFAYIARPLPRA	Anaspec/MoBiTec, ≥95%	Ringer
C5a (37 – 53)	RAARISLGPRCICKAFT	Anaspec/MoBiTec, ≥95%	C1
ESP-1	ADQKTNHEADLKNPDPQEVQRALARILCALGELDKLVK DQANAGQQEFKLPKDFTRGSKCRSLG	Gift of Dr. Pablo Chamero <sup>#</sup>	C1
<b>W-peptide library</b>			
W-Peptide	WKYMVm-NH <sub>2</sub>	Innovagen, >95%,	C1
(L)-W-Peptide	WKYMVm- NH <sub>2</sub>	Toocris, 99,2%	C1
M-peptide	MMHWAm- NH <sub>2</sub>	GenScript Corporation, >99.6%	C1
(L)-M-peptide	MMHWAM- NH <sub>2</sub>	GenScript Corporation, >96.8%	C1
W-Library Peptide 9	WKYMVVm- NH <sub>2</sub>	GenScript Corporation, >95%	C1
W-Library Peptide 10	WKYMVmm- NH <sub>2</sub>	GenScript Corporation, >97%	C1
W-Library Peptide 20	AAAWKYMVm- NH <sub>2</sub>	GenScript Corporation, >98.8%	C1
W-Library Peptide 19	AAWKYMVm- NH <sub>2</sub>	GenScript Corporation, >96.3%	C1
W-Library Peptide 12	AWKYMVm- NH <sub>2</sub>	GenScript Corporation, >98%	C1
W-Library Peptide 1	WKYMVm- NH <sub>2</sub>	GenScript Corporation, >97%	C1
W-Library Peptide 2	KYMVm- NH <sub>2</sub>	GenScript Corporation, >99%	C1
W-Library Peptide 3	YMVm- NH <sub>2</sub>	GenScript Corporation, >99%	C1
W-Library Peptide 4	MVm- NH <sub>2</sub>	GenScript Corporation, >95%	C1
W-Library Peptide 5	Vm- NH <sub>2</sub>	GenScript Corporation, >95%	C1
W-Library Peptide 11	WKYMVm	GenScript Corporation, >97%	C1
W-Library Peptide 32	WKYMVm-CHO	American peptide Company, 86.9%	C1
W-Library Peptide 47	f-MVMYKW	GenScript Corporation, >97.8%	C1

Table is continued on the next page.

Ligand	Primary structure	Provider and purity	Solvent
<b>Bacterial signal peptides</b>			
<i>Streptococcus</i> -SP1	f-MGFFIS	VCPBIO, >95.43%	C1
<i>Bacillus</i> -SP2	f-MKNFKG	VCPBIO, >96.42%	C1
<i>Staphylococcus</i> -SP3	f-MFIYYCK	VCPBIO, >97.24%	C1
<i>Salmonella</i> -SP4	f-MAMKKL	VCPBIO, >96.14%	C1
<i>Borrelia</i> -SP9	f-MLKKVY	VCPBIO, >95.24%	C1
<i>Haemophilus</i> -SP5	f-MVMKFK	VCPBIO, >95.74%	C1
<i>Staphylococcus</i> -SP22	f-MKKFNI	VCPBIO, >95.30%	C1
<i>Salmonella</i> -SP23	f-MKKFYF	VCPBIO, >97.18%	C1
<i>Salmonella</i> -SP24	f-MKKFRW	VCPBIO, >98.34%	C1
<i>Psychromonas</i> -SP6	f-MLFYFS	VCPBIO, >95.59%	DMSO
<i>Desulfotomaculum</i> -SP8	f-MLFYLA	VCPBIO, >97.04%	C1
<i>Shewanella</i> -SP7	f-MLFKYS	VCPBIO, >95.18%	C1
<i>Vibrio</i> -SP10	f-MPKLNR	United biosystems, >95.32%	Ringer
<i>Vibrio</i> -SP11	f-MVKIIF	United biosystems, >96.63%	Ringer
<i>Staphylococcus</i> -SP12	f-MNKKLL	United biosystems, >95.21%	Ringer
<i>Clostridium</i> -SP13	f-MKKNLV	United biosystems, >95.67%	Ringer
<i>Corynebacterium</i> -SP14	f-MEQQNK	United biosystems, >95.72%	Ringer
<i>Streptomyces</i> -SP15	f-MVPISI	United biosystems, >95.85%	Ringer
<i>Hydrogenobacter</i> -SP16	f-MKKFLL	United biosystems, >95.78%	Ringer
<i>Bacillus</i> -SP17	f-MMKMEG	United biosystems, >96.38%	Ringer
<i>Listeria</i> -SP18	f-MKKIML	United biosystems, >95.27%	Ringer
<i>Desulfovibrio</i> -SP19	f-MKFCTA	United biosystems, >95.44%	Ringer
<i>Zymomonas</i> -SP20	f-MTNKIS	United biosystems, >95.91%	Ringer
<i>Neisseria</i> -SP11	f-MKTSIR	United biosystems, >96.04%	Ringer
SP8 FuLe	f-MLFYALPCTLVIFVASKALYAI	VCPBIO, >95.59%	Ringer
SP1 FuLe	f-MGFFISQSKQHYGIRKYKVGVCALIALSILGTRVAA	VCPBIO, >95.18%	Ringer
SP22 FuLe1	f-MKKFNILIALFFFTSLVISPLNVKA	VCPBIO, >96.83%	C1
<b>Cytokines</b>			
MIP1-a	APYGADTPTA CCFYSRKIP RQFIVDYFET SSLCSQPGVI FLTKRNRQIC ADSKETWVQE YITDLELNA	Peprotech, >98%	Ringer
RANTES (CCL5)	SPYSSDTTPC CFAYIARPLP RAHIKEYFYT SGKCSNPAAV FVTRKNRQVC ANPEKKWVRE YINSLEMS	Peprotech, >98%	Ringer
MCP-1 (CCL2)	QPDAINAPVT CCYFTNRKI SVQRLASYRR ITSSKCPKEA VIFKTIVAKE ICADPKQKVV QDSMDHLDKQ TQTPKT	Peprotech, >98%	Ringer
<b>FPR antagonists</b>			
Boc1	N-tertbutoxy-MLF	Bachem, 98%	DMSO
Boc2	N-tertbutoxy-FIFIF	Bachem, 98%	DMSO
WRW4	WRWWWW-NH2	Tocris, 98%	C1
Cyclosporin H	C <sub>62</sub> H <sub>111</sub> N <sub>11</sub> O <sub>12</sub>	santa cruz biotechnology, inc.(≥95%)	DMSO
PBP10	RhodaminB-QRLFQVKGR	Calbiochem, ≥95%	DMSO

\*The table lists all ligands used in this study. All peptide/protein sequences are given in one letter code. Small case letters denote D-amino acids. Ac- = N-terminal acetylation, -CHO = C-terminal form aldehyde, f- = N-terminal formylation, -NH<sub>2</sub> = C-terminal amidation. # Dr. P. Chamero, Saarland University, Medical School Homburg, Department of Physiology

### 2.12.2. Imaging buffers

All buffers listed in Table 2-5 were freshly prepared from sterile stock solutions directly before use.

**Table 2-5 | Buffers used for functional imaging\***

	<b>C1</b>	<b>Ringer</b>	<b>HBSS (Ca/Mg)</b>
NaCl	130	155	138
KCl	5	4.5	5.3
CaCl <sub>2</sub>	2	1	1.3
MgCl <sub>2</sub>	/	1	0.5
MgSO <sub>4</sub>	/	/	0.4
D-Glucose	5	10	5.5
HEPES (pH7.3,NaOH)	10	5	10
Na <sub>2</sub> HPO <sub>4</sub>	/	/	0.3
KH <sub>2</sub> PO <sub>4</sub>	/	/	0.4
Used for imaging of	<b>HEK293T, mouse neurons</b>	<b>Human monocytes/neutrophils</b>	<b>Mouse leukocytes</b>

\*Shown is the composition of the used imaging buffers. Concentrations are given in mM.

### 2.12.3. Cell culture media

All media listed in Table 2-6 were stored at 4°C and kept for no longer than 6 weeks after opening.

**Table 2-6 | Cell culture media<sup>#</sup>**

<b>Supplemented with</b>	<b>Basic medium</b>		
	<b>Dulbecco's Modified Eagle Medium (Sigma, D6429)</b>	<b>RPMI-1640 (Gibco, 21875)</b>	<b>RPMI-1640 (Gibco, 21875)</b>
Penicillin/streptomycin (Sigma)	1%*	1%*	1%*
L-Glutamine (Sigma)	2 mM*	2 mM	2 mM
Serum	5% FCS (heat inactivated)*	10% FCS (heat inactivated)*	1% autologous serum*
Sodium-pyruvate (Sigma)	/	/	1%*
Used for culture of	<b>HEK293T</b>	<b>Human Monocytes</b>	<b>Human neutrophils</b>

<sup>#</sup>Shown is the composition of the used cell culture media. Heat inactivated, tetracyclin/LPS free FCS was purchased from Biochrom; 1% [v/v] penicillin/streptomycin (= 10,000 U/ml penicillin, 10 mg/ml streptomycin). \* = added manually after purchase. All media were stored at 4°C and kept for no longer than 1 month after opening.

### 2.12.4. Bacterial growth media

Bacterial growth media listed in Table 2-7 were freshly prepared and autoclaved subsequently.

**Table 2-7 | Bacterial growth media<sup>#</sup>**

	LB-medium	2x YT-medium	SOC-medium
Casein hydrolyzate	1% (w/v)	1.6% (w/v)	2% (w/v)
Yeast extract	0.5% (w/v)	1% (w/v)	5% (w/v)
NaCl	1% (w/v), pH 7	0.5% (w/v), pH 7	0.05% (w/v)
KCl	/	/	2.5 mM
MgCl <sub>2</sub>	/	/	10 mM
D-Glucose	/	/	20 mM
Ampicillin	100 µg/ml (agar plates) *	100 µg/ml, before culture start	/
pH	7	7	7.4

<sup>#</sup>Shown is the composition of the used bacterial growth media. All components were purchased from Carl Roth GmBH or VWR International. \* = For LB-agarplates 100 µg/ml ampicillin and 1.5% (w/v) agar were added

### 2.12.5. Other solutions

#### PBS (general buffer)

140 mM NaCl

10 mM Na<sub>2</sub>HPO<sub>4</sub>

2.7 mM KCl

1.76 mM KH<sub>2</sub>PO<sub>4</sub>

pH: 7.4 (NaOH)

#### TBE (Electrophoresis buffer)

89 mM tris base

89 mM boric acid

2 mM EDTA-Na<sub>2</sub>

#### HBSS (buffer for mouse leukocyte isolation)

138 mM NaCl

5.3 mM KCl

0.4 mM KH<sub>2</sub>PO<sub>4</sub>

0.3 mM Na<sub>2</sub>HPO<sub>4</sub>

5.5 mM D-Glucose

10 mM HEPES (pH7.3/NaOH)

## Chapter 3

---

### Results

---

#### 3.1. Pharmacological analysis of formyl peptide receptors of the immune and the vomeronasal system

---

##### 3.1.1. Functional analysis of formyl peptide receptors in HEK293T cells

###### 3.1.1.1. FPRs from the immune and vomeronasal system can be expressed in HEK293T cells

In order to investigate the pharmacological properties of formyl peptide receptors, the full coding sequences of all three human FPRs (hFPR1, hFPR2 and hFPR3) and seven murine FPRs (mFpr1, mFpr2, mFpr-rs1, mFpr-rs3, mFpr-rs4, mFpr-rs6, and mFpr-rs7) were cloned into expression vectors used for heterologous expression in HEK293T cells (chapter 2.1). The coding regions of all cloned receptors were sequenced for at least two times. The sequences of mFpr1, mFpr2, mFpr-rs1, mFpr-rs3, mFpr-rs4, mFpr-rs6, hFPR2 and hFPR3 did not contain nucleotide exchanges leading to altered amino acid sequences of the receptors compared to the reference sequences (Table 3-1). Two receptors, mFpr-rs7 and hFPR1 exhibited variations in their nucleotide sequence that resulted in amino acid exchanges. For mFpr-rs7, the leucine at position 147, at the N-terminal edge of the 4<sup>th</sup> transmembrane domain, was replaced by phenylalanine in the cloned construct. This single nucleotide polymorphism is also found in several BAC clones (AC154490, AC121539.7). The construct of hFPR1 showed three variations leading to exchanges in the amino acid sequence. There was a conservative substitution of valine at position 101 (3<sup>rd</sup> transmembrane helix) by leucine, which has already been described by several groups (Boulay *et al.*, 1990b; Sahagun-Ruiz *et al.*, 2001). Arginine at position 163 (4<sup>th</sup> transmembrane helix) was replaced by histidine and asparagine at position 192 (2<sup>nd</sup> extracellular loop) was replaced by lysine. The substitution N192K has already been observed by Sahagun-Ruiz and been allocated to one haplotype with V101L (Sahagun-Ruiz *et al.*, 2001).

**Table 3-1 | Overview of cloned receptors, online accession, and detected amino acid exchanges\***

Receptor	Amino acid exchanges to reference sequence	Accession (online reference)
mFpr1	/	NM_013521.2
mFpr2	/	NM_008039.2
mFpr-rs1	/	NM_008042.2
mFpr-rs3	/	NM_008040.2
mFpr-rs4	/	NM_008041.2
mFpr-rs6	/	NM_177316.2
mFpr-rs7	F147L	AF437513.1
hFPR1	V101L, R163H, N192K	NM_001193306.1
hFPR2/ALX	/	NM_001462.3
hFPR3	/	NM_002030.3

\*The table lists all cloned formyl peptide receptors investigated in this study. Observed differences in the amino acid sequence of the cloned receptors compared to the reference sequence are shown in the middle column. The first letter marks the amino acid of the reference sequence that is substituted in the cloned receptor (second letter). The number between the letters indicates the amino acid position of this substitution. The right column contains the online accession numbers of the reference sequences. Complete coding sequences are given in appendix 5. Online references are valid for BLAST ([www.ncbi.nlm.nih.gov/blast/](http://www.ncbi.nlm.nih.gov/blast/)).

In order to investigate whether these receptor constructs can be used for heterologous expression, immunocytochemistry, employing antibodies targeted against specific epitopes of the receptors were used to monitor receptor expression. Thus far, most murine FPRs lack specific antibodies. To circumvent this problem, an epitope containing the 39 most N-terminal amino acids of bovine rhodopsin was fused to the N-terminus of each receptor (Rho-tag). This enabled comparative examination of the expression levels with an antibody directed against this Rho-epitope. Figure 3-1 A depicts a representative immunocytochemistry staining of permeabilized cells transfected with *mFpr1* and the empty vector control. The staining showed prominent expression of mFpr1 in the HEK293T cells (Figure 3-1 A). Detailed quantification of total cellular expression levels for all human and mouse FPRs is given in Figure 3-1 B. The overall expression levels ranged from 47% to 87% of the cells in the visual field. Expression rates of the human FPRs were  $61 \pm 18\%$  for hFPR1,  $87 \pm 6\%$  for hFPR2 and  $61 \pm 13\%$  for hFPR3. The expression rates of the murine FPRs were as follows:  $73 \pm 6\%$  (mFpr1),  $48 \pm 6\%$  (mFpr2),  $49 \pm 13\%$  (mFpr-rs1),  $50 \pm 8\%$  (mFpr-rs3),  $58 \pm 11\%$  (mFpr-rs4),  $58 \pm 7\%$  (mFpr-rs6) and  $50 \pm 7\%$  (mFpr-rs7). The negative control (empty vector transfected cells) did not show any staining. Note that the expression levels of all human FPRs were comparable to those of the mouse Fprs. Pharmacological analysis of G protein-coupled receptors (GPCRs) requires sufficient expression and correct insertion of the receptors into the cell's plasma membrane. Therefore, the immunocytochemical staining was also performed on non-permeabilized cells. As the Rho-tag was fused to the N-terminus of the receptors, only receptors whose N-terminus was correctly located on the extracellular side could be stained (Figure 3-1 C). Figure 3-1 C shows a representative cell surface staining of unpermeabilized

cells transfected with *mFpr1*. In line with the expectations, the surface staining of unpermeabilized cells showed a clearly prominent signal located at the plasma membrane. Quantification of cell surface expression rates for all receptors is given in Figure 3-1 D.

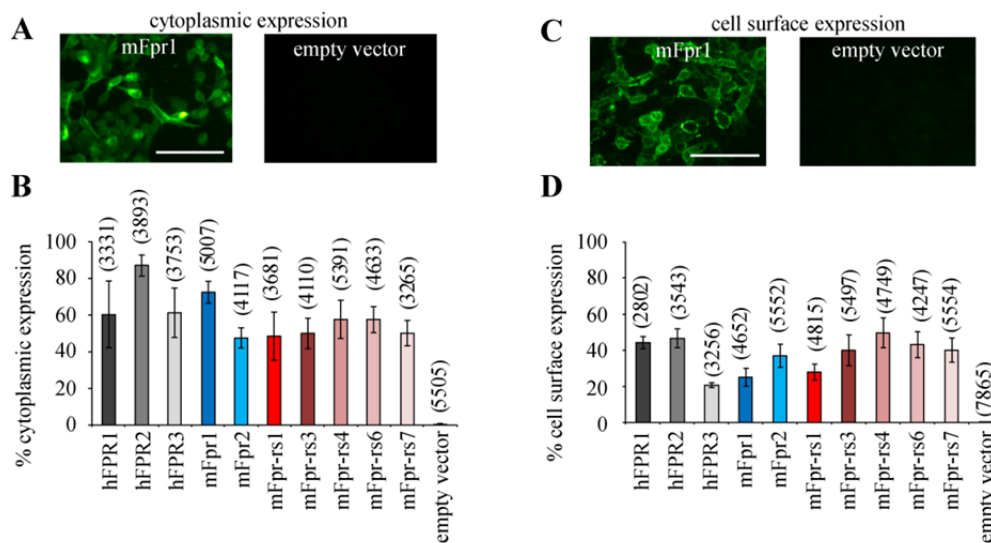


**Figure 3-1 | Expression of human and murine formyl peptide receptors in HEK293T cells**

[A] Representative immunostaining of permeabilized HEK293T cells transfected with either *mFpr1* or empty vector (mock), showing cytoplasmic localization of mFpr1. The cells were stained with an antibody directed against the Rho-tag fused to the receptor's N-terminus. [B] Quantification of cytoplasmic expression of all human and mouse receptors. Data were recorded in octuplets. [C] Representative cell surface staining using the same antibody as in A. The cells were not permeabilized to visualize receptors exclusively expressed in the cell membrane. [D] Quantification of cell surface expression of all receptors. Data are representative for one experiment measured in octuplets. Scale bar: 40  $\mu$ m; Numbers in parentheses above each bar denote the number of measured cells; error bars = standard deviation.

Surface expression rates ranged from 21% to 46%, with a mean of  $37\% \pm 6\%$ , while the background was below 0.1%. Expression rates for hFPR1 and hFPR2 were 44% and 47% respectively, while for hFPR3 it was 21%. The percentage of cells expressing vomeronasal FPRs (mFpr-rs1, mFpr-rs3, mFpr-rs4, mFpr-rs6, and mFpr-rs7) was comparable to that of cells expressing human and mouse FPR1 and FPR2. While mFpr1 and mFpr2 expression was detected in 25% and 37% of the cells respectively, the detected surface expression rates were 28% for mFpr-rs1, and over 40% for mFpr-rs3 (40%), mFpr-rs4 (50%), mFpr-rs6 (43%), and mFpr-rs7 (40%). Expression rates of 5% are already sufficient for functional studies of GPCRs, as former publications have shown (Bufe *et al.*, 2002).

This shows that the receptor constructs can be heterologously expressed in HEK293T cells and should be suited for pharmacological analysis. For this, a high-throughput calcium imaging assay was established that enables investigation of agonist-induced calcium responses of the heterologously expressed formyl peptide receptors.

### 3.1.1.2. Heterologously expressed immune FPRs can be measured in calcium imaging

To verify if receptor activation can be detected, single-cell  $\text{Ca}^{2+}$  imaging was used. To ensure efficient G protein coupling the cells were co-transfected with a plasmid encoding the human  $G_q$ -type G protein subunit  $G\alpha_{16}$ . This promiscuous G protein subunit has been shown to efficiently couple hFPR1 to the  $\text{IP}_3/\text{Ca}^{2+}$  pathway (Offermanns and Simon, 1995). For activation of the cells they were challenged with the well-known FPR agonist f-MLF. f-MLF is the prototypical high affinity agonist ( $\text{EC}_{50}$  in the upper picomolar range) for human and mouse FPR1 (Schiffmann *et al.*, 1975; Quehenberger *et al.*, 1993). It is also an agonist for human and mouse FPR2, however, with reduced affinity (Quehenberger *et al.*, 1993). In line with my expectations, 258 of 364 cells (~71%) transfected with *hFPR1*<sup>4</sup> did respond with calcium elevations when treated with 9  $\mu\text{M}$  of f-MLF (Figure 3-2 A). Notably, the cells did not respond to application of buffer. This excludes mechanical stimulation of the transfected cells. Moreover, none of the 337 control cells (empty vector transfection) responded to f-MLF. However, the cells responded to 30  $\mu\text{M}$  of ATP, an activator of endogenous purinergic receptors that served as an excitability control (Figure 3-2 A).

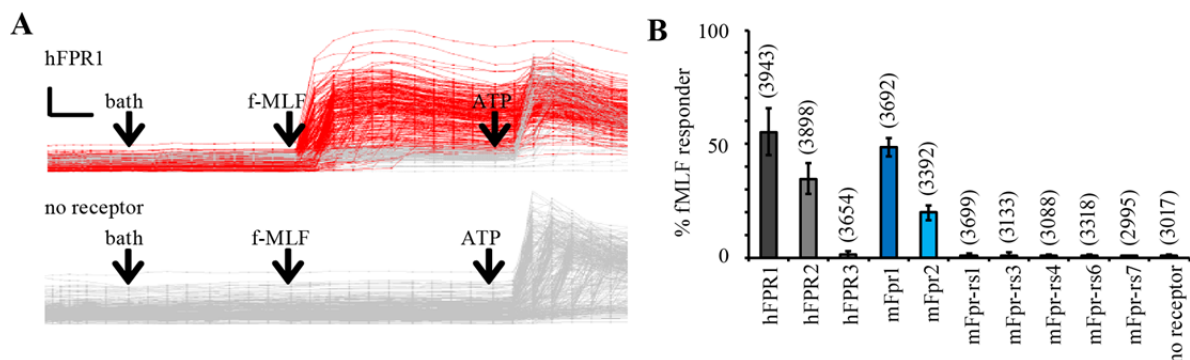


**Figure 3-2 | Single cell calcium imaging of human and murine FPRs in HEK293T cells**

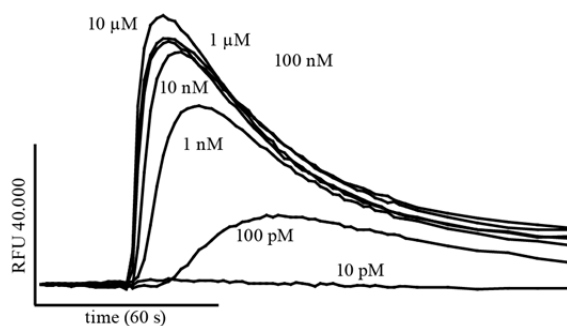
**[A]** Representative calcium imaging experiment with single cell resolution: shown are calcium transients of cells transfected with *hFPR1* or empty vector upon stimulation with 9  $\mu\text{M}$  of the prototypical agonist f-MLF. Each trace represents a single cell. Upper panel: 258 of 364 *hFPR1*-transfected cells responded to f-MLF (red traces = responding cells, gray traces = non-responder). Lower panel: 337 cells transfected with empty vector served as control. Bath solution was served as a control for application artifacts; 30  $\mu\text{M}$  ATP, an activator of endogenous purinergic was used to monitor cell excitability. Scale: y-axis ( $A_{334/380}$  ratio = 1); x-axis (time = 0.5 min). **[B]** Quantification of single cell experiments averaged over eight wells. Numbers in parentheses above each bar denote the number of measured cells. Error bars = standard deviations.

This demonstrates that heterologously expressed hFPR1 can readily be monitored in calcium imaging. Detailed quantification for all receptors showed responses for  $34 \pm 7\%$  of cells transfected with *hFPR2*,  $49 \pm 4\%$  of cells transfected with *mFpr1* and  $20 \pm 3\%$  of cells transfected with *mFpr2* (Figure 3-2 B). Note that the number of responders detected for

<sup>4</sup> The cells were transfected with the plasmid coding for the receptor hFPR1. For easier understanding, only the name of the genetic construct will be used (*hFPR1*).

*mFpr2* transfected cells is about 50% reduced compared to *mFpr1* transfected ones. Under these conditions, no responses were observed for hFPR3 or any of the mouse vomeronasal FPRs. Since no signals have been observed for the vomeronasal FPRs, I next tested other well-described FPR ligands to verify the functionality of the heterologous expression assay. The single cell calcium imaging assay grants high spatial resolution but it takes much time to test larger array of substances on several receptors. Therefore, a high-throughput calcium imaging system, which simultaneously monitors cell populations of approximately 50,000 cells/well rather than single cells in 96 well plates, was established to test several well-known FPR agonists on human and mouse receptors. First, to verify that the assay is suited for calcium imaging of heterologously expressed FPRs, f-MLF was tested in concentration-response experiments on HEK293T cells expressing hFPR1 (Figure 3-3 A). f-MLF has been described to be highly affine in calcium imaging assays, with EC<sub>50</sub> values in the upper picomolar range (Quehenberger *et al.*, 1993). As expected the ligand proved to be highly affine for hFPR1, exhibiting a threshold activation of  $\leq 100$  pM with an EC<sub>50</sub> of 544 pM. Following this, a number of well-known FPR agonists were tested on hFPR1, hFPR2, mFpr1 and mFpr2 (Figure 3-3 B). These agonists comprised the formylated mitochondrial peptides CO1 and ND1-6I (Rabiet *et al.*, 2005) and the synthetic hexapeptides W-peptide and L-W-peptide (Bae *et al.*, 2001; Baek *et al.*, 1996). All substances were able to activate human and mouse FPR1 and FPR2 (Figure 3-3 B).

### A Calcium responses of hFPR1 to f-MLF



### B Calcium responses of FPRs to several agonists

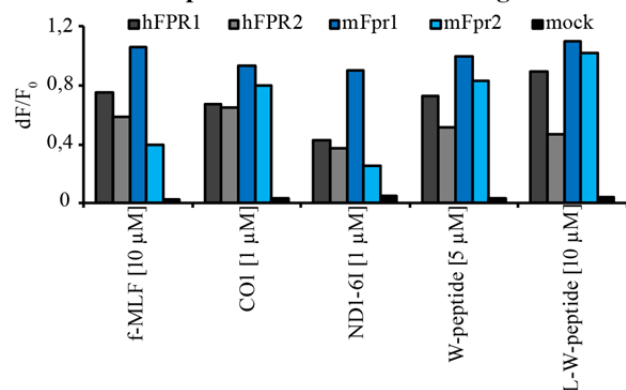


**Figure 3-3 | Mass population calcium imaging of human and murine FPRs in HEK293T cells**

**[A]** Representative concentration-response experiment as measured in the FLIPR: shown are calcium transients of cells transfected with hFPR1 upon stimulation with decreasing concentrations of f-MLF. RFU = relative fluorescence units. **[B]** Quantification of calcium responses of cells transfected with hFPR1, hFPR2, mFpr1, mFpr2 or empty vector (mock) towards various known FPR agonists (representative for at least two independent transfections).

Interestingly, the signal amplitude observed for mFpr2 was 50% reduced compared to mFpr1 when challenged with 10  $\mu$ M f-MLF. This reduction corresponds nicely to the 50% reduced number of responders observed in the single cell calcium imaging assay (Figure 3-2 B),

demonstrating the fidelity of the FLIPR assay. However, when f-MLF, CO1 and ND1 were applied on vomeronasal FPRs, no responses could be observed (not shown). To verify that the lack of response is not due to a failure in interaction with  $G\alpha_{16}$ , the cells were co-transfected with distinct G proteins or G protein-chimeras. The enzymatic body of these chimeras consisted of  $G\alpha_{16}$  but the last 44 amino acids of the C-terminal tail were substituted by those of other G protein  $\alpha$ -subunits like  $G_{i2}$  and  $G_{o1A}$  (chapter 2.6.1). Since the C-terminus of the G protein is a determinant in interaction with GPCRs, this modification enables coupling of receptors that usually interact with  $G_{i2}$  or  $G_{o1A}$  (or other respective subunits) to the  $IP_3/Ca^{2+}$  pathway (Mody *et al.*, 2000). Tests with G protein-chimeras, including those of  $G_{i2}$  and  $G_{o1A}$ , showed that immune FPRs can interact with a variety of G protein chimeras carrying C-termini from  $G_i$ ,  $G_z$ ,  $G_o$ ,  $G_{gust}$ , and  $G_{olf}$  (Fig. 3-4). Both, mFpr1 and mFpr2 showed responses towards f-MLF when co-transfected with plasmids coding for G protein-chimeras with C-termini from  $G_i$ ,  $G_z$ ,  $G_o$ , and  $G_{gust}$ . These signals were comparable to the signals observed by co-transfection of  $G\alpha_{16}$ . However, no signals were detected for the vomeronasal FPRs.  $G\alpha_{16}$  is a human G protein subunit and it is not imperative that murine FPRs can employ this G protein to its full extent. Hence, it was tested whether the mouse receptors prefer  $G\alpha_{15}$ , the murine ortholog of  $G\alpha_{16}$  (Fig. 3-4). Both, mFpr1 and mFpr2 exhibited calcium responses following stimulation with f-MLF. These responses however, were about 50% lower than those observed for  $G\alpha_{16}$ . Again: no signals for the VNO FPRs. To test whether the vomeronasal FPRs prefer interaction with olfactory G proteins, a chimera consisting of  $G\alpha_{15}$  in which the 47 C-terminal amino acids were replaced by that of the  $G_{\alpha_{olf}}$  subunit was co-transfected. Although mFpr1 and mFpr2 were able to couple to this G-protein, no signals were observed for the VNO FPRs. Very similar results have been observed with the mitochondrial peptide CO1.

These data verify the general functionality of the assay and suggest that there is no deficiency in G protein coupling.

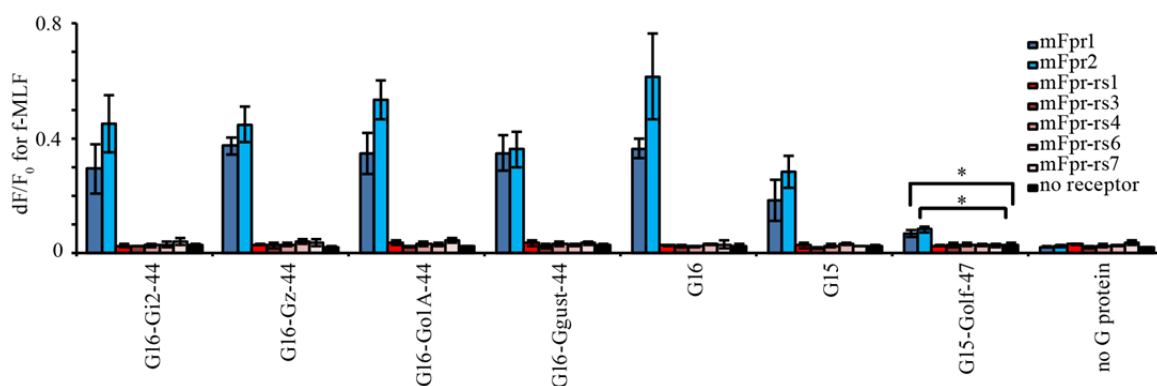


**Figure 3-4 | Influence of G protein chimeras on calcium imaging of human and murine FPRs in HEK293T cells**

Influence of G protein co-transfection on receptor-dependent calcium signal as measured in the FLIPR cell population assay (representative for two experiments). Cells were co-transfected with plasmids coding for mouse FPRs and different G proteins alpha subunits or chimeras and were stimulated with 33.3  $\mu$ M f-MLF. Each combination was averaged over three wells. The chimeras were  $G\alpha_{16}$ , carrying a C-terminal substitution of the 44 most C-terminal amino acids by those of the corresponding G protein alpha subunits ( $G\alpha_{i2}$ ,  $G\alpha_{o1A}$ ,  $G\alpha_z$ ,  $G\alpha_{gust}$ ). The  $G_{olf}$ -chimera consisted of the enzymatic body of  $G\alpha_{15}$ , carrying a C-terminal substitution of the 47 most C-terminal amino acids by that of  $G_{olf}$ . All receptors carried Rho-tags. no receptor/no G protein = empty vector. Error bars = standard deviations. *Adapted from Schumann, 2010.*

The next step involved the testing of a set of eleven substances on all three human and all eight mouse receptors to see whether the vomeronasal FPRs can be activated in general. First experiments revealed surprising results: for initial experiments hydrophobic ligands were diluted in the organic solvent DMSO. Unexpectedly, DMSO alone activated cells expressing hFPR2, mFpr1 or mFpr2 at a concentration of 2% [v/v] (= 282 mM) (Fig. 3-5 A). Cells transfected with hFPR1, hFPR3, mFpr-rs1, mFpr-rs3, mFpr-rs4, mFpr-rs6, or mFpr-rs7 showed no specific response toward 2% DMSO. The threshold of concentrations capable of inducing calcium signals in receptor transfected cells were 0.3% for mFpr1 and mFpr2 (Fig. 3-5 B) and 1% for hFPR2. Concentrations > 2% always led to unspecific signals in the control group transfected with the empty vector. The threshold concentration for these unspecific signals was 2%. However, those signals had different kinetics as those of cells transfected with mFpr1 or mFpr2 (Fig. 3-5 B). In contrast to the control group, calcium signals of mFpr1 and mFpr2 transfected cells showed a fast onset with a steep slope (Fig. 3-5 B), enabling discrimination of specific and unspecific signals. Nevertheless, to verify if these responses were indeed receptor-dependent, control experiments were performed. First, it was investigated whether the signals were mediated by the co-expressed G protein  $G\alpha_{16}$ . Indeed, DMSO-evoked signals were only seen in cells co-expressing the receptor and the G protein (Fig. 3-1-5 C). Second, it was tested whether the DMSO evoked signals seen in mFpr1 or mFpr2 transfected cells could be abolished if the receptors were desensitized by pre-application of the agonist f-MLF. The results show that cells, pre-treated with 30  $\mu$ M f-MLF,

did not respond to subsequent application of 2% DMSO (Fig. 3-5 D). Third, dose-response experiments on mouse mFpr1 and mFpr2 showed that the activation was dose-dependent, with an  $EC_{50}$  of 97 mM for mFpr1 and an  $EC_{50}$  of 55 mM for mFpr2 (Fig. 3-5 E). Together these data indicate that the calcium signals evoked by 2% DMSO are mediated by mFpr1, mFpr2 and hFPR2, respectively, as only the combination of receptor and G protein led to DMSO-dependent calcium mobilization. These results show that the use of DMSO as an organic solvent or cosolvent is critical. Therefore, concentrations  $> 0.1\%$  [v/v] were avoided in this study.

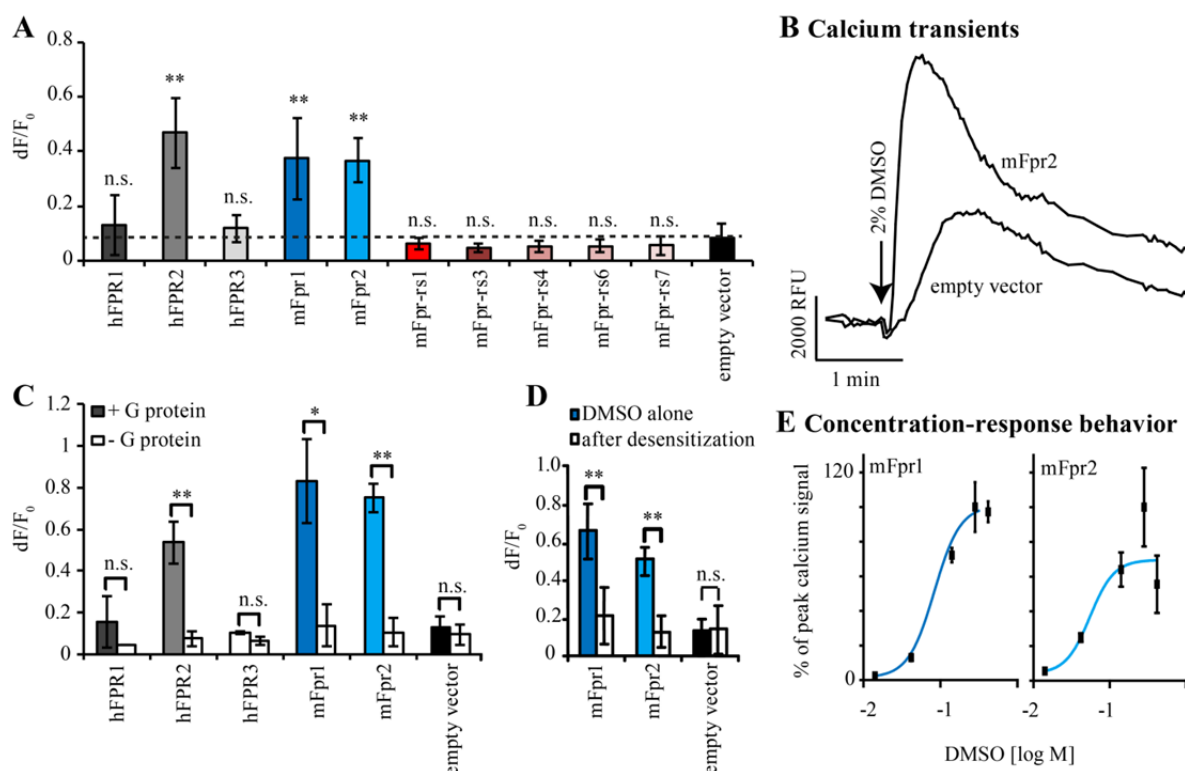


**Figure 3-5 | Specific activation of hFPR2, mFpr1 and mFpr2 by DMSO**

Mouse FPRs were heterologously expressed in HEK293T cells and responses of the receptors to DMSO were measured using calcium imaging (FLIPR). **[A]** 2% [v/v] DMSO (= 282 mM) activates the immune FPRs hFPR2, mFpr1 and mFpr2 (gray and blue) but none of the vomeronasal FPRs (red). Data averaged over three independent transfections. **[B]** Original calcium transients as measured in the FLIPR. Threshold activation for unspecific signals (empty vector) was observed at concentrations  $\geq 2\%$  [v/v]. RFU = relative fluorescence units. **[C]** Signals evoked by 2% [v/v] DMSO depended on the presence of co-transfected  $G_{\alpha 16}$ . (Data averaged over two independent transfections). **[D]** DMSO evoked signals (2% [v/v]) could be cross-desensitized by 30  $\mu$ M f-MLF. (Data averaged over three independent transfections). **[E]** mFpr activation is dose-dependent ( $EC_{50}$  mFpr1 = 97 mM,  $EC_{50}$  mFpr2 = 55 mM). To generate a dose-response profile the background signal (empty vector) was subtracted from signals obtained for FPR expressing cells. Curves are representative for five independent transfections. Black dotted line = amplitude of empty vector signal (background). Statistical significance of homoscedastic t-test: \* =  $p \leq 0.05$ , \*\* =  $p \leq 0.001$ ; n.s. = not significant (compared to empty vector control).

To perform the compound screening on the murine FPRs, at first eleven substances were tested in calcium imaging. In order to create high pharmacological variance, the chosen peptides were of different origins, thereby exhibiting highly disparate primary structures. The

well-known f-MLF was used as a control. Although the immune FPRs mFpr1 and mFpr2 were activated in nanomolar concentrations, no signals have been observed for the vomeronasal FPRs in concentrations up to 30  $\mu\text{M}$ <sup>5</sup>. Similar results have been observed for the N-terminally formylated peptide ND1-6I (Fig. 3-6 A and B). This peptide is derived from the mouse mitochondrial NADH-dehydrogenase subunit I and belongs to some of the most potent FPR ligands (Rabiet *et al.*, 2005). While it activated mFpr1 and mFpr2, no responses were monitored for the vomeronasal FPRs when applied to concentrations up to 5  $\mu\text{M}$ . FPRs are also described to respond to several peptides derived from viral hull proteins. V3 gp120 HIV (BK-130), a peptide derived from the V3 loop of HIV-1 (Shen *et al.*, 2000), was able to activate mFpr1 while another HIV-1-derived peptide, T20 (Su *et al.*, 1999b), induced calcium signals in cells expressing mFpr1 (Fig. 3-6 B). Neither of the two substances was capable of evoking responses by activating one of the vomeronasal FPRs. The human annexin A1 mimetic peptide Ac2-26 is an N-terminally acetylated peptide containing 25 amino acids (Walther *et al.*, 2000). It is known to activate hFPR1, hFPR2, hFPR3 as well as mFpr1, and mFpr2 (Ernst *et al.*, 2004). In my experiments it could clearly activate mFpr1 and mFpr2 but no vomeronasal FPR (Fig. 3-6 B). The rana temporaria-derived Temporin A amide (Chen *et al.*, 2004), which belongs to the class of anti-microbial peptides selectively activated mFpr2 but no other mouse FPR at concentrations up to 3  $\mu\text{M}$  (Figure 3-6 C). Similar results haven been observed for CRAMP39, another anti-microbial peptide known to activate mFpr2 (Kurosaka *et al.*, 2005). When *mFpr2* transfected HEK293T cells were challenged with 3  $\mu\text{M}$  CRAMP39, they responded with calcium signals (not shown). At first, it seemed that CRAMP39 was also a powerful activator of all vomeronasal FPRs. This ligand however, elicited unspecific signals in cells transfected with the empty vector when applied at 10  $\mu\text{M}$  (Appendix 1 A). mFpr2, which is a described receptor for CRAMP (Kurosaka *et al.*, 2005), showed significantly increased signals towards CRAMP. In rare occasions, such unspecific signals have been detected at concentrations of 1  $\mu\text{M}$  (Appendix 1 B). This was also observed for the isoforms CRAMP33 and rCRAMP33 (Appendix 1 B). Those three CRAMP substances were therefore excluded from further experimentation and evaluation.

So far, no responses have been observed for the vomeronasal FPRs, questioning the functional expression of this receptor subfamily. In further experiments, however, two compounds were investigated that were capable of activating at least one of the VNO-FPRs: mFpr-rs1 showed

---

<sup>5</sup> Concentrations of 100  $\mu\text{M}$  induced calcium currents in cells transfected with the mFpr-rs1 construct. The observed signals were at the detection limit (not shown).

calcium responses towards the synthetic hexapeptides W-peptide and M-peptide (Figure 3-6 D). Both substances did also activate all human FPRs as well as the mouse immune FPRs mFpr1 and mFpr2. For mFpr1, peaks of responses induced by W-peptide and M-peptide were similar to those seen for the formylated peptides f-MLF and ND1-6I (Figure 3-6).

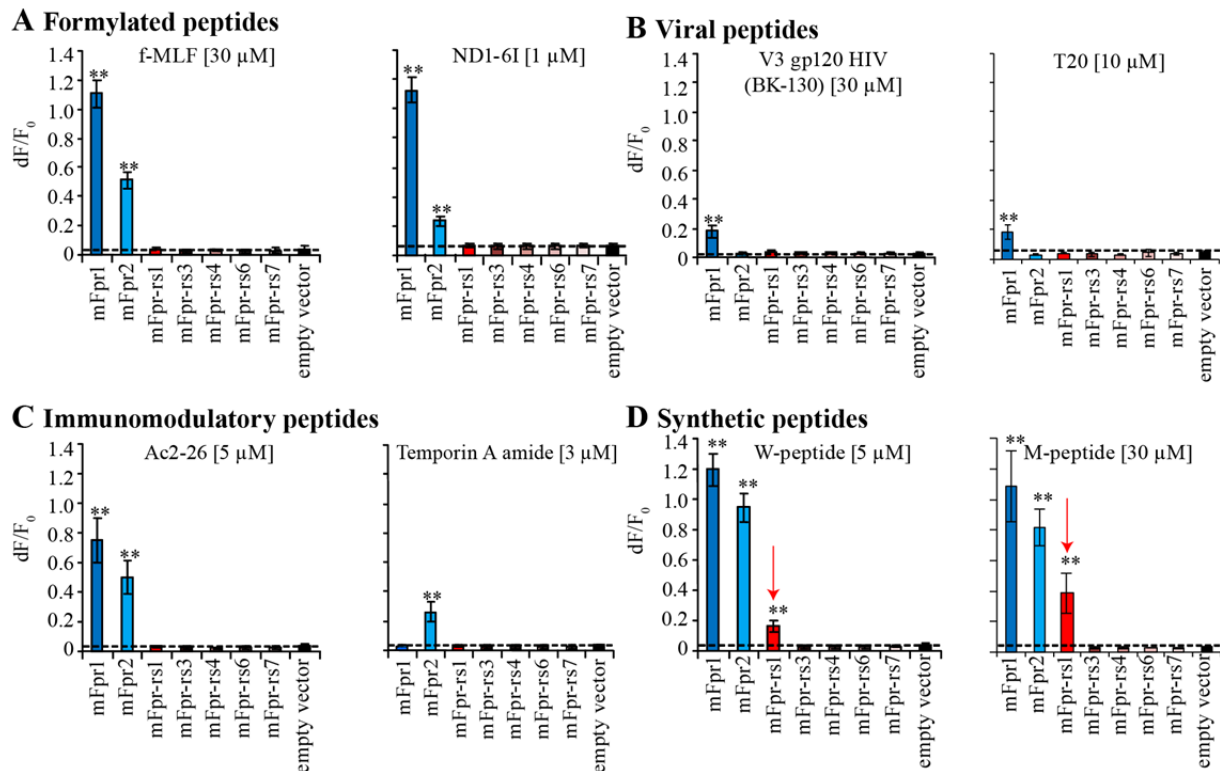


**Figure 3-6 | Cell population-based calcium imaging of heterologously expressed FPRs**

Mouse FPRs were heterologously expressed in HEK293T cells and stimulated with various FPR agonists. Calcium responses were measured with the FLIPR. mFprs naturally expressed in the immune system are shown in blue while vomeronasally expressed FPRs are shown in red. **[A]** N-terminally formylated peptides like the bacterial f-MLF or the mitochondrial ND1-6I activated mFpr1 and mFpr2 but no other tested mouse FPR. **[B]** Calcium responses towards HIV-1-derived peptides. **[C]** Calcium responses towards the human endogenous immune modulator Ac2-26 and the frog anti-microbial Temporin A amide. **[D]** mFpr-rs1 (red arrow) is activated by the synthetic immune FPR agonists W-peptide and M-peptide. Black dotted line = amplitude of background signal (empty vector). Statistical significance (compared to empty vector): \*\*  $p \leq 0.01$ . Each bar was averaged over three (two for M-peptide) independent transfections.

The results shown in Figure 3-6 demonstrate that the vomeronasal receptor mFpr-rs1 responds to W-peptide and M-peptide. The calcium transients observed for mFpr-rs1 were smaller in amplitude with a less steep slope compared to mFpr1 and mFpr2 (Figure 3-7 A), indicating a lower grade of sensitivity. In order to get deeper insights into the pharmacological profiles of W-peptide and M-peptide, the responses of mFpr1, mFpr2 and mFpr-rs1 were compared in concentration-response analyses (Figure 3-7 B). Comparison of W-peptide concentration-response curves demonstrated a remarkable functional conservation between immune system-derived mouse FPRs. The  $EC_{50}$  values for mFpr1 and mFpr2 were  $1.1 \pm 0.17$  nM and

$0.39 \pm 0.25$  nM, respectively (Figure 3-7). Similar results were observed for the M-peptide. The computed  $EC_{50}$  values were  $18.7 \pm 6.7$  nM for mFpr1 and  $87.5 \pm 20.7$  nM for mFpr2. Interestingly, both receptors showed a higher affinity towards W-peptide than M-peptide. This however, does not apply for mFpr-rs1: the calculated  $EC_{50}$  values were  $505 \pm 209$  nM for W-peptide and  $738 \pm 174$  nM for M-peptide.

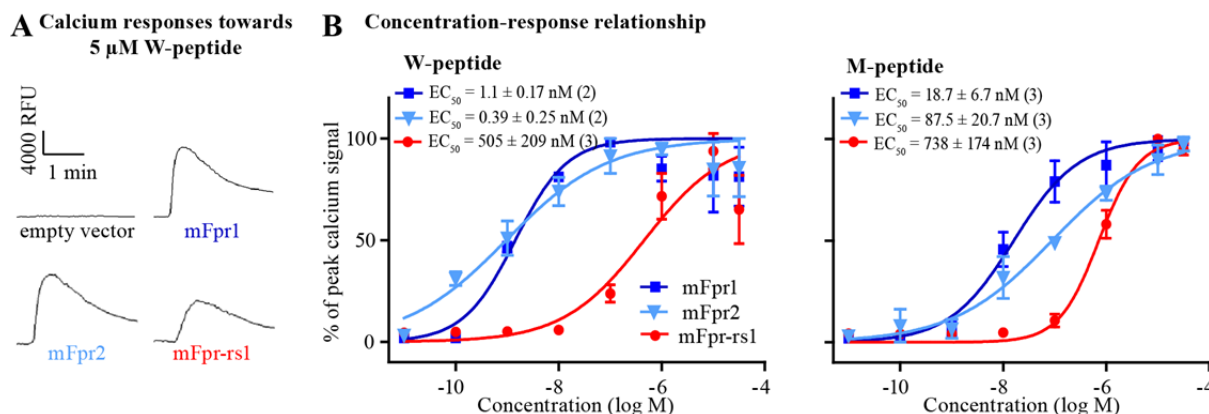


**Figure 3-7 | W-peptide and M-peptide are activators of mFpr-rs1**

Concentration-response curves of W-peptide and M-peptide on heterologously expressed mFpr-rs1 obtained by calcium imaging. [A] Typical calcium traces of cells expressing mFpr1, mFpr2 or mFpr-rs1 compared to the empty vector as monitored by the FLIPR. RFU = relative fluorescence units. Data are representative for three independent transfections [B] Dose-response-relationship of cells transfected with *mFpr-rs1* towards W-peptide and M-peptide. Number of independent experiments is given in parentheses.  $EC_{50}$  values are given in nM.

These experiments confirm that at least one vomeronasal FPR can be activated and measured in calcium imaging. It does suggest that vomeronasal FPRs can respond but that the lack of responses for mFpr-rs3, mFpr-rs4, mFpr-rs6, and mFpr-rs7 is due to the fact that they were not challenged with the appropriate stimulus. Hence, the compound screening was extended to more substances, adding up to 23 in total.

### 3.1.2. FPR agonist screening reveals divergent pharmacological profiles of immune FPRs and vomeronasal FPRs

In order to get further insights into the pharmacology of the vomeronasal FPRs, in summary a set of 23 ligands was selected for screening (chapters 3.1.1. and 3.1.2). The ligand selection was based on several parameters: First, the selected compounds should comprise well-known FPR ligands, including powerful FPR agonists. Second, the selected agonists should originate from different biological areas with distinct functions. Third, the selected ligands should comprise substances of distinct chemical classes. Fourth, since many FPR ligands are peptides, the selected peptides should exhibit diversity in amino acid sequence, peptide chain length

and chemical modifications. Fifth, to increase the structural variability, some substances were chosen as structural derivatives of known FPR ligands. 14 substances, W-peptide, M-peptide, Ac2-26, f-MLF, ND1-6I, CO1, T20, Temporin A amide, uPar 84-95, LipoxinA4, 15-(R)-Lipoxin, CRAMP39, Substance P, and WRW4 were chosen because they are described human, mouse or rabbit FPR ligands (Migeotte *et al.*, 2006). Five peptides are structural variants of already known FPR agonists: V3 gp120 HIV (JR-FL), V3 gp120 HIV (BK-130), and ADP715 HIV-I are orthologs of the V3 peptide, isolated from the HIV-1 envelope loop V3 of distinct HIV-I strains (Shen *et al.*, 2000; Moore *et al.*, 1995). CRAMP39 is an extended isomer of CRAMP33 and rCRAMP33 is its corresponding rat ortholog (Kurosaka *et al.*, 2005; Chromek *et al.*, 2006). beta amyloid 16-22 is a breakdown product of the well-known FPR2 agonist beta amyloid 1-42 (Balbach *et al.*, 2000; Le *et al.*, 2001). Two compounds, C5a 37-53 and RANTES 11-22, are derived from cytokines (Nardese *et al.*, 2001; Fujita *et al.*, 2004), molecules with proven effects on chemotactic GPCRs. One compound, Substance P, was chosen because it is assumed to activate innate immune cells via FPRs (Marasco *et al.*, 1981; Takenouchi and Munekata, 1995). The organic solvent DMSO was first used as an internal control for solubilized hydrophobic peptides (chapter 3.1.1). The structural properties of the substances and their origin are listed in Table 3-1-2.

### **3.1.2.1. Activation pattern of human FPRs**

Testing each ligand on each receptor led to an interesting picture: 15 of the chosen substances elicited receptor-dependent signals in cells transfected with human FPRs (Table 3-2). Of the 15 ligands that activated at least one human FPR, ten activated at least two receptors and only five were selective for a given hFPR. As described in the literature, M-peptide, W-peptide, and Ac2-26 activated all three human FPRs (Migeotte *et al.*, 2006). hFPR1 responded to all three tested formylated peptides, the two synthetic hexapeptides W-peptide and M-peptide, the immunomodulatory Ac2-26 and the viral peptide V3 gp120 HIV (BK-130). Interestingly, the receptor did not respond to the strain orthologs V3 gp120 HIV (JR-FL), which varies from BK-130 by substitution of two amino acids (Table 3-2). While there was no ligand that acted solely on hFPR1, two compounds, Substance P and DMSO, selectively activated hFPR2. Interestingly, hFPR2 was able to recognize each substance that activated hFPR1 in the applied concentrations. On top of that, hFPR2 was activated by the anti-microbial Temporin A amide, the cytokine fragment RANTES 11-22 and the viral T20. All these substances were also able to activate hFPR3. Besides T20, hFPR3 was also activated by two of the other three viral peptides V3 gp120 HIV (BK-130) and V3 gp120 HIV (JR-FL). Signals induced by the latter

were at the detection limit within the range of the used concentrations. V3 gp120 HIV (JR-FL) was one of the three substances that acted selectively on hFPR3. It was furthermore selectively activated by the cytokine isomer C5a and the hexapeptidic hFPR2 inhibitor WRW4.

In summary, hFPR1 was activated by seven out of 23 substances. Although the receptor was highly sensitive for all these substances, exhibiting  $EC_{50}$  values in lower nanomolar concentrations (not shown), the responses were not restricted to hFPR1. All hFPR1 activators also proved to be activators for hFPR2 and/or hFPR3. hFPR2 in contrast, responded to twelve of the 15 activators of human FPRs. Among these agonists were the organic substance DMSO and 14 peptides with variant structure, chain length and modifications like acetylation, formylation or amidation, suggesting a quite promiscuous behavior of hFPR2. This assumption is further strengthened by the fact that hFPR2 was activated by three substances that activated hFPR3. Interestingly, hFPR3 was not activated by any of the three formylated peptides which could activate hFPR1 and hFPR2 but was selective for three substances. hFPR3 was the only receptor that recognized both cytokine-derived peptides as well as three out of four viral peptides,. Together these data argue for distinct ligand binding properties of hFPR3.

### ***3.1.2.2. Activation pattern of mouse immune FPRs***

The murine receptors mFpr1 and mFpr2 showed a remarkable similarity to human FPRs with respect to ligand recognition. Of the twelve substances that activated mFpr1 or mFpr2, eleven were also recognized by the human FPRs. In contrast to the human FPRs, mFpr1 shared most of the ligands with mFpr2; out of ten ligands that activated mFpr2, nine did also induce calcium responses via mFpr1. Like hFPR1 and hFPR2, both mouse receptors responded to M-peptide, W-peptide, Ac2-26, V3 gp120 HIV (BK-130), and all three formylated peptides (Table 3-2). In addition, both murine receptors responded to Substance P and DMSO. mFpr1 proved to be selective for T20 and the murine prion fragment beta-amyloid 16-22, the latter of which did not activate any human FPR within the range of the tested concentrations. mFpr2 did selectively respond to the anti-microbial Temporin A amide .

### ***3.1.2.3. Activation pattern of mouse vomeronasal FPRs***

Unlike the human and mouse immune FPRs, the responses of the vomeronasal FPRs confined to three peptides: f-MLF (even in concentrations of 100  $\mu$ M at the detection limit), W-peptide and M-peptide were able to activate mFpr-rs1 but no other vomeronasal FPR. In order to

increase the chance of identifying possible activators for vomeronasal FPRs, the tested ligand array included a selection of structurally highly heterogeneous peptides (Table 3-2). All tested peptides that belong to the group of the eponymous N-terminally formylated peptides activated mFpr1 and mFpr2 but none of the vomeronasal FPRs in concentrations below 100  $\mu$ M (Figure 3-6). It has been shown that besides formyl peptides, N-terminally acetylated peptides are very potent FPR agonists too (Gao *et al.*, 1994). The prominent pan-immune FPR agonist Ac2-26, an acetylated mimetic of Annexin A1, was able to induce calcium responses in cells expressing mFpr1 or mFpr2. However, none of the vomeronasal FPRs showed calcium responses (Figure 3-6). V3 gp120 HIV (BK-130) was able to activate the immune receptor mFpr1 (Figure 3-6). But again, from the vomeronasal FPRs no responses were observed. Some powerful human FPR agonists are modified by an amidation at their carboxy terminus. The amidated anti-microbial Temporin A amide was able to activate mFpr2 while the viral T20 could activate cells expressing mFpr1 (Figure 3-6). Both substances were incapable of activating vomeronasal FPRs.

The complete response profile of the distinct receptors is summarized in Table 3-2. Compared to the remarkable functional similarity and the broadly tuned agonist profiles of mouse immune FPRs, a relatively narrow tuning was observed for the vomeronasal receptors (Table 3-2 and Figure 3-6), segregating the mouse FPRs into two functionally distinct groups: the promiscuous immune FPRs (including mFpr1 and mFpr2, shown in blue) and the more restrictive vomeronasal FPRs (comprising mFpr-rs1, mFpr-rs3, mFpr-rs4, mFpr-rs6, and mFpr-rs7, shown in red). This activation however is so far restricted to mFpr-rs1. mFpr-rs3, mFpr-rs4, mFpr-rs6 and mFpr-rs7 did not show specific calcium responses to any of the 23 tested ligands.

Table 3-2 | Agonist profiling of FPRs in HEK293T cells\*

Ligand	Primary structure	Ligand class	Tested concentration	hFPR1	hFPR2	hFPR3	mFpr1	mFpr2	mFpr-s1	mFpr-s3	mFpr-s4	mFpr-s6	mFpr-s7
W-peptide	WKYMVm-NH <sub>2</sub>	synthetic peptide	30 μM	●	●	(●)	●	●	●	○	○	○	○
M-peptide	MMHWA <sub>m</sub> -NH <sub>2</sub>	synthetic peptide	30 μM	●	●	●	●	●	●	○	○	○	○
Ac2-26	Ac-AMVSEFLKQAWFIENEQEYVQTVK	immunomodulatory peptide	5 μM	●	●	●	●	●	○	○	○	○	○
V3 gp120 HIV (BK-130)	RIHIGPRALYTT	viral peptide	30 μM	●	(●)	(●)	●	(●)	○	○	○	○	○
f-MLF	f-MLF	bacterial peptide	100 μM	●	●	○	●	●	(●)	○	○	○	○
CO1	f-MFINRWLFS	mitochondrial peptide	1 μM	●	●	○	●	●	○	○	○	○	○
ND1-61	f-MFFINILTL	mitochondrial peptide	1 μM	●	●	○	●	●	○	○	○	○	○
T20	Ac-YTSLIHSLEESQ <sub>N</sub> Q <sub>E</sub> KE <sub>N</sub> E <sub>L</sub> LE <sub>L</sub> DKWASLWNWF-NH <sub>2</sub>	viral peptide	10 μM	○	●	●	●	○	○	○	○	○	○
Temporin A amide	FLPLIGRVL <sub>S</sub> GIL-NH <sub>2</sub>	anti-microbial peptide	3 μM	○	●	●	○	●	○	○	○	○	○
RANTES 11-22	CFAYIARPLPRA	cytokine fragment	10 μM	○	●	●	n.d.	n.d.	○	○	○	○	○
Substance P	RPK <sub>Q</sub> QFFGLM-NH <sub>2</sub>	neuro peptide	10 μM	○	●	○	●	●	○	○	○	○	○
DMSO	C <sub>2</sub> H <sub>6</sub> O <sub>S</sub>	organic solvent	5.6 x 10 <sup>-5</sup> μM	○	●	○	●	●	○	○	○	○	○
beta-amyloid 16-22	KL <sub>V</sub> FFAE	immunomodulatory peptide	10 μM	○	○	○	●	○	○	○	○	○	○
WRW4	WR <sub>W</sub> WW-NH <sub>2</sub>	FPR2 antagonistic peptide	30 μM	○	○	●	○	○	○	○	○	○	○
C5a 37-53	RAARISL <sub>G</sub> PRC <sub>I</sub> KAFTE	synthetic antisense cytokine	10 μM	○	○	(●)	○	○	○	○	○	○	○
V3 gp120 HIV (JR-FL)	SIHIGP <sub>R</sub> AFYTT	viral peptide	30 μM	○	○	(●)	○	○	○	○	○	○	○
ADP715, HIV-1	RKRIHIGP <sub>R</sub> AFYTTKN	viral peptide	30 μM	○	○	○	○	○	○	○	○	○	○
uPAR 84-95	Ac-AVTYSRSRYLEC-NH <sub>2</sub>	immunomodulatory peptide	10 μM	○	○	○	○	○	○	○	○	○	○
Lipoxin A4	C <sub>20</sub> H <sub>32</sub> O <sub>5</sub>	immunomodulatory eicosanoid	1 μM	○	○	○	○	○	○	○	○	○	○
15-(R)-Epi-Lipoxin	C <sub>20</sub> H <sub>32</sub> O <sub>5</sub>	immunomodulatory eicosanoid	1 μM	○	○	○	○	○	○	○	○	○	○
CRAMP33	GLLRKGGEKIGEK <sub>L</sub> KKIGQKIKNFFQKLVPQPEQ	anti microbial peptide	10 μM	u.s.	u.s.	u.s.	u.s.	u.s.	u.s.	u.s.	u.s.	u.s.	u.s.
CRAMP39	ISRLAGLLRKGGEKIGEK <sub>L</sub> KKIGQKIKNFFQKLVPQPEQ	anti microbial peptide	10 μM	u.s.	u.s.	u.s.	u.s.	u.s.	u.s.	u.s.	u.s.	u.s.	u.s.
rCRAMP33	GLLRKGGEK <sub>F</sub> G <sub>E</sub> K <sub>L</sub> RKIGQKIKDFFQKLAPEIEQ	anti microbial peptide	10 μM	u.s.	u.s.	u.s.	u.s.	u.s.	u.s.	u.s.	u.s.	u.s.	u.s.

\*The table summarizes the response profiles of all tested human (h) and murine (m) receptors. The highest ligand concentrations tested are indicated. Each box represents the results from at least two independent transfections. ● = receptor-dependent calcium signal, (●) = signal at detection limit, ○ = no response, u.s. = unspecific response observed in untransfected cells, n.d. = not determined. Peptide sequences are given in one letter code. Chemical modifications: Ac = acetylation, f = formylation, m = D-methionine, NH<sub>2</sub> = amidation.

## 3.2. Structural requirements for activation of mFpr-rs1 by W-peptide

---

### 3.2.1. mFpr-rs1 shows stereo-selective tuning for related peptides containing D-amino acids

The dose-response analysis seen in Figure 3-7 shows that W-peptide and M-peptide exhibit remarkably similar affinities towards mFpr-rs1 ( $505 \pm 209$  nM for W-peptide and  $738 \pm 174$  nM for M-peptide). Both, W-peptide (WKYMVm-NH<sub>2</sub>) and M-peptide (MMHWAm-NH<sub>2</sub>) are quite different in their primary structure, i.e. the amino acid sequence. However, they share obvious structural features distinguishing them from other peptides tested in this study: first, they are rather short hexapeptides, second, they carry a C-terminal D-methionine and third, this methionine is amidated at its carboxy-terminus (Figure 3-8 A). With reference to the functional similarity, this suggests a hidden structural consensus that is necessary for the activation of mFpr-rs1.

In order to address the assumption that mFpr-rs1 exhibits structural preferences for such peptides, the pharmacology of mFpr-rs1 expressing cells was investigated on single cell resolution level. For this, a novel automated high-content single cell calcium imaging assay was established (see also chapter 2.6.2.4). To enable active removal of applied stimuli, the single cell bio-imaging system was equipped with an automated cell rinsing mechanism. Each ligand application was followed by a three minute perfusion sequence that rinsed the cells by a 256 volume buffer exchange. This assay allowed the consecutive stimulation of cells enabling investigation and comparison of calcium responses of single cells to several ligands (Figure 3-8 B). To identify cells that express mFpr-rs1, a vector coding for the green fluorescent protein eGFP was co-transfected with mFpr-rs1 in a 1/5 ratio. Since statistically only 1/5<sup>th</sup> of the plasmids were coding for eGFP it is likely that those cells expressing eGFP also express mFpr-rs1. Hence, only eGFP positive cells were investigated. 30  $\mu$ M ATP was used to verify viability/excitability of the cells at the end of the experiment.



peptides carrying an amidated C-terminal D-amino acid. To exclude that the absence of signals following the first stimulation is not due to receptor desensitization, it was checked whether the cells can be repetitively stimulated by a given stimulus (Figure 3-9). Therefore, mFpr-rs1 expressing cells were consecutively stimulated with 1  $\mu$ M W-peptide six times in five minute intervals. Of 106 viable eGFP positive cells monitored in three independent transfections,  $82 \pm 5$  % were excitable by 1  $\mu$ M W-peptide (not shown). Of 87 W-peptide excitable cells, 51 (= 58%) responded to all six consecutive applications of W-peptide.  $9 \pm 5$  % responded to five consecutive applications of W-peptide, 1% responded to four, 6% responded to three, 6% responded to two and 21% responded only to the first application of W-peptide.

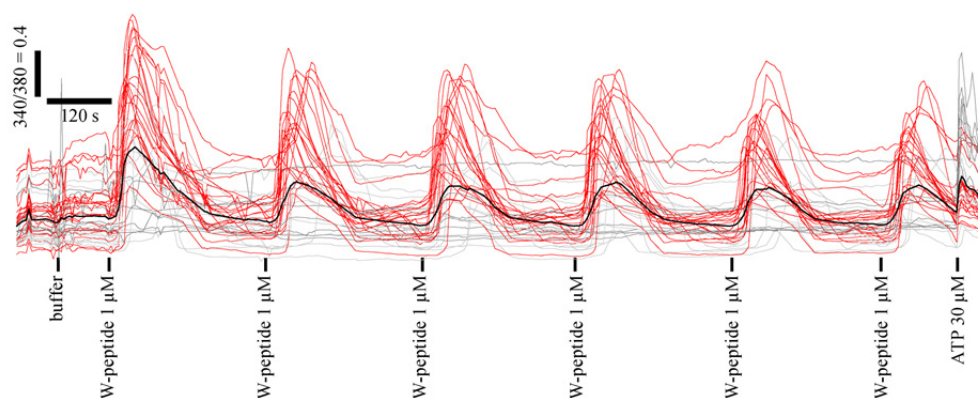


**Figure 3-9 | Single cell calcium imaging assay with buffer perfusion for repetitive stimulation**

Single cell calcium responses of HEK293T cells transfected with plasmids encoding mFpr-rs1 and GFP (ratio: 5/1) upon repeated application of W-peptide. Following each application, the cells were rinsed with 256 volumes of buffer to remove the ligand. Typical calcium imaging experiment showing that mFpr-rs1 transfected HEK293T cells can be repetitively activated by the same stimulus. Only cells expressing the green fluorescent protein eGFP were investigated. Since mFpr-rs1 was transfected in 5-fold higher amounts, it is likely that all GFP positive cells do also express mFpr-rs1. In total 32 of 39 GFP-positive cells in the visual field responded to the first stimulus. Red traces denote cells responding to the first W-peptide application. Gray = cells that did not respond to the first W-peptide stimulus. The black trace shows the averaged response. 30  $\mu$ M ATP served as excitability control. Scale bars: y-axis: Ratio 340/380 = 0.4; x-axis: 2 min. RFU = relative fluorescence units. Data are representative for three independent transfections.

Since all cells in Figure 3-9 responded to the first stimulus but not each subsequent stimulation, the averaged signal of the first calcium response is higher than the following signals. However, the average signal strength of all subsequent calcium responses is identical. This shows that mFpr-rs1 transfected cells can be stimulated by six consecutive ligand applications and that this assay is suited to monitor single cell calcium responses towards various stimulations in a row.

In order to further specify the pharmacological preferences of mFpr-rs1, additional experiments were performed in which the concentration-response behavior of W-peptide and

M-peptide was compared to their epimers, carrying the corresponding amidated L-amino acid at the C-terminus (Figure 3-10).

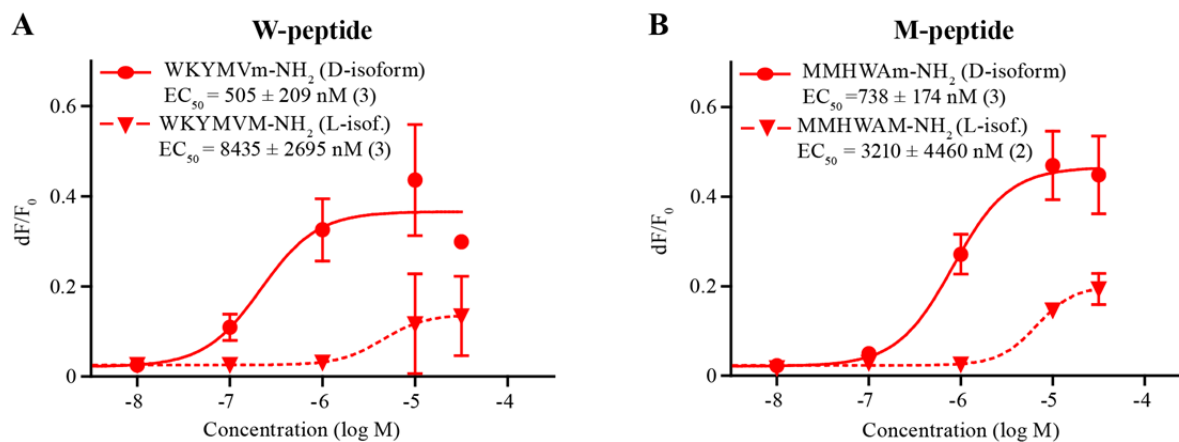


**Figure 3-10 | Heterologously expressed mFpr-rs1 prefers C-terminal D-amino acids**

Concentration-response curves of mFpr-rs1 expressed in HEK293T cells towards W-peptide and M-peptide compared to their epimers obtained by calcium imaging in the FLIPR. [A] W-peptide shows a higher affinity towards mFpr-rs1 than its epimer with a C-terminal L-amino acid. [B] M-peptide shows a higher affinity towards mFpr-rs1 than its epimer with a C-terminal L-amino acid. Amino acid sequences are given in one letter code. Lower case letters denote amino acids in D-configuration. Curves and EC<sub>50</sub> values for each substance are averaged over at least two independent experiments (see numbers in parentheses).

W-peptide exhibited an EC<sub>50</sub> value of 505 ± 209 nM on mFpr-rs1. Its epimer, L-W-peptide, showed a 16-fold increase in EC<sub>50</sub> value (Figure 3-10 A). Very similar results have been observed for M-peptide. The EC<sub>50</sub> value of L-M-peptide (3210 ± 4460 nM) was shifted to ~ 6 fold higher concentrations than that calculated for M-peptide (738 ± 174 nM) (Figure 3-10 B). In both cases the maximal signal amplitude observed after stimulation with the L-epimer was reduced around 40% compared to the amplitude caused by the D-epimer. Together, these data show that mFpr-rs1 prefers short peptides with D-amino acids rather than L-amino acids. Biogenic D-amino acids are a rather unusual feature in biosynthesized proteins. Most natural proteins and peptides consist of biogenic L-amino acids. However, certain microorganisms provide a natural source for D-amino acids (Cava *et al.*, 2011). This supports the hypothesis that mFpr-rs1 functions as a sensor for microorganisms.

### 3.2.2. Activation of mFpr-rs1 requires the four C-terminal amino acids of W-peptide

The C-terminal methionine and its stereochemistry have been shown to be important for activation of mFpr-rs1 (chapter 3.2.1). In order to identify additional key structures in W-peptide, which are necessary for activation of mFpr-rs1, a number of W-peptide derivatives with N-terminal truncations were tested on mFpr-rs1 (Figure 3-11).

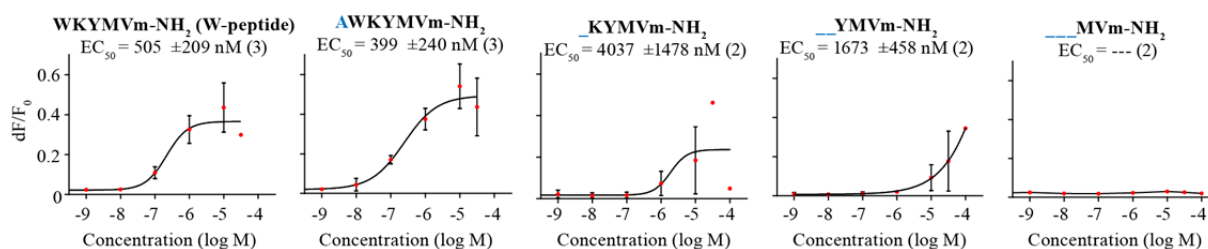


**Figure 3-11 | Amino acid residues of W-peptide critical for mFpr-rs1 activation**

Concentration-response analysis of W-peptide-derived isomers on mFpr-rs1 heterologously expressed in HEK293T cells. N-terminal truncations of W-peptide show positions that are crucial for mFpr-rs1 activation while N-terminal elongation of W-peptide did not affect affinity of the ligand towards mFpr-rs1. Blue letters indicate amino acid insertions referred to W-peptide. Blue underlines indicate elimination of amino acids referred to W-peptide. Peptide sequence is shown in one letter amino acid code. Small case letters (m) denote amino acids in D configuration. All peptides were C-terminally amidated. Experiments were in general averaged over at least two independent transfections (see numbers in parentheses). *One experiment of the MVm-NH<sub>2</sub> was conducted by Bernd Buße.*

To determine the influence of the peptide length on mFpr-rs1 activation, several elongated and truncated peptide derivatives were tested (Figure 3-11). Elongation of W-peptide by one N-terminal alanine resulted in an EC<sub>50</sub> value of 399 ± 240 nM, which is close to the EC<sub>50</sub> value gained for W-peptide (505 ± 209 nM) (Figure 3-11). This suggests that elongations at the N-terminus display minor influence on the affinity towards mFpr-rs1. However, deletion of the first N-terminal amino acid position (W<sub>1</sub>) led to a ~ 10-fold right shift of the concentration-response curve with an EC<sub>50</sub> value of 4037 ± 1478 nM (Figure 3-11). Removal of the first two N-terminal amino acids (W<sub>1</sub>, K<sub>2</sub>) showed an EC<sub>50</sub> value of 1673 ± 458 nM. Deletion of the first three N-terminal amino acids including the tyrosine in the third position (W<sub>1</sub>, K<sub>2</sub> and Y<sub>3</sub>) resulted in a complete loss of capability to activate the receptor. It seems that tyrosine at amino acid position three is a key feature for interaction between W-peptide and mFpr-rs1. These data show that the last four C-terminal amino acids are critical for receptor-ligand interaction, and that the N-terminal influence is less important. Furthermore, the tyrosine, i.e. the 4<sup>th</sup> residue, counted from the C-terminus, seems to play a key role in the interaction between mFpr-rs1 and W-peptide

### 3.2.3. Influence of C-terminal amidation of W-peptide on affinity<sup>6</sup> to mFpr-rs1

In addition to peptide length and the stereo-selective preference, the chemical modification of W-peptide and M-peptide might be important for activation of mFpr-rs1. Thus, it was tested whether this amidation could influence the peptide's affinity towards the receptor.

<sup>6</sup> The term affinity is usually used in ligand binding assays. I will refer to this term to describe the sensitivity of receptor activation by a given ligand in terms of intracellular calcium mobilization.

Comparison of concentration-response curves between the amidated W-peptide (WKYMVm-CONH<sub>2</sub>) and a non-amidated isoform (WKYMVm-COO<sup>-</sup>) showed that the presence of the amidation does indeed increase the affinity towards mFpr-rs1 (Figure 3-12). When the C-terminal amidation was removed, exhibiting the negatively charged carboxyl-tail with a delocalized electron, there was a ~ 16-fold decrease in affinity, with EC<sub>50</sub> values of 505 ± 209 nM for the amidated W-peptide and 8307 ± 3370 nM for the isomer with the free carboxyl moiety. Moreover, the peak signal observed for the carboxylated isomer was about 60% reduced compared to the amidated W-peptide. In order to determine whether the nitrogen of the amide moiety is important, the C-terminal amide group was replaced by a C-terminal formaldehyde (-CHO). This group contains the same carbonyl group (-C=O) as the amidated residue (Figure 3-12), is uncharged under physiological conditions and does not contain a nitrogen atom. Interestingly, this modification was able to rescue the loss of affinity towards mFpr-rs1. Its EC<sub>50</sub> value (1016 ± 18 nM) was only about two times higher than that of the amidated W-peptide but approximately eight times lower than that of the unmodified W-peptide. Interestingly, the maximal signal amplitudes observed for the aldehyde isomer were comparable to that of the amidated W-peptide (Figure 3-12). Together, these data demonstrate the importance of the C-terminal amidation for the W-peptide consensus motif. Moreover, they indicate that the carbonyl moiety (-C=O) rather than the amine is the determinant for W-peptide sensitivity towards mFpr-rs1.

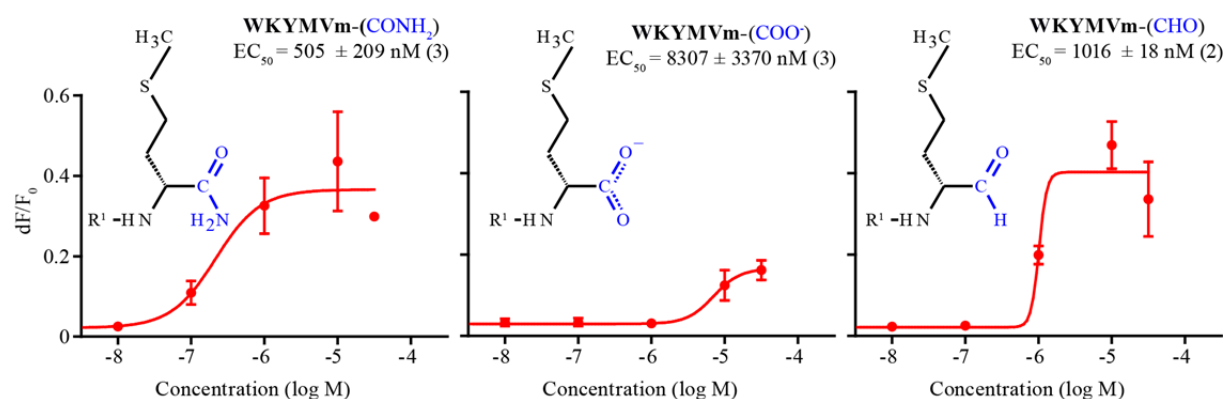


**Figure 3-12 | Heterologously expressed mFpr-rs1 is selective towards C-terminally amidated W-peptide**

Concentration-response curves of mFpr-rs1 expressed in HEK293T cells towards W-peptide, a non-amidated derivative and a derivative carrying a C-terminal aldehyde obtained by calcium imaging. Amino acid sequences are given in one letter code. Lower case letters denote amino acids in D-configuration. Curves and EC<sub>50</sub> values are averaged over at least two independent experiments (see numbers in parentheses). The chemical structures show the D-methionine of the tested peptide (m) with the corresponding C-terminal modification/moiety. Blue letters indicate the modification of the C-terminal D-methionine: (CONH<sub>2</sub>) = C-terminal amidation, (COO<sup>-</sup>) = free carboxyl group with a negative net charge (-1), (CHO) = C-terminal aldehyde.

### 3.2.4. Activation of mFpr-rs1 by N-terminally formylated peptides

The experiments described in 3.2.1 show that W-peptide, carrying a C-terminal D-methionine that has C-terminal formaldehyde is an activator of mFpr-rs1. Notably, N-terminal formylation describes the addition of formaldehyde to the N-terminus of a peptide. The only difference between an N-terminal formylation and C-terminal formaldehyde is that the N-terminal aldehyde group is added to the nitrogen of the peptide's amino moiety (Figure 3-13).

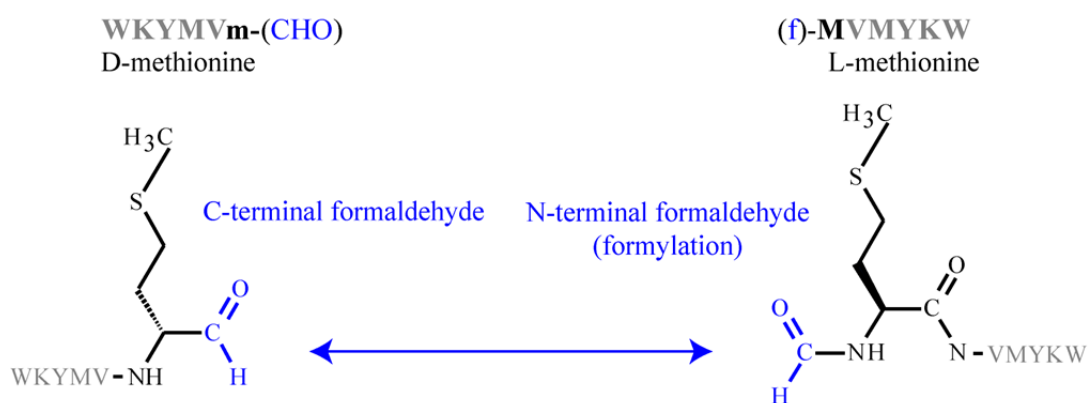


**Figure 3-13 | Stereo-chemical resemblance of D-methionine carrying a C-terminal formaldehyde function and L-methionine with N-terminal formylation**

[A] Structural comparison of C-terminal D-methionine (m) with a formaldehyde group at its carboxy-tail and a N-terminal L-methionine (M) that is formylated at its amino-terminus. The structures of the corresponding methionines are shown in natta projections (black). They are part of a peptide chain which is shown in gray capitals. The corresponding modifications are shown in blue. The D-methionine is part of a W-peptide derivative carrying a C-terminal aldehyde (left) and the L-methionine is part of the retro-inverted W-peptide (right) as measured with calcium imaging in the FLIPR.

Since both formaldehyde groups contain the essential carbonyl moiety (chapter 3.2.3), it is tempting to hypothesize that if amidated peptides activate FPRs including the vomeronasal mFpr-rs1, formylated peptides will do so as well. To address this hypothesis, an N-terminally formylated, retro-inverse<sup>7</sup> isomer of the W-peptide was synthesized. To understand the biochemistry and the structural requirements of a retro-inversion the following has to be considered: W-peptide probably binds to the receptor's binding pocket by exposing its C-terminal tail carrying an amidated methionine (or the formaldehyde, respectively). If the amino acid sequence of W-peptide (WKYMVm) was reversed i.e. turned around to mVMYKW (= retro-peptide), it would be logical that this retro-peptide would use the same receptor binding pocket as W-peptide, only with its N-terminus exposed. Formylation would

<sup>7</sup> I refer to this peptide as a retro-inverse peptide: the peptide's amino acids are assembled in reverse order but only the terminal D-methionine has been replaced by its (L-) stereoisomer. A reversed peptide in which all amino acids have been replaced by the corresponding stereoisomer is termed retro-inverso peptide.

introduce the formaldehyde group to the N-terminus of methionine. According to the rules of Cahn, Ingold and Prelog (Cahn, Ingold and Prelog, 1966), reversal of a peptide sequence results in a change of the relative chemical configuration of the amino acids because the positions of the carboxyl and amine groups in the amide bonds are exchanged. To compensate for this, the D-conformation of methionine (mVMYKW) must be inverted to the L-conformation (MVMYKW), which equals the exchange of the side chain's positions. Both changes at the same time (a retro-inversion) command a double change of absolute configuration of the methionine's chirality center. By inducing this double change of the absolute configuration, the original relative configuration is retained (Cahn, Ingold and Prelog, 1966; Brady and Dodson, 1994).

To test this hypothesis, a formylated retro-inverted peptide (f-MVMYKW) was chemically synthesized and tested on mFpr-rs1 (Figure 3-14). Interestingly, the retro-inverted peptide displayed an  $EC_{50}$  value of  $3017 \pm 1150$  nM, which is approximately three times higher than that observed for the W-peptide with the C-terminal aldehyde (WKYMVm-CHO;  $EC_{50} = 1016 \pm 18$  nM) (Figure 3-14). Although the curve of the retro-inverted W-peptide had a shallower slope than that of WKYMVm-CHO (Figure 3-14), the peak responses were comparable in height. These data suggest that there is a clear structural link between N-terminally formylated and C-terminally amidated peptides in respect to FPR activation. Furthermore, they demonstrate that heterologously expressed mFpr-rs1 can be activated by formylated peptides.

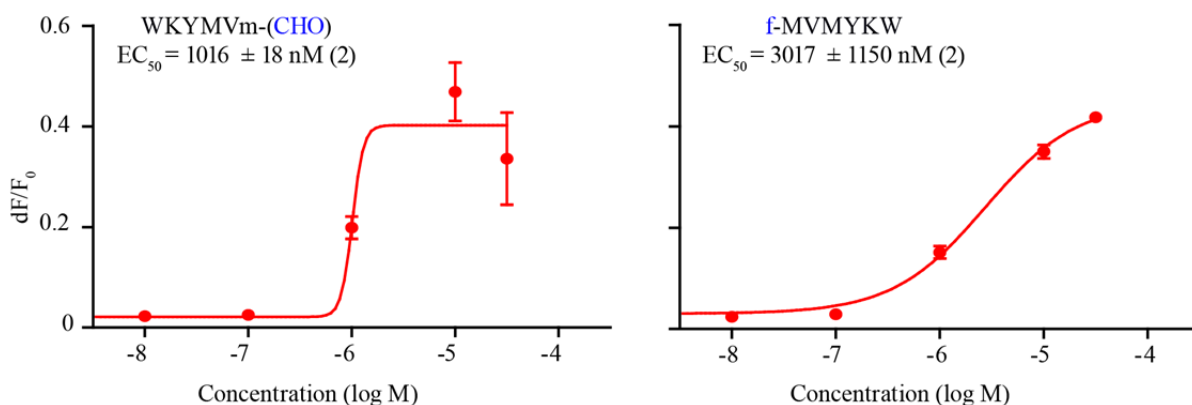


**Figure 3-14 | Heterologously expressed mFpr-rs1 can be activated by formyl peptides**

Concentration-response curves of mFpr-rs1 expressed in HEK293T cells towards a W-peptide derivative carrying a C-terminal aldehyde (left) and the retro-inverted W-peptide (right) as measured with calcium imaging in the FLIPR. The corresponding modifications of the terminal methionines are shown in blue. Data were averaged over two independent transfections. Error bars = SD.

The experiments illustrated so far have shown that heterologously expressed mFpr-rs1 is activated by W-peptide. Furthermore, it has been demonstrated, that the receptor is activated by this peptide if certain key requirements are met. First, the peptide needs a minimal length of four amino acids, second, the peptide must carry a C-terminal methionine in D-configuration and third, this methionine must be amidated or carry a formaldehyde moiety at its carboxyl-tail. Interestingly, the amino acid sequences of W-peptide and its truncated isoforms that were able to activate mFpr-rs1 are found in proteins and peptides of microbes (Table 3-3). For example, sequence blast for the sequence KYMVM yielded 367 hits in the UniProtKB database of which the majority (> 86%) refers to microorganisms like bacteria, fungi and viruses (Table 3-3 A). Interestingly, a number of these hits were identified for various pathogenic microorganisms. The sequence KYMVM for example has been identified for the Iron-regulated surface determinant protein B (A7X146) of *Staphylococcus aureus* or a DNA methylase of *Leptospira biflexa* (Table 3-3 B).

Considering that mFpr-rs1 is also activated by N-terminally formylated peptides, these data provide evidence that supports the idea that mFpr-rs1 is able to recognize pathogenic organisms or molecules.

**Table 3-3 | mFpr-rs1 agonist motifs are frequently found in proteins of various pathogenic microorganisms\***

**A**

Motif	Total hits	bacteria	fungi	virus	mouse	human
WKYMVM	1	100%	0	0	0	0
KYMVM	367	76 %	10%	0.3%	0	0
YMVM	8160	58%	8%	0.5%	0.6%	1.3%

**B**

Motif	Pathogen	Protein	Accession
WKYMVM	<i>Kribbella flavida</i>	Cyanobacterial globin	D2PTJ8
KYMVM	<i>Staphylococcus aureus</i>	Iron-regulated surface determinant protein B	A7X146
KYMVM	<i>Leptospira biflexa</i>	DNA methylase	B0SG88
KYMVM	<i>Fluoribacter gormanii</i>	FEZ-1 protein	Q9K578
YMVM	<i>Candida albicans</i>	Pheromone-regulated membrane protein 10	Q5AH11
YMVM	<i>Clostridium novyi</i>	UDP-N-acetylglucosamine 2-epimerase	A0PZ05
YMVM	<i>Burkholderia mallei</i>	Putative serine/threonine protein kinase	A5TNL9
YMVM	<i>Haemophilus influenzae</i>	Lon protease	A5UA27
YMVM	<i>Yersinia pestis</i>	Putative ABC transport integral membrane subunit	A6BSU6
YMVM	<i>Listeria monocytogenes</i>	Glycerol uptake operon antiterminator regulatory protein	Q4ETR1
YMVM	<i>Suid herpesvirus 1</i>	Major capsid protein	Q00705
YMVM	<i>Lymphocytic choriomeningitis virus</i>	RNA-directed RNA polymerase L	E2D673

\* **[A]** The table lists the number of database hits for the indicated peptide motifs and their distribution in distinct phylogenetic branches. **[B]** The table shows some examples of natural pathogens that exhibit the peptide motif in proteins. The sequences were identified via assessing UniProtKB/SwissProt, UniProtKB/ TrEMBL (July 2012) employing the ScanProsite software (release 20.83) and the taxa analysis tool.

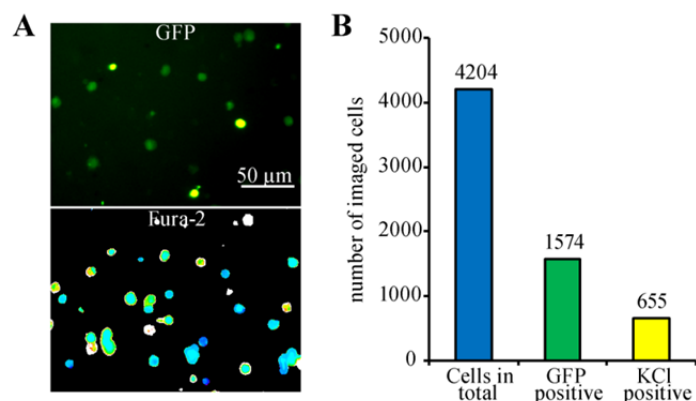
### 3.3. Vomeronasal sensory neurons of mice respond to the mFpr-rs1 ligand W-peptide

The results in chapter 3.2 have shown that the vomeronasal receptor mFpr-rs1 is activated by W-peptide when expressed in HEK293T cells. It would be interesting to see whether this substance can be recognized by neurons of the vomeronasal sensory epithelium where mFpr-rs1 is naturally expressed. Therefore, ligand-dependent responses of dissociated vomeronasal sensory neurons (VSNs) were investigated in single cell calcium imaging.

In order to investigate the pharmacology of vomeronasal sensory neurons, the VNO was extracted from mice and dissociated enzymatically (chapter 2.3.5). To visualize olfactory neurons the mice expressed the green fluorescent protein GFP under control of the OMP promoter. The olfactory marker protein (OMP) is expressed in sensory neurons of olfactory organs, i.e. all OMP positive sensory neurons express GFP and therefore, VSNs can be easily identified by green fluorescence. Fluorescence analysis showed that of 4204 cells in the visual field, isolated from 27 animals, 1574 cells (~ 37%) had intense green fluorescence (Figure 3-15). In order to investigate whether these cells are excitable, they were challenged with 80 mM KCl in single cell calcium imaging. In vomeronasal sensory neurons application of high KCl concentrations leads to calcium influx, presumably through activation of voltage gated calcium channels (Holy *et al.*, 2000; Hardingham *et al.*, 1999). Indeed, application of KCl showed that 655 of the 1574 GFP expressing cells (~ 42%) responded to KCl with calcium signals (Figure 3-15 B).

**Figure 3-15 | Identification of acutely dissociated mouse vomeronasal sensory neurons**

[A] Vomeronasal sensory neurons of OMP/GFP mice express GFP under control of the OMP promoter. GFP expressing cells show green fluorescence. Total number of cells is visualized by the calcium dye Fura-2. [B] 35% of the cells isolated via dissociation of the VNO are GFP labeled sensory neurons. Of those, ~ 30% can be activated by KCl. Data are summarized for 27 animals.



In order to test whether the neurons can be activated by chemosensory stimuli, the cells were challenged with several substances (described in the following paragraph) that are known to activate cells of the VNO in consecutive applications. If cells responded to pre-application of buffer, a control for applicational artifacts, they were removed from evaluation.

First, it was analyzed whether the neurons respond to classical VNO agonists like ESP-1 (Kimoto *et al.*, 2005) and n-pentyl acetate (Del Punta *et al.*, 2002). The exocrine gland secreted peptidic pheromone ESP-1 is a known activator of distinct V2R positive neurons and has since been used in several studies (Kimoto *et al.*, 2005; Leinders-Zufall *et al.*, 2014). The volatile pheromone n-pentyl acetate, which is found in mouse urine (Novotny *et al.*, 1986), is an activator of distinct V1R associated neurons (Del Punta *et al.*, 2002). When ESP-1 was applied to the neurons, 24 of 655 KCl positive neurons (~ 3.7%) responded to the stimulus with calcium transients (Figure 3-16 A, B and C). n-pentyl acetate induced responses in 21 of 655 (~ 3.2%) of the neurons. V1R neurons and V2R neurons reside in different anatomical zones of the VNO (chapter 1.1). It is therefore unlikely, that one neuron responds to both stimuli by GPCR-mediated signaling. Analyses showed that only three of 655 neurons (~ 0.45%) responded to both stimuli (Figure 3-16 B). This was counted as background signal. Next it was tested whether the neurons respond to application of classical immune FPR ligands: W-peptide, L-W-peptide, f-MLF, ND1-6I, and ND1-6T. The formylated peptides f-MLF, ND1-6I, and ND1-6T have already been shown to activate cells in the vomeronasal organ (Rivière *et al.*, 2009; Chamero *et al.*, 2011; Leinders-Zufall *et al.*, 2014) and served as additional positive controls. The applications scheme was based on a randomized selection. First, buffer was applied to check for application artifacts. Second, the ligands L-W-peptide, D-W-peptide, f-MLF, ND1-6I, ND1-6T, ESP-1, iso-pentyl acetate, 2-heptanone, and an additional buffer application were applied in a randomized order. Following this, the cells were stimulated with KCl to check their viability. If a cell responded to the initial buffer application, it was removed from evaluation. Although the background caused through application artifacts was below 0.5% (Figure 3-16 B and C), only the first ligand-dependent response was analyzed (Figure 3-16 D). Analyses showed that application of the formylated peptides f-MLF, ND1-6I, and ND1-6T-induced responses in 1.7%, 1.8%, and 2.3% of the neurons, respectively (Figure 3-16 D). Interestingly, 2.4% and 3.4% of the neurons responded to W-peptide and L-W-peptide, respectively (Figure 3-16 D).

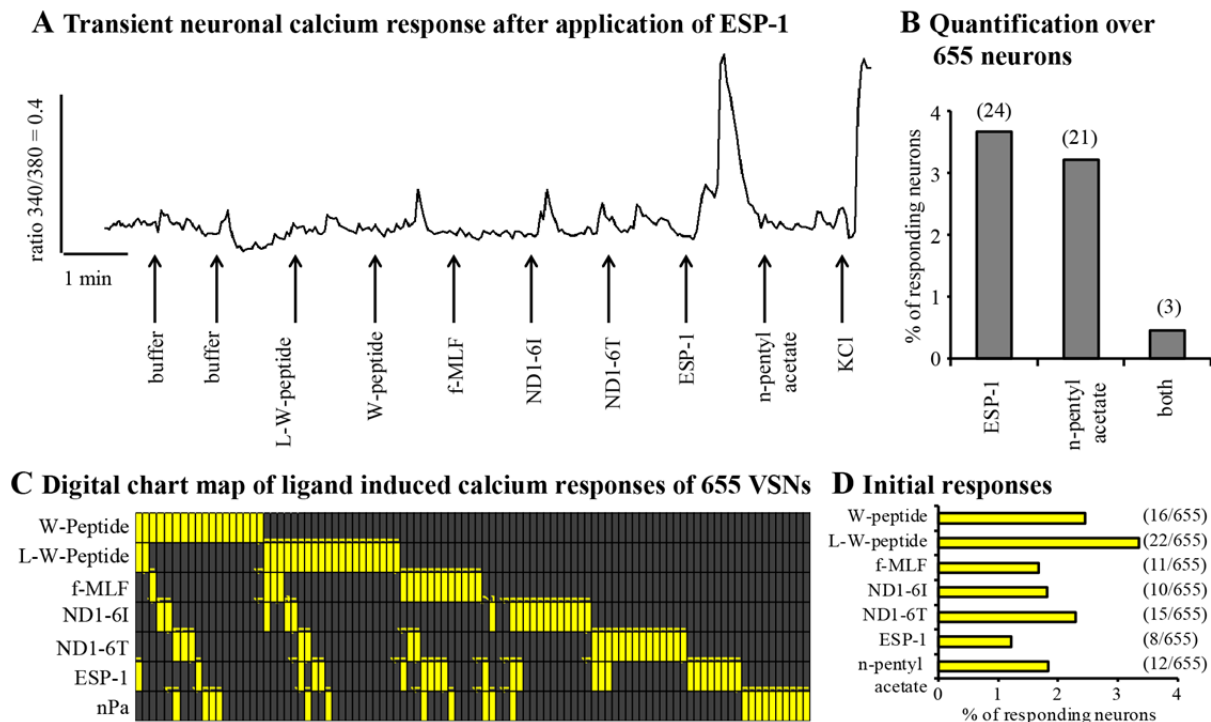


**Figure 3-16 | Calcium imaging of vomeronasal sensory neurons**

Calcium imaging of dissociated vomeronasal sensory neurons. **[A]** Representative calcium trace of VSN responding to ESP-1 from one experiment. **[B]** Quantification of ESP-1 and n-pentyl acetate responses over eight experiments. **[C]** Chart map summarizing calcium transients of KCl positive vomeronasal sensory neurons in response to diverse stimuli. Each column represents one of 655 KCl positive VSNs. Calcium responses to a certain stimulus are indicated by yellow boxes. Data are summarized over six experiments. **[D]** Quantification of responses to several stimuli. Only the first ligand-induced calcium signal was taken for the statistics. If a neuron responded to a second stimulus, this response was not counted. The used concentrations were: L-W-peptide [5  $\mu$ M], W-peptide [5  $\mu$ M], f-MLF [9  $\mu$ M], ND1-6I [1  $\mu$ M], ND1-6T [1  $\mu$ M], ESP-1 [0.9 nM], n-pentyl acetate [1  $\mu$ M], and KCl [80 mM].

These data show that the neurons can be stimulated by application of classical activators of the VNO. They furthermore indicate that neurons respond to application of the mFpr-rs1 agonist W-peptide. In order to address the specificity of the responses a set of experiments was analyzed in which the cells were stimulated with the above used ligands. In these experiments however, L-W-peptide was applied before W-peptide (both 5  $\mu$ M). 5  $\mu$ M is below the EC<sub>50</sub> value of L-W-peptide on mFpr-rs1 but about ten times higher than that of W-peptide (Figure 3-10). It was thus hypothesized that a neuron responding to W-peptide but not L-W-peptide might be activated via mFpr-rs1. Of 863 analyzed cells 27 (~ 3.1%) and 23 (~ 2.7%) responded to L-W-peptide and W-peptide, respectively, with calcium transients (Figure 3-17). Only three cells (~ 0.3%) responded to both stimuli. Interestingly, this is close to the number of responders toward W-peptide and ESP-1: only two cells (~ 0.2%) responded to both stimuli. This corresponds with the background signal: 0.2% of the neurons responded to W-peptide and an additional buffer application (Figure 3-17 B).

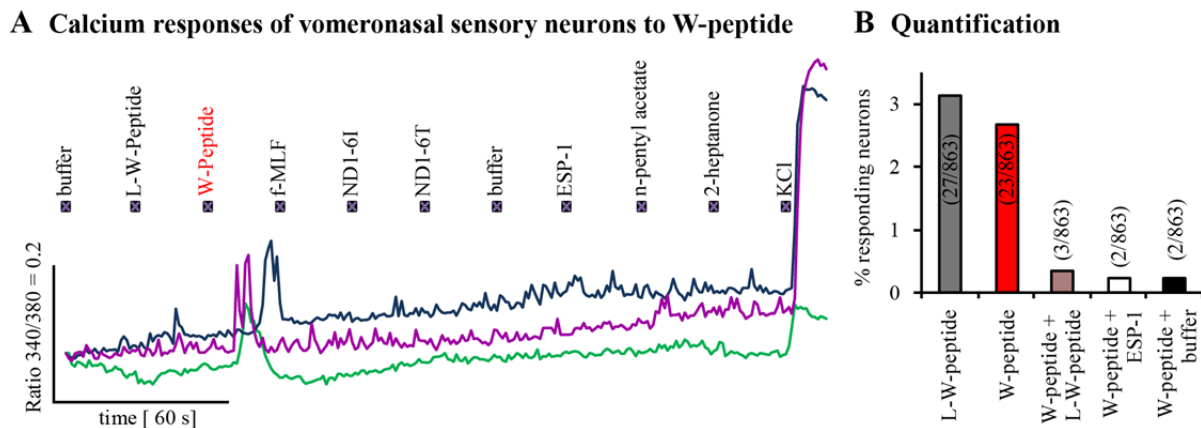


**Figure 3-17 | Vomeronasal sensory neurons respond to W-peptide**

Calcium imaging of dissociated vomeronasal sensory neurons. **[A]** Representative calcium traces of three VSNs responding to W-peptide from one experiment. **[B]** Quantification of W-peptide-induced responses over eight experiments. The used concentrations were: L-W-peptide [5  $\mu$ M], W-peptide [5  $\mu$ M], f-MLF [9  $\mu$ M], ND1-6I [1  $\mu$ M], ND1-6T [1  $\mu$ M], ESP-1 [0.9 nM], n-pentyl acetate [1  $\mu$ M], 2-heptanone [1  $\mu$ M], and KCl [80 mM].

These data show that a number of vomeronasal sensory neurons can be activated by the mFpr-rs1 agonist W-peptide in a specific manner. Since mFpr-rs1 is a receptor for W-peptide, these responses could possibly be mediated by mFpr-rs1, expressed in vomeronasal sensory neurons.

### 3.4. Formyl peptide receptor-dependent recognition of bacterial signal peptides by the mammalian innate immune system

As presented in chapter 3.2 the vomeronasal mFpr-rs1 is activated by peptides whose amino acid motifs are found in proteins of pathogens. Furthermore, mFpr-rs1 is activated by N-terminally formylated peptides, a hallmark attributed to bacteria. By employing and extending these data in a side project, conducted by Bufe and Schuman *et al.*, we could demonstrate that bacterially-derived N-terminally formylated signal peptides, and their N-terminal breakdown products are capable of activating all heterologously expressed human and mouse immune FPRs as well as mFpr-rs1 (Bufe *et al.*, 2015). Many secreted proteins or proteins inserted into the bacterial cell wall contain a cleavable signal peptide at their N-terminus. They serve as sorting tags for the proteins, recognized by the bacterial transport, export and secretion machinery and are usually cleaved from the mature protein after export (Dalbey *et al.*, 2012). Sec-dependent translocation is by far the best-investigated and apparently most common export mechanism. Signal peptides associated with the Sec machinery consist of three domains. Typically these domains contain a positively charged

N-terminal tail (n-region, 3 - 25 amino acids), a hydrophobic, helix-forming domain (h-region, 6 - 18 amino acids) and a C-region (1 - 11 amino acids) that contains the cleavage signal (Chatzi *et al.*, 2013). We could show that mouse and human immune FPRs (mFpr1, mFpr2, hFPR1, hFPR2 and hFPR3) recognize more than 20 of these signal peptides or their n-regional domains (Bufe *et al.*, 2015). Some of these peptides exhibited remarkable affinities (with EC<sub>50</sub> values in the lower picomolar range) to the immune FPRs, underlining their biological significance (Bufe *et al.*, 2015).

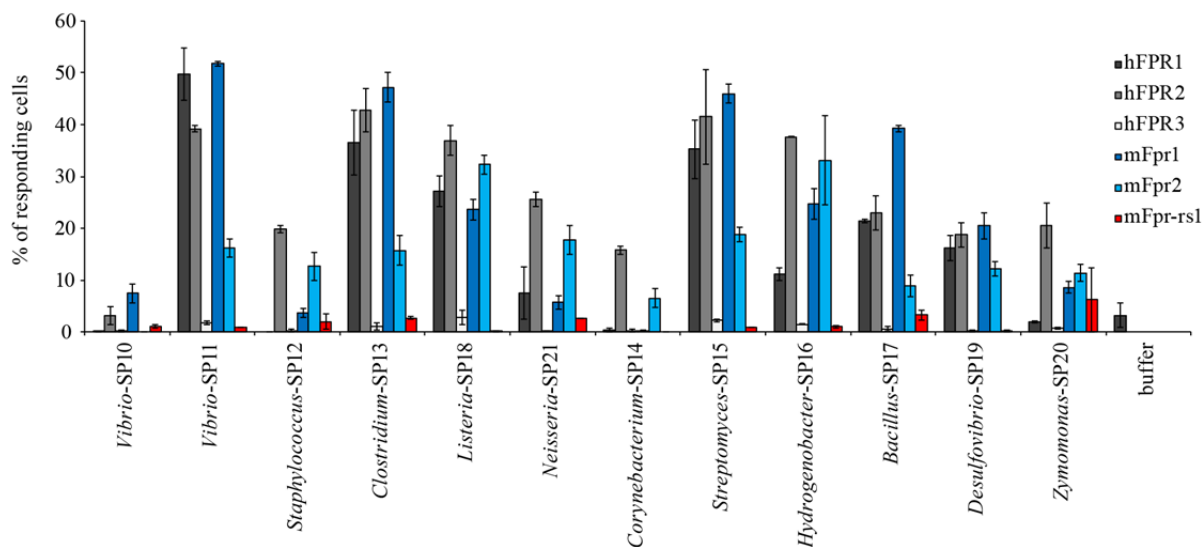


**Figure 3-18 | Heterologously expressed FPRs of human and mouse recognize bacterial signal peptides in single cell calcium imaging**

The diagram shows the result of a single cell calcium imaging experiment of FPRs heterologously expressed in HEK293T cells. Twelve out of twelve experimentally confirmed signal peptides activated at least one member of the human and mouse FPR family. On average, for each substance and each receptor  $702 \pm 246$  cells have been observed. All receptors recognize signal peptides derived from non-pathogens and pathogens as well. All agonists were applied at 10  $\mu$ M.

However, thus far the pharmacological characterization of these peptides was restricted to analysis of heterologously expressed FPRs (Figure 3-18). The next important step was to investigate whether these peptides are recognized by FPRs naturally expressed on immune cells and whether they can induce immune responses through these receptors. To address these questions I first used primary human monocytes isolated from healthy donors. They are known to express hFPR1 and hFPR2, the most prominent FPRs, in high amount (Migeotte *et al.*, 2006). In the past, naïve monocytes have frequently been used in calcium imaging to investigate the function of formyl peptide receptors. Therefore, I decided to utilize this cell type to understand whether and how bacterial signal peptides induce immune responses in cells of the innate immune system.

### 3.4.1. Formyl peptide receptor-mediated recognition of bacterial signal peptides by human monocytes

#### 3.4.1.1. Primary human monocytes can be measured by high-throughput calcium imaging

In order to get first insights into the pharmacology of signal peptides on cells of the innate immune system, human monocytes were challenged with *Streptococcus*-SP1 (SP1). This N-terminal signal peptide fragment is derived from a hyaluronidase of the zoonotic pathogen *Streptococcus suis*. It proved to be highly affine for hFPR1 in calcium imaging experiments on heterologously expressed FPRs, exhibiting an EC<sub>50</sub> value of ~ 2 nM (Bufe *et al.*, 2015). When the isolated monocytes were challenged with SP1 in first experiments, they responded with clear calcium transients (Figure 3-19). These signals were concentration-dependent, with an EC<sub>50</sub> value ( $4.8 \pm 4.7 \times 10^{-9}$  M) closely relating to that described for heterologously expressed hFPR1 (Bufe *et al.*, 2015) (Figure 3-19).

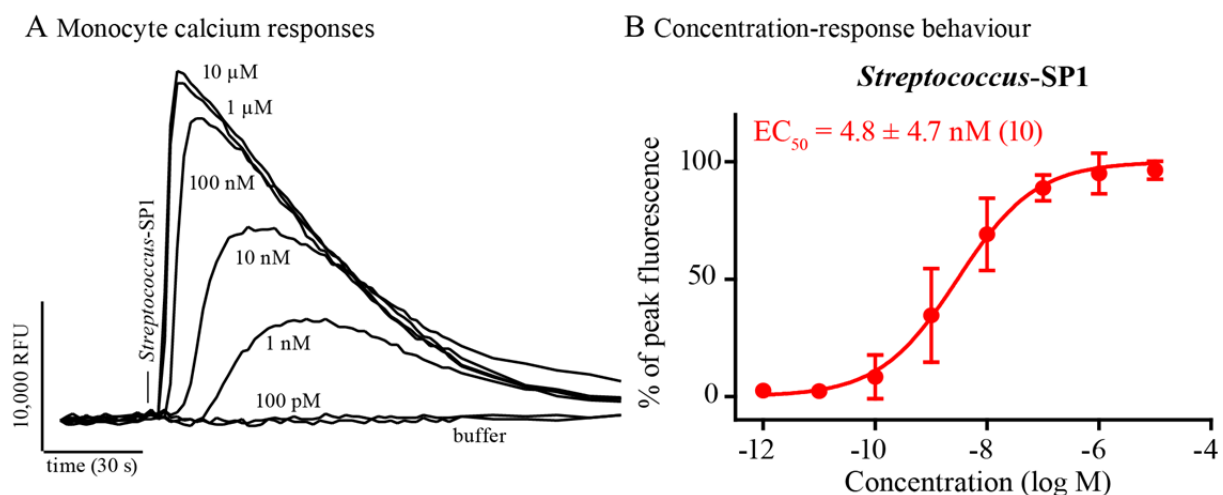


**Figure 3-19 | Calcium imaging of primary human monocytes upon stimulation with *Streptococcus*-SP1**

[A] Concentration-response experiment as measured in the FLIPR: shown are calcium transients of primary human monocytes of one donor upon stimulation with decreasing concentrations of the signal peptide fragment *Streptococcus*-SP1. RFU = relative fluorescence units. Traces are representative for ten donors. [B] Calculated concentration-response curves for monocytes stimulated with *Streptococcus*-SP1. Curve is averaged over ten donors.

These experiments show that human monocytes can be activated by the signal peptide *Streptococcus*-SP1 in calcium imaging experiments in a concentration-dependent manner. In addition, the affinity of SP1 towards monocytes is comparable to that of heterologously expressed hFPR1. So far, this does not mean that the signals are produced by monocytes and that these signals are mediated by hFPR1. In order to investigate which cells generate the calcium signals, single cell calcium imaging was used in combination with *post-hoc* immunocytochemistry. With this method, single cells are observed in calcium imaging and

then stained with antibodies directed against specific molecules like hFPR1. Employing this method should facilitate the co-localization of calcium signals with cell surface expression of hFPR1 or the monocyte marker CD14.

Before immunocytochemical analysis was performed, it was tested whether the used FPR antibodies were specific for the desired FPR. Specificity of the commercially available FPR antibody was investigated on fixated, unpermeabilized HEK293T cells, transfected with *hFPR1*, *hFPR2* or *hFPR3*<sup>8</sup> (Appendix 3). The images showed a clear, intense fluorescence of hFPR1 expressing cells stained with the anti-hFPR1 antibody (Appendix 3, upper panel). Quantification of the results (Appendix 3, lower panel) showed that  $38.5 \pm 4$  % of the cells expressed hFPR1, while no staining was detected for hFPR2 and hFPR3. The anti-hFPR2 and anti-hFPR3 antibodies were used to confirm that these receptors are expressed, underlining the specificity of the hFPR1 antibody. The anti-hFPR2 antibody stained  $25.3 \pm 7.8$ % of *hFPR2* transfected cells; no stainings were observed for *hFPR1* or *hFPR3* transfected cells. The anti-hFPR3 antibody stained  $32.5 \pm 3.6$  % of the cells transfected with *hFPR3*. No staining was observed for cells transfected with *hFPR1* or *hFPR2*. These data show that the antibodies used for immunocytochemical stainings of monocytes can differentiate between the FPRs and that they can be used for detection of FPRs expressed on the cells surface of monocytes.

Monocytes are  $\sim 10$   $\mu\text{m}$  in diameter<sup>9</sup> (in suspension) with a kidney bean shaped nucleus and express the surface marker hCD14 in high amounts (Ziegler-Heitbrock *et al.*, 1993). Therefore, first immunocytochemical stainings were done utilizing an anti-hCD14 antibody. Evaluations of these stainings showed that  $70.1 \pm 9.4$ % of all nucleated cells were positive for hCD14 (Figure 3-20 A). In contrast,  $4.4 \pm 4$ % of the cells were positive for the corresponding isotype control (MOPC-21). Of cells stained with anti-hFPR1,  $68.5 \pm 10$ % were positive, while the background, determined with the isotype control (anti-KLH), was  $5.2 \pm 3.1$ % (Figure 3-20 B). Of those stained positive for hFPR1,  $\sim 70$ % had a nucleus with a clear bean-like shape (Figure 3-20 C, red arrow). Similar results were observed for hFPR2. When incubated with an anti-hFPR2 antibody,  $\sim 70$ % of the cells were stained (Appendix 2). This number is comparable to the expression levels monitored for hFPR1. In order to confirm that the observed responses are generated by monocytes and that they are hFPR1-dependent, single cell experiments were coupled with immunocytochemistry to perform *post-hoc* analysis.

---

<sup>8</sup> Those three were unmodified receptors, without Rho-tag

<sup>9</sup> Adherent monocytes span up to 20  $\mu\text{m}$  in diameter, according to the strength of adhesive forces.

Stimulation of monocytes by 70 nM *Streptococcus*-SP1 showed a clear calcium response by 85% of the cells (Figure 3-20 D). Of those,  $92 \pm 10\%$  were positively stained for hFPR1, while the remaining  $8 \pm 10\%$  of responders were hFPR1 negative (Figure 3-20 E).

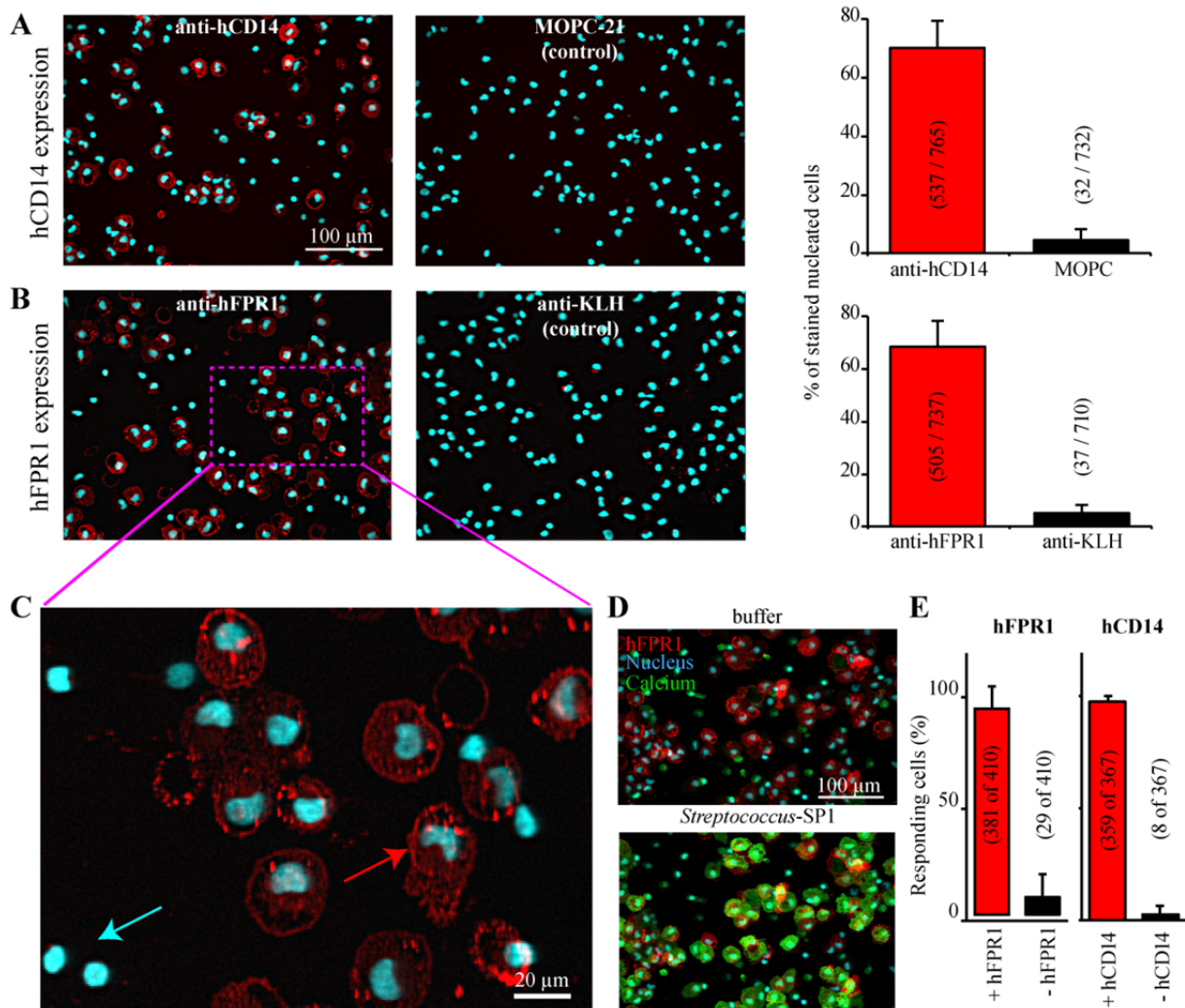


**Figure 3-20 | Immunofluorescence of surface receptors on human monocytes**

Shown are immunocytochemical cell surface stainings of primary human monocytes with antibodies directed against hCD14 and hFPR1, respectively. **[A]** Left: Representative immunostainings for the monocyte/macrophage surface marker hCD14. Right: Column chart showing that 537 of 765 nucleated cells are stained positive for hCD14. The MOPC-21 antibody served as an isotype control. **[B]** Left: Representative immunostainings for hFPR1. Right: The columns show that 505 of 737 nucleated cells are stained positive for hFPR1 while the isotype control (anti-KLH) remained negative. **[C]** Cells stained positive for hFPR1 have a bean shaped nucleus that is typical for monocytes (red arrow) while non-stained cells predominantly have a round nucleus (blue arrow). Images are representative for at least three donors. Quantifications were averaged over three donors. **[D]** *post-hoc* analysis of human monocytes after single-cell calcium imaging. Typical *post-hoc* analysis experiment. After the calcium imaging, the cells were stained for hFPR1. Images of the calcium signals and the immunostaining were then merged and analyzed. Cells stained positively for hFPR1 are shown in red, nuclear counterstain in cyan. Rise in intracellular calcium is shown in green. The images denoted with “buffer” and “*Streptococcus*-SP1” show the peak calcium responses after application of buffer or 68 nM SP1. **[E]** Quantification of the results shown in B, averaged over three donors. The chart shows the percentage of SP1-responders that are stained positively for hFPR1 or the isotype control KLH, respectively. Numbers in parentheses show how many cells responded and how many cells were present in the visual field. *D and E by courtesy of Carsten Kummerow.*

Repetitions of these experiments with hCD14 stained cells showed comparable results with 92% of the SP1 responders being positive for hCD14 (Figure 3-20 E).

These results demonstrate that responses induced by the signal peptide fragment SP1 are generated by hFPR1 expressing monocytes.

### 3.4.1.2. Bacterial signal peptides activate human monocytes by utilizing FPRs

To assess the question whether the SP1-induced responses are mediated by formyl peptide receptors, several control experiments were performed by employing *Streptococcus*-SP1. In order to get first insights into the specificity of the signal peptide SP1, the calcium responses were investigated in cross-desensitization experiments. Application of 20 nM f-MLF induced clear calcium responses in monocytes. Subsequent application of 100 nM SP1 elicited a calcium signal that was ~ 5 times reduced in amplitude (Figure 3-21).

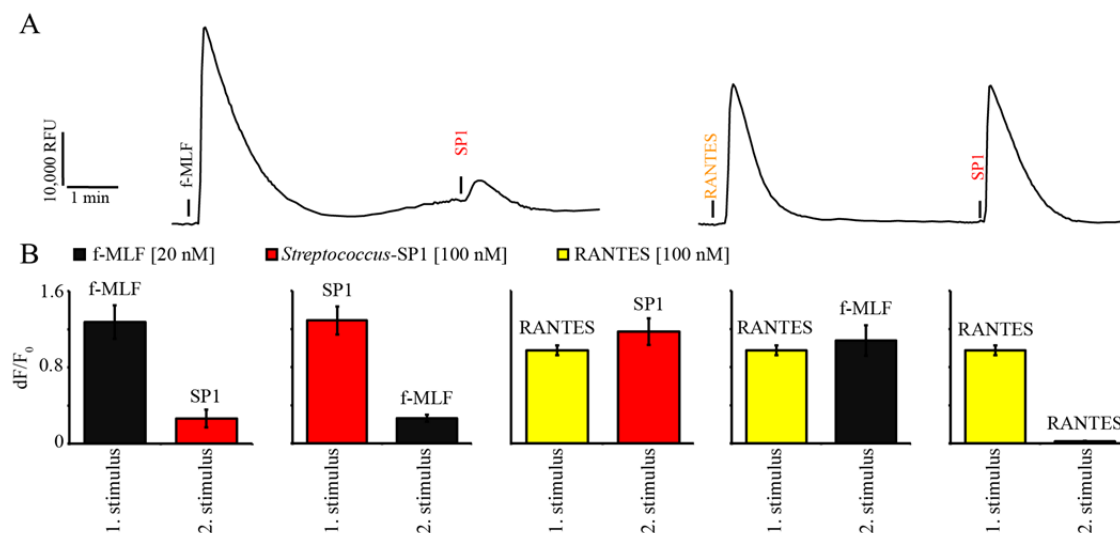


**Figure 3-21 | Cross-desensitization in human monocytes by the FPR1-preferential signal peptide SP1**

[A] Displayed are original calcium transients (measured in the FLIPR) showing the level of cross-desensitization in human monocytes to the hFPR1 preferential ligand *Streptococcus*-SP1 [100 nM] after pre-stimulation with f-MLF ([20 nM], left trace) or the CCR1 agonist RANTES ([100 nM]), right trace). Pre-application of f-MLF desensitizes the receptor that mediates the SP1 response whereas pre-application of RANTES does not. RFU = relative fluorescence units. [B] Quantification of responses shown in A together with control applications, averaged over two donors. Pre-stimulation with f-MLF desensitizes the SP1-induced response and *vice versa*. Pre-treatment with RANTES does not affect the subsequent application of SP1 or f-MLF. Subsequent application of RANTES, however, demonstrates desensitization of the RANTES receptor CCR1.

Similar results have been obtained when the sequence of the ligand application was inverted. However, pre-stimulation of monocytes with the CCR1 agonist RANTES followed by application of either SP1 or f-MLF resulted in an equivalent calcium signal for RANTES and the hFPR1 agonist. When the cells were pre-stimulated with RANTES, no signals were detected for a second RANTES application. RANTES is a well-known agonist of CCR1, a

chemokine GPCR that induces intracellular calcium mobilization upon stimulation with RANTES (Neote *et al.*, 1993). This experiment suggests that the well-known f-MLF and *Streptococcus*-SP1 likely bind the same receptor. To verify this theory, monocytes were challenged with 100 nM SP1 in concordant use with hFPR inhibitors (Figure 3-22). Cyclosporin H (CsH) is a cyclic undecapeptide, commonly used as a specific blocker for hFPR1 (Wenzel-Seifert and Seifert, 1993). tBoc2, is a competitive antagonist for hFPR1. Pre-application of 1  $\mu$ M CsH completely abolished the *Streptococcus*-SP1-dependent calcium signal. When tBoc2 (10  $\mu$ M) was mixed with SP1 before application, no calcium signal was detected (Figure 3-22 A). RANTES (100 nM) was used to show that the inhibitors did not affect general excitability or downstream signaling molecules (Figure 3-22 B).

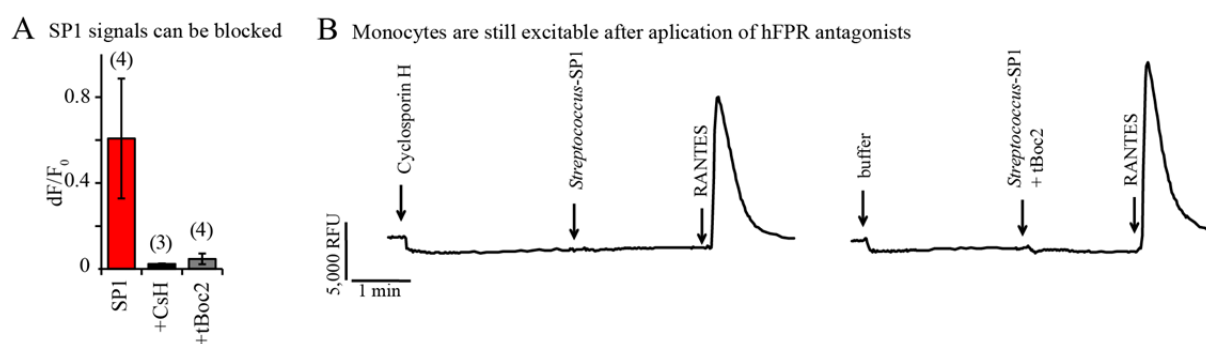


**Figure 3-22 | Inhibition of signal peptide-induced calcium responses in monocytes by hFPR blockers**

**[A]** *Streptococcus*-SP1 [100 nM] was applied either alone or in combination with the hFPR1 inhibitor CsH [1  $\mu$ M] or the FPR1 antagonist tBoc2 [10  $\mu$ M]. Data are averaged over at least three donors (exact numbers are stated in parenthesis). **[B]** Original FLIPR traces demonstrating viability of the cells after application of inhibitors, representative for at least three donors. The used concentrations are as stated in A, RANTES was applied at 100 nM. Cyclosporin H (CsH) is a blocker that has to be pre-applied (left) while Boc2 is a competitive inhibitor that is applied together with the agonist (right). In both cases, the cells can be activated by RANTES, demonstrating that intracellular GPCR associated calcium mobilization is still working and not affected by the blockers. RFU = relative fluorescence units.

These data strongly suggest that the signal peptide *Streptococcus*-SP1-induced calcium signal is mediated by hFPR1.

#### 3.4.1.3. Primary human monocytes recognize bacterial signal peptides with high sensitivity

In order to get insights into pharmacological properties and the biological role of bacterially-derived signal peptide fragments, a selection of these was tested on primary cells of the innate immune system. Monocytes were first stimulated with a selection of nine signal peptide fragments derived from the N-terminal domain (SP) and two full-length signal peptides (SP FuLe) (Figure 3-23). All nine signal peptide fragments<sup>10</sup> (*Streptococcus*-SP1,

<sup>10</sup> The peptides SP1 – SP21 have already been described (Bufe *et al.*, 2015) while the peptides SP22-24 are yet to be published as FPR agonists.

*Staphylococcus*-SP3, *Salmonella*-SP4, *Haemophilus*-SP5, *Psychromonas*-SP6, *Shewanella*-SP7, *Desulfotomaculum*-SP8, *Borrelia*-SP9 and *Staphylococcus*-SP22) were able to induce calcium responses when applied at concentrations of 10  $\mu$ M. Interestingly, the signals observed for SP1 and SP5 were about 50% higher in amplitude as those observed for the positive controls f-MLF, W-peptide and retro-inverted W-peptide. The signals induced by SP3, SP4, SP6, SP7 and SP8 were comparable to that induced by f-MLF. At 10  $\mu$ M, smaller signals were observed for SP22 and SP9, of which the latter was at the detection limit. Interestingly, the full-length signal peptides of SP8 and SP22 did induce signals that were  $\sim$ 50% (SP8 FuLe) to  $\sim$ 100% (SP22 FuLe) higher in amplitude than those induced by their N-terminal fragments (Figure 3-23).

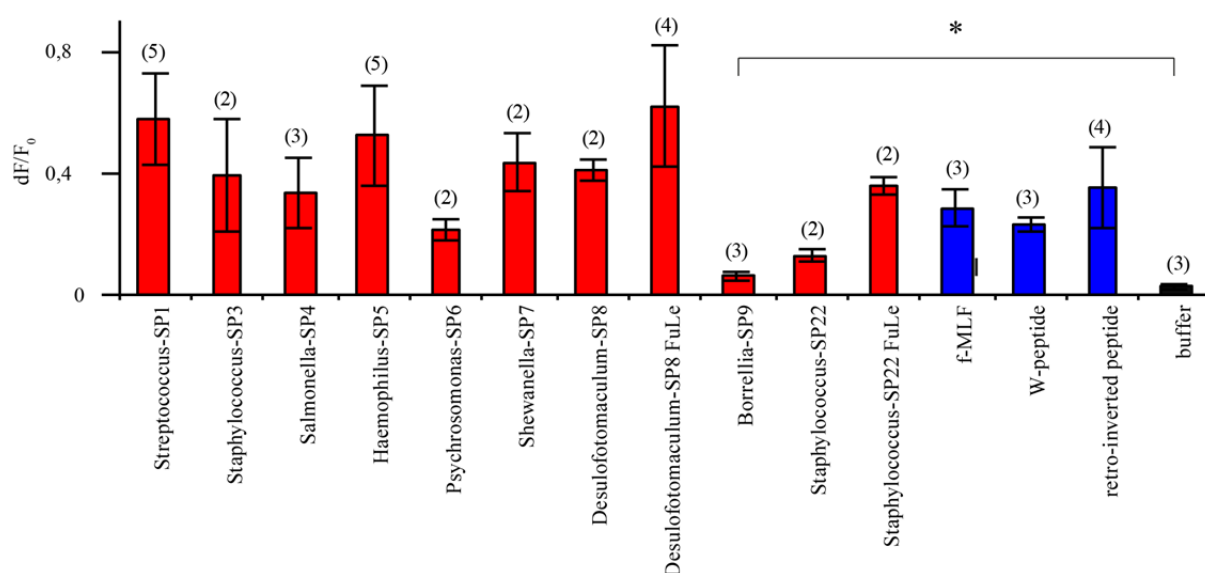


**Figure 3-23 | Human monocytes are activated by a range of bacterial signal peptides**

Calcium imaging of primary human monocytes performed with the FLIPR. Various signal peptides and single peptide fragments (red bars) were tested at 10  $\mu$ M. All peptides induced calcium responses in human monocytes. f-MLF, W-peptide and retro-inverted W-peptide (blue bars, each at 10  $\mu$ M) served as positive controls. Buffer application (black) served as control. Numbers in parentheses indicate the averaged number of independent donors. t-test: \* =  $p \leq 0.05$

The data shown above demonstrate that all tested signal peptides activated human monocytes. Bufe and Schumann *et al.* have shown that bacterial signal peptide fragments are recognized by human and mouse FPRs with extraordinary affinity (Bufe *et al.*, 2015). In order to investigate whether monocytes can detect these signal peptides with equal affinities, they were analyzed in concentration-response experiments.

When *Streptococcus*-SP1 was tested on monocytes in concentration-response experiments, the resulting curve showed a remarkable correlation in onset, shape and slope with that calculated for hFPR1 expressing HEK293T cells (Figure 3-24). The EC<sub>50</sub> calculated for the

monocytes was  $4.8 \pm 4.7$  nM. The corresponding value as determined in HEK293T cells was  $1.9 \pm 1.3$  nM (Figure 3-24). This close correlation was also observed for the control peptides f-MLF and W-peptide (Figure 3-24). When tested on monocytes, f-MLF exhibited an  $EC_{50}$  value of  $2.2 \pm 1.2$  nM, which is about four times higher than that observed for the heterologously expressed receptor ( $0.7 \pm 0.2$  nM). Again, both curves ran in parallel. W-peptide was detected with equal affinity by monocytes ( $1.9 \pm 1.2$  nM) and heterologously expressed hFPR1 ( $2.8 \pm 1.8$  nM), exhibiting closely overlaying graphs.

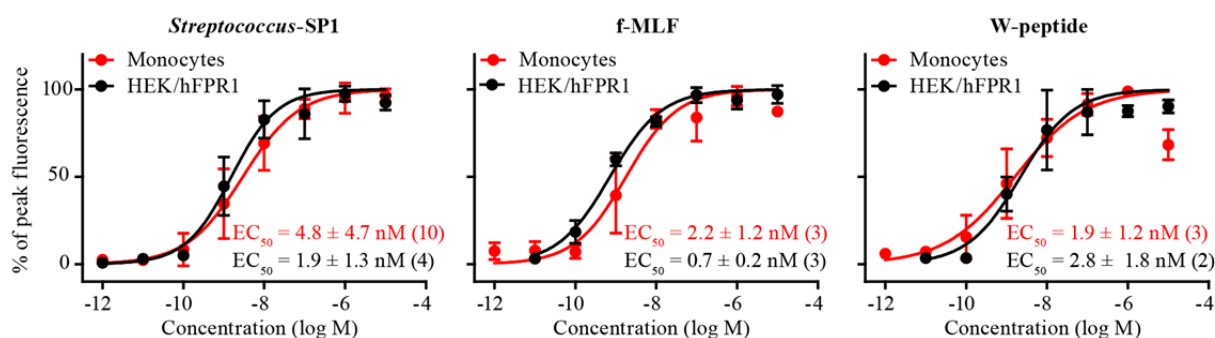


**Figure 3-24 | Direct comparison between concentration-response curves of human monocytes and hFPR1-expressing HEK293T cells**

Shown is the comparison of averaged concentration-response curves and  $EC_{50}$  values determined in calcium imaging for monocytes (red) and hFPR1 expressed in HEK293T cells (black). The exact number of averaged donors/transfections is shown in parentheses. Concentration-response curves recorded from monocytes and HEK293T cells expressing hFPR1 are identical in shape, onset, slope, and  $EC_{50}$  value for the hFPR1 preferential *Streptococcus*-SP1. The well-known f-MLF and W-peptide served as controls. *The concentration-response analysis for Streptococcus-SP1 and f-MLF on heterologously expressed hFPR1 were performed by Bernd Bufe.*

This pharmacological correlation argues for hFPR1-dependent detection of the tested peptides, including the signal peptide *Streptococcus*-SP1, contributing further evidence for the selectivity of the receptor towards the signal peptide. Hence, it was assumed that a close correlation of the concentration-response relationship between monocytes and hFPR1 expressing HEK293T cells could be used for selective analysis of given signal peptides on monocytes. In order to get further insights into signal peptide recognition by human monocytes, eleven additional signal peptide fragments were tested in concentration-response experiments (Table 3-4). The signal peptide fragments *Salmonella*-SP23 ( $EC_{50} = 5.0 \pm 2.6$  nM), *Salmonella*-SP24 ( $EC_{50} = 1.7 \pm 1.1$  nM) were similar in affinity as f-MLF ( $EC_{50} = 2.2 \pm 1.2$  nM) and W-peptide ( $EC_{50} = 1.9 \pm 1.2$  nM). Intriguingly, two signal peptides starting with the f-MLF motif exhibited high affinities on monocytes, surpassing even the prototypical f-MLF and the pan-immune FPR agonist W-peptide in affinity. With  $EC_{50}$  values of  $0.2 \pm 0.1$  nM (SP6) and  $0.2 \pm 0.2$  nM (SP8), respectively, *Psychromonas*-SP6 (f-MLFYFS) and *Desulfofotomaculum*-SP8 (f-MLFYLA) were ten times more sensitive toward monocytes than f-MLF. Although all tested signal peptides were recognized by monocytes, it did not

always occur with high affinity. Some of the peptide fragments (SP4 and SP9) exhibited EC<sub>50</sub> values close to those of low affinity agonists like Substance P (EC<sub>50</sub> > 1 μM). *Salmonella*-SP4 was the fragment with the highest calculated EC<sub>50</sub> value, reaching micromolar concentrations (1013.5 ± 500.6 nM). The EC<sub>50</sub> values determined for *Staphylococcus*-SP3, *Haemophilus*-SP5, *Shewanella*-SP7 and *Staphylococcus*-SP22 were in the lower nanomolar range (<500 nM); that measured for *Borrelia*-SP9 was in the upper nanomolar range (> 500 nM).

Up to this point, only signal peptide fragments comprising six to seven amino acids have been tested in concentration response experiments. It has been shown that heterologously expressed hFPR1 recognizes full-length peptides, containing up to more than 40 amino acids. However, this occurs with a 10- to 1000-fold loss in sensitivity (Bufe *et al.*, 2015). This is also true for monocytes (Table 3-4). The full-length peptide of *Streptococcus*-SP1 exhibited a ~ 5 times higher EC<sub>50</sub> value (24.1 ± 17.2 nM) than the hexapeptide fragment (4.8 nM). The EC<sub>50</sub> value of *Desulofotomaculum*-SP8 FuLe was shifted towards ~350-fold higher concentrations compared to the hexapeptide: 735.4 ± 17.2 nM (full-length) vs. 0.2 nM (hexapeptide). Surprisingly, the full-length version of *Staphylococcus*-SP22 was not shifted towards higher concentrations. On the contrary: the EC<sub>50</sub> value gained for the full-length peptide *Staphylococcus*-SP22 FuLe (4.6 ± 1.8 nM) was ten times lower than that for its hexapeptide (43.9 ± 26.7 nM). These data show that monocytes are able to detect full signal peptides as well as their N-terminal breakdown products albeit with different sensitivity.

**Table 3-4 | Human monocytes exhibit high affinity to bacterial signal peptides\***

Signal peptide	EC <sub>50</sub> value in [nM]	Amino acid sequence	Online accession
<i>Streptococcus</i> -SP1	4.8 ± 4.7 (10)	f-MGFFIS	Q8VLQ8
<i>Streptococcus</i> -SP1 FuLe	24.1 ± 17.2 (4)	f-MGFFISQSKQHYGIRKYKVGVC SALIALSILGTRVAA	Q8VLQ8
<i>Staphylococcus</i> -SP3	164.1 ± 133.6 (3)	f-MFIYYCK	Q6GHI8
<i>Salmonella</i> -SP4	1013.5 ± 500.6 (5)	f-MAMKKL	Q8Z9A3
<i>Haemophilus</i> -SP5	221.2 ± 103.1 (7)	f-MVMKFK	P45306
<i>Psychromonas</i> -SP6	0.2 ± 0.1 (3)	f-MLFYFS	A1ST24
<i>Shewanella</i> -SP7	64.6 ± 22.6 (3)	f-MLFKYS	A6WUI7
<i>Desulofotomaculum</i> -SP8	0.2 ± 0.2 (6)	f-MLFYLA	A4J7E6
<i>Desulofotomaculum</i> -SP8 FuLe	735.4 ± 202.7 (4)	f-MLFYALPCTLVIFVASKALYAI	A4J7E6
<i>Borrelia</i> -SP9	682.6 ± 556.2 (3)	f-MLKKVY	Q44743
<i>Staphylococcus</i> -SP22	43.9 ± 26.7 (4)	f-MKKFNILIALFFTSLVISPLNVKA	Q44743
<i>Staphylococcus</i> -SP22 FuLe	4.6 ± 1.8 (2)	f-MKKFNI	P20723
<i>Salmonella</i> -SP23	5 ± 2.6 (2)	f-MKKFYFS	P37423
<i>Salmonella</i> -SP24	1.7 ± 1.1 (2)	f-MKKFRW	Q8XG71
<b>Control peptide</b>			
f-MLF	2.2 ± 1.2 (3)	f-MLF	/
W-peptide	1.9 ± 1.2 (3)	WKYMVm-NH <sub>2</sub>	/
retro-inverted W-peptide	9.4 ± 4.8 (3)	f-MVMYKW	/
M-peptide	11.8 ± 8.6 (3)	MMHWAm-NH <sub>2</sub>	/
Substance P	1456 ± 97 (2)	RPKQQFFGLM-NH <sub>2</sub>	/

\*The table shows EC<sub>50</sub> values (in nM) from concentration-response experiments of primary human monocytes after stimulation with signal or control peptides in calcium imaging experiments. The tested amino acids are shown in one letter code. f = N-terminal formylation. Data are averaged over at least two donors (exact numbers are indicated in parenthesis). Accession numbers refer to the UniProt database.

### **3.4.2. Human granulocytes detect bacterial signal peptides through formyl peptide receptors**

As shown in chapter 3.4.1 primary human monocytes are capable of hFPR1-mediated recognition of signal peptides with high sensitivity and specificity. Human monocytes were excellent candidates for first experiments as they are frequently used for calcium imaging and they are easy to culture for primary cells. Monocytes are important elements of the innate immune defense. However, granulocytes, mainly neutrophil granulocytes (= neutrophils), are at the center of immune responses. Constituting the majority of leukocytes in the blood stream, granulocytes are easily obtained in large numbers and therefore well-investigated. Human neutrophil granulocytes have been used extensively to study FPRs in the past (Migeotte *et al.*, 2006). The cells express both, hFPR1 and hFPR2 in abundance (Migeotte *et al.*, 2006) and should therefore provide a valid tool for investigation of FPR pharmacology in primary cells. To collect more data on the effects of signal peptides on the innate immune system the study was extended to primary human granulocytes.

#### ***3.4.2.1. Primary human granulocytes recognize signal peptides in high-throughput calcium imaging***

Human granulocytes were isolated from whole blood by density gradient centrifugation and then incubated in calcium containing Ringer solution. First, it was tested whether the isolated cells can be measured in high-throughput calcium imaging. When the cells were challenged with f-MLF or the signal peptide *Streptococcus*-SP1 they responded with stable calcium transients (Figure 3-25 A). As observed for the monocytes, the strength of this response was concentration-dependent, exhibiting a minimal effective concentration of 100 pM (Figure 3-25 A + B). Calculation of concentration-response curves yielded EC<sub>50</sub> values of  $0.47 \pm 0.51$  nM (f-MLF) and  $0.62 \pm 0.43$  nM (*Streptococcus*-SP1), which are approximately four to eight times lower than those calculated for human monocytes. In a next step it was investigated whether the cells can be stimulated with several signal peptide fragments in concentrations to 10  $\mu$ M. All tested fragments (SP1, SP4, SP5, SP8 and SP22) were recognized by the granulocytes. These experiments demonstrate that human granulocytes respond to bacterial signal peptides with high sensitivity.

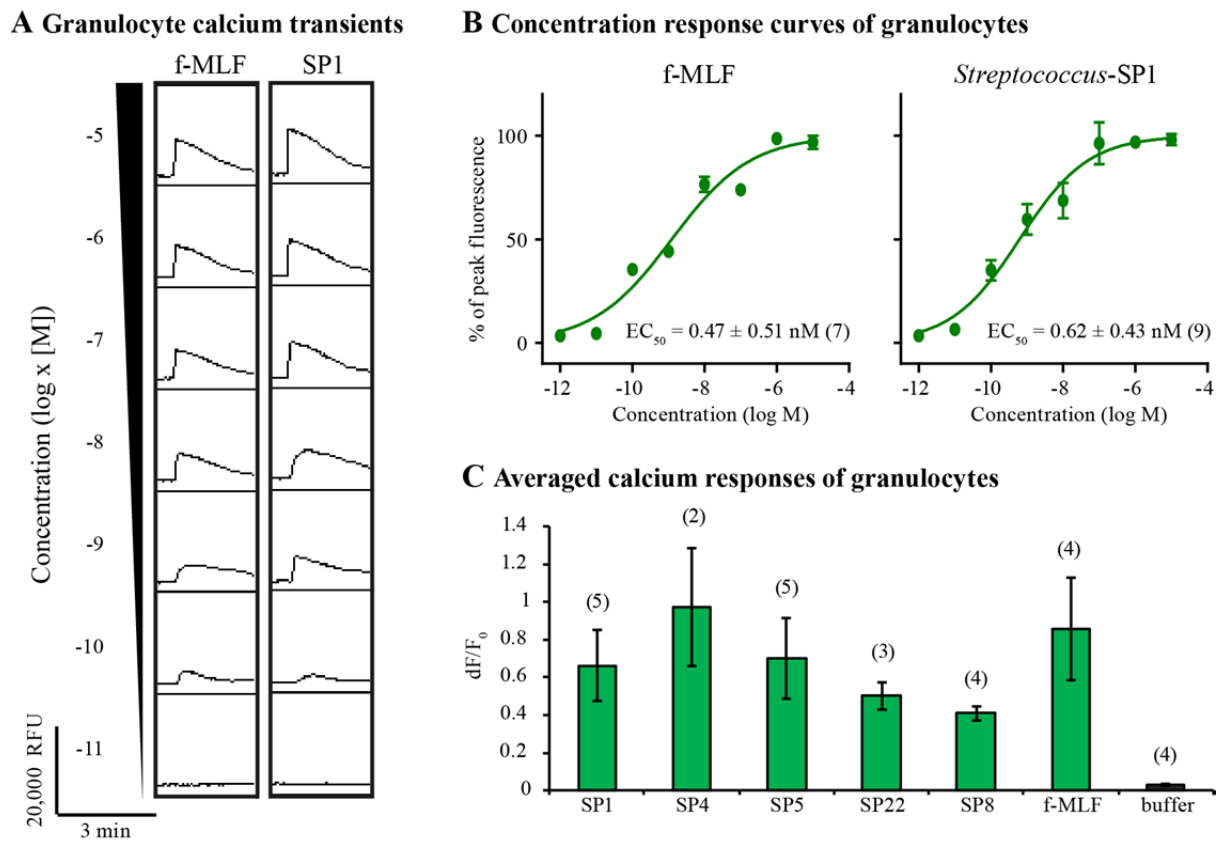


**Figure 3-25 | Primary human granulocytes are activated by various bacterial signal peptides**

Calcium imaging of primary human granulocytes performed with the FLIPR. [A] Original calcium traces of stimulated granulocytes as observed in the FLIPR. The calcium traces show calcium transients of granulocytes after application of 10  $\mu\text{M}$  *Streptococcus*-SP1 or f-MLF. RFU = relative fluorescence units. Each trace is representative for at least five donors. [B] Concentration-response analysis of granulocytes stimulated with f-MLF or SP1. Number of tested donors is given in parentheses. [C] Various single peptide fragments were tested at 10  $\mu\text{M}$ . All peptides induced calcium responses in human granulocytes. f-MLF (10  $\mu\text{M}$ ) served as positive control. Buffer application (black) served as negative control.

In a next step it was investigated which cells are responsible for the calcium signals. Therefore, immunocytochemistry was used in conjunction with single cell analysis. First, to determine the purity and morphology of the prepared cells, nuclear staining was used. Granulocytes (or polymorphonuclear leukocytes) can easily be identified in immunocytochemical analysis by the shape and morphology of their characteristic multi-lobular nuclei. The most prominent granulocyte (50-70% of all leukocytes in the human blood) is the neutrophil granulocyte. The nuclear anatomy of the mature neutrophil's chromatin is organized into two to five dense chromatin segments (Olins *et al.*, 2008). Purity analysis of the isolation showed that most cells were in fact granulocytes, since  $95.2 \pm 2.4\%$  of the cells (not shown) had a multi-lobed nucleus that is characteristic for neutrophils (Olins *et al.*, 2008). Immunocytochemistry using antibodies targeted against the neutrophil marker CD66 did also reveal staining for >95% of the cells (data not shown), confirming these results. Interestingly, the stainings showed that the granulocytes did strongly adhere to the well bottom during

incubation. Under physiological conditions, non-activated granulocytes remain in suspension. However, the Ringer solution used for incubation of the cells does not reflect physiological conditions that are found in human blood. To mimic more physiological conditions, it was tested whether the cells show different stainings when incubated in culture medium, supplemented with 1% of autologous (= donor-self) blood serum. In fact, there were about 90% less cells attached to the well bottom when incubated in autologous serum (data not shown). According to the nuclear morphology, more than 95% (183/191) of those cells were granulocytes. However, no significant differences were observed in functional analysis (data not shown). Since incubation in the Ringer solution yielded much more granulocytes, the cells were generally incubated in Ringer.

Next, the expression rates of hFPR1 and hFPR2 were addressed. Analysis of immunocytochemical stainings of human granulocytes showed that  $86.7\% \pm 3.5\%$  of the cells were positive for hFPR1 (Figure 3-26). Immunocytochemistry for hFPR2 showed that  $51.6\% \pm 16.3\%$  of the cells were stained positive (Figure 3-26). Importantly, 98% of the cells expressing hFPR1 had a multi-lobular nucleus. Of the cells stained positively for hFPR2, 97% were identified as granulocytes (Figure 3-26 C). This shows that the majority of cells is made up by granulocytes and that they express hFPR1 and hFPR2. To verify that the calcium signals are generated by granulocytes, single cell calcium imaging was used. First, the granulocytes were challenged with  $10 \mu\text{M}$  of *Streptococcus*-SP1. Of 192 cells in the visual field, 173 (= 92%) did respond with calcium elevations within 15 seconds after application of SP1 (Figure 3-26 D). In contrast, only 8 of 204 cells (= 3.9%) responded to buffer application (not shown). Quantification of these results over several experiments showed that  $\sim 70\%$  of the cells responded with calcium signals to  $10 \mu\text{M}$  of *Streptococcus*-SP1;  $\sim 50 - 60\%$  responded to  $10 \mu\text{M}$  *Desulfotomaculum*-SP8, *Hydrogenobacter*-SP16 and W-peptide, respectively (Figure 3-26 D).

The results illustrated in this chapter demonstrate that granulocytes are activated by a range of bacterially-derived signal peptide fragments and that the majority of the observed calcium signals are generated by granulocytes that express hFPR1 or hFPR2. However, so far there is no evidence that these responses are really mediated by hFPR1 or hFPR2.

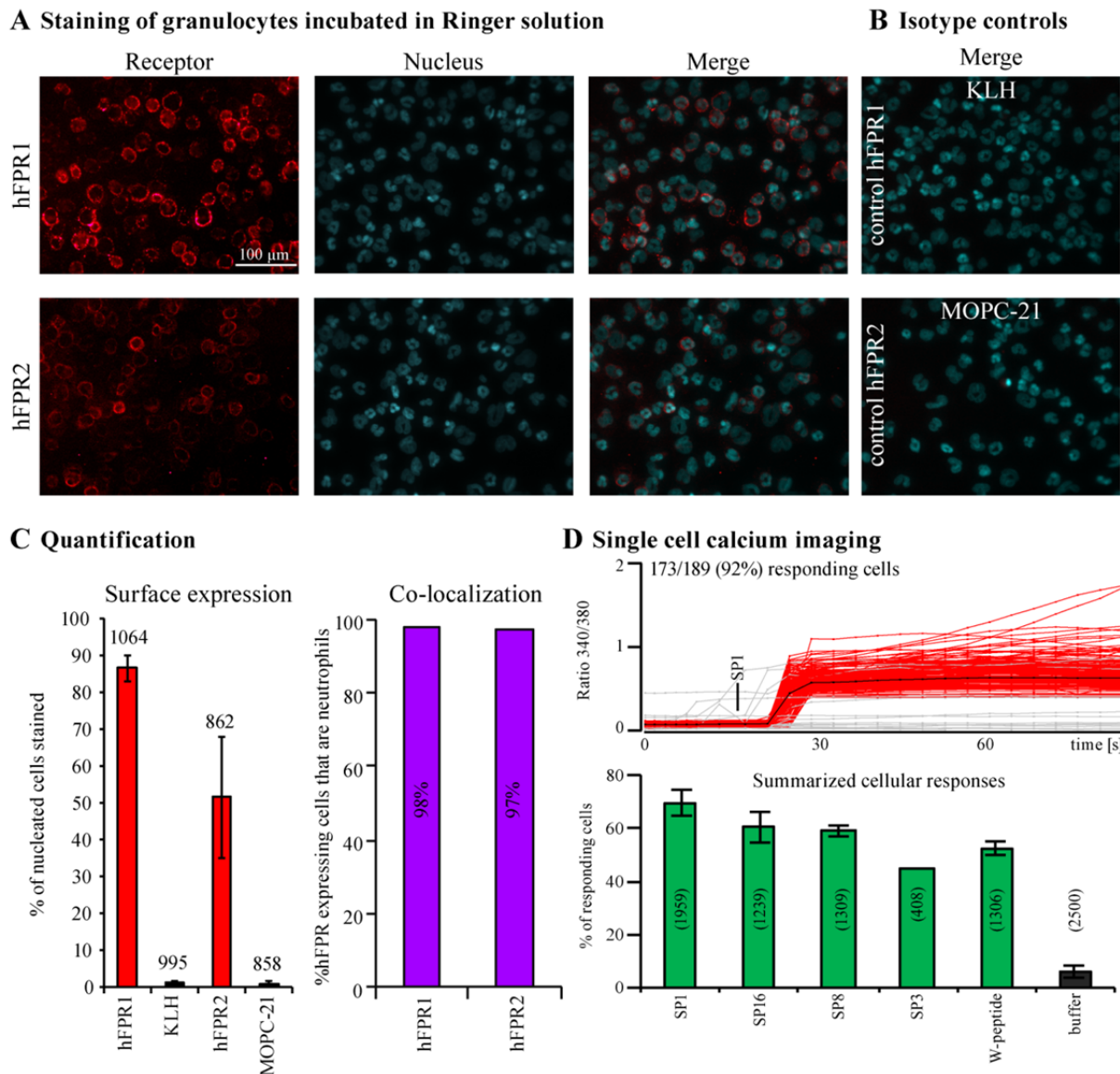


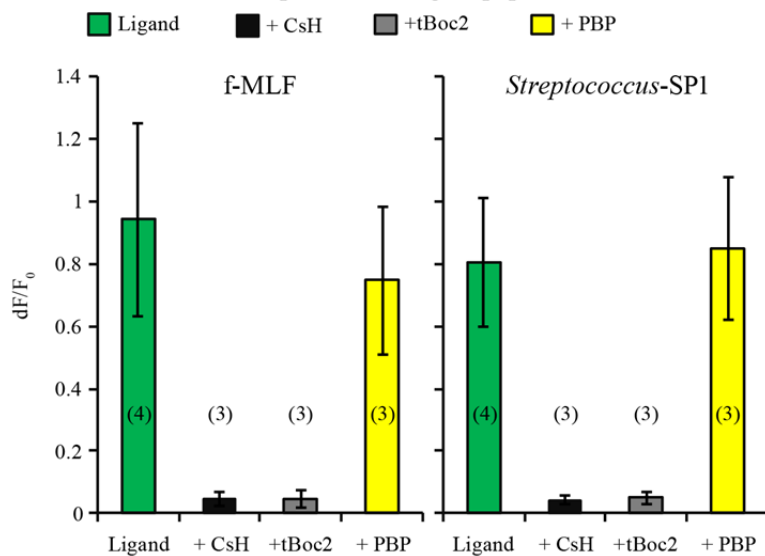
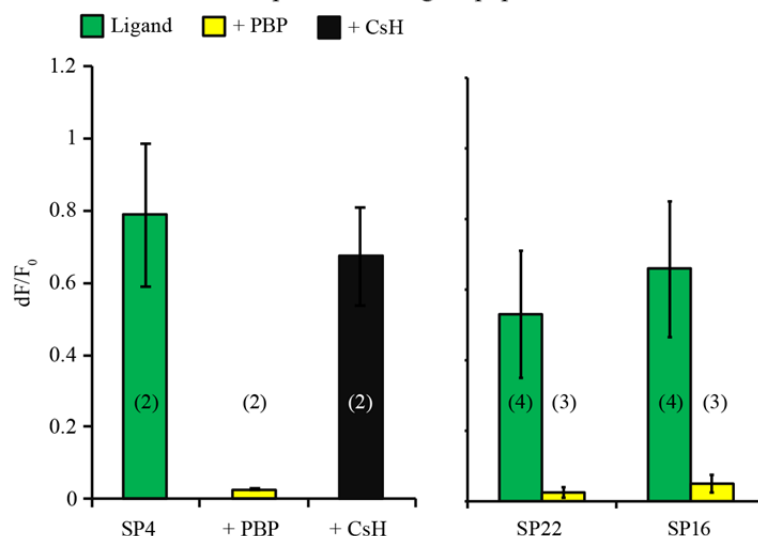
**Figure 3-26 | Signal peptide-induced calcium signals are generated by primary human granulocytes**

[A] Representative confocal immunostainings of non-permeabilized primary human granulocytes with an antibody targeted against hFPR1 (upper panel) and an antibody targeted against hFPR2 (lower panel). 321 of 337 (95%) nucleated cells had a polymorph shaped, multi-lobular nucleus typical for human neutrophil granulocytes (neutrophils). [B] Representative confocal images showing the isotype controls for the hFPR1 antibody (KLH) and the hFPR2 antibody (MOPC-21). [C] The left column chart shows that hFPR1 is expressed in 87% of the nucleated cells while hFPR2 was detected in 52% of the cells. The right chart shows that of those cells, 98% and 97%, respectively, are granulocytes. All data in A-C are representative for at least three donors. [D] Single cell calcium imaging of granulocytes. The upper panel shows that 173 of 189 cells responded to 10  $\mu$ M SP1. Each trace represents one cell. Red traces = positive responders, gray = non-responders. The lower panel shows the quantification for one representative donor experiment over at least three repetitions. Numbers in parentheses indicate the number of analyzed cells. All data are representative for two similar experiments and two donors.

#### 3.4.2.2. Signal peptide recognition of human granulocytes is mediated by FPRs

To verify that the signal peptide-induced calcium elevations are indeed mobilized through FPRs, signal peptide fragments were applied alone or in combination with blockers specific for hFPR1 or hFPR2.

First, it was tested whether *Streptococcus*-SP1-induced signals are mediated through hFPR1. Signals induced by 1 nM of *Streptococcus*-SP1 were completely abolished if it was applied together with the hFPR1 antagonist tBoc2 or after pre-application of CsH, which is another potent inhibitor of hFPR1. Very similar results were observed for 1 nM f-MLF. When SP1 or f-MLF was applied after pre-incubation with the hFPR2-specific inhibitor PBP10, these signals were not significantly reduced (Figure 3-27 A). This strongly suggests that the calcium responses are mediated by hFPR1. To verify that blocking hFPR1 with CsH does not impair the general signal transmission of the granulocytes, the above-described blocking experiments were performed with the hFPR2 preferential signal peptide fragment *Salmonella*-SP4. When applied after pre-incubation with CsH, there was no significant reduction in signal amplitude (Figure 3-27 B). This demonstrates that the general excitability is not negatively influenced by CsH. When SP4 was applied after pre-incubation with PBP10, the responses were blocked, indicating hFPR2-mediated transmission of these signals. Further experiments using the signal peptide fragments *Hydrogenobacter*-SP16 and *Staphylococcus*-SP22 showed that both peptides were sufficiently blocked by PBP10. Together these data argue for hFPR1 and hFPR2-dependent recognition of bacterial signal peptide fragments in human granulocytes.

**A** Inhibition of hFPR1 preferential signal peptides**B** Inhibition of hFPR2 preferential signal peptides**Figure 3-27 | Block of signal peptide-induced calcium signals by hFPR1 and hFPR2 inhibitors in human granulocytes**

Isolated human granulocytes were challenged with hFPR1 or hFPR2 preferential signal peptide fragments, either alone or in combination with receptor specific blockers. All data were averaged over at least two donors; the exact number of donors is given in parentheses above the columns. The used concentrations were: f-MLF [1 nM], SP1 [1 nM], SP4 [1  $\mu$ M], SP22 [10 nM], SP16 [10 nM], CsH [10  $\mu$ M], tBoc2 [10  $\mu$ M], PBP10 [5  $\mu$ M]. **[A]** Calcium signals induced by hFPR1 preferential signal peptides can be inhibited by the hFPR1 specific inhibitor CsH and tBoc2. These signals are not impaired by the hFPR2 specific blocker PBP10. **[B]** Calcium signals induced by hFPR2 preferential signal peptides can be inhibited by the hFPR2 selective blocker PBP10. The signals are not blocked by the hFPR1-specific CsH.

**3.4.2.3. Bacterial signal peptides activate primary human granulocytes with high affinity**

In order to analyze the affinity of the tested ligands on human granulocytes, concentration-response experiments were conducted. First, concentration response curves were created for *Streptococcus*-SP1 and the control substances f-MLF and W-peptide. SP1 and f-MLF are known to prefer hFPR1 while W-peptide is more affine to hFPR2 (Migeotte *et al.*, 2006). The calculated  $EC_{50}$  for SP1 on granulocytes was  $0.6 \pm 0.4$  nM; about three times lower than the value calculated for hFPR1 transfected HEK293T cells ( $1.9 \pm 1.3$  nM) (Figure 3-28). Similar results have been observed for f-MLF with  $0.2 \pm 0.07$  nM (granulocytes) and  $0.7 \pm 0.2$  nM (hFPR1 in HEK293T). The observed results for W-peptide showed an  $EC_{50}$  value of  $0.15 \pm 0.1$  nM for granulocytes. This value was almost identical to the one calculated for

HEK293T cells expressing hFPR2, which is  $0.16 \pm 0.02$  nM (Figure 3-28). The concentration-response curves of W-peptide showed a close correlation between granulocytes and hFPR2 expressed in HEK cells: they were identical in shape, onset slope and  $EC_{50}$  (Figure 3-28).

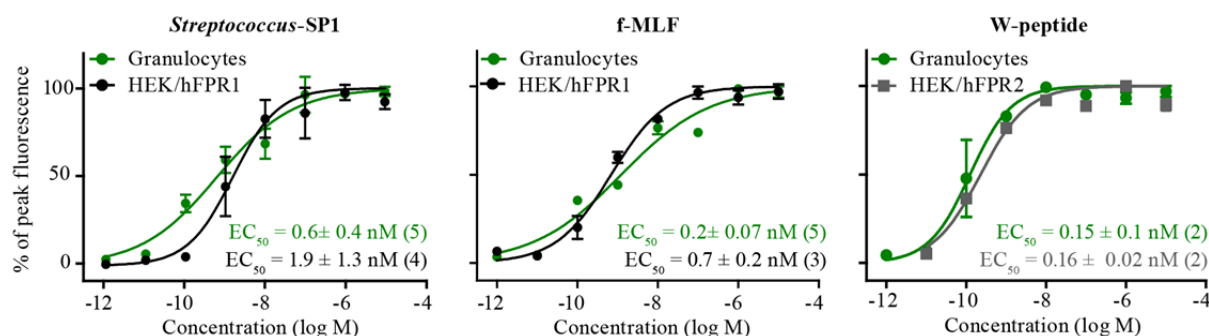


**Figure 3-28 | Direct comparison between concentration-response curves of human granulocytes and hFPR1 or hFPR2 expressed in HEK293T cells**

Shown is the comparison of averaged concentration-response curves and  $EC_{50}$  values determined in calcium imaging for granulocytes (green) and hFPR1 (black circles) or hFPR2 (gray squares) expressed in HEK293T cells. The exact number of averaged donors/transfections is shown in parentheses. Concentration-response curves recorded from granulocytes and HEK293T cells expressing hFPR1 are identical in shape, onset slope and  $EC_{50}$  value for the hFPR1 preferential *Streptococcus-SP1*. The well-known f-MLF and W-peptide served as controls. *The concentration-response analysis for Streptococcus-SP1 and f-MLF on heterologously expressed hFPR1 were performed by Bernd Bufe.*

This close correlation indicates that the concentration-response curves measured in this study can be transferred from HEK293T cells to granulocytes, underlining the selectivity of the ligands. Therefore, several signal peptides were tested on granulocytes in concentration-response experiments. The most affine of the tested peptides, *Desulfotomaculum-SP8*, exhibited an  $EC_{50}$  of  $5 \times 10^{-11}$  M. Comparison of dose-response curves between granulocytes and monocytes indicated that the granulocytes exhibit higher sensitivity towards nine of eleven compared agonists. The greatest difference in sensitivity has been observed for SP4: granulocytes exhibited  $\sim 18$  times higher sensitivity towards this peptide than monocytes (Table 3-5).

**Table 3-5 | Human granulocytes exhibit high affinity to bacterial signal peptides\***

Agonist	Granulocytes EC <sub>50</sub> [nM]	Monocytes EC <sub>50</sub> [nM]	Factor M/G
<i>Streptococcus</i> -SP1	0.62 ± 0.43 (9)	4.8 ± 4.7 (10)	6
<i>Staphylococcus</i> -SP3	116.81 ± 95.99 (2)	164.1 ± 133.6 (3)	1
<i>Salmonella</i> -SP4	56.78 ± 1.3 (3)	1013.5 ± 500.6 (5)	18
<i>Haemophilus</i> -SP5	50.06 ± 23.03 (7)	221.2 ± 103.1 (7)	4
<i>Shewanella</i> -SP7	52.32 ± 17.24 (2)	64.6 ± 22.6 (3)	1
<i>Psychromonas</i> -SP6	0.1 ± 0.09 (5)	0.2 ± 0.1 (3)	2
<i>Desulfofotomaculum</i> -SP8	0.05 ± 0.04 (4)	0.2 ± 0.2 (6)	4
<i>Hydrogenobacter</i> -SP16	5.59 ± 9.34 (8)	not determined	not tested
<i>Staphylococcus</i> -SP22	14.08 ± 5.35 (8)	43.9 ± 26.7 (4)	3
f-MLF	0.16 ± 0.07 (5)	2.2 ± 1.2 (3)	5
W-peptide	0.15 ± 0.1 (2)	1.9 ± 1.2 (3)	13
M-peptide	6.21 ± 4.13 (2)	11.8 ± 8.6 (3)	2

\*The table shows EC<sub>50</sub> values (in nM) from concentration-response experiments of primary human granulocytes and monocytes after stimulation with signal or control peptides in calcium imaging experiments. The right column contains the ratio of EC<sub>50</sub> values from monocytes/granulocytes, showing how many times the ligands were more affine on granulocytes than on monocytes. Data are averaged over at least two donors (exact numbers are indicated in parentheses).

The data presented in chapter 3.4 demonstrate that bacterially-derived signal peptides and their N-terminal fragments are recognized by cells of the innate immune system. Activation of human monocytes and granulocytes is mediated by hFPR1 and hFPR2 and leads to mobilization of intracellular calcium. It would be intriguing to investigate whether activation of monocytes and granulocytes does also induce innate immune defense mechanisms.

### 3.5. Bacterial signal peptides trigger pathogen defense mechanisms in human phagocytes

To investigate the biological actions of N-terminally formylated signal peptides it is of great use to see what actions they trigger in phagocytic cells. Cells of the innate immune system, especially monocytes and neutrophils are specialized toward pathogen recognition and their elimination; they define the first line of defense against invading pathogens. Recruitment of neutrophils from blood flow to intra-tissue sites of infection requires adhesion to the endothelium, extravasation (transmigration) through the endothelial wall and elimination of targets (Kolaczowska and Kubes, 2013). The following chapter addresses innate defense mechanisms of monocytes and granulocytes, starting from migration to elimination of pathogens.

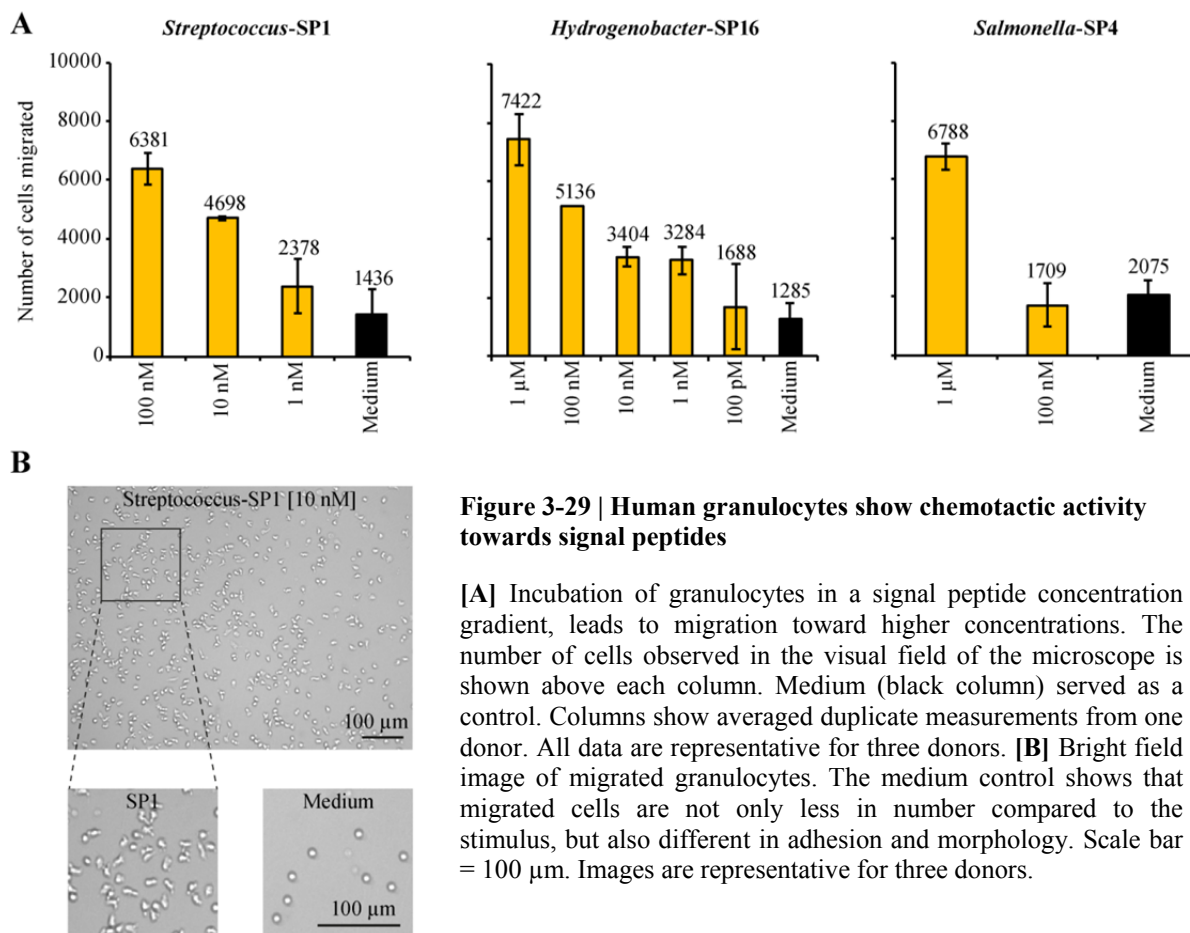
### 3.5.1. Bacterial signal peptides induce chemotaxis in neutrophils

Chemotaxis of phagocytes is one of the first events initiated during immune defense triggered by activation of GPCRs (Gambardella and Vermeren, 2013). The cells crawl towards a concentration gradient with the aim to come in close proximity to their target. hFPR1 was discovered in 1975 as the prototypic chemoattractant receptor (Schiffmann *et al.*, 1975). In order to investigate chemotaxis-inducing properties, the hFPR1 selective *Streptococcus*-SP1 and the hFPR2 selective *Salmonella*-SP4 and *Hydrogenobacter*-SP16 were tested in chemotaxis experiments. Figure 3-29 shows that all three peptides induced migration of the cells towards the higher agonist concentrations within the gradient. The bar chart displayed for *Streptococcus*-SP1 shows a typical concentration-dependent migration as has been described for f-MLF (Campbell *et al.*, 1996). For SP1, the maximal number of migrated cells was counted when stimulated with 100 nM. For SP16 and SP4 it was towards 1  $\mu$ M. Activation threshold for SP1 and SP16 was 1 nM<sup>11</sup>, the threshold for SP4 was 1  $\mu$ M (Figure 3-29 A). A typical property of activated, migrating neutrophils is the formation of lamellipodia. Granulocytes activated with 10 to 100 nM SP1 or SP16 showed a remarkable difference in morphology compared to non-stimulated cells. The cells showed elongated protrusions and strong adherence to the bottom measurement chambers (Figure 3-29). Cells incubated in medium without stimulus were of round shape and less adherent.

These experiments illustrate the chemotactic properties of signal peptides on human granulocytes. The next question was, whether the peptides can also induce anti-microbial actions as an anti-pathogenic effector function.

---

<sup>11</sup> In some occasions, signals have been observed for SP1/SP20 concentrations of < 1 nM (in one case up to 10 fM), but these were not reliably reproducible and therefore not included.



### 3.5.2. Monocytes and neutrophils produce reactive oxygen species when stimulated with bacterial signal peptides

GPCR-dependent activation of phagocytes by hostile molecules results in the release of reactive oxygen species (ROS)<sup>12</sup>, which are major contributors to host immune defense (Bedard and Krause, 2007). These highly reactive oxygen-based radicals transfer electrons to the closest target (e.g. pathogens), thereby breaking covalent bonds of proteins, sugars, fatty acids, etc. Controlled formation of these radicals requires NADPH-dependent oxidases (NOX) that reside in intracellular vesicles (Bedard and Krause, 2007). In phagocytes, GPCR-dependent activation leads to assembly and activation of the well-investigated NOX2 enzyme complex, whose vesicle is fused with the plasma membrane (Bedard and Krause, 2007). NOX-dependent reduction of oxygen results in the formation of superoxide radicals ( $\bullet\text{O}_2^-$ ). This radical reacts with water molecules forming additional ROS species like hydrogen peroxide ( $\text{H}_2\text{O}_2$ ) that supports the antimicrobial mode of action (Bedard and Krause, 2007). One possibility to monitor the formation of  $\text{H}_2\text{O}_2$  requires the use of the fluorescent dye

<sup>12</sup> The rapid release of reactive oxygen species is known as respiratory burst or oxidative burst

Amplex®UltraRed (Amplex). Amplex is a fluorogenic substrate for horseradish peroxidase (HRP). Upon H<sub>2</sub>O<sub>2</sub> formation, the HRP catalyzes the H<sub>2</sub>O<sub>2</sub>-dependent reduction of Amplex to a fluorescent dye, which can be monitored in ELISA readouts.

In order to investigate whether signal peptides can induce the formation of reactive oxygen species, a high-throughput, Amplex®UltraRed-based fluorescence assay was used to test a number of stimuli. Notably, Amplex®UltraRed is not membrane permeable and does only indicate extracellularly produced H<sub>2</sub>O<sub>2</sub> (Bogeski *et al.*, 2011). All tested signal peptides (SP1, SP3, SP4 and SP5) were able to induce the formation of H<sub>2</sub>O<sub>2</sub> (Figure 3-30 A). The fluorescence measured for f-MLF was two times higher than for SP1. SP5 seemed to be three times more potent in inducing formation of H<sub>2</sub>O<sub>2</sub> than SP1, indicating that these peptides show different potencies in ROS production. In order to investigate the sensitivity of hydrogen peroxide formation, a kinetic measurement was performed (Figure 3-30 B). Steady concentration-response effects of SP1-induced signals stabilized 3 minutes after beginning of the measurement. Similar results were obtained for f-MLF (not shown). As expected, signal peptides, namely SP1 and SP16, also induce peroxide formation in human granulocytes (Figure 3-30 C). To determine whether this effect is FPR-dependent, the hFPR1 preferential SP1 (100 nM) was also applied in conjunction with hFPR1 inhibiting concentrations of tBoc2 (10 μM). As expected, the SP1-induced signal was completely abrogated (Figure 3-30 B). The same experiment was performed with the hFPR2 preferential SP16 (1 μM). Signals generated via SP16 were not diminished when applied together with tBoc2. This suggests that the hydrogen peroxide generation induced by *Streptococcus*-SP1 is dependent on hFPR1. The next step was to acquire the sensitivity of these peptides with respect to radical production in monocytes and granulocytes. In monocytes both, f-MLF and SP1 produced superoxide with EC<sub>50</sub> values in the lower nanomolar range. The calculated EC<sub>50</sub> values were 34 ± 13 nM for f-MLF and 74 ± 32 nM for SP1. This corresponds to a ~14-fold (SP1) to 20-fold (f-MLF) shift to higher concentrations in the dose-response curves compared to the calcium signals (Figure 3-30 C). This is in agreement with previously observed data on superoxide production in human monocytes (Kemmerich and Pennington, 1988). Similar results have been observed for human neutrophils (Figure 3-30 D). Regarding ROS release, *Streptococcus*-SP1 exhibited an EC<sub>50</sub> value of 39.3 ± 23.5%, which is about 60 times higher than that calculated for calcium mobilization (Figure 3-30 D). Hydrogenobacter-SP16 stimulated the ROS production in neutrophils with an EC<sub>50</sub> of 104 ± 9.8 nM, approximately twenty times higher than that for calcium mobilization (Figure 3-30 D). Similar results have been described before (Gao *et al.*, 1994).

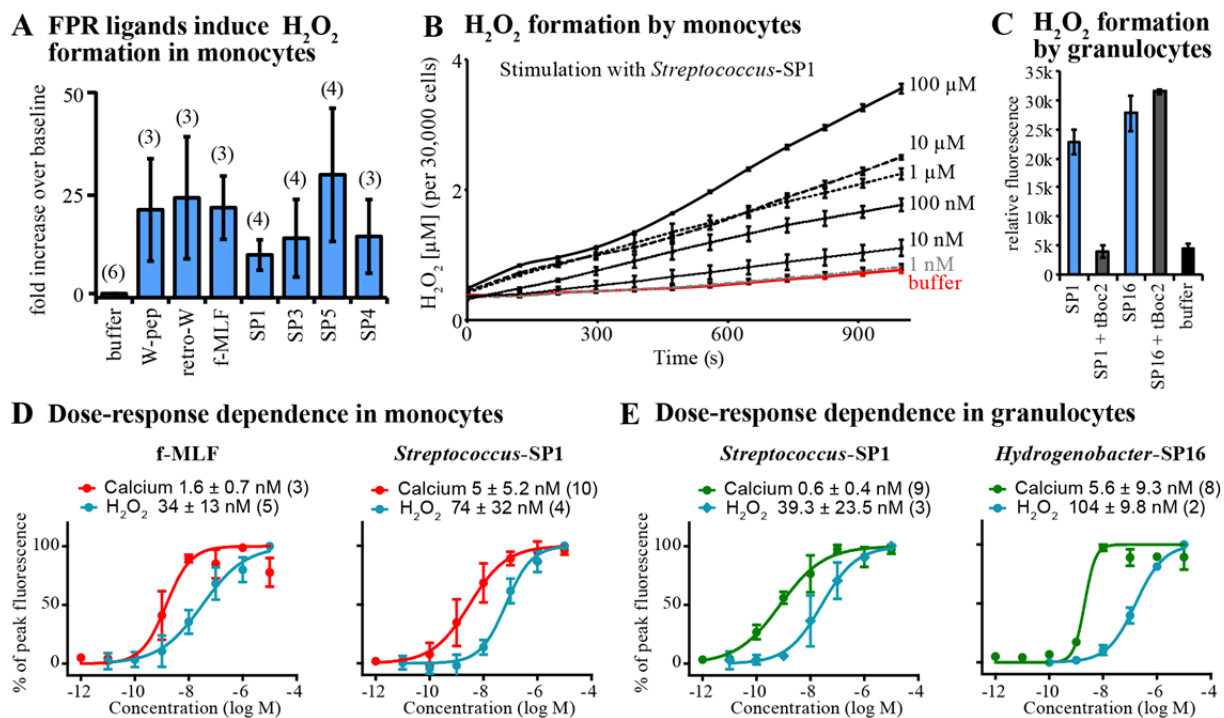


**Figure 3-30 | Signal peptide-dependent formation of reactive oxygen species by human monocytes and granulocytes**

Amplex-based detection of H<sub>2</sub>O<sub>2</sub> formation by monocytes and granulocytes after stimulation with distinct signal peptides. **[A]** Average H<sub>2</sub>O<sub>2</sub> production (number of donors in parentheses) stimulated with four signal peptides. f-MLF, W-peptide (W-pep), and retro-inverted W-peptide (retro-W) were used as positive controls. Buffer was used as baseline control. The columns show the x-fold increase in fluorescence over baseline fluorescence 10 minutes after stimulation with a given substance. All peptides were used at 10 μM, except SP4 (100 μM). **[B]** Concentration-dependent kinetics measurement of H<sub>2</sub>O<sub>2</sub> formation after stimulation with SP1 (representative for four donors). **[C]** Signal peptide-induced H<sub>2</sub>O<sub>2</sub> formation observed in granulocytes. The effect induced by the hFPR1 selective SP1 (100 nM) can be inhibited by tBoc2 (10 μM) while the hFPR2 selective SP16 (1 μM) is unaffected. **[D]** Dose-response analysis of H<sub>2</sub>O<sub>2</sub> formation (blue) by monocytes. The curve's EC<sub>50</sub> values are shifted towards higher concentrations, compared to those of the calcium measurements (red). **[E]** Comparison of concentration-dependent calcium mobilization (green) and H<sub>2</sub>O<sub>2</sub> formation (blue) in human granulocytes after stimulation with signal peptides. EC<sub>50</sub> values of C and D are stated above the graphs. Number of donors used for calculation of the graphs is given in parentheses.

In summary, these data demonstrate that bacterial signal peptides activate classical cascades of innate defense mechanisms formed during immune responses. First, the signal peptides utilize FPRs to induce calcium responses. Second, the cells migrate toward higher concentrations of these peptides and third, if a certain concentration threshold is exceeded, they start producing reactive oxygen species in the extracellular milieu.

## 3.6. Formyl peptide receptor-dependent activation of murine leukocytes by bacterial signal peptides

---

The chapters 3.4.1.2 and 3.4.2.2 delivered pharmacological arguments that signal peptide recognition of human innate immune cells is mediated by FPRs. However, pharmacological manipulation alone does not provide substantial evidence. Hence, a genetic model was used to address the specificity of signal peptide recognition in *Fpr1* knockout mice.

First, to investigate whether signal peptides activate mouse FPRs in primary leukocytes, cells - including monocytes and granulocytes - were isolated from mouse bone marrow and challenged with distinct signal peptides.

### 3.6.1. Signal peptides activate neutrophils isolated from mouse bone marrow

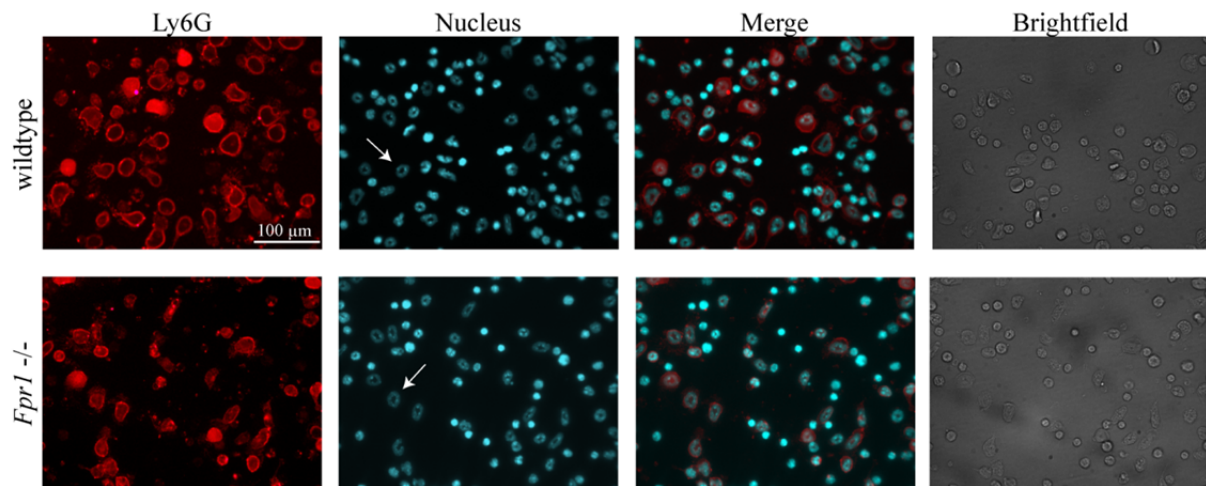
#### 3.6.1.1. Immunocytochemical analysis of isolated bone marrow cells

Bone marrow from long bones like tibia and femur of C57BL/6J mice contain many different cell types. With about 40% of the total cell number, neutrophils are the dominant cell type in femur bone marrow (Yang *et al.*, 2013). I investigated the purity and quality of my preparation using immunocytochemistry. First, crude bone marrow cell extracts were compared to granulocytes isolated from whole blood with beads targeted against the mouse neutrophil marker Ly6G. No obvious difference was observed for cell morphology, viability, calcium signals and dose-response behavior of the cells towards f-MLF, SP1, and SP16 (not shown). The bead-isolated cells showed a high degree of purity for mature granulocytes. However, this procedure yielded ~10 times less numbers of neutrophils than the bone marrow extracts. Therefore, bone marrow isolates were used for further investigation.

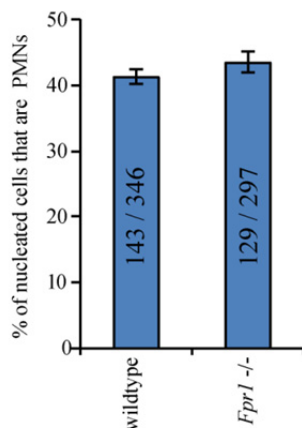
Knockout of the *Fpr1* gene could lead to differences in composition of cell populations and the differentiation states of the isolated granulocytes. To exclude such experimental bias the number and maturity of the cells in knockout mice was compared to that of wild type mice (Figure 3-31). Immunocytochemistry showed that  $42\% \pm 1.1\%$  and  $44\% \pm 1.7\%$  (wild type and knockout, respectively) of the cells had a clearly polymorph, ring-like shaped nucleus, identifying them as polymorphonuclear leukocytes (PMNs) (Figure 3-31 A and B).  $94 \pm 1.2\%$  and  $90 \pm 4\%$  (wild type and knockout, respectively) of those cells were positively stained for the mouse neutrophil marker Ly6G (Figure 3-31 C). The overall number of cells purified and

observed in the visual field was also comparable (143 cells for wild type, 129 cells for knockout). Morphological differences were not observed. This implies that the health status of neutrophils, isolated from *Fpr1*<sup>-/-</sup> mice is not compromised by the knockout.

### A Staining of mouse bone marrow cells with anti-Ly6G



### B Percentage of polymorphonuclear cells



### C Percentage of PMNs stained positive for Ly6G

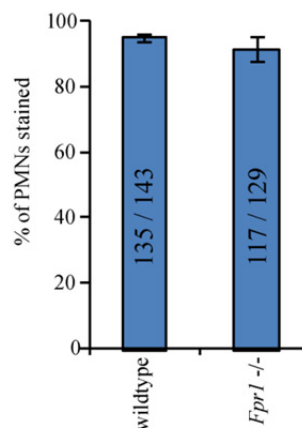


**Figure 3-31 | Immunocytochemical analysis of mouse bone marrow leukocytes**

The figure compares anatomical aspects of neutrophil granulocytes of bone marrow isolates from wildtype and *Fpr1*<sup>-/-</sup> mice. All data and images are representative for three independent experiments. **[A]** Confocal images of non-permeabilized bone marrow isolates from wildtype mice (upper panel) and *Fpr1*<sup>-/-</sup> mice (lower panel) stained with the Ly6G antibody. Ly6G is a surface marker for mature neutrophil granulocytes in mice. Nuclear counterstaining enables additional identification of polymorphonuclear leukocytes by their typical multi-lobular, circular nucleus (white arrows). **[B]** 42% (wildtype mice) and 44% (*Fpr1*<sup>-/-</sup> mice) of all nucleated cells are polymorphonuclear leukocytes (PMNs). The number of analyzed cells (polymorphonuclear / total number) is shown inside the columns. Data were analyzed in triplicates. **[C]** Overlay of Ly6G stained cells with polymorph shaped nuclei shows that 94% (wildtype) and 91% (*Fpr1*<sup>-/-</sup>) of the PMNs are stained positively for Ly6G. The number of analyzed cells (polymorphonuclear / total number) is shown inside the columns. Data were analyzed in triplicates.

### 3.6.1.2. Bone marrow leukocytes isolated from mice heterozygous for *Fpr1* can be activated by bacterial signal peptides

In order to see if murine leukocytes respond to signal peptides, a selection of six signal peptides with dissimilar peptide sequences was tested in calcium imaging on leukocytes isolated from mice heterozygous for *mFpr1* (Figure 3-32). Application of 1  $\mu\text{M}$  *Streptococcus*-SP1, *Staphylococcus*-SP3, *Hydrogenobacter*-SP16 or *Bacillus*-SP2-induced clear calcium signals that were even higher than those observed for the positive control f-MLF or the CCR1 agonist MIP1- $\alpha$ .

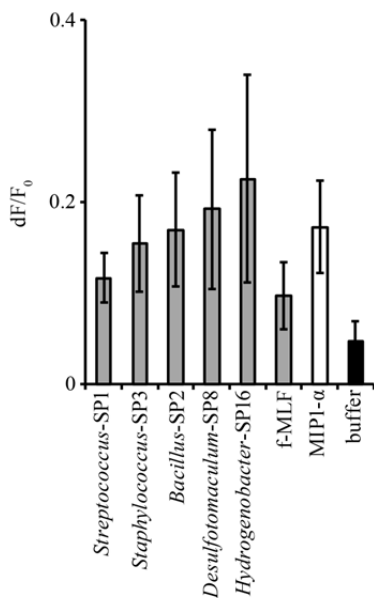


**Figure 3-32 | Bone marrow leukocytes isolated from *Fpr1*<sup>+/-</sup> mice respond to signal peptides with intracellular calcium mobilization**

Stimulation of bone marrow leukocytes (BMLs) with signal peptides (all 1  $\mu\text{M}$ ) leads to induction of calcium transients. f-MLF (1  $\mu\text{M}$ ) and MIP1- $\alpha$  (10  $\mu\text{M}$ ) (white), a CCR agonist, serve as positive controls; buffer (black) as a negative control. Data are averaged over two independent experiments; all data points were measured in triplicates.

### 3.6.2. Signals induced by mFpr1-selective concentrations of *Streptococcus*-SP1 are abolished in *Fpr1*<sup>-/-</sup> mice

Leukocytes of *Fpr1* knockout mice were challenged with 1  $\mu\text{M}$  of the mFpr1 preferential *Streptococcus*-SP1 or f-MLF, respectively, and compared to leukocytes from heterozygous and wildtype mice in calcium imaging. Both, the SP1 and the f-MLF-induced responses were abolished in cells of the knockout mice (Figure 3-33 A). The cells of wild type and knockout mice did respond to MIP1- $\alpha$ , a CCR agonist, with comparable intensity. Cells isolated from heterozygous animals showed a stronger response to all stimuli than those of wild type mice. However, they seem to expose a higher baseline activity because the signals monitored after buffer application were also higher than those of wild type mice. These data indicate mFpr1-dependent transduction of *Streptococcus*-SP1-induced signals. When SP1 was applied in a concentration of 10  $\mu\text{M}$ , which activated mouse Fpr2 in the heterologous expression system, the ligand induces a signal in the knockout mice. This signal was 30% smaller compared to

the signal of wild type mice, implying activation of mFpr2 by SP1 (Figure 3-33 B). Similar results have been observed for f-MLF (not shown). These data are consistent with the literature (Southgate *et al.*, 2008) and demonstrate that intracellular calcium mobilization, induced by the signal peptide is mediated via mouse formyl peptide receptors.

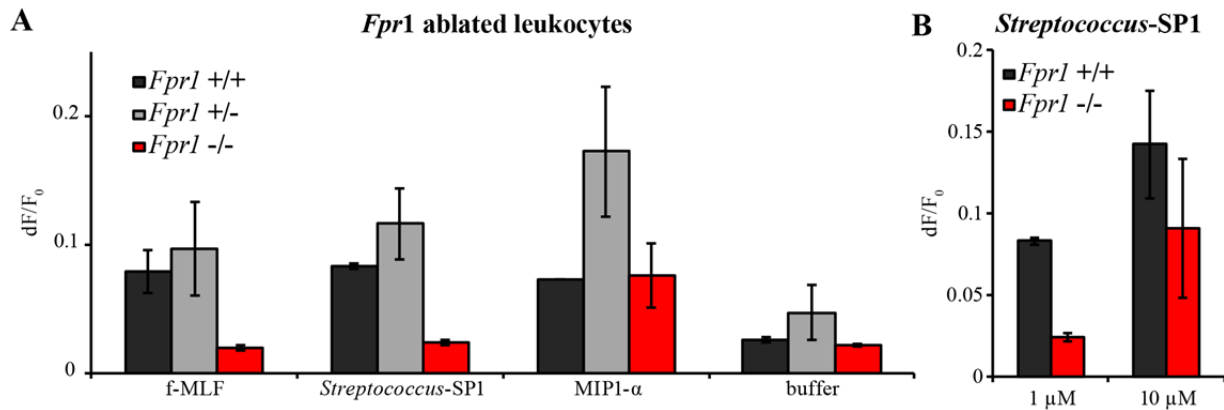


**Figure 3-33 | Calcium signals in murine bone marrow leukocytes induced by 1  $\mu$ M *Streptococcus*-SP1 are abolished in *Fpr1*<sup>-/-</sup> mice**

Calcium imaging of mouse bone marrow leukocytes (BMLs). The cells were isolated from wildtype (*Fpr1*<sup>+/+</sup>, shown in black) mice and mice heterozygous (*Fpr1*<sup>+/-</sup>, shown in gray) or deficient (*Fpr1*<sup>-/-</sup>, shown in red) for *Fpr1*. All data were averaged over two independent experiments; each condition was tested in triplicates. **[A]** Stimulation of BMLs by 1  $\mu$ M SP1 (mFpr1 selective) leads to calcium responses of cells expressing at least one genetic copy of *Fpr1*. These responses are absent in *Fpr1*<sup>-/-</sup> mice. This is also observed for 1  $\mu$ M f-MLF. MIP1- $\alpha$  (10  $\mu$ M) that served as excitability control, proves the functionality of the signaling pathway in *FPR1*<sup>-/-</sup> mice. **[B]** When the BMLs are stimulated by SP1 in a concentration that activated heterologous expressed mFpr2 (10  $\mu$ M), they respond with a strongly diminished calcium signal.

## Chapter 4

---

### Discussion

---

Several major findings emerge from the current thesis. I show for the first time that the vomeronasal formyl peptide receptor mFpr-rs1 can be activated by peptides that are derived from microorganisms. W-peptide, one of the best mFpr-rs1 activators so far, is capable of inducing calcium responses in vomeronasal sensory neurons. This supports the theory that vomeronasal FPRs can mediate olfactory detection of pathogens. Furthermore, the data provide substantial evidence for a novel FPR-mediated pattern-recognition mechanism. Cells from the innate immune system utilize FPRs for highly sensitive detection of bacterial signal peptides. Therefore, my data provide first evidence for a mechanism by which mammalian immune cells could sense the presence of bacteria.

#### 4.1. DMSO is a newly identified FPR agonist with therapeutic potential

---

In order to compare the pharmacology of vomeronasal and immune FPRs a variety of substances was tested on heterologously expressed FPRs. Surprisingly, DMSO, used as a co-solvent for organic compounds and hydrophobic peptides, induced strong calcium signals in *hFPR2*, *mFpr1* and *mFpr2* transfected HEK293T cells. This is very interesting because DMSO has been used in anti-inflammatory treatment of acute ectopic lesions like rheumatic disorders for years (Matsumoto, 1965; Trice, 1985). The drug exhibits extraordinary skin-penetrating capabilities, which is why it has been used as a transdermal penetration enhancer in targeting neoplastic cancers (Hagemann and Evans, 1968; Williams and Barry, 2012). Because of its cell-permeating properties, DMSO-induced signals must be investigated with special care; DMSO evoked FPR-independent signals in HEK293T cells transfected with the empty vector control at concentrations  $\geq 2\%$  [v/v]. However, the shape of the calcium transients of the mFpr1, mFpr2, and hFPR2-dependent signals showed a faster onset and had

a steeper slope than that observed for the empty vector control, providing first evidence for receptor-mediated signaling. Importantly, responses observed for concentrations below 2% [v/v] were certainly mediated by the above mentioned receptors (hFPR2, mFpr1 and mFpr2) because no signals have been observed for the empty vector control or other functional FPRs like hFPR1, hFPR3, and mFpr-rs1. To verify that DMSO activates the receptor, desensitization experiments were conducted. Signals induced by *mFpr1* and *mFpr2* expressing cells were absent after desensitization of the receptors by pre-stimulation with the mFpr1 and mFpr2 agonist f-MLF, further arguing for receptor-mediated signaling. More importantly, the DMSO evoked signals were completely dependent on co-expression of the G protein alpha subunit  $G_{\alpha 16}$ . Only the combination of receptor and G protein led to the calcium transients induced by DMSO at concentrations  $> 0.1\%$  [v/v]. These evidences strongly support the argumentation that DMSO mediates calcium signals via mFpr1, mFpr2, and hFPR2. As mentioned above, DMSO has been described to mediate anti-inflammatory actions in rheumatic disorders. In this regard, the illustrated data provide first evidence for a possible FPR-mediated anti-inflammatory mechanism. There are many studies providing evidence for an inflammation-resolving role of hFPR2 in human monocytes and granulocytes (Krishnamoorthy *et al.*, 2010; Corminboeuf and Leroy, 2015). In addition, hFPR2 has been proposed to be involved in the homeostasis of rheumatic inflammation: application of the organic hFPR2 ligand Lipoxin A4 led to a marked reduction of inflammatory cytokines in human synovial fibroblasts (Fiore *et al.*, 2005). It is possible that the anti-inflammatory potential of DMSO during rheumatic lesions is triggered by DMSO-dependent activation of hFPR2. Dose-response analysis of mFpr1 and mFpr2 showed dose-dependent activation of both receptors with  $EC_{50}$  values of  $\sim 100$  mM ( $\sim 1\%$  [v/v] DMSO). At first, this might seem like a very high concentration. However, application of 50 – 100% DMSO is the standard concentration in medication of rheumatic lesions (Matsumoto, 1965; Trice, 1985). Due to its remarkable skin-penetrating potential (spilling DMSO on the finger makes one taste it after a few seconds; Williams and Barry, 2012) it is realistic that at least 1% DMSO will reach hFPR2 expressing inflammatory leukocytes.

The results provide first insights into a possible new mechanism in which FPR2 is utilized to treat immune diseases. If this theory proved right, DMSO could be used to treat many of the perilous auto-immune diseases that scourge humanity. Therefore, it would be highly interesting to see whether DMSO is able to trigger FPR2-dependent anti-inflammatory responses in cells of the innate immune system.

## 4.2. Recognition of pathogen-derived peptides by vomeronasal mFpr-rs1

---

In the early course of this study a variety of substances was tested in order to determine whether they can activate vomeronasal FPRs when expressed in HEK293T cells. The results of this compound screening revealed a number of agonists for the vomeronasal receptor mFpr-rs1. The best agonists identified during this screening, W-peptide and M-peptide, proved to be very useful pharmacological tools to investigate the receptor's binding properties. Therefore, these peptides were used in structure-function analyses of mFpr-rs1.

### 4.2.1. Activation of the vomeronasal receptor mFpr-rs1 by W-peptide and M-peptide

The experiments illustrated in chapter 3.2 clearly show that mFpr-rs1 can be activated by M-peptide and W-peptide. Both peptides have been intensively studied in several calcium imaging assays. At the time when these substances were identified as mFpr-rs1 activators, not even a handful of agonists were known for the entire vomeronasal FPR subfamily (Bufe *et al.*, 2012). Furthermore, W-peptide was the most sensitive peptide agonist described for vomeronasal FPRs so far ( $EC_{50}$  values in the upper nanomolar range). This has been verified by the laboratory of Richard Ye; they reported degranulation of mFpr-rs1-transfected rat basic leukemia cells (RBL-2H3) upon stimulation with 100 nM W-peptide (He *et al.*, 2013). As W-peptide has been demonstrated to be a potent agonist, it was used as a tool to investigate pharmacological properties of mFpr-rs1 in structure-function analyses. Results from these are discussed below.

### 4.2.2. Key structures for activation of mFpr-rs1 by small peptides

During a compound screening to identify agonists for vomeronasal FPRs, W-peptide and M-peptide were identified as activators of mFpr-rs1 (chapter 3.2). Both are synthetic peptides described as two of the most potent hFPR1 and hFPR2 activators known so far (Bae *et al.*, 2001; Bae *et al.*, 2012). Dose-response analyses performed in the current work proved that both peptides activate hFPR1, hFPR2, and hFPR3 as well as mFpr1, Fpr2, and mFpr-rs1. Interestingly, W-peptide displayed a conserved concentration-response profile between FPR1 and FPR2 of human and mouse. Thus, the results imply that W-peptide inherits a peptide motif that is conserved with respect to FPR activation. To test whether such a motif exists, a

structure-function analysis including several carefully selected derivatives of W-peptide was performed. The results of this analysis led to the prediction of a binding motif for short peptides by mFpr-rs1.

#### ***4.2.2.1. A core motif of four amino acids is necessary to activate mFpr-rs1***

Testing N-terminal truncated isomers of W-peptide revealed a core motif of four residues that are crucial for mFpr-rs1 activation. When mFpr-rs1 was challenged with shorter W-peptide isomers, no responses have been observed. However, small calcium signals were observed when f-MLF was tested in high concentrations (100  $\mu$ M). This indicates that mFpr-rs1 can be activated by tripeptides although the motif may be incomplete as four amino acids are required for full activation.

#### ***4.2.2.2. mFpr-rs1 prefers peptides with C-terminal D-amino acids rather than L-amino acids***

W-peptide and M-peptide are potent activators of mFpr-rs1 with similar EC<sub>50</sub> values. It was hypothesized that this functional conservation may be due to a common structural feature that was unique in the tested array of ligands: both peptides carry a C-terminally-amidated D-methionine at the C-terminus (Table 3-2 and Figure 3-8). To investigate the importance of these features in terms of mFpr-rs1 activation they were analyzed in structure-function analyses.

The current work provides fundamental evidence that mFpr-rs1 prefers hexapeptides with C-terminal D-amino acids rather than L-amino acids. When the D-methionine of W-peptide or M-peptide is substituted by its L-isomer, the affinity towards the receptor was reduced by at least 14-times. This strongly argues for a stereo-selective preference of mFpr-rs1 for D-amino acids. Furthermore, the signal amplitudes induced by the L-isoforms were approximately 50% smaller than those observed for the corresponding D-isomers, indicating lesser efficacy of the L-isoforms. Similar results have been observed when the methionine of W-peptide was replaced by cysteine, another biogenic sulfuric amino acid (Bufe *et al.*, 2012). These data demonstrate that although the L-epimers are recognized by the receptor, C-terminal D-amino acids are clearly preferred.

#### ***4.2.2.3. The double-bonded oxygen of terminal carbonyl groups is important for affinity of peptides to mFpr-rs1***

Experiments to determine whether the C-terminal amidation is necessary for activation of mFpr-rs1 revealed that the amidation is important to preserve the affinity to the receptor.

Further investigations revealed that the double-bonded oxygen present in the amidation is the determining factor for activation of mFpr-rs1. This is discussed in following the section.

The importance of the double-bonded oxygen in the carbonyl group has been addressed mainly by substitution of the C-terminal amidation (CONH<sub>2</sub>) in W-peptide. To elucidate whether the nitrogen is necessary for receptor activation, a W-peptide derivative carrying a formaldehyde (CHO) at its C-terminus was tested on mFpr-rs1 in concentration-response experiments. There were almost no differences in EC<sub>50</sub> values and efficacy between W-peptide carrying an amidation (CONH<sub>2</sub>) or W-peptide carrying a formaldehyde (CHO) when tested on mFpr-rs1. Since the aldehyde does not contain a nitrogen atom, nitrogen can be excluded as the determinant factor. However, the amide and the formaldehyde contain a carbonyl group (C=O). When W-peptide was synthesized without a C-terminal modification, exposing the free carboxyl group (COO<sup>-</sup>), the affinity and efficacy to the receptor were significantly reduced. The major physicochemical difference between the carboxy group and the distinct carbonyl moieties is that the carboxy group contains no double-covalent-bonded oxygen (C=O). Instead, a carboxyl group harbors a delocalized electron, adding a negative net charge to the oxygen. These revelations provided enough evidence to hypothesize that, in terms of activation, the C-terminal amidation and aldehyde group are equivalent to the N-terminal formylation. To test this hypothesis, the retro-inverted W-peptide was synthesized and tested. As assumed, the retro-inverted peptide showed very similar properties to W-peptide with respect to affinity and efficacy. More recently, this has also been demonstrated for the human and mouse FPR1 and FPR2 (Bufe *et al.*, 2015). The strong pharmacological correlation between the retro-inversed W-peptide and the “native” W-peptide proved the validity of this hypothesis. Computer-based structural modelling of both substances shows that W-peptide and the retro-inverted isomer can adopt conformations with aligning folding states (Bufe *et al.*, 2015; Figure 4-1). The rendered three-dimensional structures envision the close spatial orientation between the amidation of the C-terminal D-methionine and the N-terminal formyl-methionine.

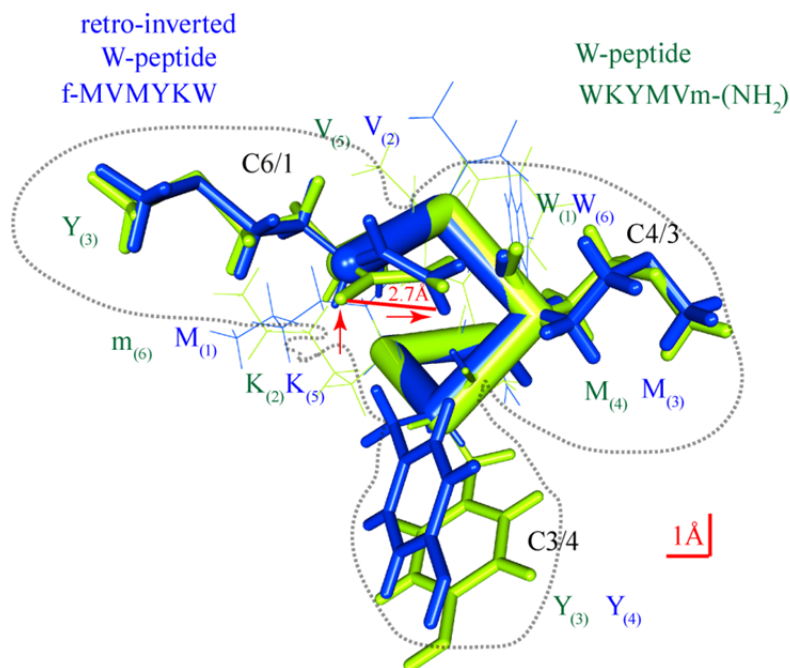


**Figure 4-1 | Retro-inversion of W-peptide reveals a common structural motif of N-terminally formylated and C-terminally amidated peptides**

Three-dimensional computer model predicting the secondary alpha-helical structure of W-peptide (green) and the retro-inverted W-peptide (dark blue). The spatial overlay shows that both structures align in proximity and orientation. The carbonyl double-bonded oxygen (red arrows) of the C-terminal amidation (W-peptide) and the N-terminal formylation (retro-inverted W-peptide) share a distance of 2.7Å (red line). The black letters indicate the amino acid position of W-peptide and retro-inverted W-peptide, respectively. The colored letters name the amino acids of the indicated peptides. *By courtesy of Reinhard Kappl.*

The importance of the N-terminal formylation in order to reach high performance in FPR activation is known since the discovery of FPR1 (Schiffmann *et al.*, 1975; Showell *et al.*, 1976). Considering this, it is not very surprising that DMSO also activates FPRs in high concentrations. DMSO contains a central sulfoxide consisting of a sulfur atom with a covalently double-bonded uncharged oxygen (S=O). With this, the chemical structure distantly resembles the carbonyl moiety. This sulfoxide probably retains a residual activation potential towards the FPRs. It is also known, that N-terminally acetylated peptides can be as effective as formylated ones, underlining the role of the carbonyl group (Gao *et al.*, 1994).

In my opinion, the current investigation provides the most thorough study of mFpr-rs1. It does not only demonstrate activation of mFpr-rs1 by several ligands but also provides a solid pharmacological analysis of the structural properties required for activation of the receptor. The issues discussed above show that mFpr-rs1 is activated by peptides with certain modifications like C-terminal amidation or N-terminal formylation. It is, however, important to mention that binding to mFpr-rs1 by peptides takes additional requirements. C-terminal amidation alone is not sufficient to activate the receptor, as shown in single cell and cell

population calcium imaging. First, only peptides with an amidated methionine were capable of activating the receptor in nanomolar concentrations. Second, a minimal motif of four amino acids is necessary for complete activation. Third, as shown in our latest publication (Bufe *et al.*, 2015), the motif requires a hydrophobic or positively charged amino acid at amino acid position C4 (the fourth amino acid if counted from the C-terminus). This does also apply for formylated or acetylated peptides. I could show that mFpr-rs1 is activated by formylated peptides. However, single cell experiments have shown that formylated peptides like ND1 and CO1 cannot activate the receptor. In addition, only very few of more than 20 tested N-terminally formylated signal peptides derived from bacteria could activate the receptor (Bufe *et al.*, 2015). This implies that the discovered peptide motif necessary for mFpr-rs1 activation is not fully understood and requires further investigation.

#### **4.2.3. mFpr-rs1 detects pathogen-derived peptides: possible novel mechanisms to sense microbes**

Former publications have shown that the vomeronasal organ (VNO) recognizes disease-related molecules (Shirasu and Touhara, 2011), including bacterial products like f-MLF (Rivière *et al.*, 2009). More recently, it has been shown that the vomeronasal organ (VNO) mediates the avoidance of sick or parasitized conspecifics (Boillat *et al.*, 2015). FPRs expressed in the innate immune system are well-known for their capability to detect many disease-related and microbial products, including the bacterial f-MLF (Migeotte *et al.*, 2006). Since a subfamily of FPRs is found in neurons of the VNO, they provide excellent candidates as detectors of these avoidance-mediating molecules. As described in the chapters 3.2 and 3.4 the vomeronasal FPR mFpr-rs1 is activated by several peptides that are derived from bacteria or exhibit posttranslational modifications that are typical for bacterial proteins/peptides. This is consistent with the idea that vomeronasal FPRs mediate the detection of microbes. Arguments supporting this hypothesis are discussed below.

##### **4.2.3.1. Detection of D-amino acid-containing peptides by mFpr-rs1**

The results illustrated in chapter 3.2 show that W-peptide and L-W-peptide are agonists for mFpr-rs1. The peptide sequence of L-W-peptide (WKYMVM) was found to be present in a protein of the bacterium *Kribella flavida*. Interestingly, both peptides were able to activate a subset of vomeronasal sensory neurons, a cell type that naturally expresses mFpr-rs1 (Liberles *et al.*, 2009). As discussed in chapter 4.2.2, the motif for mFpr-rs1 activation requires at least

four amino acids. Database analyses have shown that both, the five-amino acid and the four-amino acid core motif of W-peptide (KYMVM and YMVM, respectively) can predominantly be found in various micro-organisms. Most of these motifs have been identified in bacteria but were also identified in viruses and fungi. Some of them are well known human and mouse pathogens like *L. monocytogenes* or *S. aureus*. This means that mFpr-rs1 is able to detect bacterially-derived peptides. More interestingly, the affinity of W-peptide and M-peptide to mFpr-rs1 is significantly increased when the C-terminal L-methionine is substituted by its corresponding D-enantiomer. In nature, D-amino acids are often found in microbial products (Martínez-Rodríguez *et al.*, 2010). It is well known that D-alanine and D-glutamate are necessary for the composition of the peptidoglycan layer of bacteria. D-amino acids can also be introduced into peptides by non-ribosomal proteins (NRPs). These are non-ribosomal peptide/protein complexes in fungi and bacteria that are able to biosynthesize peptides and proteins. Their hallmark is the use of very unusual amino acids (e.g. in D-configuration) and the addition of various formerly unknown amino acid modifications (Schwarzer *et al.*, 2003; Caboche *et al.*, 2007). The results presented in chapter 3.2.3 show that C-terminal modifications like amidation or formaldehyde boost the affinity of W-peptide toward mFpr-rs1. It would be interesting to see if these modifications are regularly formed by NRPs or if other NRP-based modifications are capable of activating mFpr-rs1. Expansion of this knowledge could lead to a novel mechanism for detecting products of microbial metabolism.

These results further support the theory that mFpr-rs1 functions as a pathogen detector.

#### ***4.2.3.2. Detection of N-terminally formylated peptides by mFpr-rs1***

The experiments depicted in chapter 3.2.4 show that mFpr-rs1 is activated by the formylated retro-inverted W-peptide. Although the retro-inverted sequence of W-peptide has not been identified in microorganisms so far, this experiment demonstrates that mFpr-rs1 is capable of recognizing formyl peptides. When f-MLF was applied at concentrations of 100  $\mu$ M, small calcium signals were observed, further supporting the thesis that mFpr-rs1 acts as a receptor for formyl peptides. This finding has more recently been verified by our group (Bufe *et al.*, 2015): N-terminally formylated bacterial signal peptides, including such from mouse pathogens, emerged to be activators of mFpr-rs1. One of these peptides, *Desulfotomaculum*-SP8 exhibits the f-MLF motif at the N-terminus and was capable of activating mFpr-rs1 at high nanomolar concentrations. This verifies two things: (1) f-MLF activates mFpr-rs1 and (2) if the peptide contains more than three amino acids, thereby fulfilling the minimal requirements for the binding motif discussed in 4.2.2.1, its sensitivity is markedly increased.

Although the receptor was activated by several signal peptides with nearly identical  $EC_{50}$  values, thus far no tested agonist revealed significantly higher affinity than W-peptide. This could mean that the identified molecules are not the primary targets of mFpr-rs1. Further studies should address this issue.

#### ***4.2.3.3. Activation of vomeronasal sensory neurons by the mFpr-rs1 agonist W-peptide***

An important question following receptor characterization is whether W-peptide is able to activate cells of the vomeronasal organ, where mFpr-rs1 is naturally expressed. The data illustrated in chapter 3.3 clearly show that 5  $\mu$ M W-peptide and L-W-peptide each induced calcium transients in about 2% of the investigated neurons. Activation of vomeronasal sensory neurons (VSNs) by W-peptide has been independently determined by other members of our laboratory. P. Chamero and B. Stein showed W-peptide activation in VSNs infected with viruses encoding mFpr-rs1 (unpublished results). A. Schmid observed calcium responses of dendritic knobs in whole mount preparations of the VNO sensory epithelium induced by 100 nM W-peptide (unpublished results). Similarly, field potential measures in vomeronasal sensory epithelia, revealed that W-peptide induces electrical currents (unpublished results, P. Hendrix).

Further evidence is needed to prove that these responses are mediated by mFpr-rs1. One possibility to do so is to co-localize receptor expression with calcium signals induced by mFpr-rs1 agonists. Co-localization of both, the receptor and the calcium signal will hint to mFpr-rs1-mediated signaling. H. Stempel, a PhD student in our laboratory, has already purified anti-mFpr-rs1 antibodies that can be used for surface staining of VSNs. However, to prove mFpr-rs1-mediated activation of VSNs by W-peptide and signal peptides, investigation of mFpr-rs1 knock-out mice is mandatory. Those could be used for calcium imaging of vomeronasal sensory neurons after stimulation with mFpr-rs1 agonists. Furthermore, these mice would provide an excellent tool for *in-vivo* characterization of the receptor, e.g. in behavioral avoidance experiments. I expect that if bacterial signal peptides were presented to mice expressing intact copies of *mFpr-rs1*, they would avoid the presented samples. In theory, this behavior is likely to be absent in *mFpr-rs1*-deficient mice.

### 4.3. Neo-functionalization of mouse Fpr-rs receptors expressed in the VNO

---

The results of the structure-function analysis of peptide ligands reveal a clear difference between immune FPRs (hFPR1-3, mFpr1-2) and the vomeronasal FPRs (mFpr-rs1, mFpr-rs3, mFpr-rs4, mFpr-rs6, and mFpr-rs7). While the immune FPRs responded to the majority of the tested substances, particularly the peptides, the vomeronasal FPRs remained silent, with the only exception of mFpr-rs1. The tested ligands encompassed more than 30 substances from distinct chemical classes like arachidonic acid derivatives, sulfoxides and peptides. The tested peptides were varying in primary structure, peptide length and either unmodified or carrying distinct naturally-occurring N- or C-terminal modifications (e.g. formylation). Some of the peptides are naturally-occurring microbial products (like the bacterial f-MLF) or fragments of viral glycoproteins (e.g. T20). I also tested several eukaryotic peptides, like the Temporin A amide that is usually found on amphibian skin, or human immune modulators like Ac2-26. Among the tested peptides were damage-associated molecular pattern (DAMP) molecules: peptides derived from the mitochondrial proteins ND1 and CO1. None of these agonists, whose functionality was proven by testing them on immune FPRs (Table 3-2), was able to activate the vomeronasal FPRs. The receptors also did not respond to the pan-immune FPR agonists W-peptide, M-peptide or their epimers. Bacterially-derived signal peptides that were identified as highly affine FPR agonists based on a hidden consensus motif for immune FPR activation, could not induce responses in cells transfected with plasmids coding for mFpr-rs3, mFpr-rs4, mFpr-rs6, and mFpr-rs7 (data not shown). All peptides were used up to concentration of 10 - 30  $\mu$ M, which are very high for receptors expressed in sensory neurons (Leinders-Zufall *et al.*, 2009). Immunocytochemical analysis of the Rho-tagged FPRs showed that they are inserted into the plasma membrane in the correct orientation. Their expression levels were comparable to those observed for the immune FPRs and mFpr-rs1, all of which could readily be activated by several substances. However, the receptors mFpr-rs3, mFpr-rs4, mFpr-rs6, and mFpr-rs7 did not respond to any stimulus. The number of viable cells present in the visual field was highly similar, arguing against lethal effects due to receptor expression.

In addition, the cells were readily excitable by the positive control stimulus ATP in single cell experiments, excluding lethal damage taken by the transfected constructs. The cloned constructs were carefully sequenced several times: besides mFpr-rs7, which had a F147L amino acid substitution, no amino acid exchanges were observed for the vomeronasal receptors, excluding bias caused by structural deviations from the reference sequences. Since all vomeronasal FPRs (besides mFpr-rs1) are expressed in the  $G_{\alpha i2}$  enriched zone of the

vomer nasal organ I tested whether they can interact with G protein chimeras derived from distinct G proteins, including  $G_{\alpha i2}$ . Although those were functional (they readily interacted with mFpr1 and mFpr2), no calcium signals were observed for mFpr-rs3, mFpr-rs4, mFpr-rs6 and mFpr-rs7. To couple the FPRs to PLC dependent calcium mobilization pathways in HEK293T cells the human  $G_{\alpha i6}$  was co-transfected in most experiments. Although this alpha subunit is described to be highly promiscuous in receptor-coupling (Offermanns and Simon, 1995) it was checked whether the murine FPRs prefer the murine ortholog  $G_{\alpha i5}$ . Although equally promiscuous in receptor-coupling (Offermanns, 1995), co-transfection of  $G_{\alpha i5}$  did not lead to improvement in calcium signaling of the murine FPRs. There are two obvious explanations standing to reason. First, the vomeronasal receptors utilize special downstream signaling components not present or incomplete in the used cell line. Second, they specialized on ligands that remain to be identified. A combination of both might as well be possible. It is possible that the vomeronasal FPRs other than mFpr-rs1 are tuned towards recognition of substances that are not recognized by immune FPRs, thereby expanding the repertoire of detectable molecules. Since those receptors are expressed in the  $G_{\alpha i2}$  enriched zone of the VNO, it is reasonable to assume that they rather recognize lipophilic, volatile substances, which are classical activators of neurons in this zone (Chamero *et al.*, 2012). On the other hand, mFpr-rs3, mFpr-rs4, mFpr-rs6 and mFpr-rs7 exhibit a striking pattern in structural alignment, distinguishing them from FPRs expressed in the immune system. All of them lack a certain five amino-acid motif located in the third extracellular loop (Migeotte *et al.*, 2006). This gap is also found in the corresponding vomeronasal orthologs found in rat (Liberles *et al.*, 2009). It is possible that this deletion causes conformational changes of the receptor which influence ligand binding or signal transduction behavior. Recent phylogenetic analyses of the FPR family in mammals provide genetic evidence for a rodent-specific neo-functionalization of the vomeronasal FPRs (Liberles *et al.*, 2009). It is unlikely that a family of conserved immune receptors (i.e. immune FPRs) develops into a bigger subfamily (vomeronasal FPRs) that will eventually turn out to be non-functional. In 2009, Rivière *et al.* reported activation of heterologously expressed vomeronasal FPRs for the first time. Thus far, this is the only publication describing activation of vomeronasal FPRs. Many other studies, including my own (Bufe *et al.*, 2012; Liberles *et al.*, 2009; Southgate *et al.*, 2008; Gao *et al.*, 2007; Wang *et al.*, 2002) failed to report activation of those vomeronasal FPRs. One possible explanation for this discrepancy could be due to structure-related utilization of distinct signaling cascades. The signaling apparatus of the VNO is not completely discovered and this organ is known for its molecular complexity (Tirindelli *et al.*, 2009). Furthermore, several reports indicate that

FPR signaling is dependent on additional interaction partners at the surface of the plasma membrane, like CD38 (Partida-Sánchez *et al.*, 2001), RAGE (Slowik *et al.*, 2012) or MARCO (Brandenburg *et al.*, 2010). Since Rivière *et al.* (2009) employed a specialized HEK293 cell line, which was formerly used for heterologous expression of taste and olfactory receptors, it is possible that this cell line provided factors not present in commercially available cell lines. It might therefore be profitable to test the receptors in cell lines that are derived from murine sensory neurons or similar cells, increasing the chance to hit the right button.

#### **4.4. Recognition of bacterial signal peptides of innate immune cells is mediated by FPRs – evidence for a novel pattern recognition mechanism**

---

Heterologously expressed FPRs are, without doubt, activated by signal peptides that are derived from naturally occurring pathogens (Bufe *et al.*, 2015). However, an important question is whether, and how, these peptide cues are detected by cells in a natural environment. To demonstrate that these cues are indeed detected in native cells, I used primary leukocytes of the innate immune system of human and mouse.

##### **4.4.1. Detection of signal peptides by innate immune cells occurs with extraordinary high affinity and receptor specificity**

Over one-third of the bacterial proteome is inserted into, or secreted across the bacterial membrane (Papanikou *et al.*, 2007). These processes are mediated by export systems that translocate proteins depending on their sorting tags or signal peptides (Blobel, 1980). So far, more than 16 such systems are known (Papanikou *et al.*, 2007).

These transport systems can roughly be classified into two groups: Sec-dependent and Sec-independent. The Sec-dependent pathway, which is the best-understood pathway thus far, is ubiquitous and essential for viability in all three domains of life (Papanikou *et al.*, 2007). All proteins that are secreted via Sec-dependent mechanisms are synthesized as pre-(pro-)proteins carrying an N-terminal signal sequence (Chatzi *et al.*, 2013). This sequence typically has a three-domain structure which is found in eukaryotes and prokaryotes (von Heinje, 1990). Although not mandatory, the typical signal peptide contains a positively charged N-terminus (1-8 amino acids), a hydrophobic helix-forming core (4-16 amino acids) and a polar

C-terminal domain that carries a cleavage site (Chatzi *et al.*, 2013). Most secretory pre-proteins are exported post-translationally by binding to the SecB/SecA chaperones with the signal sequence or the nascent peptide chain as soon as they emerge from the ribosome exit tunnel (Chatzi *et al.*, 2013). In gram-negative bacteria<sup>13</sup> the pre-pro-protein is then targeted to the inner membrane by docking to SecYEG translocase (Chatzi *et al.*, 2013). The signal peptide is then cleaved at the C-terminal domain by signal peptidase I, releasing the pro-protein into the periplasmic space (Dalbey *et al.*, 2012). For full secretion of the protein across the outer membrane, distinct pathways can be used (Papanikou *et al.*, 2007). The cleaved signal peptide is usually further degraded into smaller fragments by signal peptide peptidases (Dalbey *et al.*, 2012). It is important to mention that the utilization of N-terminal signal peptides is not restricted to Sec-dependent pathways. There are other pathways that mediate export of proteins across the membrane that employ a pathway-specific signal peptide sequence at the N-terminus, similar to the Sec-dependent signal peptide. These include the twin-arginine-transporter (TAT) signal sequence, the lipoprotein signal peptide, the prepilin and the preflagilin signal peptides.

In this work, several N-terminal signal peptide fragments as well as four full-length signal peptides were tested on primary human and murine leukocytes of the innate immune system. All of them were able to induce calcium signals through at least one human and mouse FPR. However, more important: some signal peptides are recognized with extraordinary sensitivity and specificity. Concentration-response experiments showed that several of the signal peptides showed extraordinarily high affinity for hFPR1 or hFPR2 when expressed in HEK293T cells (Bufe *et al.*, 2015). With EC<sub>50</sub> values in the lower picomolar range they are among the most affine naturally-derived agonists for FPRs described so far (Ye *et al.*, 2009). In addition, these highly affine ligands were also very selective for a particular FPR. SP1, for example, showed > 1,000 times higher affinity towards hFPR1 than hFPR2. This high affinity paired with the strong selectivity provides an excellent pharmacological tool for the characterization of FPRs. Importantly, the current study on primary leukocytes demonstrates that these responses are indeed highly specific in primary cells. This has predominantly been proven with the hFPR1 selective ligand *Streptococcus*-SP1. The high affinity SP1 exhibited on hFPR1-transfected HEK293T cells (EC<sub>50</sub> = 1.9 nM) was almost identical to that observed for human monocytes and granulocytes. Even the shape and onset of the curves were highly comparable. This pharmacological resemblance was further strengthened by the fact, that

---

<sup>13</sup> Gram-positive bacteria use a very similar mechanism, which is, however, owed to its higher complexity, not that well described in current publications.

elongation of SP1 (extending it to its full-length) caused an almost identical reduction of sensitivity in HEK293T cells and monocytes (Bufe *et al.*, 2015). Similar behavior was also observed in human monocytes. The resulting concentration-response curves were again highly comparable in shape and onset. Very similar results have been observed with the control substances f-MLF and W-peptide in both, human monocytes and granulocytes. This is valid pharmacological evidence arguing for hFPR1-mediated signals in human monocytes and granulocytes. Monocyte single cell experiments performed by Carsten Kummerow (Saarland University, Medical School Homburg, Department of Biophysics) in which the calcium signal was co-localized with hFPR1 expression showed that > 90% of the responding cells were positive for hFPR1 and the monocyte marker CD14, further strengthening my argumentation. The specificity has further been addressed by the desensitization experiments in human monocytes. Only the hFPR1 preferential agonists f-MLF and SP1 were able to induce desensitization towards additional application of hFPR1 selective agonists. This desensitization was not observed when RANTES, an agonist for the chemokine G protein-coupled receptor CCR1, was applied prior to SP1 stimulation. On the contrary, the signal induced by SP1 after stimulation with RANTES had the same amplitude as the signal caused by the RANTES stimulation. This implies that RANTES and SP1 utilize different receptors, in contrast to f-MLF and SP1, which both signal through hFPR1. Further pharmacological evidence is provided by the hFPR1-selective blockers CsH and tBoc2. Both were able to block the SP1-mediated signaling in monocytes whereas calcium transients induced by RANTES were unaffected despite presence of the blockers. This has also been shown in human neutrophils: CsH was able to abolish the SP1-induced signals but signals evoked by SP2 preferential agonists like *Staphylococcus*-SP22 were not impaired. Finally, the specificity of the signals has been validated in *Fpr1*-deficient animals. Unlike the wild type and the heterozygous controls, leukocytes of *Fpr1* *-/-* mice were unable to respond to SP1 or f-MLF when applied in concentrations below 10  $\mu$ M. In order to test whether the function of mFpr2 is impaired I challenged the cells with higher concentrations of f-MLF and SP1. mFpr2 is activated by both substances, however with EC<sub>50</sub> values in the micromolar range (Southgate *et al.*, 2008; Bufo *et al.*, 2015). In line with the literature the cells were able to respond to 10  $\mu$ M SP1, although these responses were strongly reduced in cells of the *Fpr1*-deficient mice, strongly arguing for mFpr2-mediated signaling. These data prove that the detection of SP1 by monocytes and granulocytes is indeed committed by FPR1. This careful pharmacological characterization of SP1-dependent signals proves that the concentration-response correlation of this highly affine agonist is a valid tool to investigate receptor-specific

signaling in primary cells. Therefore, I concluded that all signal peptides that induced responses in human monocytes and granulocytes were mediated by FPRs, if a great overlap between the published  $EC_{50}$  values of transfected HEK293T cells (Bufe *et al.*, 2015) and the values of primary cells was observed. This was generally the case for hFPR1 preferential ligands. However, this was not applicable for hFPR2 preferential signal peptides. There was no such strong correlation between the dose-response curves for heterologous hFPR2 and monocytes/granulocytes as observed for hFPR1. In one case (SP22) the dose-response curve was shifted to higher concentrations by a factor of 77 from heterologously expressed hFPR2 to monocytes. Similar results have been published by Kretschmer (Kretschmer *et al.*, 2010). They showed that  $EC_{50}$  values of the hFPR2 preferential agonists PSM $\alpha$ 3 and PSM $\beta$ 2 measured in HL60 cells were shifted to higher concentrations in human neutrophils in calcium imaging experiments. Utilizing the well-described hFPR2 blocker PBP10, I could show that the signals induced by the hFPR2 preferential signal peptides SP4, SP16 and SP22 were mediated by hFPR2. PBP10 is a RhodaminB-coupled cell membrane permeable decapeptide that has been shown to act via allosteric binding at the C-terminus of hFPR2 but not hFPR1 (Forsman *et al.*, 2012). My experiments confirm these results: following pre-incubation with PBP10, calcium signals have only been observed in human neutrophils when SP1 or f-MLF was applied in hFPR1 specific concentrations. Signals mediated by SP4, SP16 and SP22 in hFPR2 specific concentrations, however, were completely abolished when applied after pre-incubation with PBP10. This discrepancy in dose-response behavior cannot be explained by differences in receptor structure or expression. The hFPR2 containing plasmid was sequenced several times and the nucleotide sequence corresponds to the reference sequence. Expression levels and patterns of hFPR2 were comparable to that of hFPR1 in HEK293T cells (Figures 3-1-1 and 3-3-2). This was also true for monocytes. Although the stainings for granulocytes showed lower expression rates for hFPR2 than for hFPR1, the number of hFPR2-positive granulocytes was still higher than the number of stained HEK293T cells, excluding a failure in receptor expression. However, this pharmacological effect could be due to distinct glycosylation patterns caused by the distinct cell types. Another explanation could be the use of distinct downstream signaling molecules. For heterologous analysis the human  $G_{\alpha 16}$ , which is known to be expressed exclusively in hematopoietic cells of the myeloid lineage (Rhee, 2001) was co-transfected. However, this does not mean that this G protein subunit is predominantly used by hFPR2 in monocytes and granulocytes. Besides, the possible influence of beta and gamma subunits of the heterotrimeric G proteins was not addressed in this work. It is also possible that hFPR2 employs co-receptors like CD38 (Partida-Sánchez *et al.*, 2001),

MARCO (Brandenburg *et al.*, 2010) or RAGE (Slowik *et al.*, 2012), which has been observed for hFPR1. Interesting in this course is that the grade of the observed affinity shift between HEK293T cells and monocytes/granulocytes was dependent on the ligand (also seen by Kretschmer *et al.*, 2010). It has been proposed, that hFPR2 comprises multiple ligand binding sites (Cattaneo *et al.*, 2013). It could even be possible to have several co-receptors or accessory molecules modulating the distinct binding pockets. Furthermore, Cooray *et al.* (2013) have shown that hFPR2 is able to undergo homo- and heterodimerization, which leads to activation of distinct intracellular signaling pathways, adding more items to the complex conformational landscape of this receptor. Ligand-dependent activation of distinct signaling pathways of a single receptor, a phenomenon called functional selectivity, has been described for several GPCRs (Zhou, 2014).

#### **4.4.2. Biological significance of signal peptide detection by innate immune cells – evidence for a novel pattern recognition receptor**

Detection of signal peptides occurred with very high affinity and specificity for formyl peptide receptors in HEK293T cells as well as in primary human granulocytes and monocytes. Several peptides tested in concentration-response experiments were able to activate hFPR1 or hFPR2 in the sub-nanomolar range. These peptides belong to the most affine naturally-derived FPR peptide agonists described so far (Cattaneo *et al.*, 2013; Ye *et al.*, 2009; Migeotte *et al.*, 2006). Even in complex cellular systems like the primary leukocytes which express myriads of chemosensory receptors, these ligand-induced responses were FPR specific. Moreover, the peptides were able to induce cellular responses in human granulocytes that are characteristic for neutrophil-dependent inflammation: (I) receptor activation leading to downstream cellular signaling (in this case calcium), (II) induction of adhesion/cell migration towards higher stimulus concentrations, (III) release of matrix-metalloproteases to enable tissue invasion and migration towards the threat (Bufe *et al.*, 2015), and (IV) formation of reactive oxygen species during respiratory bursts in order to eliminate pathogenic microorganisms (Kolaczowska and Kubes, 2013; Witko-Sarsat *et al.*, 2000). The latter needed higher concentrations of the stimuli for activation. Similar results have already been described for f-MLF and some synthetic peptides (Kemmerich and Pennington, 1988; Gao *et al.*, 1994). This is not very surprising as the cells usually need very low stimulus concentrations to migrate into the direction of the assumed target. The onset of eliminatory processes is shifted towards higher concentrations since the concentration of the stimulus is

increased in close proximity to the pathogen. If such processes would start early on, they would primarily harm surrounding host tissue instead of the acquired target.

Many of the above-mentioned arguments are transferable to the murine immune FPRs. The displayed affinities and FPR-discriminating selectivity observed for human FPRs also apply to the mouse FPRs, emphasizing their evolutionary conservation. For receptors of both species the N-terminal formylation is not mandatory for receptor activation but is required for preserving the high affinity (Bufe *et al.*, 2015). This is a valid molecular model for distinction between eukaryotic signal peptides, which are not N-terminally formylated, and prokaryotic signal peptides. Because of this, FPRs have been proposed as pattern recognition receptors (PRRs) for several times already (Thomas and Schroder, 2013), as the structural requirements for activation, the N-terminal formylation, fulfills requirements to be defined as PRRs. However, to define FPRs as pattern recognition receptors certain experimental evidence is missing.

PRRs, per definition, possess several common characteristics (Akira *et al.*, 2006). First, they recognize microbial components, so-called pathogen-associated molecular patterns (PAMPs). These components are essential for bacterial survival and hence, are highly conserved. Second, PRRs are constitutively expressed in the host and are therefore capable of recognizing the pathogenic pattern at each stage of the host's life cycle. Third, PRRs are germ line encoded, independent of immunologic memory and expressed on all cells of a certain cell type. In addition, PRRs are highly conserved among species. Activation of a given PRR results in activation of distinct signaling pathways and leads to distinct anti-pathogen responses. Formyl peptide receptors are expressed in many developmental stages of myeloid cells like native monocytes as well as mature macrophages and dendritic cells (Migeotte *et al.*, 2005). Orthologs of FPR1 and/or FPR2 have been found in different species like human, rat and mouse (Liberles *et al.*, 2009). Mammalian FPRs (human, mouse, rat, rabbit, dog, horse, ape, etc.) are highly conserved in structure and, at least those that have been tested, in function. My data strongly support these arguments as signal peptide detection was conserved between human and mouse. According to the literature, FPRs are generally expressed by granulocytes and lead, upon activation, to anti-pathogenic responses. This has also been confirmed by data presented in the current work. With this, FPRs seem to share all characteristics common to PRRs with one exception: as far as I know, there is no evidence that formylated peptides, as part of a functional group, are essential for bacterial survival. However, with 20 - 30% of all proteins in bacterial cells localized outside the cytosol, proving the necessity of protein

targeting for cell survival, signal peptides are vital for bacterial existence (Kudva *et al.*, 2013). All these characteristics have more or less been addressed and confirmed in the scope of this work and should enable to classify FPRs as pattern recognition receptors.

#### **4.4.3. Occurrence of signal peptides and their N-terminal fragments in nature**

Interpolation of the results discussed in chapter 4.4.2 underlines the biological relevance of signal peptide detection by cells of the innate immune system. However, it is not exactly known how these peptides are found in nature and what structural properties they possess in the end. This will be discussed in the following section.

##### ***4.4.3.1. Natural occurrence of bacterial peptides starting with N-terminally formylated methionine***

Since the late 1960s it is widely known that bacterial protein synthesis generally starts with N-terminally formylated methionine (Capecchi, 1966). According to the literature (Frottin *et al.*, 2006), 35 - 70% of those peptides are either deformylated after exiting the ribosomal machinery or targeted by N-terminal methionine excision (NME). In the past however, there have been plenty of publications reporting the occurrence of N-formyl methionine-containing peptides in bacterial supernatants of many bacterial species (Stead *et al.*, 2013; Liu *et al.*, 2011; Ravipaty and Reilly, 2010; Wang *et al.*, 2007, Watson *et al.*, 1988; Rot *et al.*, 1987; Marasco *et al.*, 1984; Fitton *et al.*, 1980; Smith and Shaw, 1981). Besides, investigations by Smith and Shaw have shown that the method used for purification of bacterial proteins does in part distinguish between non-formylated and formylated peptides (Smith and Shaw, 1981), questioning the real extent of N-terminal deformylation or NME. It has been proposed that f-MLF, which is present in several signal peptide sequences, is released during a process similar to NME (Broom *et al.*, 1993; Schiffmann *et al.*, 1975). However, there are possibilities that the N-terminal formyl-methionine of signal peptides is not hydrolyzed at all. The nascent peptide chains of proteins that are co-translationally transported via Sec-dependent pathways are bound by SecB/SecA after exiting the ribosome. This protein could serve as a capping molecule, masking the formyl-methionine. Analyses of Frey (Frey *et al.*, 1987) show that rubredoxin was found in the cytoplasm of *Desulfovibrio gigas*, still carrying its N-terminal formyl-methionyl signal peptide.

In line with this, there have been reports suggesting that secreted proteins, starting with formyl-methionine, still carry their N-terminal signal sequence (Watson *et al.*, 1988). Stead *et al.* identified several proteins in the supernatant that are supposed to be transported via a Sec-

dependent pathway, still carrying their N-terminally formylated signal sequence (Stead *et al.*, 2013).

#### ***4.4.3.2. Release of signal peptides and N-terminal signal peptide fragments in nature***

Two major questions arise from the data discussed above. First, what is the exact mechanism by which the signal peptides are released? Second, in which form are they presented so that formyl peptide receptors can access them *in vivo*? The following section proposes six scenarios (I - VI) describing potent sources of N-terminally formylated bacterial signal peptides or their breakdown products in nature.

(I) Sec-dependent and TAT-dependent signal sequences are cleaved off the pre-protein by the bacterial signal peptidase I, releasing the premature protein (Dalbey *et al.*, 2012). The cleaved signal peptide is then typically further degraded by signal peptide peptidases (Dalbey *et al.*, 2012). It has been shown that signal peptide fragments of secreted proteins were found in the growth medium of *Staphylococcus aureus* (Ravipaty and Reilly, 2010). Interestingly, the same study proved the presence of five stable full-length signal peptides in the extracellular medium of which four start with the N-terminal MKK motif. It is possible that these fragments or small full-length peptides escape the periplasm and cross the outer membrane/wall via active or passive transport or diffusion. Such a scenario would easily explain the presence of f-MLF in the supernatant of gram-negative *E.coli* (Marasco *et al.*, 1984).

(II) For intercellular chemical communication bacteria employ several quorum sensing pathways that make use of peptide pheromones. It has been shown that secreted enterococcal sex-pheromones are contained within N-terminal signal sequences of several proteins (Cook and Federle, 2014). To excise the residing pheromone from the signal sequence, the signal peptide is cleaved upon translocation by EEP1 (Chandler and Dunny, 2008), leading to release of the pheromone and the remaining N-terminal residue (Cook and Federle, 2014). It has been shown that N-terminal cleavage products of AgrD quorum sensing peptides, containing the N-terminally formylated methionine, can be found in cell free culture supernatants of *Staphylococcus aureus* (Gonzalez *et al.*, 2014).

(III) It is not imperative that N-terminal signal peptides are cleaved off the exported protein at all. As stated above, some signal peptides are needed fully intact for unmitigated secretion of short proteins (Stead *et al.*, 2013; Watson *et al.*, 1988). Loss of these signal sequences leads to a failure in the secretion process (Stead *et al.*, 2013). Furthermore, Bennet *et al.* (1980)

have shown that the pre-mature penicillinase of *Bacillus licheniformis*, carrying its signal sequence, stimulated  $\beta$ -glucuronidase release in rabbit neutrophils. This effect was absent when the signal peptide sequence was removed (Bennet *et al.*, 1980). We have shown that the immune FPRs of human and mouse detected all tested signal peptides, including the full-length sequences comprising up to 37 amino acids (Bufe *et al.*, 2015). Thus, it is possible that the signal sequence is still recognized by FPRs as part of the premature protein.

(IV) Protein export is not restricted to secretion. It is also important for proteins that are inserted into membranes. Proteins with non-cleavable signal peptide sequences can be inserted into the outer membrane as well, without losing the N-terminal leader peptide. Such peptides can be part of pili or the injectosome machinery (Cornelis, 2006). The latter introduces virulence factors, so called effectors, into the mammalian host cell. Since bacteria contain intracellular formyl-methionylated proteins (Frey *et al.*, 1987), it is possible that these peptides are retained in the host cell until it becomes necrotic and lyses. It has been shown that formylated mitochondrially-translated peptides, potent FPR activators, exit the mitochondria of necrotic cells (Carp, 1982; Zhang *et al.*, 2010).

(V) It has been shown that the FPR ligand f-MIVIL, originating from pathogenic *Listeria monocytogenes*, is presented by the non-classical murine MHC receptor H2M3 (Gulden *et al.*, 1996). Interestingly, this peptide is part of an N-terminal leader sequence (Princiotta *et al.*, 1998) and can be found in the signal peptide database (<http://www.signalpeptide.de/>). Presentation of bacterial peptides by MHC class II molecules by antigen presenting cells like monocytes is a key mechanism in activation of adaptive immune response. It is imaginable that such peptides escape the antigen presentation and are further available for FPRs.

(VI) Bacteria, no matter if growing intra- or extracellularly, will, for the sake of their community, constitutively undergo a process of programmed cell death (Lewis *et al.*, 2000; Allocati *et al.*, 2015). Several of these autolytic processes are mainly dependent on autolysins that are activated/up-regulated during certain growth phases of the bacterial community. Upon autolysis complex intracellular components like DNA or proteins are released into the growth medium or substrate, including bacterial biofilms (Målen *et al.*, 2007). Especially biofilms would provide a potent source of bacterial signal peptides detectable by the immune system and the vomeronasal organ.

## 4.5. Conclusion and Outlook

---

The current work will certainly be of interest for many research areas. To my knowledge, it provides the most extensive study on vomeronasal FPRs so far. It led to the discovery that vomeronasal mFpr-rs1 is able to discriminate peptides with molecular signatures that are attributed to bacteria, like peptides containing D-amino acids as well as N-terminally formylated peptides. Together with our findings that bacterial signal peptides activate this receptor, it supports the validity of the underlying hypothesis that vomeronasal FPRs mediate pathogen sensing. Hence, my data provide first pharmacological insights into a possible new mechanism by which animals can smell the presence of bacteria. Moreover, by recognition of these peptides the vomeronasal mFpr-rs1 shares a common ligand repertoire with FPRs from the innate immune system, providing first functional evidence for a molecular link between the olfactory and the immune system. Further experiments should address whether mFpr-rs1 does recognize these substances *in vivo*, and if so, whether this affects the animal's behavior.

The major finding of this work is that bacterial signal peptides act as novel activators of immune responses and that these are mediated by FPRs. This introduces a possible novel mechanism of pattern recognition in the innate immune system. Employing this knowledge will certainly lead to a better understanding of immune surveillance by innate immune cells. Understanding the connection between *in vivo* signal peptide release and recognition by FPRs will certainly yield clinical implications. This could lead to new strategies for fighting bacterial diseases in general. FPRs display a very broad expression pattern that is not restricted to tissues of the immune system and the vomeronasal organ (Migeotte *et al.*, 2006). There is growing evidence for the FPR's influence in general physiological and pathophysiological processes. Their role in neurogenic inflammation is slowly emerging (Mollica *et al.*, 2012) and signal peptide-induced MMP-9 release and oxidative burst would easily explain the perilous damage caused by bacteria infiltrating the central nervous system (Obermeier *et al.*, 2013). Furthermore, recent reports show impairment of bacterium-dependent homeostasis in colonic crypts of *Fpr2*-deficient mice (Chen *et al.*, 2013). Bacterial signal peptides could be major determinants in controlling the microbial homeostasis in the human intestine. My findings could also help to understand the complex regulatory mechanisms of the human microbiome (Chu and Mazmanian, 2013). Since FPRs are expressed in several other epithelia like the lung (Shao *et al.*, 2011) it is possible that they contribute to general management of the microbiome in the host body. On this view, there are two major points that should be addressed in future works. The most important one should

directly address the key question: how do FPRs meet bacterial signal peptides *in vivo*. The first simple step could be to show that signal peptides that activate FPRs, are secreted by bacteria, or *vice versa*, that secreted peptides activate FPRs. Stead *et al.* (2013) reported Sec-dependent secretion of five peptides still carrying their N-terminal signal peptide sequence. Studies by de Souza *et al.* reported the presence of numerous secretory proteins that carried their uncleaved signal peptide sequence in *Mycobacterium tuberculosis* cultures (de Souza *et al.*, 2011). Moreover, recent reports (Ravipaty and Reilly, 2010) verified the presence of four full-length signal peptides starting with the MKK motif in supernatants of *Staphylococcus aureus*. The group of Woolf has shown that N-terminally formylated peptides released by heat-inactivated bacteria (*S. aureus* among others) directly activate mFpr1 in nociceptor neurons of the dorsal root ganglia of mice (Chiu *et al.*, 2013). However, it is vital to elucidate the release mechanisms of bacterial signal peptides in nature. More experiments are required assessing the whereabouts, the post-cleavage fate, the final concentration and the actual phenotype of the signal peptides. It is also important to discriminate between signal peptides of the distinct export pathways. It is imaginable that hFPR1 and hFPR2 are tuned toward the recognition of signal peptides derived from distinct signal peptide pathways. It would also be a great asset to apprehend possible differences in signal peptide usage between pathogenic bacteria and non-pathogenic strains. Purposeful growth of bacteria could include nuclear/fluorescence-labeling strategies to follow the fate of single molecules. Nano-high-performance liquid chromatography coupled with mass spectrometry would be a very powerful tool to analyze the fate of bacterial signal peptides, their subcellular localization and their concentration. In my opinion, the presented work paves the way for a better understanding of the mammalian immune system, which might eventually lead to the discovery of completely new mechanisms for treating perilous bacterial diseases.

---

## Literature

---

1. Allocati N, Masulli M, Di Ilio C, De Laurenzi V (2015) Die for the community: an overview of programmed cell death in bacteria. *Cell Death Dis.* 6:e1609
2. Akira S, Uematsu S, Takeuchi O (2006) Pathogen recognition and innate immunity. *Cell* 124(4):783-801
3. Bäck M, Powell WS, Dahlén SE, Drazen JM, Evans JF, Serhan CN, Shimizu T, Yokomizo T, Rovati GE (2014) Update on leukotriene, lipoxin and oxoeicosanoid receptors: IUPHAR Review 7. *Br J Pharmacol.* 171(15):3551-74
4. Bae YS, Bae H, Kim Y, Lee TG, Suh PG, Ryu SH (2001) Identification of novel chemoattractant peptides for human leukocytes. *Blood* 97(9):2854-62
5. Bae YS, Lee HY, Jo EJ, Kim JI, Kang HK, Ye RD, Kwak JY, Ryu SH (2004) Identification of peptides that antagonize formyl peptide receptor-like 1-mediated signaling. *J Immunol.* 173(1):607-14
6. Bae GH, Lee HY, Jung YS, Shim JW, Kim SD, Baek SH, Kwon JY, Park JS, Bae YS (2012) Identification of novel peptides that stimulate human neutrophils. *Exp Mol Med.* 44(2):130-7
7. Baek SH, Seo JK, Chae CB, Suh PG, Ryu SH (1996) Identification of the peptides that stimulate the phosphoinositide hydrolysis in lymphocyte cell lines from peptide libraries. *J Biol Chem.* 271(14):8170-5.
8. Balbach JJ, Ishii Y, Antzutkin ON, Leapman RD, Rizzo NW, Dyda F, Reed J, Tycko R (2000) Amyloid fibril formation by A beta 16-22, a seven-residue fragment of the Alzheimer's beta-amyloid peptide, and structural characterization by solid state NMR. *Biochemistry* 39(45):13748-59.
9. Bedard K, Krause KH (2007) The NOX family of ROS-generating NADPH oxidases: physiology and pathophysiology. *Physiol Rev.* 87(1):245-313.
10. Benelli D, Londei P (2009) Begin at the beginning: evolution of translational initiation. *Res Microbiol.* 160(7):493-501
11. Bennet J.P, Hirth KP, Fuchs E, Sarvas M, Warren GB (1980) The bacterial factors which stimulate neutrophils may be derived from procaryote signal peptides. *FEBS Lett.* 116(1):57-61.
12. Berghard A, Buck LB (1996) Sensory transduction in vomeronasal neurons: evidence for G alpha o, G alpha i2, and adenylyl cyclase II as major components of a pheromone signaling cascade. *J Neurosci.* 16(3):909-18
13. Blobel G (1980) Intracellular protein topogenesis. *Proc Natl Acad Sci U S A* 77(3):1496-500
14. Bogeski I, Kappl R, Kummerow C, Gulaboski R, Hoth M, Niemeyer BA (2011) Redox regulation of calcium ion channels: chemical and physiological aspects. *Cell Calcium* 50(5):407-23
15. Boillat M, Challet L, Rossier D, Kan C, Carleton A, Rodriguez I (2015) The vomeronasal system mediates sick conspecific avoidance. *Curr Biol.* 25(2):251-5.
16. Boulay F, Tardif M, Brouchon L, Vignais P (1990) Synthesis and use of a novel N-formyl peptide derivative to isolate a human N-formyl peptide receptor cDNA. *Biochem Biophys Res Commun.* 168(3):1103-9
17. Boulay F, Tardif M, Brouchon L, Vignais P (1990b) The human N-formylpeptide receptor. Characterization of two cDNA isolates and evidence for a new subfamily of G-protein-coupled receptors. *Biochemistry* 29(50):11123-33.
18. Boxio R, Bossenmeyer-Pourie C, Steinckwich N, Dourmon C, Nüsse O (2003) Mouse bone marrow contains large numbers of functionally competent neutrophils. *J Leukoc Biol.* 75(4):604-11
19. Brady L, Dodson G (1994) Drug design. Reflections on a peptide. *Nature* 368(6473):692-3.
20. Brandenburg LO, Konrad M, Wruck CJ, Koch T, Lucius R, Pufe T (2010) Functional and physical interactions between formyl-peptide-receptors and scavenger receptor MARCO and their involvement in amyloid beta 1-42-induced signal transduction in glial cells. *J Neurochem.* 113(3):749-60
21. Brooks BR, Brooks CL 3rd, Mackerell AD Jr, Nilsson L, Petrella RJ, Roux B, Won Y, Archontis G, Bartels C, Boresch S, Caffisch A, Caves L, Cui Q, Dinner AR, Feig M, Fischer S, Gao J, Hodoseck M, Im W,

- Kuczera K, Lazaridis T, Ma J, Ovchinnikov V, Paci E, Pastor RW, Post CB, Pu JZ, Schaefer M, Tidor B, Venable RM, Woodcock HL, Wu X, Yang W, York DM, Karplus M (2009) CHARMM: the biomolecular simulation program. *J Comput Chem.* 30(10):1545-614
22. Broom MF, Sherriff RM, Ferry DM, Chadwick VS (1993) Formylmethionyl-leucylphenylalanine and the SOS operon in *Escherichia coli*: a model of host-bacterial interactions. *Biochem J.* 291 ( Pt 3):895-900
  23. Bufe B, Hofmann T, Krautwurst D, Raguse JD, Meyerhof W (2002) The human TAS2R16 receptor mediates bitter taste in response to beta-glucopyranosides. *Nat Genet.* 32(3):397-401
  24. Bufe B, Schumann T, Zufall F (2012) Formyl peptide receptors from immune and vomeronasal system exhibit distinct agonist properties. *J Biol Chem.* 287(40):33644-55
  25. Bufe B, Schumann T, Kappl R, Bogeski I, Kummerow C, Podgórska M, Smola S, Hoth M, Zufall F (2015) Recognition of bacterial signal peptides by mammalian formyl peptide receptors: a new mechanism for sensing pathogens. *J Biol Chem.* jbc.M114.626747 (ahead of print)
  26. Caboche S, Pupin M, Leclère V, Fontaine A, Jacques P, Kucherov G (2008) NORINE: a database of nonribosomal peptides. *Nucleic Acids Res.* PMID:17913739
  27. Cahn, R. S., Ingold, C. and Prelog, V (1966) Spezifikation der molekularen Chiralität. *Angew. Chem.*, 78: 413-447
  28. Campbell JJ, Qin S, Bacon KB, Mackay CR, Butcher EC (1996) Biology of chemokine and classical chemoattractant receptors: differential requirements for adhesion-triggering versus chemotactic responses in lymphoid cells. *J Cell Biol.* 134(1):255-66
  29. Capecchi MR (1966) Initiation of *E. coli* proteins. *Proc Natl Acad Sci U S A* 55(6):1517-24
  30. Carp H (1982) Mitochondrial N-formylmethionyl proteins as chemoattractants for neutrophils. *J Exp Med.* 155(1):264-75
  31. Cattaneo F, Parisi M, Ammendola R (2103) Distinct signaling cascades elicited by different formyl Peptide receptor 2 (FPR2) agonists. *Int J Mol Sci.* 14(4):7193-230
  32. Cava F, Lam H, de Pedro MA, Waldor MK (2011) Emerging knowledge of regulatory roles of D-amino acids in bacteria. *Cell Mol Life Sci.* 68(5):817-31
  33. Chamero P, Marton TF, Logan DW, Flanagan K, Cruz JR, Saghatelian A, Cravatt BF, Stowers L (2007) Identification of protein pheromones that promote aggressive behaviour. *Nature* 450(7171):899-902.
  34. Chamero P, Katsoulidou V, Hendrix P, Bufe B, Roberts R, Matsunami H, Abramowitz J, Birnbaumer L, Zufall F, Leinders-Zufall T (2011) G protein G(alpha)o is essential for vomeronasal function and aggressive behavior in mice. *Proc Natl Acad Sci U S A* 108(31):12898-903
  35. Chamero P, Leinders-Zufall T, Zufall F (2012) From genes to social communication: molecular sensing by the vomeronasal organ. *Trends Neurosci.* 35(10):597-606
  36. Chandler JR, Dunny GM (2008) Characterization of the sequence specificity determinants required for processing and control of sex pheromone by the intramembrane protease Eep and the plasmid-encoded protein PrgY. *J Bacteriol.* 190(4):1172-83
  37. Chatzi KE, Sardis MF, Karamanou S, Economou A (2013) Breaking on through to the other side: protein export through the bacterial Sec system. *Biochem J.* 449(1):25-37
  38. Chen Q, Wade D, Kurosaka K, Wang ZY, Oppenheim JJ, Yang D (2004) Temporin A and related frog antimicrobial peptides use formyl peptide receptor-like 1 as a receptor to chemoattract phagocytes. *J Immunol.* 173(4):2652-9.
  39. Chen K, Liu M, Liu Y, Yoshimura T, Shen W, Le Y, Durum S, Gong W, Wang C, Gao JL, Murphy PM, Wang JM (2013) Formylpeptide receptor-2 contributes to colonic epithelial homeostasis, inflammation, and tumorigenesis. *J Clin Invest.* 123(4):1694-704
  40. Chiu IM, Heesters BA, Ghasemlou N, Von Hehn CA, Zhao F, Tran J, Wainger B, Strominger A, Muralidharan S, Horswill AR, Bubeck Wardenburg J, Hwang SW, Carroll MC, Woolf CJ (2013) Bacteria activate sensory neurons that modulate pain and inflammation. *Nature* 501(7465):52-7
  41. Chromek M, Slamová Z, Bergman P, Kovács L, Podracká L, Ehrén I, Hökfelt T, Gudmundsson GH, Gallo RL, Agerberth B, Brauner A (2006) The antimicrobial peptide cathelicidin protects the urinary tract against invasive bacterial infection. *Nat Med.* 12(6):636-41
  42. Chu H, Mazmanian SK (2013) Innate immune recognition of the microbiota promotes host-microbial symbiosis. *Nat Immunol.* 14(7):668-75

43. Chupin V, Killian JA, Breg J, de Jongh HH, Boelens R, Kaptein R, de Kruijff B (1995) PhoE signal peptide inserts into micelles as a dynamic helix-break-helix structure, which is modulated by the environment. A two-dimensional <sup>1</sup>H NMR study. *Biochemistry* 34(36):11617-24
44. Clewell DB, An FY, Flannagan SE, Antiporta M, Dunny GM (2000) Enterococcal sex pheromone precursors are part of signal sequences for surface lipoproteins. *Mol Microbiol.* 35(1):246-7
45. Cook LC, Federle MJ (2014) Peptide pheromone signaling in *Streptococcus* and *Enterococcus*. *FEMS Microbiol Rev.* 38(3):473-92
46. Cooray SN, Gobetti T, Montero-Melendez T, McArthur S, Thompson D, Clark AJ, Flower RJ, Perretti M (2013) Ligand-specific conformational change of the G-protein-coupled receptor ALX/FPR2 determines proresolving functional responses. *Proc Natl Acad Sci U S A* 110(45):18232-7
47. Corminboeuf O, Leroy X (2015) FPR2/ALXR agonists and the resolution of inflammation. *J Med Chem.* 58(2):537-59
48. Cornelis GR (2006) The type III secretion injectisome. *Nat Rev Microbiol.* 4(11):811-25
49. Dalbey RE, Wang P, van Dijl JM (2012) Membrane proteases in the bacterial protein secretion and quality control pathway. *Microbiol Mol Biol Rev.* 76(2):311-30
50. de Souza GA, Leversen NA, Målen H, Wiker HG (2011) Bacterial proteins with cleaved or uncleaved signal peptides of the general secretory pathway. *J Proteomics* 75(2):502-10
51. Del Punta K, Leinders-Zufall T, Rodriguez I, Jukam D, Wysocki CJ, Ogawa S, Zufall F, Mombaerts P (2002) Deficient pheromone responses in mice lacking a cluster of vomeronasal receptor genes. *Nature* 419(6902):70-4
52. Di Virgilio F, Pizzo P, Zanovello P, Bronte V, Collavo D (1990) Extracellular ATP as a possible mediator of cell-mediated cytotoxicity. *Immunol Today* 11(8):274-7
53. Døving KB1, Trotier D (1998) Structure and function of the vomeronasal organ. *J Exp Biol.* 201(Pt 21):2913-25
54. Durstin M, Gao JL, Tiffany HL, McDermott D, Murphy PM (1994) Differential expression of members of the N-formylpeptide receptor gene cluster in human phagocytes. *Biochem Biophys Res Commun.* 201(1):174-9
55. Ernst S, Lange C, Wilbers A, Goebeler V, Gerke V, Rescher U (2004) An annexin 1 N-terminal peptide activates leukocytes by triggering different members of the formyl peptide receptor family. *J Immunol.* 172(12):7669-76
56. Fiore S, Antico G, Aloman M, Sodin-Semrl S (2005) Lipoxin A4 biology in the human synovium. Role of the ALX signaling pathways in modulation of inflammatory arthritis. *Prostaglandins Leukot Essent Fatty Acids* 73(3-4):189-96
57. Fitton JE, Dell A, Shaw WV (1980) The amino acid sequence of the delta haemolysin of *Staphylococcus aureus*. *FEBS Lett.* 115(2):209-12
58. Forsman H, Onnheim K, Andreasson E, Dahlgren C (2011) What formyl peptide receptors, if any, are triggered by compound 43 and lipoxin A4? *Scand J Immunol.* 74(3):227-34
59. Forsman H, Andréasson E, Karlsson J, Boulay F, Rabiet MJ, Dahlgren C (2012) Structural characterization and inhibitory profile of formyl peptide receptor 2 selective peptides descending from a PIP2-binding domain of gelsolin. *J Immunol.* 189(2):629-37
60. Freer RJ, Day AR, Muthukumaraswamy N, Pinon D, Wu A, Showell HJ, Becker EL (1982) Formyl peptide chemoattractants: a model of the receptor on rabbit neutrophils. *Biochemistry* 21(2):257-63
61. Freer RJ, Day AR, Radding JA, Schiffmann E, Aswanikumar S, Showell HJ, Becker EL (1980) Further studies on the structural requirements for synthetic peptide chemoattractants. *Biochemistry* 19(11):2404-10
62. Frey M, Sieker L, Payan F, Haser R, Bruschi M, Pepe G, LeGall J. (1987) Rubredoxin from *Desulfovibrio gigas*. A molecular model of the oxidized form at 1.4 Å resolution. *J Mol Biol.* 197(3):525-41
63. Frottin F, Martinez A, Peynot P, Mitra S, Holz RC, Giglione C, Meinnel T (2006) The proteomics of N-terminal methionine cleavage. *Mol Cell Proteomics* 5(12):2336-49
64. Fujita E, Farkas I, Campbell W, Baranyi L, Okada H, Okada N (2004) Inactivation of C5a anaphylatoxin by a peptide that is complementary to a region of C5a. *J Immunol.* 172(10):6382-7.
65. Gambardella L, Vermeren S (2013) Molecular players in neutrophil chemotaxis--focus on PI3K and small GTPases. *J Leukoc Biol.* 94(4):603-12
66. Gao JL, Becker EL, Freer RJ, Muthukumaraswamy N, Murphy PM (1994) A high potency nonformylated peptide agonist for the phagocyte N-formylpeptide chemotactic receptor. *J Exp Med.* 180(6):2191-7

67. Gao JL, Chen H, Filie JD, Kozak CA, Murphy PM (1998) Differential expansion of the N-formylpeptide receptor gene cluster in human and mouse. *Genomics* 51(2):270-6
68. Gao JL, Lee EJ, Murphy PM (1999) Impaired antibacterial host defense in mice lacking the N-formylpeptide receptor. *J Exp Med.* 189(4):657-62
69. Gao JL, Guillabert A, Hu J, Le Y, Urizar E, Seligman E, Fang KJ, Yuan X, Imbault V, Communi D, Wang JM, Parmentier M, Murphy PM, Migeotte I (2007) F2L, a peptide derived from heme-binding protein, chemoattracts mouse neutrophils by specifically activating Fpr2, the low-affinity N-formylpeptide receptor. *J Immunol.* 178(3):1450-6
70. Gesty-Palmer D, Luttrell LM (2011) Refining efficacy: exploiting functional selectivity for drug discovery. *Adv Pharmacol.* 62:79-107
71. David J. Gonzalez, Ross Corriden, Kathryn Akong-Moore, Joshua Olson, Pieter C. Dorrestein, Victor Nizet (2014) N-Terminal ArgD Peptides from the Classical *Staphylococcus aureus* Agr System Have Cytotoxic and Proinflammatory Activities. *Chemistry & Biology* (in press)
72. Grynkiewicz G, Poenie M, Tsien RY (1985) A new generation of Ca<sup>2+</sup> indicators with greatly improved fluorescence properties. *J Biol Chem.* 260(6):3440-50
73. Gulden PH, Fischer P 3rd, Sherman NE, Wang W, Engelhard VH, Shabanowitz J, Hunt DF, Pamer EG (1996) A *Listeria monocytogenes* pentapeptide is presented to cytolytic T lymphocytes by the H2-M3 MHC class Ib molecule. *Immunity* 5(1):73-9
74. Hagemann RF, Evans TC (1968) Influence of dimethyl sulphoxide on glycine transport in sarcoma 180 tumour cells. *Nature* 218(5141):583-4.
75. Hanson J, Ferreirós N, Pirotte B, Geisslinger G, Offermanns S (2013) Heterologously expressed formyl peptide receptor 2 (FPR2/ALX) does not respond to lipoxin A<sub>4</sub>. *Biochem Pharmacol.* 85(12):1795-802
76. Hardingham GE, Chawla S, Cruzalegui FH, Bading H (1999) Control of recruitment and transcription-activating function of CBP determines gene regulation by NMDA receptors and L-type calcium channels. *Neuron* 22(4):789-98.
77. Harrison RS, Shepherd NE, Hoang HN, Ruiz-Gómez G, Hill TA, Driver RW, Desai VS, Young PR, Abbenante G, Fairlie DP (2010) Downsizing human, bacterial, and viral proteins to short water-stable alpha helices that maintain biological potency. *Proc Natl Acad Sci U S A* 107(26):11686-91
78. He HQ, Liao D, Wang ZG, Wang ZL, Zhou HC, Wang MW, Ye RD (2013) Functional characterization of three mouse formyl peptide receptors. *Mol Pharmacol.* 83(2):389-98
79. He HQ, Troksa EL, Caltabiano G, Pardo L, Ye RD (2014) Structural determinants for the interaction of formyl peptide receptor 2 with peptide ligands. *J Biol Chem.* 289(4):2295-306
80. Holy TE, Dulac C, Meister M (2000) Responses of vomeronasal neurons to natural stimuli. *Science* 289(5484):1569-72.
81. Ibarra-Soria X, Levitin MO, Saraiva LR, Logan DW (2014) The olfactory transcriptomes of mice. *PLoS Genet.* 10(9):e1004593
82. Ishii T, Hirota J, Mombaerts P (2003) Combinatorial coexpression of neural and immune multigene families in mouse vomeronasal sensory neurons. *Curr Biol.* 13(5):394-400
83. Jia C, Halpern M (1996) Subclasses of vomeronasal receptor neurons: differential expression of G proteins (Gi alpha 2 and G(o alpha)) and segregated projections to the accessory olfactory bulb. *Brain Res.* 719(1-2):117-28
84. Kavaliers M, Choleris E, Pfaff DW (2005) Genes, odours and the recognition of parasitized individuals by rodents. *Trends Parasitol.* 21(9):423-9
85. Kemmerich B, Pennington JE. (1988) Different calcium and oxidative metabolic responses in human blood monocytes during exposure to various agonists. *J Leukoc Biol.* 43(2):125-32.
86. Kimoto H, Haga S, Sato K, Touhara K (2005) Sex-specific peptides from exocrine glands stimulate mouse vomeronasal sensory neurons. *Nature* 437(7060):898-901
87. Klebanoff SJ (2005) Myeloperoxidase: friend and foe. *J Leukoc Biol.* 77(5):598-625
88. Kolaczowska E, Kuberski P (2013) Neutrophil recruitment and function in health and inflammation. *Nat Rev Immunol.* 13(3):159-75
89. Kretschmer D, Gleske AK, Rautenberg M, Wang R, Köberle M, Bohn E, Schöneberg T, Rabiet MJ, Boulay F, Klebanoff SJ, van Kessel KA, van Strijp JA, Otto M, Peschel A (2010) Human formyl peptide receptor 2 senses highly pathogenic *Staphylococcus aureus*. *Cell Host Microbe* 7(6):463-73

90. Krishnamoorthy S, Recchiuti A, Chiang N, Yacoubian S, Lee CH, Yang R, Petasis NA, Serhan CN (2010) Resolvin D1 binds human phagocytes with evidence for proresolving receptors. *Proc Natl Acad Sci U S A* 107(4):1660-5
91. Kudva R, Denks K, Kuhn P, Vogt A, Müller M, Koch HG (2013) Protein translocation across the inner membrane of Gram-negative bacteria: the Sec and Tat dependent protein transport pathways. *Res Microbiol.* 164(6):505-34
92. Kurosaka K, Chen Q, Yarovinsky F, Oppenheim JJ, Yang D (2005) Mouse cathelin-related antimicrobial peptide chemoattracts leukocytes using formyl peptide receptor-like 1/mouse formyl peptide receptor-like 2 as the receptor and acts as an immune adjuvant. *J Immunol.* 174(10):6257-65.
93. Lacy M, Jones J, Whitemore SR, Haviland DL, Wetsel RA, Barnum SR (1995) Expression of the receptors for the C5a anaphylatoxin, interleukin-8 and FMLP by human astrocytes and microglia. *J Neuroimmunol.* 61(1):71-8
94. Lad PM, Olson CV, Smiley PA (1985) Association of the N-formyl-Met-Leu-Phe receptor in human neutrophils with a GTP-binding protein sensitive to pertussis toxin. *Proc Natl Acad Sci U S A* 82(3):869-73
95. Le Y, Gong W, Tiffany HL, Tumanov A, Nedospasov S, Shen W, Dunlop NM, Gao JL, Murphy PM, Oppenheim JJ, Wang JM (2001) Amyloid (beta)42 activates a G-protein-coupled chemoattractant receptor, FPR-like-1. *J Neurosci.* 21(2):RC123
96. Leinders-Zufall T, Lane AP, Puche AC, Ma W, Novotny MV, Shipley MT, Zufall F (2000) Ultrasensitive pheromone detection by mammalian vomeronasal neurons. *Nature* 405(6788):792-6
97. Leinders-Zufall T, Brennan P, Widmayer P, S PC, Maul-Pavicic A, Jäger M, Li XH, Breer H, Zufall F, Boehm T (2004) MHC class I peptides as chemosensory signals in the vomeronasal organ. *Science* 306(5698):1033-7.
98. Leinders-Zufall T, Ishii T, Mombaerts P, Zufall F, Boehm T (2009) Structural requirements for the activation of vomeronasal sensory neurons by MHC peptides. *Nat Neurosci.* 12(12):1551-8
99. Leinders-Zufall T, Ishii T, Chamero P, Hendrix P, Oboti L, Schmid A, Kircher S, Pyrski M, Akiyoshi S, Khan M, Vaes E, Zufall F, Mombaerts P (2014) A family of nonclassical class I MHC genes contributes to ultrasensitive chemodetection by mouse vomeronasal sensory neurons. *J Neurosci.* 34(15):5121-33
100. Lewis K (2000) Programmed death in bacteria. *Microbiol Mol Biol Rev.* 64(3):503-14
101. Li Y, Ye D (2013) Molecular biology for formyl peptide receptors in human diseases. *J Mol Med (Berl)* 91(7):781-9
102. Liberles SD, Horowitz LF, Kuang D, Contos JJ, Wilson KL, Siltberg-Liberles J, Liberles DA, Buck LB (2009) Formyl peptide receptors are candidate chemosensory receptors in the vomeronasal organ. *Proc Natl Acad Sci U S A.* 106(24):9842-7
103. Liu X, Vederas JC, Whittal RM, Zheng J, Stiles ME, Carlson D, Franz CM, McMullen LM, van Belkum MJ (2011) Identification of an N-terminal formylated, two-peptide bacteriocin from *Enterococcus faecalis* 710C. *J Agric Food Chem.* 59(10):5602-8
104. Liu M, Chen K, Yoshimura T, Liu Y, Gong W, Wang A, Gao JL, Murphy PM, Wang JM (2012) Formylpeptide receptors are critical for rapid neutrophil mobilization in host defense against *Listeria monocytogenes*. *Sci Rep.* 2:786
105. Loconto J, Papes F, Chang E, Stowers L, Jones EP, Takada T, Kumánovics A, Fischer Lindahl K, Dulac C (2003) Functional expression of murine V2R pheromone receptors involves selective association with the M10 and M1 families of MHC class Ib molecules. *Cell* 112(5):607-18
106. Målen H, Berven FS, Fladmark KE, Wiker HG (2007) Comprehensive analysis of exported proteins from *Mycobacterium tuberculosis* H37Rv. *Proteomics* 7(10):1702-18
107. Marasco WA, Phan SH, Krutzsch H, Showell HJ, Feltner DE, Nairn R, Becker EL, Ward PA (1984) Purification and identification of formyl-methionyl-leucyl-phenylalanine as the major peptide neutrophil chemotactic factor produced by *Escherichia coli*. *J Biol Chem.* 259(9):5430-9
108. Marasco WA, Showell HJ, Becker EL (1981) Substance P binds to the formylpeptide chemotaxis receptor on the rabbit neutrophil. *Biochem Biophys Res Commun.* 30:99(4):1065-72
109. Martínez-Rodríguez S, Martínez-Gómez AI, Rodríguez-Vico F, Clemente-Jiménez JM, Las Heras-Vázquez FJ (2010) Natural occurrence and industrial applications of D-amino acids: an overview. *Chem Biodivers.* 7(6):1531-48
110. Matsumoto J (1965) Clinical trials of dimethyl sulfoxide in rheumatoid arthritis patients in Japan. *Ann N Y Acad Sci.* 141(1):560-8

111. Migeotte I, Riboldi E, Franssen JD, Grégoire F, Loison C, Wittamer V, Detheux M, Robberecht P, Costagliola S, Vassart G, Sozzani S, Parmentier M, Communi D (2005) Identification and characterization of an endogenous chemotactic ligand specific for FPRL2. *J Exp Med.* 201(1):83-93
112. Migeotte I, Communi D, Parmentier M (2006) Formyl peptide receptors: a promiscuous subfamily of G protein-coupled receptors controlling immune responses. *Cytokine Growth Factor Rev.* 17(6):501-19
113. Mills JS, Miettinen HM, Cummings D, Jesaitis AJ (2000) Characterization of the binding site on the formyl peptide receptor using three receptor mutants and analogs of Met-Leu-Phe and Met-Met-Trp-Leu-Leu. *J Biol Chem.* 275(50):39012-7
114. Mody SM, Ho MK, Joshi SA, Wong YH (2000) Incorporation of Galpha(z)-specific sequence at the carboxyl terminus increases the promiscuity of galpha(16) toward G(i)-coupled receptors. *Mol Pharmacol.* 57(1):13-23
115. Mollica A, Stefanucci A, Costante R, Pinnen F (2012) Role of formyl peptide receptors (FPR) in abnormal inflammation responses involved in neurodegenerative diseases. *Antiinflamm Antiallergy Agents Med Chem.* 11(1):20-36
116. Moore JP, Trkola A, Korber B, Boots LJ, Kessler JA 2nd, McCutchan FE, Mascola J, Ho DD, Robinson J, Conley AJ (1995) A human monoclonal antibody to a complex epitope in the V3 region of gp120 of human immunodeficiency virus type 1 has broad reactivity within and outside clade B. *J Virol.* 69(1):122-30.
117. Nardese V, Longhi R, Polo S, Sironi F, Arcelloni C, Paroni R, DeSantis C, Sarmientos P, Rizzi M, Bolognesi M, Pavone V, Lusso P (2001) Structural determinants of CCR5 recognition and HIV-1 blockade in RANTES. *Nat Struct Biol.* 8(7):611-5.
118. Neote K, DiGregorio D, Mak JY, Horuk R, Schall TJ (1993) Molecular cloning, functional expression, and signaling characteristics of a C-C chemokine receptor. *Cell* 72(3):415-25
119. Nguyen MD, Julien JP, Rivest S (2002) Innate immunity: the missing link in neuroprotection and neurodegeneration? *Nat Rev Neurosci.* 3(3):216-27
120. Nodari F, Hsu FF, Fu X, Holekamp TF, Kao LF, Turk J, Holy TE (2008) Sulfated steroids as natural ligands of mouse pheromone-sensing neurons. *J Neurosci.* 28(25):6407-18.
121. Novotny M, Jemiolo B, Harvey S, Wiesler D, Marchlewska-Koj A (1986) Adrenal-mediated endogenous metabolites inhibit puberty in female mice. *Science* 231(4739):722-5.
122. Obermeier B, Daneman R, Ransohoff RM (2013) Development, maintenance and disruption of the blood-brain barrier. *Nat Med.* 19(12):1584-96
123. Offermanns S, Simon MI (1995) G alpha 15 and G alpha 16 couple a wide variety of receptors to phospholipase C. *J Biol Chem.* 270(25):15175-80
124. Olins AL, Zwerger M, Herrmann H, Zentgraf H, Simon AJ, Monestier M, Olins DE (2008) The human granulocyte nucleus: Unusual nuclear envelope and heterochromatin composition. *Eur J Cell Biol.* 87(5):279-90
125. Panaro MA, Cianciulli A, Lisi S, Sisto M, Acquafredda A, Mitolo V (2007) Formyl peptide receptor expression in birds. *Immunopharmacol Immunotoxicol.* 29(1):1-16
126. Papanikou E, Karamanou S, Economou A (2007) Bacterial protein secretion through the translocase nanomachine. *Nat Rev Microbiol.* 5(11):839-51
127. Partida-Sánchez S, Cockayne DA, Monard S, Jacobson EL, Oppenheimer N, Garvy B, Kusser K, Goodrich S, Howard M, Harmsen A, Randall TD, Lund FE (2001) Cyclic ADP-ribose production by CD38 regulates intracellular calcium release, extracellular calcium influx and chemotaxis in neutrophils and is required for bacterial clearance in vivo. *Nat Med.* 7(11):1209-16
128. Pittman K, Kubes P (2013) Damage-associated molecular patterns control neutrophil recruitment. *J Innate Immun.* 5(4):315-23
129. Potter SM, Zheng C, Koos DS, Feinstein P, Fraser SE, Mombaerts P (2001) Structure and emergence of specific olfactory glomeruli in the mouse. *J Neurosci.* 21(24):9713-23.
130. Princiotta MF, Lenz LL, Bevan MJ, Staerz UD (1998) H2-M3 restricted presentation of a *Listeria* derived leader peptide. *J Exp Med.* 187(10):1711-9
131. Quehenberger O, Prossnitz ER, Cavanagh SL, Cochrane CG, Ye RD (1993) Multiple domains of the N-formyl peptide receptor are required for high-affinity ligand binding. Construction and analysis of chimeric N-formyl peptide receptors. *J Biol Chem.* 268(24):18167-75

132. Rabiet MJ, Huet E, Boulay F (2005) Human mitochondria derived N-formylated peptides are novel agonists equally active on FPR and FPRL1, while *Listeria monocytogenes* derived peptides preferentially activate FPR. *Eur J Immunol.* 35(8):2486-95
133. Ravipaty S, Reilly JP (2010) Comprehensive characterization of methicillin-resistant *Staphylococcus aureus* subsp. *aureus* COL secretome by two-dimensional liquid chromatography and mass spectrometry. *Mol Cell Proteomics* 9(9):1898-919
134. Resnati M, Pallavicini I, Wang JM, Oppenheim J, Serhan CN, Romano M, Blasi F (2002) The fibrinolytic receptor for urokinase activates the G protein-coupled chemotactic receptor FPRL1/LXA4R. *Proc Natl Acad Sci U S A* 99(3):1359-64
135. Rhee SG (2001) Regulation of phosphoinositide-specific phospholipase C. *Annu Rev Biochem.* 70:281-312
136. Rienstra CM, Tucker-Kellogg L, Jaroniec CP, Hohwy M, Reif B, McMahon MT, Tidor B, Lozano-Pérez T, Griffin RG (2002) De novo determination of peptide structure with solid-state magic-angle spinning NMR spectroscopy. *Proc Natl Acad Sci U S A* 99(16):10260-5
137. Rivière S, Challet L, Fluegge D, Spehr M, Rodriguez I (2009) Formyl peptide receptor-like proteins are a novel family of vomeronasal chemosensors. *Nature* 459(7246):574-7
138. Rot A, Henderson LE, Copeland TD, Leonard EJ (1987) A series of six ligands for the human formyl peptide receptor: tetrapeptides with high chemotactic potency and efficacy. *Proc Natl Acad Sci U S A* 84(22):7967-71
139. Ryba NJ, Tirindelli R (1997) A new multigene family of putative pheromone receptors. *Neuron* 19(2):371-9
140. Sahagun-Ruiz A, Colla JS, Juhn J, Gao JL, Murphy PM, McDermott DH (2001) Contrasting evolution of the human leukocyte N-formylpeptide receptor subtypes FPR and FPRL1R. *Genes Immun.* 2(6):335-42.
141. Schepetkin IA, Kirpotina LN, Khlebnikov AI, Leopoldo M, Lucente E, Lacivita E, De Giorgio P, Quinn MT (2013) 3-(1H-indol-3-yl)-2-[3-(4-nitrophenyl)ureido]propanamide enantiomers with human formyl-peptide receptor agonist activity: molecular modeling of chiral recognition by FPR2. *Biochem Pharmacol.* 85(3):404-16
142. Schiffmann E, Corcoran BA, Wahl SM (1975) N-formylmethionyl peptides as chemoattractants for leucocytes. *Proc Natl Acad Sci USA* 72(3):1059-62.
143. Schumann T (2010) Functional characterization of Formyl peptide receptors in mice and rats. Diploma Thesis, Zentrum für Human- und Molekularbiologie; Saarland University, Faculty III
144. Schwarzer D, Finking R, Marahiel MA (2003) Nonribosomal peptides: from genes to products. *Nat Prod Rep.* 20(3):275-87
145. Selvatici R, Falzarano S, Mollica A, Spisani S (2006) Signal transduction pathways triggered by selective formylpeptide analogues in human neutrophils. *Eur J Pharmacol.* 534(1-3):1-11
146. Serra MC, Calzetti F, Ceska M, Cassatella MA (1994) Effect of substance P on superoxide anion and IL-8 production by human PMNL. *Immunology.* 82(1):63-9
147. Shao G, Julian MW, Bao S, McCullers MK, Lai JP, Knoell DL, Crouser ED (2011) Formyl peptide receptor ligands promote wound closure in lung epithelial cells. *Am J Respir Cell Mol Biol.* 44(3):264-9
148. Shen W, Proost P, Li B, Gong W, Le Y, Sargeant R, Murphy PM, Van Damme J, Wang JM (2000) Activation of the chemotactic peptide receptor FPRL1 in monocytes phosphorylates the chemokine receptor CCR5 and attenuates cell responses to selected chemokines. *Biochem Biophys Res Commun.* 272(1):276-83.
149. Shi G, Partida-Sánchez S, Misra RS, Tighe M, Borchers MT, Lee JJ, Simon MI, Lund FE (2007) Identification of an alternative G $\alpha$ q-dependent chemokine receptor signal transduction pathway in dendritic cells and granulocytes. *J Exp Med.* 204(11):2705-18
150. Shirasu M, Touhara K (2011) The scent of disease: volatile organic compounds of the human body related to disease and disorder. *J Biochem.* 150(3):257-66
151. Showell HJ, Freer RJ, Zigmond SH, Schiffmann E, Aswanikumar S, Corcoran B, Becker EL (1976) The structure-activity relations of synthetic peptides as chemotactic factors and inducers of lysosomal secretion for neutrophils. *J Exp Med.* 143(5):1154-69
152. Slowik A, Merres J, Elfgen A, Jansen S, Mohr F, Wruck CJ, Pufe T, Brandenburg LO (2012) Involvement of formyl peptide receptors in receptor for advanced glycation end products (RAGE)--and amyloid beta 1-42-induced signal transduction in glial cells. *Mol Neurodegener.* 7:55
153. Smith GM, Shaw WV (1981) Comparison of three methods for the purification of the delta haemolysin of *Staphylococcus aureus*. *J Gen Microbiol.* 124(2):365-74

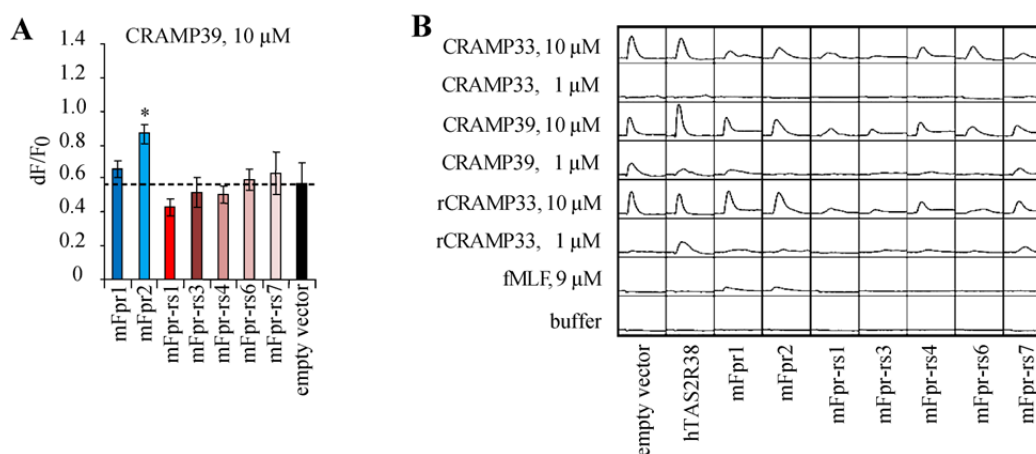
154. Smola-Hess S, Schnitzler R, Hadaschik D, Smola H, Mauch C, Krieg T, Pfister H (2001) CD40L induces matrix-metalloproteinase-9 but not tissue inhibitor of metalloproteinases-1 in cervical carcinoma cells: imbalance between NF-kappaB and STAT3 activation. *Exp Cell Res.* 267(2):205-15
155. Southgate EL, He RL, Gao JL, Murphy PM, Nanamori M, Ye RD (2008) Identification of formyl peptides from *Listeria monocytogenes* and *Staphylococcus aureus* as potent chemoattractants for mouse neutrophils. *J Immunol.* 181(2):1429-37
156. Stead CM, Omsland A, Beare PA, Sandoz KM, Heinzen RA (2013) Sec-mediated secretion by *Coxiella burnetii*. *BMC Microbiol.* 13:222
157. Stenfeldt AL, Karlsson J, Wennerås C, Bylund J, Fu H, Dahlgren C (2007) Cyclosporin H, Boc-MLF and Boc-FLFLF are antagonists that preferentially inhibit activity triggered through the formyl peptide receptor. *Inflammation* 30(6):224-9
158. Su SB, Gong W, Gao JL, Shen W, Murphy PM, Oppenheim JJ, Wang JM (1999a) A seven-transmembrane, G protein-coupled receptor, FPRL1, mediates the chemotactic activity of serum amyloid A for human phagocytic cells. *J Exp Med.* 189(2):395-402
159. Su SB, Gong WH, Gao JL, Shen WP, Grimm MC, Deng X, Murphy PM, Oppenheim JJ, Wang JM (1999b) T20/DP178, an ectodomain peptide of human immunodeficiency virus type 1 gp41, is an activator of human phagocyte N-formyl peptide receptor. *Blood* 93(11):3885-92.
160. Takano T, Fiore S, Maddox JF, Brady HR, Petasis NA, Serhan CN (1997) Aspirin-triggered 15-epi-lipoxin A4 (LXA4) and LXA4 stable analogues are potent inhibitors of acute inflammation: evidence for anti-inflammatory receptors. *J Exp Med.* 185(9):1693-704
161. Takenouchi T, Munekata E (1995) beta-Amyloid peptide, substance P, and SEC receptor ligand activate cytoplasmic Ca<sup>2+</sup> in neutrophil-like HL-60 cells: effect of chemotactic peptide antagonist BocMLF. *Peptides* 16(6):1019-24
162. Tenailleau S, Corre I, Hermouet S (1997) Specific expression of heterotrimeric G proteins G12 and G16 during human myeloid differentiation. *Exp Hematol.* 25(9):927-34.
163. Thomas CJ, Schroder K (2013) Pattern recognition receptor function in neutrophils. *Trends Immunol.* 34(7):317-28
164. Tirindelli R, Dibattista M, Pifferi S, Menini A (2009) From pheromones to behavior. *Physiol Rev.* 89(3):921-56
165. Trice JM, Pinals RS (1985) Dimethyl sulfoxide: a review of its use in the rheumatic disorders. *Semin Arthritis Rheum.* 15(1):45-60
166. von Heijne G (1990) The signal peptide. *J Membr Biol.* 115(3):195-201
167. Walther A, Riehemann K, Gerke V (2000) A novel ligand of the formyl peptide receptor: annexin I regulates neutrophil extravasation by interacting with the FPR. *Mol Cell.* 5(5):831-40.
168. Wang R, Braughton KR, Kretschmer D, Bach TH, Queck SY, Li M, Kennedy AD, Dorward DW, Klebanoff SJ, Peschel A, DeLeo FR, Otto M (2007) Identification of novel cytolytic peptides as key virulence determinants for community-associated MRSA. *Nat Med.* 13(12):1510-4
169. Wang ZG, Ye RD (2002) Characterization of two new members of the formyl peptide receptor gene family from 129S6 mice. *Gene.* 299(1-2):57-63
170. Watson DC, Yaguchi M, Bisaillon JG, Beaudet R, Morosoli R (1988) The amino acid sequence of a gonococcal growth inhibitor from *Staphylococcus haemolyticus*. *Biochem J.* 252(1):87-93
171. Wenzel-Seifert K, Grünbaum L, Seifert R (1991) Differential inhibition of human neutrophil activation by cyclosporins A, D, and H. Cyclosporin H is a potent and effective inhibitor of formyl peptide-induced superoxide formation. *J Immunol.* 147(6):1940-6
172. Wenzel-Seifert K, Seifert R (1993) Cyclosporin H is a potent and selective formyl peptide receptor antagonist. Comparison with N-t-butoxycarbonyl-L-phenylalanyl-L-leucyl-L-phenylalanyl-L-leucyl-L-phenylalanine and cyclosporins A, B, C, D, and E. *J Immunol.* 150(10):4591-9
173. Wenzel-Seifert K, Hurt CM, Seifert R (1998) High constitutive activity of the human formyl peptide receptor. *J Biol Chem.* 273(37):24181-9
174. Wenzel-Seifert K, Arthur JM, Liu HY, Seifert R (1999) Quantitative analysis of formyl peptide receptor coupling to g(i)alpha(1), g(i)alpha(2), and g(i)alpha(3). *J Biol Chem.* 274(47):33259-66
175. Williams AC, Barry BW (2004) Penetration enhancers. *Adv Drug Deliv Rev.* 56(5):603-18.
176. Witko-Sarsat V, Rieu P, Descamps-Latscha B, Lesavre P, Halbwachs-Mecarelli L (2000) Neutrophils: molecules, functions and pathophysiological aspects. *Lab Invest.* 80(5):617-53

177. Yan L, Borregaard N, Kjeldsen L, Moses MA (2001) The high molecular weight urinary matrix metalloproteinase (MMP) activity is a complex of gelatinase B/MMP-9 and neutrophil gelatinase-associated lipocalin (NGAL). Modulation of MMP-9 activity by NGAL. *J Biol Chem.* 276(40):37258-65
178. Yang M, Büsche G, Ganser A, Li Z (2013) Morphology and quantitative composition of hematopoietic cells in murine bone marrow and spleen of healthy subjects. *Ann Hematol.* 92(5):587-94
179. Ye RD, Boulay F, Wang JM, Dahlgren C, Gerard C, Parmentier M, Serhan CN, Murphy PM (2009) International Union of Basic and Clinical Pharmacology. LXXIII. Nomenclature for the formyl peptide receptor (FPR) family. *Pharmacol Rev.* 61(2):119-61
180. Ying G, Iribarren P, Zhou Y, Gong W, Zhang N, Yu ZX, Le Y, Cui Y, Wang JM (2004) Humanin, a newly identified neuroprotective factor, uses the G protein-coupled formylpeptide receptor-like-1 as a functional receptor. *J Immunol.* 172(11):7078-85
181. Zhang Q, Raoof M, Chen Y, Sumi Y, Sursal T, Junger W, Brohi K, Itagaki K, Hauser CJ (2010) Circulating mitochondrial DAMPs cause inflammatory responses to injury. *Nature* 464(7285):104-7
182. Zhou L, Bohn LM (2014) Functional selectivity of GPCR signaling in animals. *Curr Opin Cell Biol.* 27:102-8
183. Ziegler-Heitbrock HW, Fingerle G, Ströbel M, Schraut W, Stelter F, Schütt C, Passlick B, Pforte A (1993) The novel subset of CD14<sup>+</sup>/CD16<sup>+</sup> blood monocytes exhibits features of tissue macrophages. *Eur J Immunol.* 23(9):2053-8

## Appendix

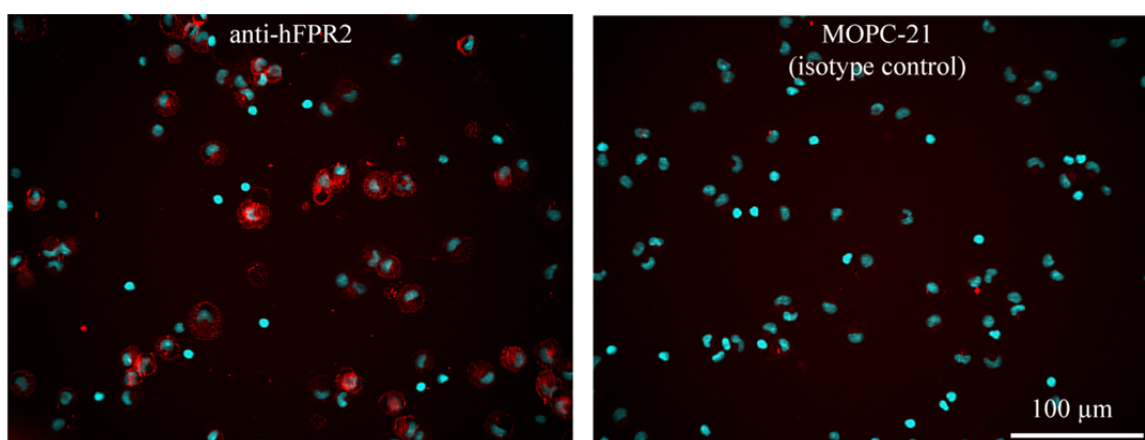
### Appendix 1 | The mFpr2 agonist CRAMP can elicit unspecific responses in HEK293T cells

Mouse FPRs were heterologously expressed in HEK293T cells and stimulated with various CRAMP isoforms. Calcium responses were measured with the FLIPR. **[A]** mFpr2 significantly responds to 10  $\mu\text{M}$  of CRAMP39. Data are averaged over three independent transfections. **[B]** 10  $\mu\text{M}$  of CRAMP33, CRAMP39 and rCRAMP33 elicit unspecific responses in HEK cells transfected with empty vector and the control plasmid encoding the taste receptor hTAS2R38. Occasionally, cells are activated by 1  $\mu\text{M}$  of a given CRAMP substance. T-test: \* =  $p \leq 0.05$ . All other calcium signals were not significant compared to the control. Figure A modified after Bufo, 2012. B is modified after Schumann, 2010. In this case the mFpr-rs1 plasmid was encoding a non-functional receptor.



### Appendix 2 | hFPR2 expression in human monocytes

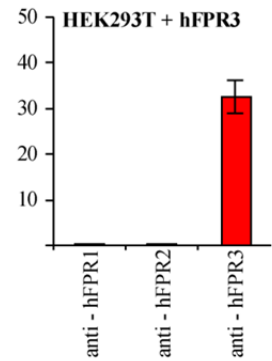
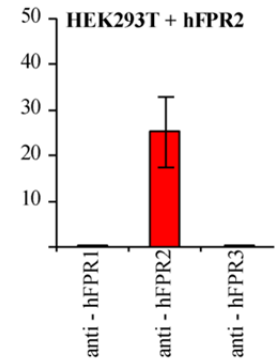
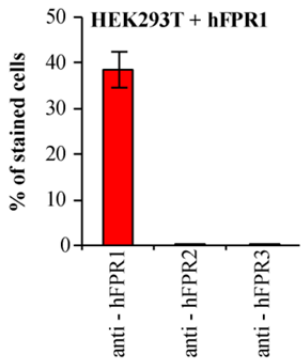
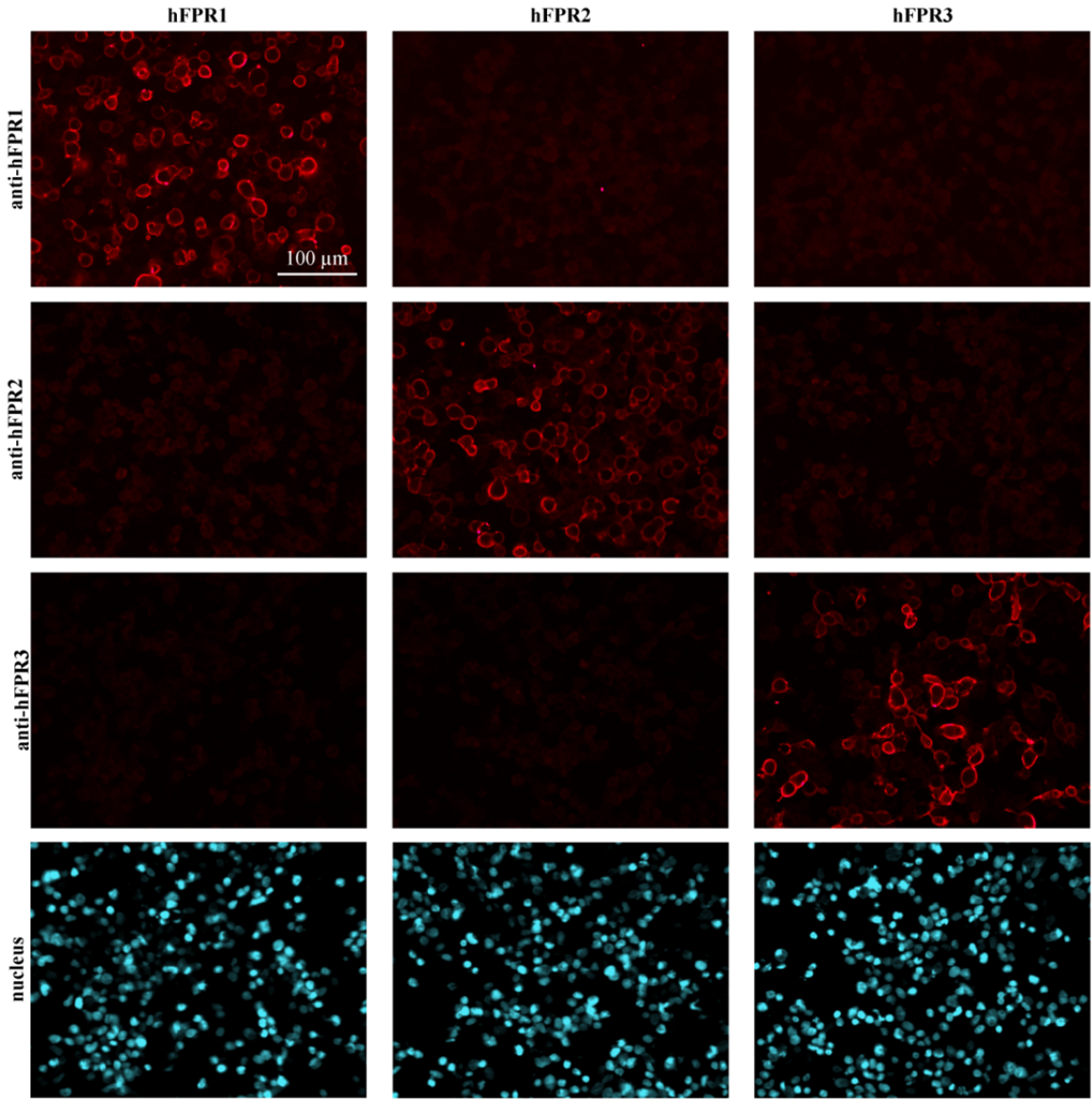
Immunocytochemical staining of primary human monocytes stained with an anti-hFPR2 antibody or the isotype control MOPC-21. Antibody-dependent fluorescence is shown in red, nuclear counterstain in cyan.



**Appendix 3 | Determination of cross-reactivity of anti-hFPR antibodies with heterologously expressed FPRs**

Primary antibodies directed against hFPR1, hFPR2 or hFPR3, respectively, were used for staining of HEK293T cells, transfected with plasmids encoding either hFPR1, hFPR2 or hFPR3. All hFPR antibodies were treated with a secondary antibody conjugated with the Alexa555 fluorophore. Shown are confocal fluorescence images of non-permeabilized cells transfected with plasmids for a given receptor (red stainings). Hoechst 33342 counterstaining of cell nuclei (cyan) is exemplified for the cells stained with the anti-hFPR3 antibody. Quantification of the surface stainings is shown in the lowest panel. All three antibodies stain only their original target receptor and do not cross react with the other FPRs, although they are expressed in equal amounts. Notably, the percentage of specifically stained cells is comparable to that of Rho-tagged FPRs by staining with an anti-Rho antibody (Figure 3-1-1). Results are representable for at least three independent transfections.

HEK293T cells transfected with



**Appendix 4 | Nucleotide sequence of the rhodopsin fusion element (figure 2.1)**

5' atgaacgggaccgagggcccaacttctacgtgcctttccaacaagacgggcgtggtgcgcagccccttcgaggccccgcagt  
actacctggcggagccatggcagttctccatgg 3'

**Appendix 5 | Full coding sequences of the cloned formyl peptide receptors****mFpr1**

atggacaccaacatgtctctctcatgaacaagtctgcagtgaacctcatgaatgtatctgggagtactcaatcagtatctgctggctacat  
cgttctggatgcttctcatatftgatctttgccgtcacattgtccttggggttctgggcaacgggctcgtgatctgggtgctggttccgc  
atgaaacacactgtcaccacctcttacttgaacttggccattgctgacttttcttcaacttccactttgccattttacattgccagcatggt  
catgggaggacattggccatttggttggttcatgtgcaaatcatatatactgtaatagacataaacctatttggagtgcttctctgattgcc  
ctcattgcactggaccgctgtattgttctacatccagctctgggctcagaaccaccgactgtgagcctagccaagaaggtaatcatcg  
tacctggatttgtcatttcttctacattgccagttatcattcgttggaccacagtcctaatagtagacttggaccagggaacagcctg  
tacttgcacttctccccctggaccaaaagatcctgtagagaagagggaaggtggccgtcaccatgctcactgtcagaggaatcatcaggtt  
catcattgggttcagcactcccatgtccattgttgcatttgcctatgggtaataaccactaaaattcacaggcaggccctgatcaaatcca  
gccgtcctttgggggttctctcttggttggtgctccttttctctgctggtgcccatttcaagtagtggccctcatatccacaatccaagtc  
cgtgaacggttgaagaacatgactccaggcattgtaactgccttgaaaatcacaagccccttggcttcttcaacagctgcctcaatccaa  
tgccttatgtctttatgggcccaggacttcagagaaagactaatccactcttacctgccagcctagagaggccctgactgaggactcag  
ctcagaccagtgatacaggccaatttggggaccaactctacttcccttctgaaaacactttaaataatgcaatgtga

**mFpr2**

atggaatccaactactccatccatctgaatggatcagaagtgggtggttatgattctaccatctccagattctgtggatcctctcaatgggtg  
gttctctccatcactttctcttgggtgctgctgggcaatggactagtattgggtagctggattccggatgccacacactgtcaccactatc  
tggtatttgaatctagcattggctgacttttcttccagcaactctaccattccttctgttgaatggctatgaaagaaaaatggccttttgg  
ctggttctgtgtaaattagttcacatttggttagatgtaaacctgttggagtgcttcttctgattgctctcattgccttggaccgctgcattg  
gttctgcacccagctcgggctcagaaccaccgactgtgagcctggctaggaaggtggttggggccctggattttgctctgattctca  
ctttgccatttttcttctgactactgttagaattcctggaggagatgtgtattgtacattcaacttggatcctgggctcaaacgatgaag  
aaaagttgaacacagctatcacttttgaacaactagagggatcatcaggttccttattggttccagcatgccatgcaatgttctgctgtttg  
ctatggactcattgctgcaagatcaacagaagaacctgttaattccagccgtcctttacgagtccttacagcagttgtggcttctcttctt  
atctgctggttcccttccagcttggccctttggggcacagtctggttaaaagagacattgcttagtggtagtataaaattcttgacatgttt  
gtaaccaacaagctcattggcttactcaatagttgtctcaatccgatgctctatgtttcatgggcccaggacttctgtgagagattattca  
ttccctgccttatagcttgagagagccctgagtgaggattctggtcaaacagtgattcaagcaccagttctacttccctctcgcagaca  
ttgagttaaagggcccatga

**mFpr-rs1**

atggaaaccaactactctatcccttgaatggatcagatgtggtgatctatgattctaccatctccagggttctgtggatcctctcaatgggtg  
gttctctccatcactttctcttgggtgctgctgggaaatggactagtatctgggttagctggattccggatgccacacactgtcaccactatc  
tggtatctgaatctagcattggctgacttcttcttccagcaactctaccattccttctgttgaatggctatgaaagaaaaatggccttttgg  
ctggttctgtgtaaattagttcacattgcagtagatgtaaacctatttggagtgcttcttctgattgctgtcattgccttggaccgctgtattg  
gttctgcacccagctcgggctcagaaccaccgactgtgagcctggctagaaatgtggttgggtcctggattttgctctcatttctca  
ctttgcccttttcttcttctgactacagtagatgctagaggggatgtcactgtagattgagcttcttatcctggggcaactctgttga  
ggaaaggttgaacacagctatcacgttgaacaactagagggatcatcaggttcattgttagcttcagcttggccatgtcctttgttgcct  
ctgctatggactcatcactacaaagattcacaanaagcctttgtaattccagccgtccttccgagttcttacaggagttgtggcttctctc  
ttatctgttgggttcttccaattgggtggcccttttaggcacagctctgctcaaaagagatgcagtttagtggtagtataaaattattggcag  
gttggtaataccaacagttcattggccttttcaatagctgcctcaatcaatctctatgtttctatgggcccaggacttcaagaaagactg

attcattccctgtcttctcgtctgcagagagccctgagtgaggactctggcatatcagtgatacaagaaccaattggcttcacttctgaa  
gacattgaaataaaggcaatatga

## hFPR1

atggagacaaattcctctctccccacgaacatctctggagggacacctgctgtatctctggctatcttcttctggatatcatcacttctg  
gtattgcagtcaccttctcctcgggctctgggcaacgggcttctgctctgggtggctggattccggatgacacacacagttaccacc  
atcagttacctgaacctggccgtggctgacttctgtttcacctccactttgccattcttcatggtcaggaaggccatgggaggacattggc  
cttctggctggctctgtgcaaattcctctttaccatagtgacatcaactgttcggaagtgtcttctgatcgcctcattgctctggaccg  
ctgtgttgcctcctcatccagctctggaccagaaccaccgcaccgtgagcctggccaagaagggtgatcattgggcccctgggtgatg  
gctctgctcctcacattgccagttatcattcatgtgactacagctacctggtaaacggggacagtagcctgcacttttaacttttgcctgg  
accaacgacctaaagagaggataaagggtggccgttgcctgttgacgggtgagaggcatcatccggttcatcattggcttcagcgcac  
cctatgctcatcgttctgtcagttatggccttattgccaccaagatccacaagcaaggctgattaagtccagctgctccctacgggtcctc  
tcttctgtcgcagcagcctttttctctgctggctcccatatcaggtgggtggccttatagccacagtcagaatccgtgagttattgcaaggc  
atgtacaaagaaattggattgcagtggtatgacaagtgcctggccttcttaacagctgctcaacccatgctctatgtcttcatggg  
ccaggacttccgggagaggctgatccacgcccctcccgcagctggagagggcctgaccgaggactcaacccaaaccagtga  
cagctaccaattctacttctctgcagaggtggagttacaggcaaatgga

## hFPR2

atggaaccaacttctccactcctctgaatgaatatgaagaagtgcctatgagctgctggctacactgttctcggatcctcccattggg  
ggctgttggggtcaccttctcctcggggtcctgggcaatgggcttctgctctgggtggctggattccggatgacacgcacagtcacca  
cctctgttacctgaacctggccctggctgactttcttccagggccacattaccattcctcattgtctccatggccatgggagaaaaatgg  
ccttttggctggttctgttaagtaattcacatcgtggtggacatcaacctcttggaaagtgtcttcttgattggttccattgactggaccg  
ctgcaattgtctcctcatccagctctggcccagaaccaccgcactgtgagctggccatgaagggtgatcgtcggaccttggattcttctg  
ctagtccttacctgcccagtttctcttcttactacagtaactattccaaatggggacacatactgtactttcaactttgcatcctggggtg  
caccctgaggagaggctgaagggtggccattaccatgctgacagccagagggtattccggttctcattggcttttagcttgcgatg  
cattgttccatctgctatgggctcattgcagccaagatccacaaaaagggtatgattaatccagccgtcccttacgggtcctcactgct  
gtggtggcttcttcttctctgttggttcccttcaactggttgccttctgggcaccgtctggctcaaagagatgttcttctatggcaagta  
caaaatcattgacatcctggttaaccaacgagctccctggccttcttaacagctgctcaacccatgctttactgttcttgggccaag  
acttccgagagagactgatccactccctgccaccagctggagagggcctgtctgaggactcagcccaactaatgacacggctg  
ccaattctgcttcactcctcgcagagactgagttacaggcaatgga

## hFPR3

atggaaccaacttctccactcctctgaatgaaactgaggaggtgctcctgagcctgctggccacaccgttctgtggatcttctcattgct  
agtccacggagtcaccttctcctcggggtcctgggcaatgggcttctgctctgggtggctggattccggatgacacgcacagtcaca  
cctctgttacctgaacctggccctagctgacttcttctcagtgccatcctaccattccgaatggtctcagtcgccatgagagaaaaatgg  
ccttttggctcattcctatgtaagttatgctatgtagatcaacctgttctcagtgctacctgatcaccatcattgctctggaccgc  
tgtatttctcctgcatccagcctggcccagaaccatcgccatgagctggccaagagggtgatgacgggactctggattttcacc  
atagtccttaccttaccaaatttctcttctggactacaataagtagctacgaatggggacacatactgtattttcaactttgacttctggggtga  
cactgctgtagagaggtgaacgtgttccattaccatggccaaggcttctgactcctccacttatttggcttcagcgtgctatgtccatc  
atcacagtctgctatgggatcctgctgcccataacacagaaaccacatgattaatccagccgtcccttacgtctctcgtctgtggt  
ggcttcttctcctctgttgggtcccttatgaaactaattggcattctaatggcagctctggctcaaagagatgttgttaaatggcaatacaaaa  
tcaattctgctgattaaccaacaagctccttggccttttttaacagctgctcaacccaaattctctacgtctttatgggtcgttaacttcaa  
gaaagactgattcgtcttctggccactagtttggagagggcctgactgaggtccctgactcagcccagaccagcaacacagacacca  
cttctgcttcactcctgaggagacggagttacaagcaatgga

## mFpr-rs3

atggaagccaactcctccatcccactgaatggctcagaagtgggtgtttatgattctaccacctccagagttctatggatcctctcagtgat  
agtctctccataaccttctccttgggtgctaggtaatgggcttctgatttgggtggctgggttccggatggcacacactgtgaccacca  
tctgttatctgaacctggccttgggtgacttcttcttcatggttactttaccactacacatcatctcaatggtcatgaaaggaaaaatggctttttg

gttggtcctttgcaaattgttctcagcattgtgcacataaaccttttgaagtgtttcttaactctcattgcatggatcggtgacttgt  
 gtctgcaccagatgggttcagaatcaccgaactgtgagctggccaggaaagtattgttgagcttgattctttctctgctgttac  
 attgccacattttctcttctgactacagtgagagatgcaagaggcgaagtgcactgtacatgtaacttgaatctgtggtgcaaaccctg  
 aggagcaattaaagggtcaattaccgtgagcagcaacaggaaatcatcagttttatttggcttcagcctacctatgctctcattgcc  
 gctgctatggactcatggctgccaagattttagaaaaggcttttgaactccagccgtcctttacgtgttctcactgctgtagaatttct  
 tctttatgtgttggtccctttcaactgattattctctaggaataatctggaataaggagacaccaagcagcattcacatttgtgaaccag  
 caagcacactggcttctcaacagctgtctcaaccaatactctatgtctttcttggcaagaatttagagagaaactgatatctcctgtc  
 tggcagctggagagggcgctgcgagaagactcagctctaagcagtggaagcagcaacttttctcatgtctcggactctgaac  
 tatga

## mFpr-rs4

atggaagtcaacattcaatgcctctgaatggatcagaagttgtgtttatgattctaccacctcaagagttctatggatcctctcattagtgg  
 tctctttataacctttgtctcgggtgttaggtaatgggctgtgatttgggtggctgggtccagatggcacacactgtgaccactgtctct  
 atctgaacttggctttagtgatttattcttcatggctactctaccactcacaatcctcaatggctcatgagaggaaatggcttttgggtggt  
 ttctttgcaaattggtcacataaattgcaaacataaaccttttgaagtattctctaatcactcttattgcatggatcgctgtatttgtctctg  
 tggccagatgggtctcagaatcaccgaactgtgagctggccagaaaagtgggtcttggagcttggatatttgcctctgctgtaccttggc  
 acatttctcttctgactacagtgagagatgcaagaggggatgtgactgtatatctaaattgaaatcctgggtgcaacctctgaagagca  
 gttaaagggtgtctgttattgctgccacagctcaggaatcatcaattcatttggattcagcatgccatgctttcattgctatctgctatgg  
 actcatggctgccaagatctcagaagaggcttgaattcagctcctttacgtgtcctcactgctgtagcagttcctcttctgtctgtt  
 ggttccctttcaattaattatgcttttaggcaacatcttaacaatgagacactgagcatttcatatgttggttaaccagcaataaccttg  
 gcttctttaacagctgctcaaccaatactctatgtattcctgggtcaggaattcagagacagactaatctattctctgtatgccagctca  
 gagagggccctgaggggaagactga

## mFpr-rs6

atggaagccaacttctccataacctcagaatggatcagaagtggtgtttatgattctaccacctccagagttatgtatcttcttagttgtggt  
 cctctctataacctttctccttgggtgtgataggaatgggcttgtgatttattgtggctgggttccggatgacacacactgtgacaacaatctgt  
 tatctgaacctggcattgtctgacttctttacatggcaagctaccattcagatcacctcaattgtcatgaatggagaatggcttttgggtg  
 gttcctttgcaaattgttcacatgattataaacgtaaaccttttctaagtattcttctgattacttcttccatggatcggttatttgttctg  
 catccagatgggctcagaatcatcgaactgtgaatgtggcaacgaaagtgatcttggagcttggatacttgttctgatcttatattcca  
 cattgtatctctgactacagtgaagatgaaagtgggaaagtacattgcatatgtaatttgaatcctgggctgcaaccctgaggagc  
 aagtaaaagtatctatgactgtgagtttaattcagtaacctcagttcatttggcttcagcataccaatgatcttcattgtcatctgttatg  
 gactcatggctgccaagataggcagaagaggttttgaattccagctcctttacgtgtcctcactgctgtagcaatttcttttctgtctgt  
 tggttccctttcaattgattttcttttaggcaatattgggaacaaggagacacagaataatattgacacgtgggtgaacacagcaagcact  
 ctggcctcctcaatagttgcctcaaccaatactctatgtttcttaggtcagcaattcagagagagactgatctactccctatcagctagt  
 ctggagagggccctgagggaggactcagccctgaacagtgacaaaaccagaaactgtcttcacaaagactctga

## mFpr-rs7

atggaagccaacttctccataacctcagaatggatcagaagtggtgtttatgattctaccacatccagagttatgtatcttcttagttgtggt  
 cctctctataacctttctccttgggtgtgataggaatgggcttgtgatttattgtggctgggttccggatgacacatactgtgacaacaatctgt  
 tatctgaacctggcattgtctgacttctttacatgacaagctaccattcagatcacctcaattgtcatgaatggagaatggcttttgggtg  
 gttcctttgcaaattgttcacatgattataaatgtaaaccttttctaagtattcttctgattacttcttccatggatcgctgtatttgttctg  
 catccagatgggctcagaatcatcgaactgtgaatctggcaaggaagtatttgggacttggatacttgttctgatcttatattcca  
 catttttcttctgactacagtgaagatgaaagtggtaagtacactgtatgcaatttgaatcctgggctgcaaccctgaggagca  
 ggtaaacatgtctatgactgtgagtttaattcagtaacctcagttcattgttggcttcagcataccaatgatcttcattgtcatctgctatgg  
 actcatggctgccaagataggcagaagaggttggtaattccagctcctttacgtgtcctcactgctgtagcattttctttctgtctgtt  
 ggttccctttcaattgattttcttttaggcaatattgggaacaaggagacacagaataatattgacgctgggtgaaccagcaagcact  
 ctggcctcctcaatagttgcctcaaccaatactctatgtttcttaggtcagcaattcagagagagactgatctactccctatcagctagt  
 ctggagagggccctgagggaggactcagccctgaacagtgacaaaaccagaaactgtcttcacaaactta

---

## Publications

---

### Journal articles

#### **Bacterial signal peptides as pharmacological tools to detect FPRs (in preparation)**

Schumann T, Podgórska M, Kappl R, Bogeski I, Smola S, Zufall F, Bufe B

#### **Recognition of bacterial signal peptides by mammalian formyl peptide receptors: a new mechanism for sensing pathogens.**

**J Biol Chem.** 2015 Jan 20. pii: jbc.M114.626747. [Epub ahead of print]

Bufe B\*, Schumann T\*, Kappl R, Bogeski I, Kummerow C, Podgórska M, Smola S, Hoth M, Zufall F

\* Both authors contributed equally to this work

#### **Formyl peptide receptors from immune and vomeronasal system exhibit distinct agonist properties.**

**J Biol Chem.** 2012 Sep 28;287(40):33644-55. Epub 2012 Aug 2.

Bufe B\*, Schumann T\*, Zufall F.

\* Both authors contributed equally to this work

## Abstracts

### **12th International Congress of Neuroimmunology, 9-13 November 2014, Mainz, Germany**

Formyl peptide receptors from the innate immune system and the vomeronasal organ recognize pathogen derived peptides

Schumann T, Bufe B and Zufall F

### **17th STS Meeting 2013: Signal Transduction - Receptors, Mediators and Genes, 4-6 November, 2013, Weimar, Germany**

Evolution of formyl peptide receptor function in mammals

Bufe B, Schumann T, Stempel H, Zufall F

### **XXIInd Congress of the European Chemoreception Research Organization, ECRO 2013, 27-29 August 2013, Leuven, Belgium**

RNA-editing alters the function of vomeronasal formyl peptide receptors

Stempel H, Schumann T, Bufe B, , Zufall F

Evolution of formyl peptide receptor function in mammals

Bufe B, Schumann T, Stempel H, Zufall F

### **92nd Annual Meeting | Deutsche Physiologische Gesellschaft, 2-5 March, 2013, Heidelberg, Germany,**

Evolution of formyl peptide receptor function in mammals

Bufe B, Schumann T, Zufall F,

**XVI International Symposium on Olfaction and Taste, ISOT/ECRO 2012, 23-27 June, 2012, Stockholm, Sweden**

Formyl peptide detection by vomeronasal sensory neurons is mediated by functionally distinct cell populations

Schumann T, Bufe B and Zufall F

Agonist profiling of the mouse formyl peptide receptors reveals a stereoselective tuning of mFpr-rs1

Bufe B, Schumann T, Stempel H and Zufall F

Functional characterization of G-protein coupled vomeronasal receptors using a virus-based expression system

Stein B, Cvijetic S, Schumann T, Bufe B, Zufall F and Chamero P

---

## Acknowledgments and Contributions

---

### Statement and declaration of experimental contributions

The essence of science is to discover, understand and explain what is to be explained; to create and gather as much knowledge as possible. Demand for quality and scientific correctness, should hence be the most important and exalted traits of scientific research. A task not easily completed, especially in times where episodes of time pressure urge scientists to increase data quantity without any loss of quality. In my opinion, requirements of this research philosophy are easily fulfilled by allegorizing three simple traits: honesty, candor and teamwork. Following this idea, I will try my best to reveal contributions by other people as frank, honest and correct as demanded.

*Cell stock handling, cell culture and transfection were from time to time performed by Sabine Plant, Saarland University, Medical School Homburg, Department of Physiology.*

*Blood collection for human granulocyte isolation was performed by Dr. Martina Pyrski (Saarland University, Medical School Homburg, Department of Physiology) and Regina Bender-Omlor (Saarland University Hospital, Department of Virology).*

*Enrichment of PBMCs was in general performed by Carmen Hässig (Saarland University, Medical School Homburg, Department of Biophysics). Overnight incubations of monocytes were sometimes performed by Sabine Plant (Saarland University, Medical School Homburg, Department of Physiology).*

*Ficoll separations were generally performed by Marta Podgórska (Saarland University Hospital, Department of Virology)*

*Mouse keeping and breeding was performed by the staff of the animal facility of Trese Leinders-Zufall (Saarland University, Medical School Homburg, Department of Physiology), namely Angelika Ströer and Sarah Boll.*

*Single cell calcium imaging of human monocytes was performed by Carsten Kummerow (Saarland University, Medical School Homburg, Department of Biophysics).*

*Calcium imaging of HEK293T cells was in rare cases performed by Dr. Bernd Buße (Saarland University, Medical School Homburg, Department of Physiology).*

*I cloned the genes for mFpr1, mFpr2, and mFpr-rs3 during my diploma thesis (Schumann, 2010).*

**Einverständniserklärung/ statement of agreement**

Ich bin damit einverstanden, dass Herr Timo Schumann die von ihm angegebenen Daten zur inhaltlichen Darstellung seiner Dissertation verwenden darf. Die Daten wurden unentgeltlich erstellt und freiwillig zur Verwendung genehmigt.

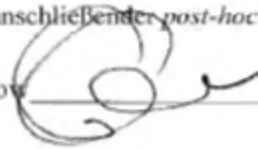
- (1) Konzentrations-Wirkungskurven für MVm-NH<sub>2</sub> auf mFpr-rs1 und für *Streptococcus*-SPI + f-MLF auf hFPR1. Hilfe beim Klonieren des mFpr-rs1.

Mit freundlicher Genehmigung: Bernd Bufe



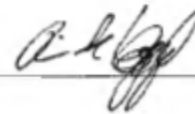
- (2) Einzel-Zell Messungen humaner Monozyten mit anschließender *post-hoc* Färbung.

Mit freundlicher Genehmigung: Carsten Kummerow



- (3) Modellierung der 3D Struktur von W-peptide und retro-inverted W-peptide

Mit freundlicher Genehmigung: Reinhard Kappl



Alle Angaben wurden nach bestem Wissen und Gewissen erstellt.



## Copyright Permission Policy of the American Society for Biochemistry and Molecular Biology

### Copyright Permission Policy

---

These guidelines apply to the reuse of articles, figures, charts and photos in the *Journal of Biological Chemistry*, *Molecular & Cellular Proteomics* and the *Journal of Lipid Research*.

#### For authors reusing their own material:

Authors need **NOT** contact the journal to obtain rights to reuse their own material. They are automatically granted permission to do the following:

- Reuse the article in print collections of their own writing.
- Present a work orally in its entirety.
- Use an article in a thesis and/or dissertation.
- Reproduce an article for use in the author's courses. (If the author is employed by an academic institution, that institution also may reproduce the article for teaching purposes.)
- Reuse a figure, photo and/or table in future commercial and noncommercial works.
- Post a copy of the paper in PDF that you submitted via BenchPress.
- Link to the journal site containing the final edited PDFs created by the publisher.

EXCEPTION: If authors select the Author's Choice publishing option:

- The final version of the manuscript will be covered under the Creative Commons Attribution license (CC BY), the most accommodating of licenses offered.
- The final version of the manuscript will be released immediately on the publisher's website and PubMed Central.

Please note that authors must include the following citation when using material that appeared in an ASBMB journal:

"This research was originally published in Journal Name. Author(s). Title. *Journal Name*. Year; Vol:pp-pp. © the American Society for Biochemistry and Molecular Biology."

Updated March 20, 2013

## Acknowledgments and Contributions

First of all, I thank **Prof. Dr. Dr. Frank Zufall** to give me the chance to investigate the FPR-family and to enable me a start for a career in science. I very much appreciate that he left me free to develop my project in unforeseen directions. I would like to thank him for his support of my projects and the easy access to expensive working material. I would like to thank him for enabling me traveling to scientific meetings and presenting my work. I thank him for his open words and for his forthright teaching lessons one cannot learn from books. Finally, I would like to thank him for sharing some of his vast knowledge of science, its rules and laws.

I thank **Dr. Bernd Bufe** for his advice in nearly all situations, professionally and in private. I would like to thank him for his complaisant mentoring, his academical advice and his support and the critical evaluation of my work and my conceptual skills. Furthermore I want to thank him for introducing me into his FLIPR assay and the daily laboratory routine. I would like to thank him for some of the FLIPR experiments and his help in cloning of mFpr-rs1. I would like to thank him for his cooperation and many discussions. Finally I would like to say that even though our ways of working are not always compatible, I am very happy to have a friend in science in who I know I can rely on.

I would like to thank **Prof. Dr. Markus Hoth** very much for his candid and sincere nature. Our conversations were very encouraging. Furthermore, I would like to thank him for his scientific advice and his uncomplicated cooperation.

I thank **Prof. Dr. Trese Leinders-Zufall** for her technical and “political” advice and for her constructive criticism. Though none of my business, I especially thank her for her dedication toward her students. I thank her for the continuous and well planned support with genetically modified mice and for sharing some aliquots of different chemicals in times of need.

I thank **Prof. Dr. Sigrun Smola** for successful and inspiring cooperation.

I would like to thank **Sabine Plant** for her friendly and benevolent support and advice in many issues; in business and in private. Furthermore, I would like to thank her for sharing her professional expertise in heterologous cell culture and her dedication in solving upcoming problems. Finally, I would like to thank her for providing me with cells whenever my time schedule was blasted and I thank her for purifying plasmids whenever needed.

I thank **Carmen Hässig** for continuous support with human monocytes.

Thanks go also to **Regina Bender-Omlor** for the blood taking, which was necessary for leukocyte isolation.

I thank **Marta Podgórska** for the isolation of the human granulocytes and her technical advice in observing granulocyte chemotaxis.

My thanks go to **Carsten Kummerow** for conducting the *post-hoc* experiments on human monocytes.

I would like to thank **Dr. Reinhard Kappel** for his committed support in calculating and modeling the structures of D-W-peptide and the corresponding mirror variant. Furthermore, I thank him for his always present calm and kind mood.

I thank **PD Dr. Ivan Bogeski** for nicely introducing me into detection of reactive oxygen species in monocytes.

I thank my classmate **Stephanie Saul** for her technical advice in purifying and culturing human PBMCs.

In addition, I would like to thank **Dr. Pablo Chamero** for showing me how to isolate, cultivate and measure the vomeronasal sensory neurons. I very much appreciate your readiness to help.

I thank **Petra Hammes** for providing me with lab stuff I could not find and for many friendly conversations.

I thank **Michael Konzmann** for providing me with aliquots of dissolved peptides ND1-6I, ND1-6T and CO1-3I.

I very much thank all the people who critically read my thesis for their comments and help. Special thanks go to **Dr. Anabel Pérez-Gómez, Dr. Bernd Bufe, Thomas Blum, Henrike Reder, Hendrik Stempel**, and my dear friend **Dr. Katja Schmitt**.

I thank the animal staff facility **Monika Vorndran, Andrea Degreif, Sarah Boll, Angelika Ströer, Kerstin Becker, and Lisa Knieriemen** for the animal caretaking and their professional support.

I would like to thank my fellow PhD and graduate students of which some have become close friends over the past years: **Dennis Bakker, Katherin Bleymehl, Thomas Blum, Florian Bolz, Michael Dieli, Eugenia Eckstein, Dr. Phil(ipp) Hendrix, Henrike Reder, Dr. Christian Schauer, Benjamin Stein, Hendrik Stempel, and Tong Tong**. We have had a wonderful time.

Many thanks go to all people who donated blood for my studies.

## Special thanks go to ...

... the GradUS committee for granting me the scholarship.

... my fellow-sufferer **Hendrik Stempel** for working together; for the many scientific discussions, for his helping hand and for the many moments he cheered me up. It was a great time.

... my office partner **Henrike Reder** for being the jolly natured woman she is and for becoming a close friend.

... “always lending a helping hand in technical issues” **Holger Frisch**; “you keep the whole system running”.

... **Martina Pyrski**. No matter how limited her own time is, what scientific challenges she is meeting, she always listens to others; and always in a very kind fashion.

... **Gabi Mörschbacher**: “without your support, I would have left the road too early!”

... my parents **Doris Schumann** and **Willi Schumann** who always supported me, no matter what problem there was. You made it possible to achieve what I achieved. You taught me what really matters in life; this might be the most important lesson at all.

... my brother **Björn Schumann**, the best friend I will ever have.

... my wife **Eva Schumann** who always supports me to her best; you are a greater help than you know. And thank you for showing me the value of a happy marriage.

My last thanks go to my daughter **Emily Schumann** and her little still unborn sib “**Gummibärchen**”, both of whom taught me a kind of inexplicable, unique love: “you give me the power to endure almost anything.”

---

## Curriculum vitae

---

### Personal information

---

Date of birth	March 7th, 1983
Nationality	German
Family status	married, 1 child

### Research experience

---

05/2011 - today	PhD student and research associate, Molecular Medicine of Sensory Systems group, Department of Physiology, Universität des Saarlandes/Germany
01/2011 - 04/2011	Research Associate, Dept. Molecular Medicine of Sensory Systems, Universität des Saarlandes/Germany <i>Pharmacological analysis of GPCRs in neurosensory epithelia</i>
07/2008 - 04/2009	Research assistant, Dept. of Neurophysiology, Universität des Saarlandes <i>“Histone H3 (K9) acetylation-mediated behavioral regulation of MAPK p44/42, PKA and PKC expression in the honey bee”</i>

## Higher Education and Training

---

Since 01/2011	Work on my doctoral thesis, graduation as <b>Dr. rer. nat.</b> expected June 2015 <i>„Formyl peptide receptors are highly sensitive detectors of bacterial signal peptides“</i>
12/2010	German <b>Diploma in Biology</b> , Universität des Saarlandes <i>„Functional characterization of formyl peptide receptors in mice and rats“</i>
10/2005 - 12/2010	<b>Studies of Biology, Focus on human/-molecular-biology</b> , Universität des Saarlandes
6/2003 - 12/2005	Pre-qualifying period to finance my studies, including working as a postman
08/2002 - 05/2003	Community service in the ambulance service, Malteser Hilfsdienst (MHD) Tholey
1993 - 6/2002	High School Diploma (Abitur), Cusanus-Gymnasium, St. Wendel

## Additional academic training

---

11/2014	Graduate school seminar – Leading techniques
05/2014 - 07/2014	Rhetoric for PhD students
10/2013	„Teaching Assistant Program“ – How to teach and to learn

## Languages

---

German	Native Speaker
English	Fluent
French	Advanced knowledge
Spanish	Advanced knowledge
Japanese	Basic knowledge

## Computer skills

---

Profound knowledge	Adobe Illustrator, Microsoft Excel/ PP/Word, Graph Pad Prism, PyRAT
Advanced knowledge	Wavemetrics-IGOR, Origin, Endnote, Adobe Photoshop, Corel Draw

## Raised funding

---

01/2011 - 07/2014	<b>GradUS Research Fellowship</b> , <i>Graduiertenförderung UdS</i>
06/2012	<b>Travel grant</b> - ISOT XVI

## Memberships

---

Since 2014	International Society of Neuroimmunology
Since 2013	Signal Transduction Society
Since 2012	European Chemoreception Research Organisation
2012	Graduate Research School: Calcium-Signaling and Cellular Nanodomains (GK 1326), Universität des Saarlandes

## Voluntary work

---

03/2004 - 05/2004	Inpatient care (practical), MKH Hospital, St. Wendel
07/2003 - 03/2004	Ambulance station, MHD Tholey